Complex organic molecules in the interstellar medium: IRAM 30 m line survey of Sagittarius B2(N) and (M)[⋆,⋆⋆,⋆⋆⋆]

A. Belloche[1], H. S. P. Müller[1,2], K. M. Menten[1], P. Schilke[1,2], and C. Comito[1]

[1] Max-Planck-Institut für Radioastronomie, Auf dem Hügel 69, 53121 Bonn, Germany
e-mail: belloche@mpifr-bonn.mpg.de
[2] I. Physikalisches Institut, Universität zu Köln, Zülpicher Str. 77, 50937 Köln, Germany

ABSTRACT

Context. The discovery of amino acids in meteorites fallen to Earth and the detection of glycine, the simplest of them, in samples returned from a comet to Earth strongly suggest that the chemistry of the interstellar medium is capable of producing such complex organic molecules and that they may be widespread in our Galaxy.

Aims. Our goal is to investigate the degree of chemical complexity that can be reached in the interstellar medium, in particular in dense star-forming regions.

Methods. We performed an unbiased, spectral line survey toward Sgr B2(N) and (M), two regions where high-mass stars are formed, with the IRAM 30 m telescope in the 3 mm atmospheric transmission window. Partial surveys at 2 and 1.3 mm were performed in parallel. The spectra were analyzed with a simple radiative transfer model that assumes local thermodynamic equilibrium but takes optical depth effects into account.

Results. About 3675 and 945 spectral lines with a peak signal-to-noise ratio higher than 4 are detected at 3 mm toward Sgr B2(N) and (M), i.e. about 102 and 26 lines per GHz, respectively. This represents an increase by about a factor of two over previous surveys of Sgr B2. About 70% and 47% of the lines detected toward Sgr B2(N) and (M) are identified and assigned to 56 and 46 distinct molecules as well as to 66 and 54 less abundant isotopologues of these molecules, respectively. In addition, we report the detection of transitions from 59 and 24 catalog entries corresponding to vibrationally or torsionally excited states of some of these molecules, respectively, up to a vibration energy of 1400 cm^{-1} (2000 K). Excitation temperatures and column densities were derived for each species but should be used with caution. The rotation temperatures of the detected complex molecules typically range from ∼50 to 200 K. Among the detected molecules, aminoacetonitrile, *n*-propyl cyanide, and ethyl formate were reported for the first time in space based on this survey, as were five rare isotopologues of vinyl cyanide, cyanoacetylene, and hydrogen cyanide. We also report the detection of transitions from within twelve new vibrationally or torsionally excited states of known molecules. Absorption features produced by diffuse clouds along the line of sight are detected in transitions with low rotation quantum numbers of many simple molecules and are modeled with ∼30–40 velocity components with typical linewidths of ∼3–5 km s^{-1}.

Conclusions. Although the large number of unidentified lines may still allow future identification of new molecules, we expect most of these lines to belong to vibrationally or torsionally excited states or to rare isotopologues of known molecules for which spectroscopic predictions are currently missing. Significant progress in extending the inventory of complex organic molecules in Sgr B2(N) and deriving tighter constraints on their location, origin, and abundance is expected in the near future thanks to an ongoing spectral line survey at 3 mm with ALMA in its cycles 0 and 1. The present single-dish survey will serve as a solid basis for the line identification and analysis of such an interferometric survey.

Key words. astrobiology – astrochemistry – line: identification – stars: formation – ISM: individual objects: Sagittarius B2 – ISM: molecules

1. Introduction

In the field of astrochemistry, organic molecules are considered to be complex if they contain six atoms or more (Herbst & van Dishoeck 2009). The search for such complex organic molecules in the interstellar medium is in part motivated by the discovery of more than 80 distinct amino acids in meteorites fallen to Earth. The isotopic composition and racemic distribution of these amino acids, in particular, suggest that they, or at least their direct precursors, have an extraterrestrial origin (see, e.g., Ehrenfreund et al. 2001; Bernstein et al. 2002; Elsila et al. 2007, and references therein). More recently, the detection of glycine (NH_2CH_2COOH), the simplest amino acid, has even been claimed in samples from comet 81P/Wild 2 returned to Earth by NASA's Stardust spacecraft (Elsila et al. 2009). Even if it is unclear whether the meteoritic amino acids and the cometary glycine represent pristine *interstellar* molecules, these discoveries strongly suggest that interstellar chemistry is capable of producing such complex molecules and that they could be widespread in our Galaxy.

A direct detection of amino acids and other similarly complex molecules in the interstellar medium is challenging because of their large partition functions and the related weakness of their

---

⋆ Based on observations carried out with the IRAM 30 m telescope. IRAM is supported by INSU/CNRS (France), MPG (Germany), and IGN (Spain).

⋆⋆ Figures 2–7 and Tables 6–107 are available in electronic form at http://www.aanda.org

⋆⋆⋆ The observed and synthetic 3 mm spectra of Sgr B2(N) and (M), as well as the lists of line identifications corresponding to the blue labels in Figs. 2–7, are only available at the CDS via anonymous ftp to cdsarc.u-strasbg.fr (130.79.128.5) or via http://cdsarc.u-strasbg.fr/viz-bin/qcat?J/A+A/559/A47

molecular line emission. The most efficient and least ambiguous way to search for such complex molecules is to perform unbiased spectral line surveys of suitable astronomical sources over a broad frequency range, as was realized three decades ago already (see, e.g., the spectral survey of Cummins et al. 1986). The reliability of a new detection is significantly improved by checking the presence of a molecule as a whole instead of relying on only detecting a few specific transitions (see, e.g., Snyder et al. 2005, for the disputed case of interstellar glycine). Such an approach also allows the contribution of all known molecules to be modeled at once and reduces the risks of misassignment.

The best hunting ground for complex organic molecules has turned out to be the Sagittarius B2 molecular cloud – hereafter Sgr B2. It is the most massive star-forming region in our Galaxy, at a projected distance of ~100 pc from the Galactic center, which is located at 7.9 ± 0.8 kpc from the Sun (Reid et al. 2009). Sgr B2 has a diameter of 34 pc (Scoville et al. 1975, after correction for the distance) and contains two main sites of star formation, Sgr B2(N) and Sgr B2(M), which are separated by ~48″ (~1.8 pc in projection). Their luminosities are 8.6×10^5 and 6.5×10^6 $L_\odot$ (Goldsmith et al. 1992, after correction for the distance), and their masses are $3-10 \times 10^4$ and $1.5-4.1 \times 10^4$ $M_\odot$, respectively, which are small fractions of the total mass of the cloud, $5-10 \times 10^6$ $M_\odot$ (Lis & Goldsmith 1990). Both Sgr B2(N) and (M) contain a number of ultracompact H II regions (see, e.g., Gaume & Claussen 1990; Mehringer et al. 1993; Gaume et al. 1995). The star formation rate of Sgr B2 is about 0.04 $M_\odot$ yr^{-1}, which qualifies Sgr B2 as a ministarburst (see Appendix A).

Most complex organic molecules reported so far, such as acetic acid (CH_3COOH, Mehringer et al. 1997), glycolaldehyde ($CH_2(OH)CHO$, Hollis et al. 2000), acetamide (CH_3CONH_2, Hollis et al. 2006), aminoacetonitrile (NH_2CH_2CN, Belloche et al. 2008), or ethyl formate (C_2H_5OCHO, Belloche et al. 2009), were found for the first time in space toward Sgr B2(N). This source contains two hot cores separated by 5″ (~0.2 pc in projection) in the north–south direction, the less prominent one being located north of the most prominent one. The positions of these hot cores as obtained with the IRAM Plateau de Bure interferometer are ($\alpha_{J2000} = 17^h47^m19\overset{s}{.}886 \pm 0\overset{s}{.}005$, $\delta_{J2000} = -28°22′18.4″ \pm 0.1″$) and ($\alpha_{J2000} = 17^h47^m19\overset{s}{.}88 \pm 0\overset{s}{.}01$, $\delta_{J2000} = -28°22′13.5″ \pm 0.2″$) (Belloche et al. 2008, see also the SMA map of Qin et al. 2011). Their molecular emissions have similar linewidths (~7 km s^{-1}), but significantly different systemic velocities of 64 and ~73 km s^{-1}, respectively, which allows their emissions to be separated even with single-dish telescopes that do not resolve them spatially. Their immense hydrogen column densities of $>10^{25}$ cm^{-2} on scales of a few arcseconds (Belloche et al. 2008; Qin et al. 2011) boost weak lines from rare species into detectability.

Here, we report the analysis of a deep, unbiased, spectral line survey obtained at 3 mm toward Sgr B2(N) and (M) with the IRAM 30 m telescope. The main goal of the survey was to search for new complex organic molecules in the gas phase of the interstellar medium. This has been partially addressed in a number of earlier publications (Belloche et al. 2008, 2009; Müller et al. 2008; Brünken et al. 2010; Braakman et al. 2010; Møllendal et al. 2012; Ordu et al. 2012). This article now presents the complete analysis of the full survey, the main goal being to provide a reliable identification of the detected lines. Section 2 summarizes the observational details. The procedure to model the line survey is described in Sect. 3. The results are presented in Sect. 4 and are discussed in Sect. 5. Section 6 summarizes our conclusions.

2. Observations and data reduction

2.1. Observations

We carried out millimeter line observations with the IRAM 30 m telescope on Pico Veleta, Spain, in 2004 January (project 217-03), 2004 September (project 102-04), and 2005 January (project D18-04). Four SIS heterodyne receivers were used simultaneously, two in the 3 mm window connected to the autocorrelation spectrometer VESPA and two in the 1.3 mm window with filter banks as backends. A few selected frequency ranges were also observed with one SIS receiver at 2 mm in 2004 January. The channel spacing and bandwidth were 0.313 and 420 MHz for each receiver at 3 and 2 mm, and 1 and 512 MHz for each receiver at 1.3 mm, respectively. The channel spacing corresponds to 0.8–1.2, 0.5–0.7, and 1.1–1.5 km s^{-1} in velocity scale at 3, 2, and 1 mm, respectively. The observations were done in single-sideband mode with sideband rejection gains of ~1–3% at 3 mm, ~5–7% at 2 mm, and ~5–8% at 1.3 mm. The half-power beamwidth can be computed with the equation $HPBW('') = \frac{2460}{\nu(GHz)}$. The forward efficiencies, F_{eff}, were 0.95 at 3 mm, 0.93 at 2 mm, and 0.91 at 1.3 mm, respectively. The main-beam efficiencies were computed using the Ruze function $B_{eff} = 1.2\epsilon\, e^{-(4\pi R\sigma/\lambda)^2}$, with $\epsilon = 0.69$, $R\sigma = 0.07$, and λ the wavelength in mm[1]. The system temperatures ranged from 96 to 600 K at 3 mm, from 220 to 720 K at 2 mm (except at 176 GHz where they ranged from 2400 to 3000 K), and from 280 to 1200 K at 1.3 mm. The telescope pointing was checked every ~1.5 h on Mercury, Mars, 1757−240, or G10.62-0.38, and was found to be accurate to 2″–3″ (rms). The telescope focus was optimized on Mercury, Jupiter, Mars, or G34.3+0.2 every ~1.5–3 h. The observations were performed toward both sources Sgr B2(N) ($\alpha_{J2000} = 17^h47^m20\overset{s}{.}0$, $\delta_{J2000} = -28°22′19.0″$, $V_{lsr} = 64$ km s^{-1}) and Sgr B2(M) ($\alpha_{J2000} = 17^h47^m20\overset{s}{.}4$, $\delta_{J2000} = -28°23′07.0″$, $V_{lsr} = 62$ km s^{-1}) in position-switching mode with a reference position offset by $(\Delta\alpha, \Delta\delta) = (-752″, +342″)$ with respect to the former. The emission toward this reference position was found to be weak: $T_a^\star(^{12}CO\ 1-0) \sim 2$ K, $T_a^\star(CS\ 2-1) \lesssim 0.05$ K, $T_a^\star(^{12}CO\ 2-1) \sim 1.5$ K, $T_a^\star(^{13}CO\ 2-1) \lesssim 0.1$ K, and it is negligible for higher excitation lines and/or complex species.

We observed the full 3 mm window between 79.990 and 115.985 GHz toward both sources. The step between two adjacent tuning frequencies was 395 MHz, which yielded an overlap of 50 MHz. Half of the integration time at each tuning frequency was spent with the backend shifted by 50 MHz. At 2 mm, we observed Sgr B2(M) at only six selected frequencies (136.250, 145.300, 154.500, 163.500, 172.650, and 176.200 GHz) and Sgr B2(N) at 8 frequencies (the same ones plus 147.600 and 166.400 GHz). At 1.3 mm, we covered the frequency ranges 201.805 to 204.615 GHz and 205.025 to 217.750 GHz, plus a number of selected spots at higher frequency between 219.285 and 267.175 GHz, 26 for Sgr B2(N) and 19 for Sgr B2(M). The total observing time from 2004 January to 2005 January was on the order of 100 h.

2.2. Data reduction

The data were reduced with the Fortran 77 version of the CLASS software, which was part of the GILDAS software package[2]

---

[1] See the system summary of the IRAM 30 m telescope as of September 2007 on http://www.iram.es/IRAMES/telescope/telescopeSummary/telescope_summary.html

[2] See http://www.iram.fr/IRAMFR/GILDAS

Table 1. Estimated rms noise level achieved toward Sgr B2(N) and (M).

Frequency range (GHz)	Sgr B2(N)		Sgr B2(M)	
	Estimated rms noise level (mK)			
	range	median	range	median
80.0–89.9	10–25	13	12–22	15
89.9–100.2	10–23	17	14–42	18
100.2–114.6	12–35	22	14–34	22
114.6–116.0	42–56	43	43–57	45
136.0–147.9	17–21	20	24–26	25
154.2–154.8	74	74	75	75
163.2–172.9	25–42	28	47–55	51
176.0–176.5	227	227	289	289
201.8–204.6	66–220	91	72–118	85
205.0–217.8	19–169	44	18–91	44
219.2–228.0	47–155	54	42–69	52
230.9–236.6	10–100	22	9–123	115
240.7–241.3	114	114	169	169
243.9–247.5	21–49	32	36–40	38
251.9–254.5	16–21	19	14–19	17
255.2–259.3	107–784	551	98–339	263
260.0–267.2	37–200	49	50–85	84

Notes. The rms noise levels are given in $T_a^\star$ scale and are estimated from the radiometer formula, assuming a spectral resolution of 1.2 times the channel spacing below 180 GHz and 1.1 above. Some frequency ranges listed in the first column above 116 GHz include holes that were not covered by the observations.

Fig. 1. Diagram illustrating how the radiative transfer of N_e emission components and N_a absorption components is computed with XCLASS (see Sect. 3.1).

until 2010. The autocorrelator VESPA produces artificial spikes with a width of 3–5 channels at the junction between subbands (typically two or three spikes per spectrum). We used the redundancy provided by our observing strategy of shifting the backend for half of the integration time (see Sect. 2.1) to get rid of these artefacts at 3 mm without producing any hole in the frequency coverage of the final average spectra. In each 3 mm spectrum, we removed five channels at each of the six junctions between subbands that were possibly affected by this phenomenon. The artificial spikes at 2 mm were removed in the same way, but without redundancy, thus producing some holes in each frequency band.

For each individual spectrum, we removed a zeroth-order (constant) baseline by selecting a group of channels which seemed to be free of emission or absorption. However, many spectra are full of lines and we may have overestimated the level of the baseline in many cases, especially at 1.3 mm where the confusion limit was often reached.

The spectra obtained toward Sgr B2(N) and (M) have a very high density of spectral lines (see Sect. 4.1), which makes a direct measurement of the rms noise level difficult to perform in many cases. Instead, we estimate the rms noise level with the radiometer formula:

$$\sigma = 2T_{sys}/\sqrt{Bt_{int}} \qquad (1)$$

with T_{sys} the system temperature, B the *effective* spectral resolution, and t_{int} the sum of the on- and off-source integration times. The spectral resolution of the autocorrelator VESPA is worse than the channel spacing by a factor of about 1.2 (G. Paubert, priv. comm.). We verified on the spectra taken toward the reference position, which consist mostly of noise apart from the narrow frequency range over which weak emission of CO is detected (see Sect. 2.1), that the rms noise level estimated with the radiometer formula assuming this factor 1.2 is consistent with the measured noise level. As far as the 1 MHz filter banks are concerned, the measured rms noise levels toward the reference
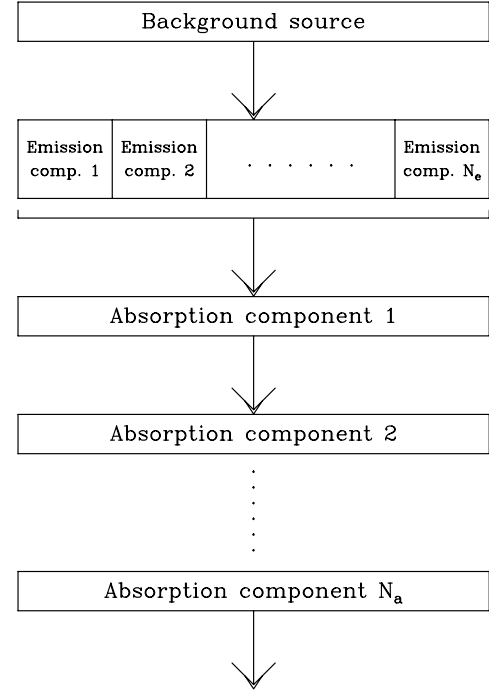
position are consistent with the radiometer formula when we use a factor ∼1.1. Table 1 lists for Sgr B2(N) and (M) the rms noise levels estimated with the radiometer formula as described above. For both sources, the median noise levels at 3 and 1.3 mm are 18 and 53 mK, respectively, in T_a^* scale. The median noise level at 2 mm is 27 mK for Sgr B2(N) and 51 mK for Sgr B2(M).

3. Modeling of the line survey

Given the high line density of the Sgr B2(N) and (M) spectra (see Sect. 4.1), the assignment of a line to a given molecule can be trusted only if all lines emitted by this molecule in our frequency coverage are detected with the right intensity predicted by a model (see below) and no predicted line is missing in the observed spectrum. This approach of modeling the full spectrum at once helps reducing the risks of misassignment and allows to deal with lines that overlap in frequency.

3.1. Radiative transfer with XCLASS

We used the XCLASS software[3] to model both the emission and absorption lines. The method used to compute the radiative transfer is described in the next paragraphs and illustrated in Fig. 1. The molecular spectroscopic parameters are taken from our line catalog which contains all entries from the catalog of the Cologne Database for Molecular Spectroscopy (CDMS[4], see Müller et al. 2001, 2005) and most entries from the molecular spectroscopic database of the Jet Propulsion Laboratory (JPL[5], see Pickett et al. 1998), as well as additional "private" entries. In

---

[3] See http://www.astro.uni-koeln.de/projects/schilke/XCLASS. Details about the software can also be found in Schilke et al. (1999), Comito et al. (2005), Hieret (2005), and Zernickel et al. (2012).
[4] See http://www.cdms.de
[5] See http://spec.jpl.nasa.gov

Table 2. Velocity ranges and isotopic ratios of the Galactic emission and absorption components along the line of sight of Sgr B2.

Velocity range[a] (km s^{-1})	^{12}C/^{13}C[b]	^{16}O/^{18}O[c]	^{18}O/^{17}O[d]	^{14}N/^{15}N[e]	Location[a]
(1)	(2)	(3)	(4)	(5)	(6)
~62	20	250	2.88	300	Galactic Center, Sgr B2
39–25	40	327	4.16	350	Scutum/Crux arm
22–12	60	560	4.16	450	Sagittarius arm
8––9	20	250	2.88	300	Galactic Center
−13––50	40	327	4.16	350	3-kpc arm
< −53	20	250	2.88	300	Galactic Center

Notes. The following isotopic ratios were assumed to be constant: ^{32}S/^{34}S = 22^c, ^{34}S/^{33}S = 5^f, ^{28}SiO/^{29}SiO = 20^g, ^{29}SiO/^{30}SiO = 1.5^g.

References. $^{(a)}$ Menten et al. (2011) and references therein; $^{(b)}$ Milam et al. (2005); $^{(c)}$ Wilson & Rood (1994); $^{(d)}$ Wouterloot et al. (2008); $^{(e)}$ Dahmen et al. (1995); $^{(f)}$ Nummelin et al. (2000); $^{(g)}$ Penzias (1981).

the version of XCLASS used for this work, a global linear fit to the tabulated values of the partition function between 9.375 and 300 K is performed in log-log space for each species. The parameters of this fit are used to interpolate or extrapolate the partition functions at any temperature. The extrapolation at temperatures below 9.375 K, which concerns the species seen in absorption, is in some cases significantly wrong. In the following, we will mention when the column densities were corrected a posteriori for the inaccuracy of the linear extrapolation.

The modeling was done species per species, a species being one molecule, or only one particular vibrationally or torsionally excited state of a molecule. The rare isotopologues of each main species were also modeled separately, but we tried to stay close to the isotopic ratios listed in Table 2. For each species, XCLASS assumes that the level populations are described by a single excitation temperature, which we refer to as the rotation temperature, T_{rot}. This assumption is valid in two cases: at high density where collisions are frequent enough for the local thermodynamic equilibrium (LTE) approximation to be valid, and at very low density, where T_{rot} equals the temperature of the cosmic microwave background, $T_{CMB} = 2.73$ K.

For each species m, several components can be modeled at once. For each component c, the fixed parameters are the diameter of the telescope, D, and the spectral resolution, and the free parameters are: source size, $\theta_{m,c}$, temperature, $T_{rot}^{m,c}$, column density, $N_{tot}^{m,c}$, velocity linewidth, $\Delta v^{m,c}$ (FWHM), velocity offset, $v_{off}^{m,c}$, with respect to the systemic velocity of the source, and a flag indicating if it belongs to the "emission" or "absorption" group. The velocity components in the "emission" group are supposed to be non-interacting, i.e. the intensities add up linearly. This approximation is valid for two distinct, non-overlapping sources smaller than the beam of the telescope, but it is a priori less good for, e.g., a source that consists of a hot, compact region surrounded by a cold, extended envelope or for two angularly-overlapping sources with spectrally-overlapping optically-thick emissions. The radiative transfer is performed in the following way. The full spectrum of the "emission" group is computed in a first step. In a second step, this spectrum is taken as a background for the calculation of the contribution of the components in the "absorption" group (see Fig. 1).

The set of equations used to compute the spectrum of the "emission" group is the following:

$$T_{emg}(f) = \sum_m \sum_c \eta_f^{m,c} \left(J_f(T_{rot}^{m,c}) - J_f(T_{bg}) \right) \left(1 - e^{-\tau_f^{m,c}} \right), \quad (2)$$

with

$$J_f(T) = \frac{hf/k}{e^{hf/kT} - 1}, \quad (3)$$

$$\eta_f^{m,c} = \frac{\theta_{m,c}{}^2}{\Theta_f{}^2 + \theta_{m,c}{}^2}, \quad (4)$$

with

$$\Theta_f = 1.22 \frac{c_1}{fD}, \quad (5)$$

and

$$\tau_f^{m,c} = \sum_t \tau_f^{m,c,t}, \quad (6)$$

where

$$\tau_f^{m,c,t} = \frac{c_1^2}{8\pi f^2} g_u^t A_{ul}^t \frac{N_{tot}^{m,c}}{Q_m(T_{ex}^{m,c})} \left(e^{-E_l^t/kT_{rot}^{m,c}} - e^{-E_u^t/kT_{rot}^{m,c}} \right) \phi_f^{m,c} \quad (7)$$

and

$$\phi_f^{m,c} = \frac{1}{\sqrt{2\pi}\,\sigma_f} e^{-\frac{(f - f_t - f_{off}^{m,c})^2}{2\sigma_f^2}}, \quad (8)$$

with

$$f_{off}^{m,c} = -\frac{v_{off}^{m,c}}{c_1} f_t \quad (9)$$

and

$$\sigma_f = \frac{1}{\sqrt{8\ln 2}} \frac{\Delta v^{m,c}}{c_1} \left(f_t + f_{off}^{m,c} \right), \quad (10)$$

with f the frequency, c_1 the speed of light, m the index on the species, Q_m the partition function of species m, c the index on the components in the "emission" group, t the index on the transitions of each species, f_t the transition rest frequency, g_u^t the upper state degeneracy, A_{ul}^t the Einstein coefficient for spontaneous emission, and E_l^t and E_u^t the lower and upper state energy levels, respectively.

The spectrum of the "absorption" group is computed with the following equation, c being now the index on the components in the "absorption" group:

$$T_{abg}(f) = \sum_m \sum_c$$
$$T_{c-1}(f)\, e^{-\tau_f^{m,c}} + \eta_f^{m,c} \left(J_f(T_{rot}^{m,c}) - J_f(T_{bg}) \right) \left(1 - e^{-\tau_f^{m,c}} \right), \quad (11)$$

where T_{c-1} is initialized to the spectrum of the "emission" group and then contains in addition the contribution of each component of the "absorption" group up to index $c - 1$.

Table 3. Effective background temperatures used to model the spectra of Sgr B2(N) and (M).

Atmospheric window	Sgr B2(N)	Sgr B2(M)
3 mm	5.2	5.9
2 mm	6.5	7.0
1.3 mm	10.0	8.5

Notes. The background temperatures, T_{bg}, are given in K.

3.2. Background temperature and continuum emission

The effective background temperature, T_{bg}, was estimated from the absorption lines that looked saturated, assuming a beam filling factor of unity. Its values for each source are listed in Table 3. It is only an effective temperature related to the beam-averaged continuum emission, and its values may not be physically meaningful especially if the continuum emission is optically thin, which is very likely at scales comparable to the beam.

For simplicity reasons and because we do not know the structure of the continuum emission at small scales very well, we use the background temperature T_{bg} derived from the saturated absorption lines to compute the spectrum of the "emission" group (Eq. (2)). This assumption is, strictly speaking, not correct, especially for the components that are much more compact than the beam because the continuum emission is certainly not uniform within the single-dish beam. To evaluate the error introduced by this, we compare the continuum and molecular emissions in Table 4. We compiled continuum measurements (Cols. 2 and 3) made at different frequencies (Col. 1) and small scales (Col. 4) from the literature. We compute $\Omega B(T_{rot})$, the product of the solid angle over which the continuum emission was measured (Col. 5) and the Planck function at typical rotation temperatures of the molecular transitions (Col. 6). The ratio of the flux density of the continuum emission to $\Omega B(T_{rot})$ is given in Col. 7. It is equal to the ratio $R = J_f(T_{bg})/J_f(T_{rot})$ (see Eq. (2)), provided the continuum emission is a true background, i.e. the particles producing the continuum emission are not mixed with the molecules. Under this assumption, we see that the error done in Eq. (2) is on the order of 10–20% at 3 mm for a source size of ∼3″ for the main hot core of Sgr B2(N). This error will propagate to the derived column density in case of optically thin emission or to the derived rotation temperature/beam filling factor in case of optically thick emission. The error is less than 10% for sizes ≳7″ at 3 mm. For Sgr B2(M), the error can be as high as 30–60% for a source size of ∼4″ at 3 mm[6]. At 227 GHz, the error is on the order of 15–30% for a source size of ∼4″ in Sgr B2(N), and somewhat smaller (9–18%) in Sgr B2(M).

However, the assumption that the continuum emission is a true background for the molecular emission is not correct. It is probably a good approximation for the free-free continuum emission which is concentrated in the ultra-compact H II regions of size ∼0.1″ (de Pree et al. 1998) and contributes to more than 50% of the continuum flux density of Sgr B2(M) at 3 mm on scales of 10–20″ (Kuan et al. 1996). But it is certainly not a good approximation for the thermal dust emission because we expect the dust particles and the molecules in the gas phase to be well mixed together. In this case, Eq. (2) is not fully correct: attenuation of the molecular emission by dust should also be taken into account. This can be done in XCLASS by multiplying Eq. (2) by

---

[6] We note, however, that the continuum measurements performed at 85 and 91 GHz toward Sgr B2(M) do not seem to be consistent with each other.

Table 4. Properties of the continuum emission toward Sgr B2(N) and (M).

f^a (GHz) (1)	F_f^b (Jy/beam) (2)	S_f^c (Jy) (3)	Size^d (″ × ″) (4)	Ω^e (10^{-10} sr) (5)	T^f (K) (6)	$S_f/\Omega B_f^g$ (7)
Sgr B2(N)						
85	–	0.90	3.2 × 2.8	2.1	200	0.10
					150	0.13
					100	0.20
91	2.0	–	12.2 × 4.4	14.3	200	0.03
					150	0.04
					100	0.06
227	20.0	–	4.5 × 3.7	4.4	200	0.15
					150	0.20
					100	0.30
Sgr B2(M)						
85	–	4.38	4.8 × 3.2	3.6	200	0.28
					150	0.37
					100	0.56
91	3.0	–	10.5 × 4.9	13.7	200	0.04
					150	0.06
					100	0.09
153	3.5	–	6.5 × 3.0	5.2	200	0.05
					150	0.06
					100	0.10
227	12.0	–	4.5 × 3.7	4.4	200	0.09
					150	0.12
					100	0.18

Notes. [a] Frequency. [b] Peak flux density from de Vicente et al. (2000) at 91 GHz, Furuya et al. (2003) at 153 GHz, Lis et al. (1993) at 227 GHz. [c] Flux density from Liu & Snyder (1999) at 85 GHz. [d] Beam size or size of the box over which the flux density was integrated. [e] Solid angle of the beam or integration box. [f] Assumed temperature for the Planck function. [g] Ratio of the measured continuum flux density to the product of the solid angle Ω and the Planck function $B_f(T)$.

a factor $e^{-\tau_{dust}}$ (see Eq. (1) of Zernickel et al. 2012). It is, however, not completely correct either because it assumes that all the absorbing dust is in front of the gas while dust and gas are likely well mixed. Given that the 2 and 1.3 mm spectra are also severely affected by the uncertainty on the baseline level due to line confusion, it is difficult to break the degeneracy between dust attenuation and overestimate of the baseline level, and we did not use this option of dust attenuation.

At 1.3 mm, the continuum emission is dominated by the thermal dust emission. Column 7 of Table 4 is then equivalent to the dust optical depth. At 3 mm, it is only an upper limit, because the continuum flux density includes a (significant) contribution from the free-free emission. This dust attenuation effect should thus be small at 3 mm, but significantly more important at 1.3 mm, especially for Sgr B2(N) with maybe 30–40% of attenuation for a source size of 3″.

3.3. Optimization

The input parameters ($\theta_{m,c}$, $T_{rot}^{m,c}$, $N_{tot}^{m,c}$, $\Delta v^{m,c}$, $v_{off}^{m,c}$) were varied until a good fit to the data was obtained for each species. The whole spectrum including all the identified species was then computed at once, and the parameters for each species were adjusted again when necessary. The quality of the fit was checked

by eye for each species over the whole frequency coverage of the 3 mm line survey.

We limited the fit optimization to the 3 mm range because the synthetic spectrum systematically overestimates by a significant amount (factor two or even more) the molecular emission of the compact components at 2 and 1.3 mm. This could be the combined result of at least four effects, some of them already mentioned before. First, the confusion limit is reached in most parts of the 1.3 mm spectrum, which hides the true continuum level (baseline subtraction) and implies that the level of the baseline must have been significantly overestimated. Second, the distance between the two hot cores of Sgr B2(N), 5″, is about half the size of the beam at 1.3 mm, which means that the observed emission of the northern hot core is attenuated by nearly a factor of two. The model does not take this into account because the 3 and 1.3 mm ranges are modeled with the same parameters. Finally, the last two effects are related to the radiative transfer. As detailed in Sect. 3.2, the contribution of the "background" term in Eq. (2) was likely underestimated and the attenuation by the dust was not taken into account, both effects being more pronounced at 1.3 mm than at 3 mm. Because of these limitations, we used the information provided by the 2 and 1.3 mm ranges only in few cases (extended components).

4. Results

4.1. Overview of the detected lines and molecules

The 3 mm spectra of Sgr B2(N) and (M) contain, respectively, about 3675 and 945 lines detected with a main-beam peak temperature higher than 90 mK, about four times the median noise level (4σ). These numbers correspond to an average line density of 102 and 26 lines per GHz for Sgr B2(N) and (M), respectively. For a higher threshold of 0.3 K ($\sim 13\sigma$), we found 1377 and 193 lines toward Sgr B2(N) and (M), i.e. an average line density of 38 and 5.4 lines per GHz, respectively.

The counting mentioned in the previous paragraph was performed by eye. Many transitions toward Sgr B2(N), which consists of two hot cores separated by about 5″, have a double-peaked profile because they are emitted by both hot cores with a difference in line-of-sight velocity of 9–10 km s^{-1} (see Sect. 1). Distinguishing between a true double-peaked line profile and the chance juxtaposition of two independent lines is possible only once the modeling has been performed. The counting mentioned above being purely observational, such transitions with a "true" double-peaked profile were counted twice.

So far, we have identified 56 molecules and 66 of their isotopologues toward Sgr B2(N). In addition, transitions from 59 catalog entries corresponding to vibrationally or torsionally excited states of some of the identified molecules or their isotopologues were also identified. For Sgr B2(M), the corresponding numbers are 46, 54, and 24, respectively.

The spectra observed toward Sgr B2(N) in the 3, 2, and 1.3 mm atmospheric windows are shown in Figs. 2–4, respectively (online material). The corresponding spectra toward Sgr B2(M) are shown in Figs. 5–7, respectively (online material). For each source, the best-fit synthetic model produced with XCLASS is overlaid in green, and the relevant molecular lines are marked with the name of the emitting or absorbing molecule in blue. Recombination lines cannot be modeled with XCLASS but some of them are clearly detected toward Sgr B2(N) (several H α, H β, and H γ lines) and Sgr B2(M) (several H α, H β, H γ, and He α lines). They are labeled in pink in all figures. Finally, because of the high dynamic range of our spectra (~ 2000),

strong lines from the image band can contaminate the signal band. We address this issue only for the 3 mm window. With a typical sideband rejection gain of ~ 1–3% (see Sect. 2.1), we estimate that only lines with a peak temperature higher than ~ 2 K in $T_{\rm mb}$ scale can significantly contaminate the spectra. We find 120 and 116 locations in the full 3 mm spectra of Sgr B2(N) and (M), respectively, where contamination by a strong line from the image band may occur, depending on the exact sideband rejection gain which is not precisely known. These locations are marked with red labels in Figs. 2 to 7. Among these, an inspection by eye reveals only a few cases where the contamination is obvious: at 81.246 and 94.254 GHz by CH$_3$OH (image band frequencies: 84.521 and 97.583 GHz), at 112.111 and 112.124 GHz by CO (115.275 and 115.263 GHz) for Sgr B2(N); at 81.246 GHz by CH$_3$OH (84.521 GHz), at 94.642 and 94.651 GHz by CS (97.984 and 97.975 GHz), at 112.111 and 112.123 GHz by CO (115.275 and 115.263 GHz) for Sgr B2(M).

4.2. Statistics

The synthetic spectra of Sgr B2(N) and (M) containing all the detected species are used to estimate the fraction of lines that remain unidentified in the 3 mm range. The statistics about the identification are summarized in Table 5. The analysis is performed over four frequency ranges, as well as over the full frequency coverage from 80 to 116 GHz. The goal is to estimate the fraction of channels for which the detected emission (or absorption) can be considered as identified based on our model. For each source, the calculation is done twice, once including both the parts in emission and in absorption, and the second time including only the emission part. The analysis is performed on the channels that have a main-beam temperature higher than 90 mK (4σ) in absolute value. The number of such "detected" channels is given in Col. 4. About 50% of all channels are "detected" toward Sgr B2(N), and 19% toward Sgr B2(M) (Col. 12). Given that the detected lines have wings extending below the 4σ threshold and other lines exist between 3 and 4σ, we can conclude that less than 50% of all channels are free of emission or absorption toward Sgr B2(N), meaning that its 3 mm spectrum is close to the confusion limit.

We measure the performance of our model in two ways. First we compute the average fraction of the observed spectrum that is accounted for by our model based on the integrated intensities. The integrated intensities of the observed and synthetic spectra are listed in Cols. 7 and 8. Their difference is given in Col. 9, but, given that the model sometimes overestimates the observed signal[7], a more relevant quantity is the integrated intensity of the difference spectrum after clipping the synthetic spectrum to the observed one in the channels where the former overestimates the latter. The resulting integrated intensity is given in Col. 10. It corresponds to the integrated intensity of the signal that is not accounted for by the model. Using the values of Cols. 7 and 10, we find that 83% of the part of the spectrum of Sgr B2(N) detected in emission is well reproduced by our model, and 62% for Sgr B2(M) (Col. 13). This estimate is biased in the

---

[7] As described in Sect. 3.1, XCLASS adds the contributions of different emission components linearly. This can lead the model to overestimate the observed emission when spectrally blended transitions of two different molecules or two components of the same molecule with similar velocities (e.g. a cold one and a warm one) overlap along the line of sight and the one in the front is partially optically thick. The model can also overestimate the observed emission if the level of the baseline of the observed spectrum is overestimated due to line confusion, or if there is a gradient of kinetic temperature along the line of sight.

Table 5. Statistics about the identification of the lines detected above a threshold of 90 mK in the 3 mm spectra of Sgr B2(N) and (M).

Frequency range (GHz)	N_{tot}[a]	N_{sel}[b]	N_{det}[c]	N_{id}[d]	L_{det}[e]	I_{obs}[f] (K km s^{-1})	I_{mod}[g]	I_{diff}[h] (K km s^{-1})	$I_{diffPos}$[i]	$f_{N,sel}$[j] (%)	$f_{N,det}$[k] (%)	$f_{I,rec}$[l] (%)	$f_{N,rec}$[m] (%)	$f_{N,id}$[n] (%)
(1)	(2)	(3)	(4)	(5)	(6)	(7)	(8)	(9)	(10)	(11)	(12)	(13)	(14)	(15)
Sgr B2(N)														
79.98 – 90.00	32 033	32 033	11 444	8393	–	4820	4467	353	895	100.0	35.7	81.4	70.5	73.3
90.00 – 100.00	32 000	32 000	14 408	10 444	–	5048	4914	134	880	100.0	45.0	82.6	70.4	72.5
100.00 – 110.00	32 000	31 990	17 978	12 612	–	6575	7141	–566	958	100.0	56.2	85.4	69.6	70.2
110.00 – 116.00	19 152	19 152	13 465	9454	–	7318	7340	–22	1158	100.0	70.3	84.2	69.9	70.2
79.98 – 116.00	115 185	115 175	57 295	40 903	–	23 761	23 861	–101	3890	100.0	49.7	83.6	70.0	71.4
Sgr B2(N) without absorption parts														
79.98 – 90.00	32 033	30 733	10 144	7160	803	4027	3574	453	858	95.9	33.0	78.7	67.8	70.6
90.00 – 100.00	32 000	31 634	14 042	10 109	993	4874	4712	163	864	98.9	44.4	82.3	70.0	72.0
100.00 – 110.00	32 000	31 645	17 633	12 337	1131	6465	6978	–514	947	98.9	55.7	85.4	69.4	70.0
110.00 – 116.00	19 152	18 296	12 609	8688	752	6618	6555	62	1159	95.5	68.9	82.5	68.2	68.9
79.98 – 116.00	115 185	112 308	54 428	38 294	3680	21 984	21 820	164	3828	97.5	48.5	82.6	69.0	70.4
Sgr B2(M)														
79.98 – 90.00	32 033	32 033	4619	3221	–	2928	2702	225	464	100.0	14.4	84.1	66.3	69.7
90.00 – 100.00	32 000	31 984	5050	2523	–	2115	1725	389	649	100.0	15.8	69.3	49.4	50.0
100.00 – 110.00	32 000	31 997	6538	3144	–	2145	1602	543	661	100.0	20.4	69.2	47.7	48.1
110.00 – 116.00	19 152	19 152	5329	2686	–	4862	3683	1180	1630	100.0	27.8	66.5	50.1	50.4
79.98 – 116.00	115 185	115 166	21 536	11 574	–	12 050	9713	2337	3405	100.0	18.7	71.7	52.7	53.7
Sgr B2(M) without absorption parts														
79.98 – 90.00	32 033	30 332	2918	1670	186	1468	1156	312	426	94.7	9.6	71.0	51.7	57.2
90.00 – 100.00	32 000	31 124	4190	1948	238	1670	1206	464	627	97.3	13.5	62.4	44.8	46.5
100.00 – 110.00	32 000	31 510	6051	2777	314	2011	1479	532	632	98.5	19.2	68.6	46.0	45.9
110.00 – 116.00	19 152	18 056	4233	1734	203	3762	2389	1373	1699	94.3	23.4	54.8	37.0	41.0
79.98 – 116.00	115 185	111 022	17 392	8129	942	8911	6229	2682	3384	96.4	15.7	62.0	44.5	46.7

Notes. [a] Total number of channels in the selected frequency range. [b] Number of selected channels, excluding the blanked channels, and those in the absorption parts of the spectrum when explicitly mentioned. [c] Number of channels above the detection threshold (90 mK in main-beam temperature scale). [d] Number of identified channels, i.e. channels for which the temperature of the synthetic spectrum reaches at least 50% of the observed temperature. [e] Estimated number of lines detected in emission. [f] Integrated intensity of the absolute value of the observed spectrum over the range of detected channels. [g] Integrated intensity of the synthetic spectrum over the range of detected channels. [h] Difference between Cols. 7 and 8 ($I_{obs} - I_{mod}$). [i] Integrated intensity of the difference between the absolute value of the observed spectrum and the absolute value of the clipped synthetic spectrum over the range of detected channels. The synthetic spectrum is clipped to the observed spectrum in the channels for which the synthetic temperature is higher than the observed temperature in absolute value. [j] Fraction of selected channels (N_{sel}/N_{tot}). [k] Fraction of detected channels (N_{det}/N_{sel}). [l] Fraction of recovered integrated intensity ($1 - I_{diffPos}/I_{obs}$). [m] Average fraction of recovered temperature per channel, after clipping the synthetic spectrum like in Col. 10. [n] Fraction of identified channels (N_{id}/N_{det}).

sense that channels that have strong emission or absorption have more weight than channels that have weak emission or absorption.

The second method, which does not suffer from the previous bias, is performed channel-wise. For each "detected" channel, we compute the fraction of its emission that is recovered by the model (clipping this fraction to 1 when the model overestimates the observed signal). We find that, on average, 69% of the emission of the "detected" channels toward Sgr B2(N) is recovered by the model, and 45% toward Sgr B2(M) (Col. 14).

We set the identification threshold to 50%, i.e. we consider the emission/absorption in a channel to be identified when the synthetic spectrum accounts for at least 50% of the detected level of emission/absorption. The number of such "identified" channels is given in Col. 5. They represent 70% of the channels "detected" in emission toward Sgr B2(N), and 47% toward Sgr B2(M) (Col. 15). These fractions are very similar to the ones obtained in the previous paragraph because we assumed an identification threshold of 50%. They would be lower if we would increase this threshold.

Finally, Col. 6 gives an *estimate* of the number of detected lines. This estimate is done by assuming a typical line width in velocity (a priori *not* equal to the typical FWHM) such that

the derived number of lines detected in the full 3 mm window corresponds to the one obtained by eye in Sect. 4.1. The typical line widths we had to use to have a good match are 13.9 and 17.2 km s^{-1} for Sgr B2(N) and (M), respectively. Column 6 shows that the density of detected lines increases with frequency for both sources, by a factor of 1.6 for Sgr B2(N) and 1.7 for Sgr B2(M) from 80 to 116 GHz.

Figure 8 plots the fraction of identified channels as a function of frequency for each source. This calculation was done for different thresholds in main-beam temperature, from 90 to 900 mK (4 to 40σ). There is no obvious trend in frequency, except maybe for Sgr B2(M) with a slight decrease in the fraction of identified channels with increasing frequency. But there is a clear increase in the fraction of identified channels as a function of temperature threshold, from 70% to 95% for Sgr B2(N) and from 47% to 75% for Sgr B2(M).

The fraction of identified lines above a threshold of 0.9 K estimated in the previous paragraph is affected by the shortcomings of the model. We counted by eye 388 identified lines out of 411 lines detected above this threshold toward Sgr B2(N), and 80 out of 103 toward Sgr B2(M). However, the observed CO and ^{13}CO 1–0 lines are very strong and consist of multiple components both in emission and absorption. The model was not
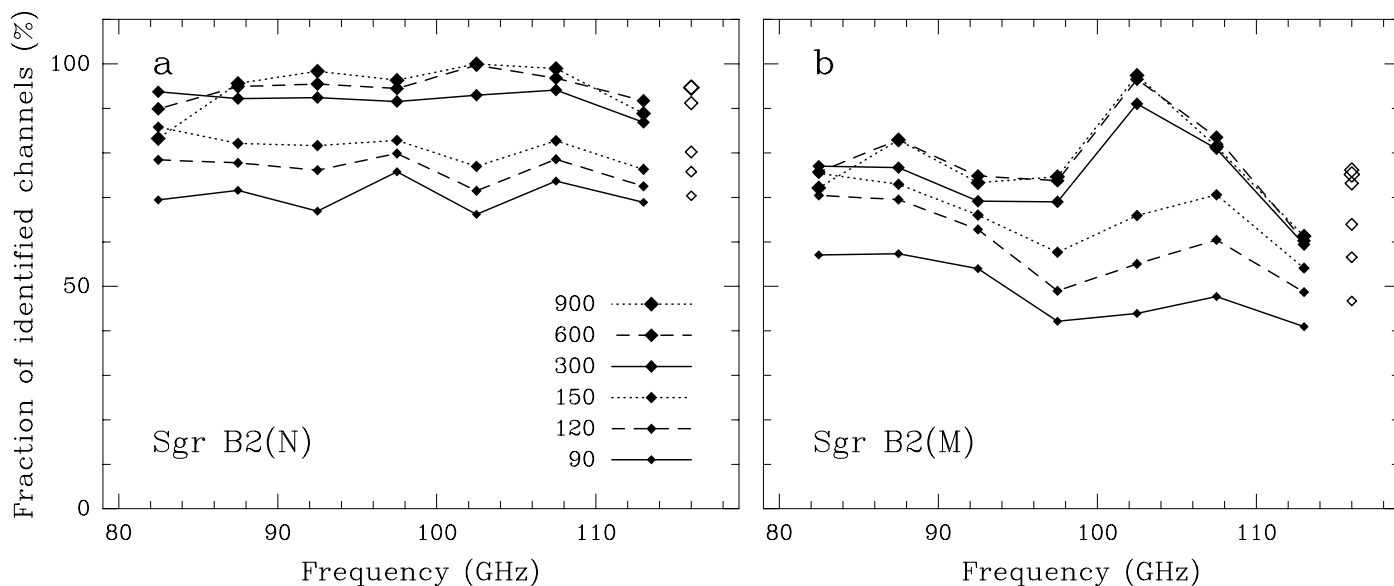
Fig. 8. Fraction of identified channels in the spectra of **a)** Sgr B2(N) and **b)** Sgr B2(M) as a function of frequency. Each curve corresponds to a different temperature threshold, which is given in mK in the lower right corner of panel **a)**. Each data point (filled diamond) corresponds to the average fraction of identified channels over a frequency range of 5 GHz, except for the point at highest frequency which is an average over 6 GHz. The unfilled diamonds to the right of each panel are the average fractions over the full frequency range 80 to 116 GHz, for the same temperature thresholds. The size of the filled and unfilled diamonds increases with the temperature threshold.

fine-tuned to fit all the emission components because the LTE assumption is certainly wrong for these components. If we ignore the frequency ranges where the CO and ^{13}CO 1−0 transitions are detected, then we find 367 identified lines out of 371 detected toward Sgr B2(N) and 68 out of 72 toward Sgr B2(M). The four lines missing in the model of each source correspond to Hα recombination lines that cannot be modeled with XCLASS, at 85.7, 92.0, 99.0, and 106.7 GHz. All the lines (100%) stronger than 0.9 K are therefore identified in the 3 mm spectra of Sgr B2(N) and (M). The somewhat lower fractions obtained in the previous paragraph (95% and 75%, respectively) are due to the unmodeled Hα emission, the complicated CO and ^{13}CO 1−0 emission, and a significant underestimate of the strength of the methanol transitions at 84.5 and 95.2 GHz (see Sects. 4.4.23 and 5.4).

4.3. Overview of the source properties

Sgr B2(N): about 75% of the molecules (main isotopologues) tracing warm/hot gas (>30 K) toward Sgr B2(N) emit in two velocity components at LSR velocities of ~63–64 and 73−74 km s^{-1} (e.g., CH$_3$C$_3$N, CH$_3$CHO). They correspond to the two hot cores embedded in Sgr B2(N) and separated by 5″ in the north-south direction (see Sect. 1). The linewidth of each velocity component is typically on the order of 7 km s^{-1}. Six complex organic molecules emit in only one component (C$_2$H$_5$OCHO, c-C$_2$H$_4$O, aGg′-(CH$_2$OH)$_2$, CH$_2$(OH)CHO, CH$_3$C(O)NH$_2$, NH$_2$CH$_2$CN). This is most likely due to a lack of sensitivity to the less prominent, northern hot core.

A few species with strong emission show the presence of additional wing emission (e.g., HC$_3$N, C$_2$H$_5$CN). At higher angular resolution, this wing emission is resolved in the east-west direction (see, e.g., HC$_3$N, v_7 = 1 in Figs. 5k, l, and m of Belloche et al. 2008, or Lis et al. 1993; Liu & Snyder 1999; Hollis et al. 2003). Given that this wing emission is also traced by SO, SO$_2$, and SiO, it may be due to an outflow (see, e.g., Rodríguez-Fernández et al. 2010; Tafalla et al. 2010, which show

that these molecules are good outflow tracers). Higher angular resolution with, e.g., ALMA will certainly help in understanding the physical origin of this wing emission. Here, we use one or several additional (Gaussian) component(s) at blue- and/or red-shifted velocities to account for the extra wing emission when necessary. The Gaussian approximation is a priori not optimum to model wing emission if it is produced by an outflow. This can prevent us from perfectly matching the model to the observed emission in the cases where wing emission is present.

Most simple molecules are less sensitive to the two hot cores embedded in Sgr B2(N) and rather trace colder, more extended emission in the envelope. They are often self-absorbed, and also suffer from absorption by multiple diffuse clouds along the line of sight.

The rotation temperatures derived for the complex molecules detected toward Sgr B2(N) range from 50 K (e.g., aGg′-(CH$_2$OH)$_2$) to 200 K (e.g., CH$_3$CN, CH$_3$OH). A few vibrationally or torsionally excited states seem to require higher rotation temperatures (230 K for HC$_3$N, v_7 = 1, 500 K for HCN, v_2 = 1).

Sgr B2(M): the emission of most complex molecules detected toward Sgr B2(M) is relatively well reproduced with only one velocity component, with linewidths ranging from ~6 to 15 km s^{-1} and LSR velocities from ~60 to 66 km s^{-1}. The simpler molecules tracing colder, more extended emission have linewidths up to ~22 km s^{-1}.

The rotation temperatures derived for the complex molecules detected toward Sgr B2(M) range from 30–40 K (e.g., CH$_3$C(O)CH$_3$, CH$_3$CHO) to 200 K (e.g., CH$_3$CN, CH$_3$OH).

4.4. Detected molecules

The model parameters for each detected molecule are listed in Tables 6 to 107 (online material). In this section we briefly describe the fit to the emission or absorption lines of each detected

molecule. When the frequency range is not mentioned (e.g., when the maximum opacity of the modeled transitions is mentioned), it is by default the 3 mm range.

For a catalog entry containing a vibrationally or torsionally excited state (with the level energies including the vibrational or torsional energy), each column density given in Tables 6 to 107 represents the total column density of the molecule (assuming LTE), not the partial column density of the excited state only. If all levels of a molecule are populated following LTE, then our modeling should yield the same column density parameter for the entry of the ground state and the entries of all vibrationally or torsionally excited states. When this is not the case, we estimate a vibration (or torsion) temperature for each excited state with the following equation:

$$\frac{N_j}{N_i} = \frac{\mathrm{e}^{-\Delta E_{\mathrm{vib}}/kT_{\mathrm{vib}}}}{\mathrm{e}^{-\Delta E_{\mathrm{vib}}/kT_{\mathrm{LTE}}}}, \tag{12}$$

which yields

$$T_{\mathrm{vib}} = \frac{1}{\frac{1}{T_{\mathrm{LTE}}} - \frac{k}{\Delta E_{\mathrm{vib}}} \ln \frac{N_j}{N_i}}, \tag{13}$$

with T_{vib} the vibration (or torsion) temperature, T_{LTE} the LTE temperature (equal to the rotation temperature), E_j the vibration (or torsion) energy of the excited state, E_i the vibration (or torsion) energy of the reference state, $\Delta E_{\mathrm{vib}} = E_j - E_i$, N_j and N_i the column density parameters (i.e. total column density of the molecule, see above) derived from our LTE modeling and corresponding to the entries of the excited and reference states, respectively, and k the Boltzmann constant. When the LTE models for the ground state and all vibrationally or torsionally excited states have the same source size and rotation temperature, we use the ground state as reference state to compute the vibration (or torsion) temperature of each excited state. When it is not the case, we indicate which excited state is used as reference to compute the vibration (or torsion) temperature of each higher excited state. Assuming that the relative uncertainty U_{vib} on T_{vib} only depends on the relative uncertainty U_N on the column density ratio, we derive

$$U_{\mathrm{vib}} = \frac{\Delta T_{\mathrm{vib}}}{T_{\mathrm{vib}}} = \frac{kT_{\mathrm{vib}}}{\Delta E_{\mathrm{vib}}} U_N. \tag{14}$$

With a typical relative uncertainty ($\sim 3\sigma$) of 10% on each column density N_i and N_j (for source sizes and rotation temperatures kept fixed), U_N is about 14%.

Uncertainties are not given in Tables 6 to 107. Because of the blendings of multiple components and species, degeneracies of the parameters in certain cases (e.g., between source size and column density for optically thin emission), small number or limited energy range of detected transitions for some molecules (preventing a reliable estimate of the temperature), limitations due to the simplicity of the model (e.g., uniform temperature, non-interacting components, same background temperature for compact and extended components, dust attenuation not accounted for), uncertainties are very hard to quantify in a satisfactory way. Cases when some or even all parameters are poorly or not even constrained are explicitly mentioned in the following subsections and we invite the reader to carefully read them before using the values listed in Tables 6 to 107. In the general case, the uncertainties on source size, temperature, and column density are probably not smaller than 20–30%. Linewidth and velocity are certainly better constrained.

Population (or "Boltzmann" or "rotation") diagrams are not shown in this article. Examples of such diagrams can be found in Belloche et al. (2008, 2009), where the optical depths effects were properly taken into account. Belloche et al. (2009) even showed an improved version of such diagrams by removing the contribution of contaminating species, based on the complete model presented in the present article. These diagrams illustrate the reliability of our modeling approach.

We provide information on the source of the rest frequencies, e.g. the CDMS or JPL catalogs, as well as information on the laboratory data on which these rest frequencies are based[8]. The number of detected species reported in this section is large. Therefore we limit the information on laboratory data somewhat because the number of references is rather large for some species. We provide in all instances a primary reference that usually summarizes the (mostly laboratory) rest frequencies used to generate the catalog entry or that provides spectroscopic parameters most closely resembling those employed for the catalog entry. The primary reference may or may not contain measurements in the frequency ranges of our line survey. We also mention references for rest frequencies that cover the ranges of this survey. Dipole moment information is given in special cases only. Not all entries from the CDMS or JPL catalogs or from private sources include all of the presently available data. This shortcoming should have a small, probably negligible effect on our results. Several of the very old entries as well as a small number of recent entries provide incomplete lists of references in the corresponding documentation files. We have inspected the references given in the documentation files for previous original rest frequency determinations in the range of our survey.

As described in Sect. 3.1, the partition function at any temperature T is computed based on a global linear fit performed by XCLASS in log-log space to the values tabulated between 9.375 and 300 K. This method is not very accurate when the partition function contains contributions of vibrationally or torsionally excited states in addition to the ground state. The extrapolation at temperatures below 9.375 K (for the absorption components) or above 300 K based on this fit is sometimes also inaccurate. Therefore, in order to compensate for these inaccuracies, we applied a correction to the derived column densities a posteriori. The corrected partition functions were computed with a piecewise, linear interpolation in the range 9.375 to 300 K. Most species with components below 9.375 K have partition function values at 2.725 and 5 K in the CDMS catalog which allowed for a similar piecewise interpolation. For the species lacking these low-temperature values, we extrapolated the partition function from a linear fit (in log-log space) to the values at 9.375 and 18.75 K. We also corrected the partition functions for the contribution of excited states, for as many species as we could. The global correction factor used to rescale the column density is listed in Col. 7 of the table listing the model parameters for each species.

---

[8] It is worthwhile mentioning that the CDMS and JPL catalogs are intended to be available together in a database environment in the near future. Recommendations, information on laboratory rest frequencies, as well as additional information will eventually be automatically provided with each request. The implementation of the CDMS into a database environment within the framework of the Virtual Atomic and Molecular Data Centre (VAMDC; Dubernet et al. 2010) is approaching the official release of a test version.

4.4.1. Vinyl cyanide C_2H_3CN

We use the CDMS entries for the ground state of the ^{12}C and ^{13}C isotopologues (tags 53 515, 54 506, 54 507, 54 508, all version 1). The entries were based on data described in Müller et al. (2008). This work includes in particular laboratory data from Gerry & Winnewisser (1973), Baskakov (1996), and Cazzoli & Kisiel (1988) providing rest frequencies for the main isotopic species in the range of our line survey. In the case of the ^{13}C isotopologues, Colmont et al. (1997) cover additional frequency ranges similar to the ones of our survey.

Recently, Kraśnicki & Kisiel (2011) redetermined the dipole moment components of vinyl cyanide and ethyl cyanide. While most values agreed well with previous measurements, the b-component of vinyl cyanide turned out to be 23% smaller than the value currently used in the CDMS. This has not been taken into account in our model yet.

The catalog entries for the vibrationally excited states of the main isotopologue were prepared by one of us (HSPM). The predictions were based on assignments by Cazzoli & Kisiel (1988) for $v_{11} = 1$, $v_{15} = 1$, $v_{11} = 2$, and $v_{11} = 3$ obtained in the frequency range 20–40 GHz as well as parts of the 100–184 GHz range. Additional $v_{11} = 1$ data (350–630 GHz) were taken from Demaison et al. (1994). Further measurements of selected transition frequencies pertaining to a variety of vibrational states were made between 64 and 119 GHz as well as between 239 and 353 GHz as described for the ground state of the main species and the singly ^{13}C and ^{15}N isotopic species (Müller et al. 2008). Broader scans were also taken in the lower frequency range.

Pseudoequilibrium spectroscopic parameters were determined in that unpublished study. Vibrational corrections for v_{11} up to third order ensured a good reproduction for $v_{11} = 1$, a reasonably good reproduction for $v_{11} = 2$ and a somewhat satisfactory reproduction for $v_{11} = 3$. Systematic deviations between measured and calculated frequencies suggested $v_{11} = 3$ to be severely perturbed by one or more vibrational states. Some of these deviations were already observed by Cazzoli & Kisiel (1988), but were not discussed, presumably because they appeared to be rather random. Assignments in the 3 mm range and below were secure at least in most cases even if the frequencies were not reproduced well. Assignments in the 239–353 GHz range are less certain for $v_{11} = 3$.

First order v_{15} corrections for some spectroscopic parameters not only accounted quite well for the $v_{15} = 1$ data, but also permitted assignments for $v_{15} = 2$ and for $v_{11} = v_{15} = 1$ to be made for the first time. These transition frequencies were better reproduced by including a small number of second order vibrational corrections. Some of the assignments in the 3 mm region and below appear to be safe, those at higher frequencies are probably less certain as both states are perturbed, the former possibly by $v_{11} = 3$ and very likely by $v_{14} = 1$, the latter by $v_{10} = 1$.

Kisiel et al. (2009) recently extended the analyses of vinyl cyanide in its ground and first excited $v_{11} = 1$ states considerably in frequency. Even though $v_{11} = 1$ is much higher than the ground vibrational state, these authors observed perturbations between these states which permitted the $v_{11} = 1$ origin to be determined very accurately to 228.300 cm^{-1} or 328.47 K. The effective matrix elements of such interactions usually decrease rapidly with increasing ΔK_a, but the effect for a given ΔK_a increases with J and K_a. Very local effects were observed for rather high values of ΔK_a (6 and 5) with resonant interactions beyond $J = 100$. There were also more pronounced near-resonant $\Delta K_a = 4$ interactions, however, these occured at rather high values of K_a (21/17 and 22/18), and the effects became noticeable

in the spectrum only above $J \approx 40$; their strong a-type R-branch transitions are at almost 400 GHz or higher. Transitions within $v_{11} = 1$ observed in our line survey are thus unaffected by these perturbations.

More recently, Kraśnicki et al. (2011a) investigated perturbations between the ground state and $v_{11} = 1$ for four singly substituted isotopic species and published also data for the ground vibrational states of some doubly substituted species. The investigations of the main isotopologue were extended to $v_{15} = 1$ and $v_{11} = 2$ which perturb each other as well as $v_{11} = 1$ (Kisiel et al. 2012). The band origins were determined very accurately to 332.678 and 457.175 cm^{-1}, respectively. Transitions within $v_{15} = 1$ observed in our line survey are probably unaffected by perturbations. The situation is less clear for $v_{11} = 2$. Transitions pertaining to even higher lying vibrational states may well be affected by perturbations, and identifications in our survey should be viewed with some caution.

Sgr B2(N): the parameters of all entries related to vinyl cyanide are listed in Table 6. The first detection in space of the ^{13}C isotopologues based on this survey was already reported in Müller et al. (2008). A ^{12}C to ^{13}C isotopic ratio of 21 was derived in that work, in excellent agreement with the value of 20 determined by Wilson & Rood (1994). The lines of these isotopologues are optically thin ($\tau_{max} \sim 0.3$), so their relative intensities give a direct constraint on the temperature, which is relatively high due to the detection of transitions with E_1/k up to ~200 K (e.g., 168 K at 113.45 GHz, 235 K at 103.96 GHz). Many transitions of the main isotopologue are optically thick ($\tau_{max} \sim 7$). With the temperature derived from the ^{13}C isotopologues, the optically thick ^{12}C transitions in turn constrain the size of the emitting region. The column density is then constrained by the optically thin lines. We see no obvious sign of column density differences, i.e. differential fractionation, between the three ^{13}C isotopologues.

The northern hot core is also clearly detected at, e.g., 84.95 and 85.30 GHz for the main isotopologue, and 85.00 and 85.28 GHz for the ^{13}C isotopologues. In addition, a third velocity component is necessary to reproduce the blue wing of the optically thick ^{12}C transitions (e.g., 84.95 and 85.30 GHz). Its temperature and source size are not well constrained. We use the same values as for the two main components.

We also detect emission lines from within six vibrationally excited states of the main isotopologue: $v_{11} = 1$, $v_{15} = 1$, $v_{11} = 2$, $v_{11} = v_{15} = 1$, $v_{15} = 2$, $v_{11} = 3$ (229.4, 333.3, 458.8, 562.7, 666.6, 688.2 cm^{-1}, respectively, derived from the apparent band centers of ν_{11} and ν_{15} in the far-infrared spectrum, Cole & Green 1973). We fixed the rotation temperature to the value obtained from the ground state transitions but we had to reduce the source size to fit the optically thick lines of $v_{11} = 1$ and $v_{15} = 1$ ($\tau_{max} \sim 4$ and 3, respectively). The northern hot core is also clearly detected for $v_{11} = 1$, $v_{15} = 1$, and $v_{11} = 2$ (e.g., 85.99, 106.75, and 105.64 GHz, respectively) and it is likely detected for $v_{11} = v_{15} = 1$ (e.g., 114.38 GHz). There may be signs of an additional blueshifted component for $v_{11} = 1$ at certain frequencies (e.g., 114.25 and 114.28 GHz), but it is less obvious at other frequencies so we did not include it in the model. The transitions in the higher vibrational states ($v_{11} = 2$ and higher) are optically thin ($\tau_{max} = 0.4$–0.9), so their source size is not constrained. We set it to the size derived for $v_{11} = 1$ and $v_{15} = 1$. Finally, we note that transitions from within $v_{10} = 1$ (560 cm^{-1}) should be easily detected, but no spectroscopic data are available yet. They may be as strong and numerous as the transitions from

within $v_{11} = v_{15} = 1$ detected here (a dozen at 3 mm with peak temperatures ranging from 0.1 to 0.4 K).

While the rotation temperature derived from the ground state fits the relative intensities of the lines from within the vibrationally excited states well, the column density parameter required to fit these excited states increases with their energy, which means that the "vibration" temperature is actually higher than the rotation temperature (170 K). This could be due to radiative pumping. Using Eq. (13) with $v_{11} = 1$ as reference state and only for the first velocity component, we derive vibration temperatures of $230\pm50, 210\pm20, 200\pm10, 230\pm10$, and 240 ± 10 K for the other excited states in the same order as in Table 6. If a direct pumping mechanism from the ground state exists for each of the six excited states listed above, then it has to occur at ∼44, 30, 22, 18, 15, and 14.5 μm, respectively. However, the vibrational band ν_{11} is fairly weak, and ν_{15} is weak. Therefore, direct infrared pumping is unlikely to explain the apparent higher vibration temperatures of $v_{11} = 1$ and $v_{15} = 1$. The combination and overtone bands seem similarly too weak to permit direct pumping of the associated states.

Schilke et al. (1997) and Nummelin & Bergman (1999) reported the detection of transitions pertaining to the $v_{11} = 1$ and $v_{15} = 1$ excited states in Orion KL and Sgr B2(N), respectively. The higher-lying vibrational states have been detected here for the first time as far as we know.

Sgr B2(M): the parameters of all entries related to vinyl cyanide are listed in Table 62. Many transitions of vinyl cyanide are detected at 3 mm with lower-level energies ranging from 16 K (84.95 GHz) to 136 K (113.93 GHz). We note that a few transitions with even higher energies ($E_l/k = 159, 163$, and 205 K at 94.96, 104.46, and 113.99 GHz, respectively) coincide with detected lines but are significantly underestimated by the current low-temperature model. Increasing the temperature to, e.g., 150 K improves the fit to these high-energy transitions, but degrades it for some of the lower-energy ones and produces too strong lines at 1.3 mm. The level of the baseline at 1.3 mm is uncertain and the spectrum may be affected by dust attenuation, but both effects may not be sufficient to make the 1.3 mm spectrum of vinyl cyanide consistent with a higher temperature. In any case, the model parameters should be viewed with caution. In addition, the lines of the current model being optically thin ($\tau_{max} \sim 0.25$), the source size is not constrained. The ^{13}C isotopologues are not detected.

A few emission lines from within the vibrationally excited state $v_{11} = 1$ are detected (e.g., 85.67, 104.51, 114.24, and 114.28 GHz). Because the lines have low signal-to-noise ratios, the detection and the model parameters should be viewed with caution. A temperature of 150 K fits the ratios of the five transitions detected around 114.3 GHz a bit better than the temperature of 50 K used for the ground state. In addition, the latter would require a column density parameter 30 times higher than the former to fit roughly the detected transitions.

4.4.2. Ethyl cyanide C_2H_5CN

We use the CDMS entries for the ground state of the ^{12}C, ^{13}C, and ^{15}N isotopologues (tags 55 502, 56 504, 56 505, 56 506, and 56 508, all version 2). The entry of the main isotopologue is based on Brauer et al. (2009) which contained measurements in the frequency range of our survey from Fukuyama et al. (1996). The entries for the ^{13}C and ^{15}N isotopologues are based on Richard et al. (2012) and Margulès et al. (2009), respectively.

Entries for the vibrationally excited states $v_{13} + v_{21} = 1$, $v_{20} = 1$, and $v_{12} = 1$ of the main isotopologue were provided by J. Pearson. They are based on unpublished, preliminary, though rather extensive analyses involving these vibrational states[9]. A limited and preliminary account on the first three vibrational states was given by Fukuyama et al. (1999). A more extensive analysis of $v_{13} + v_{21} = 1$ was described by Mehringer et al. (2004). The low-lying vibrational states of ethyl cyanide form polyads, groups of vibrational states which are fairly close in energy. The first group is a dyad described by $v_{13} + v_{21} = 1$. Both states are rather close, at 206.5 and 212.7 cm^{-1}, respectively, and they are interacting very strongly (Fukuyama et al. 1999; Mehringer et al. 2004). The next group is a tetrad described by $v_{13} + 2v_{20} + v_{21} = 2$. $v_{20} = 1$ at 378 cm^{-1} is somewhat lower than the three states described by $v_{13} + v_{21} = 2$ near 400 cm^{-1}. Even though some transitions show torsional splitting, transition frequencies pertaining to this state can be fitted quite well as isolated state up to fairly high quantum numbers (Pearson et al. 2009). No data have been published for the remaining three states. The next higher group of states is already a heptad described by $3v_{12} + v_{13} + 2v_{20} + v_{21} = 3$. We have only data for the lowest, apparently fairly isolated state $v_{12} = 1$ at 523 cm^{-1}.

Sgr B2(N): the parameters of all entries related to ethyl cyanide are listed in Table 7. The model for the ground state of ethyl cyanide ($\tau_{max} \sim 10$) was already reported in Sect. 4.4 of Belloche et al. (2009) and for the ^{13}C isotopologues ($\tau_{max} \sim 0.35$) in Sect. 6 of Müller et al. (2008). The source sizes derived for the main isotopologue from our Plateau de Bure interferometric observations (Belloche et al. 2008) are $2.2'' \pm 0.2''$ and $1.5'' \pm 0.2''$ for the southern and northern hot cores, respectively. Our model uses slightly larger sizes in order to fit better both the optically thick and thin transitions of the main isotopologue. Some optically thick transitions are too strong by about 20–30% (e.g. 80.60, 89.57, 96.92, and 107.49 GHz), but other optically thick lines with similar lower-level energies and similar opacities are well reproduced, so the reason for this discrepancy is unclear. Many optically thin lines of the main isotopologue with a broad range of lower-level energies from 1.6 to ∼500 K are also detected and well fitted, implying that the temperature is well constrained. Three velocity components (both hot cores and an additional blue wing) are clearly detected with the ^{12}C and ^{13}C isotopologues (see discussion in Sect. 4.4 of Belloche et al. 2009). There is no significant difference in column density between the three ^{13}C isotopologues. The column density ratio of the ^{12}C to ^{13}C isotopologues is about 30 for the hot core components, which is puzzling given the isotopic ratio of ∼20 usually found toward the Galactic center. We note that a model with source sizes closer to the sizes derived interferometrically requires a temperature of 280 K to reproduce the intensities of the optically thick transitions of the main isotopologue and yields a ^{12}C to ^{13}C isotopic ratio of ∼24. However, this alternative model overestimates the (optically thin) high-energy ($E_l/k > 300$ K) transitions of the main isotopologue. We favored the (simple) model with the slightly larger sizes in order to better fit *all* the detected transitions. A more complex model would probably help in deriving a physically more consistent description of the structure of the hot core. The ^{15}N isotopologue is not detected. With a $\frac{^{14}N}{^{15}N}$ isotopic ratio of 300, we expect emission above the 3σ level,

---

but it is always blended with emission of other species (e.g., 87.01, 95.72, and 95.75 GHz), which prevents a secure identification. It is for that reason not included in the full model.

We detect emission lines from within four vibrationally excited states of the main isotopologue: $v_{13} + v_{21} = 1$, $v_{20} = 1$, and $v_{12} = 1$ (206.5/212.7, 378, and 523 cm^{-1}). The peak opacities of the synthetic model are 6.5, 1.2, and 0.36, respectively. We fixed the temperature to the value derived for the ground state. The source size had to be reduced for the excited states to simultaneously match their optically thick and thin lines. Both hot-core components are clearly detected in all four states (e.g., 89.45 GHz for $v_{12} = 1$). The third, blueshifted component is well detected for $v_{13} + v_{21} = 1$ and reasonably well detected for $v_{20} = 1$. It is less secure for $v_{12} = 1$ but the model including this component gives a good match (e.g., 98.38 GHz). Like for vinyl cyanide (see Sect. 4.4.1), the column density parameter required to fit the vibrationally excited states is higher than for the ground state, which suggests the presence of radiative pumping[10]. However, surprisingly, it does not increase monotonically with energy: $v_{20} = 1$ has a lower column density parameter than the lower-energy states $v_{13} = 1$ and $v_{21} = 1$. We note that our catalog file for $v_{13} + v_{21} = 1$ contains intensities at 200 K instead of 300 K, but correcting for this does not solve the discrepancy and we have not identified the origin of the problem so far. Given this issue, we do not attempt to estimate any vibration temperature.

Given the detections above, we expect all vibrationally excited states with $v_{13} + v_{21} = 2$ to be easy to detect in our 3 mm survey but no predictions are available yet. The transitions from within each of these three states may be as strong and numerous as the transitions from within $v_{20} = 1$ detected here (about two dozens with peak temperatures ranging from 0.2 to 0.9 K). Transitions from within $v_{13} + v_{21} = 3$ (4 states) or from within $v_{20} = 1/v_{13} + v_{21} = 1$ (2 states) may even be detected once predictions become available, each of them maybe as strong and numerous as the transitions from within $v_{12} = 1$ detected here (about 30 with peak temperatures ranging from 0.1 to 0.3 K). We also expect a few transitions of the ^{13}C isotopologues from within the vibrationally excited states with $v_{13} + v_{21} = 1$ to be detectable in our survey at 3 mm.

Gibb et al. (2000) and Mehringer et al. (2004) report the detection of transitions in the $v_{13} = 1$ and $v_{21} = 1$ excited states toward G327.3-0.6 and Sgr B2(N), respectively. Daly et al. (2013) report the detection of transitions in the $v_{20} = 1$ and $v_{12} = 1$ excited states toward Orion KL during the reviewing process of this article. Both states are detected here toward Sgr B2(N) for the first time as far as we know.

Sgr B2(M): the parameters of all entries related to ethyl cyanide are listed in Table 63. The lower-level energies of the detected transitions range from 19 K (88.32 GHz) to 74 K (80.60 GHz). The optical depths are low ($\tau_{max} \sim 0.25$), which lets the source size unconstrained. The temperature is somewhat constrained around, e.g., 80.6, 89.6, and 98.6 GHz, where group of transitions with different lower-level energies are detected. The ^{13}C isotopologues are not unambiguously detected.

Emission lines from within the $v_{13} = 1$ and $v_{21} = 1$ vibrationally excited states are detected at, e.g., 89.65, 97.15, 98.62,

and 98.74 GHz. The temperature is not constrained at 3 mm, but detections at 1.3 mm favor a model with a temperature higher than the one derived for the ground state. The source size is not constrained. One transition from within the $v_{20} = 1$ vibrationally excited state may be detected at 98.60 GHz, but this is not sufficient to claim a detection and we do not include this state in the complete model.

4.4.3. Ethyl formate C$_2$H$_5$OCHO

We use the CDMS entry (tag 74 514 version 1) which is based on Medvedev et al. (2009).

Sgr B2(N): the parameters of ethyl formate are listed in Table 8. The detection of this complex organic molecule was reported for the first time in space in Belloche et al. (2009). Kalenskii & Johansson (2010) claim a (somewhat indirect) detection of this molecule toward the W51 e1/e2 star-forming region based on a stacking analysis of their 3 mm spectral survey obtained with the Onsala 20 m telescope.

Sgr B2(M): ethyl formate is not detected.

4.4.4. Ethanol C$_2$H$_5$OH

We use the JPL entry for the main isotopologue (tag 46 004 version 4) based on the very extensive analysis in Pearson et al. (2008). Additional data in the range of our survey were taken from Pearson et al. (1995, 1996, 1997). We use the CDMS entries for the ^{13}C isotopologues (tags 47 511 and 47 512, both version 1) which are based on Bouchez et al. (2012).

Sgr B2(N): the parameters of ethanol are listed in Table 9. The synthetic spectrum is optically thin ($\tau_{max} \sim 0.6$). The source size is therefore not constrained and was fixed to 3″. The temperature is well constrained thanks to many transitions detected over a broad range of lower-level energies (from 2 K at 112.81 GHz to $\sim$430 K at 97.86 GHz). The other parameters were slightly readjusted compared to the model reported in Belloche et al. (2009). The northern hot core is clearly detected in addition to the main one. Two low-energy transitions (at 85.27 and 90.12 GHz with $E_1/k = 13$ and 5 K, respectively) are underestimated by the model by a factor of about 2. However, other transitions with similar energies are well reproduced (at 84.60, 87.72, and 112.81 GHz with $E_1/k = 9$, 13, and 2 K, respectively), so we exclude the additional presence of a significant, low-excitation (and extended?) component. The model overestimates by a factor $\gtrsim 3$ the observed spectrum for two transitions at 99.54 and 101.36 GHz with $E_1/k = 223$ and 158 K. Many other transitions with similar energies (e.g., the nearby transition at 99.52 GHz with $E_1/k = 137$ K) are well fitted however. The two problematic transitions are close to large gauche-gauche perturbations and their line strengths could be wrong because of that (J. Pearson, priv. comm.).

With a $\frac{^{12}C}{^{13}C}$ isotopic ratio of 20, the emission of the ^{13}C isotopologues of ethanol is expected to be weak. It is consistent with the observed spectrum within the noise, with possible detection at 100.70 and 101.40 GHz (CH$_3$^{13}CH$_2$OH and ^{13}CH$_3$CH$_2$OH, respectively). Even if one transition per species is not sufficient to claim a secure detection, we include the ^{13}C isotopologues in the complete model.

---

[10] If a direct pumping mechanism from the ground state exists for each of the four excited states listed above, then it has to occur at $\sim$48, 47, 26, and 19 μm, respectively. The intensities of the infrared bands v_{13}, v_{20}, and v_{12} are sufficiently high to facilitate direct infrared pumping. The weak torsional mode v_{21} may be pumped through the Coriolis interaction with v_{13}.

Sgr B2(M): the parameters of ethanol are listed in Table 64. Most lines detected at 3 mm are reasonably well fitted with a low-excitation component. Several higher-energy transitions, however, seem to be detected too and suggest the presence of an additional, warm component (e.g., E_1/k = 94 K at 87.96 GHz, 154 K at 98.59 GHz). All lines are optically thin (τ_{max} = 0.018 for the low-excitation component, 0.030 for the warm component), implying that the source size of each component is not constrained. There are two issues with the current model at 84.60 GHz (E_1/k = 9 K) and 112.81 GHz (2 K). The reason for this discrepancy is unclear because the transition at 114.06 GHz (E_1/k = 2 K), for instance, is well reproduced. The ^{13}C isotopologues are not detected.

4.4.5. n-propyl cyanide n-C$_3$H$_7$CN

We use the CDMS entry (tag 69 505 version 1) which is based on the analysis in Belloche et al. (2009). Transition frequencies related to the range of our survey were published by Wlodarczak et al. (1988).

Sgr B2(N): the parameters of n-propyl cyanide are listed in Table 10. The detection of this complex organic molecule was reported in Belloche et al. (2009). It has only been detected in Sgr B2(N) so far.

Sgr B2(M): n-propyl cyanide is not detected.

4.4.6. Ethylene oxide c-C$_2$H$_4$O

We use the CDMS entry (tag 44 504 version 2). The entry is based on data summarized in Pan et al. (1998). The spectroscopic parameters are very different from those in that work and have been mentioned in a very recent far-infrared study (Medcraft et al. 2012) which improves predictions somewhat at very high frequencies. Hirose (1974) published transition frequencies that in part fall into the frequency ranges of our survey.

Sgr B2(N): the parameters of ethylene oxide are listed in Table 11. The synthetic spectrum is optically thin ($\tau_{max} \sim 0.15$), so the source size is not constrained and was set to 3″. The model is based on eight clearly detected transitions, plus a number of other transitions that are partly blended with emission from other species. The detected transitions span a range of lower-level energies from 5 K (at 94.66 GHz) to 147 K (at 110.81 GHz). At this low level of detection, there is no evidence for emission from the northern hot core (see, e.g., 102.42 GHz).

Sgr B2(M): ethylene oxide is not detected.

4.4.7. Cyclopropenylidene c-C$_3$H$_2$

We use the CDMS entries for the ^{12}C and ^{13}C isotopologues (tags 38 508, version 2, as well as 39 509 and 39 510, both version 1). The entries are based roughly on the spectroscopic parameters reported by Bogey et al. (1987). Most of the rest frequencies for the ^{13}C isotopologues were also taken from that work. Transition frequencies for the main isotopic species were largely taken from Bogey et al. (1986). Spectroscopic information for a number of isotopic species, though mostly outside the frequency range of our survey, were published by

Spezzano et al. (2012). A small number of transition frequencies for the main isotopologue in the range of our survey were reported by Vrtílek et al. (1987).

Sgr B2(N): the parameters of all entries related to cyclopropenylidene are listed in Table 12. The molecule is detected both in emission (at 82.96, 84.73, and 85.65 GHz) and in absorption (at 82.09 and 85.34 GHz). The absorption consists of contributions from the envelope of Sgr B2(N) itself and several diffuse clouds along the line of sight (see Menten et al. 2011, for more details). The temperature of the emission component is not very well constrained because of the narrow range of lower-level energies of the few detected transitions.

One of the ^{13}C isotopologue (c-CC^{13}CH$_2$) is clearly detected in absorption (at 80.05 and 84.18 GHz). Only the self-absorption components are detected, but the diffuse-cloud components are included in the model with the isotopic ratios listed in Table 2. The situation for the other isotopologue (c-^{13}CC$_2$H$_2$) is less clear: its predicted absorption ($\sim$−0.2 K) is blended with emission from C$_2$H$_5$OCHO, HCC^{13}CN, $v_5 = 1/v_7 = 3$, and HC$_3$N, $v_6 = v_7 = 1$ at 82.30 GHz. The synthetic spectrum including all species is not consistent with the observed spectrum at this frequency: either the contribution in absorption of c-^{13}CC$_2$H$_2$ is overestimated or the contribution in emission of the contaminating species is underestimated. The situation at 81.15 GHz is similar, the absorption due to c-^{13}CC$_2$H$_2$ being likely blended with emission from other (still unidentified) species. Despite these uncertainties, we kept both isotopologues in the complete model, with the same column densities.

Sgr B2(M): the parameters of all entries related to cyclopropenylidene are listed in Table 65. The model for the main isotopologue was already reported in Menten et al. (2011). The self-absorption component of the ^{13}C isotopologues is clearly detected at 80.05, 84.19 (c-CC^{13}CH$_2$), and 82.30 GHz (c-^{13}CC$_2$H$_2$). The latter is somewhat overestimated and the transition of the same isotopologue expected at 81.15 GHz seems to be blended with an unidentified line in emission (see similar issues for Sgr B2(N) above). The model for the ^{13}C isotopologues also contains the diffuse-cloud components derived for the main isotopologue and scaled with the isotopic ratios listed in Table 2, but these components are too weak to be detected, except for a hint of weak detection at 80.06 GHz.

4.4.8. Ethynyl CCH

We use the CDMS entries for the ^{12}C and ^{13}C isotopologues (tags 25 501 version 3, 26 502 version 1, and 26 503 version 2) which are based on Padovani et al. (2009), McCarthy et al. (1995), and Sakai et al. (2010), respectively.

Sgr B2(N): the parameters of all entries related to ethynyl are listed in Table 13. The molecule is clearly detected in absorption, both from the envelope of Sgr B2(N) itself and from the diffuse clouds along the line of sight. Including a component in emission turns out to be necessary to consistently reproduce the self-absorption features of all three transitions at 87.28, 87.32, and 87.33 GHz, but the parameters of this emission component are very poorly constrained. Such a very extended emission component is seen in the large-scale maps of Jones et al. (2008) taken with the Mopra telescope. Like for c-C$_3$H$_2$, only one of the ^{13}C isotopologues (^{13}CCH) is detected, in absorption

at the 3σ level at 84.12 GHz, with a further hint of detection at 84.21 GHz. The other isotopologue ($C^{13}CH$) is not detected at 85.23 GHz, probably because of blends with emission from other (unidentified) species. It is still included in the complete model.

Sgr B2(M): the parameters of all entries related to ethynyl are listed in Table 66. Ethynyl is detected both in emission and in absorption. The emission part is modeled with two components, one for the core of the line and one for the redshifted wing. Their parameters are poorly constrained. The presence of a blueshifted wing cannot be seen in our data because, if it exists, it is masked by the deep absorption components of spiral-arm diffuse clouds. The diffuse-cloud components were fitted on the first group of hyperfine transitions (at 87.28, 87.32, and 87.33 GHz). The second group of hyperfine transitions (at 87.40, 87.41, and 87.45 GHz) is well fitted with the same parameters.

There are hints of detection of the ^{13}C isotopologues at 84.1–84.2 GHz (^{13}CCH) and 85.2–85.3 GHz ($C^{13}CH$). Both are included in the complete model, with the same parameters as the main isotopologue after rescaling the column densities using the isotopic ratios listed in Table 2. The first one is partly contaminated by absorption lines of c-$H^{13}CCCH$.

4.4.9. Thioethenyl CCS

We use the CDMS entry for the main isotopologue (tag 56 502 version 1) which is based mainly on Saito et al. (1987).

Sgr B2(N): the parameters of thioethenyl are listed in Table 14. It is detected with no or little contamination at 81.51, 86.18, 93.87, 103.64, and 106.35 GHz (with E_1/k = 11, 19, 15, 26, and 20 K, respectively). The energy range of the detected transitions is too narrow to fully constrain the temperature. A comparison of the 30 m detection to the peak temperatures obtained by Friedel et al. (2004) with the NRAO 12 m telescope suggests that the emission is more extended than the 30 m beam but less extended than the 12 m beam, which led us to assume a source size of 60″. The emission is optically thin (τ_{max} = 0.03). The ^{13}C and ^{34}S isotopologues are not detected.

Sgr B2(M): the parameters of thioethynyl are listed in Table 67. It is clearly detected at the same frequencies as toward Sgr B2(N). We assume the same source size as for the latter source. The emission is optically thin (τ_{max} = 0.03). The ^{13}C and ^{34}S isotopologues are not detected.

4.4.10. Methylenimine CH_2NH

We use the CDMS entry (tag 29 518, version 1), which is based largely on Dore et al. (2012). Transition frequencies in the range of our survey were published by Dore et al. (2010). These transitions display hyperfine splitting and we use the CDMS entry that accounts for it.

Sgr B2(N): the parameters of methylenimine are listed in Table 15. The detection relies, at 3 mm, on only four lines with no or little contamination from other species (at 87.53, 95.31, 95.51, and 114.55 GHz with E_1/k = 270, 114, 597, and 492 K). The transition at 85.21 GHz is blended with diffuse-cloud absorption components of $HC^{18}O^+$ 1–0. There are five additional

lines with little contamination detected in the 2 mm and 1.3 mm windows. The emission is optically thin at 3 mm (τ_{max} = 0.85), which allows for a reasonable estimate of the rotation temperature. The lines detected at 1.3 mm are optically thick (τ_{max} = 5.5) and in turn constrain the source size (but see Sect. 3.3 for the caveats about the modeling at 1.3 mm). The ^{13}C and ^{15}N isotopologues are not detected.

Sgr B2(M): the parameters of methylenimine are listed in Table 68. The observed spectrum is not consistent with a warm component like in Sgr B2(N), for instance at 87.53 GHz. Only one transition is detected at 3 mm (at 105.79 GHz with E_1/k = 26 K), with a high signal-to-noise ratio. This transition is severely blended with the second velocity component of $H^{13}CCCN$ toward Sgr B2(N) but only its blueshifted wing is partially blended toward Sgr B2(M) because this source does not harbor such a second velocity component.

4.4.11. Ethylene glycol aGg'-$(CH_2OH)_2$

We use the CDMS entry for the two lowest-state conformers (tags 62 503 and 62 504, both version 1) which are based on Christen & Müller (2003) and Müller & Christen (2004).

Sgr B2(N): the parameters of ethylene glycol are listed in Table 16. The 3 mm emission of the lowest state conformer, aGg', is weak and optically thin (τ_{max} = 0.024), so the source size is not constrained. A comparison of our 30 m spectrum around 93.0 GHz to the NRAO 12 m spectrum of Hollis et al. (2002) suggests that the emission of ethylene glycol and gly-colaldehyde are in the same proportion more extended than the emission of ethyl cyanide. As a result, we arbitrarily set the source size to 10″. The detection relies on about 13 weak lines that are not or only weakly blended with emission from other species. The lower-level energies of the detected transitions range from 13 K (83.62 GHz) to 40 K (95.53 GHz), which implies that the rotation temperature is not very well constrained. There is no evidence for the presence of several velocity components (e.g., 87.56, 99.51 GHz). The second lowest state conformer, gGg', is not detected.

Sgr B2(M): ethylene glycol is not detected.

4.4.12. Glycolaldehyde $CH_2(OH)CHO$

We use the CDMS entry for the vibrational ground state (tag 60 501 version 2) for technical reasons, the quality of the CDMS and JPL entries being about the same in the frequency range of our survey. We use a subset of the JPL entry for the first vibrationally excited state (tag 60 006 version 2). The ground state data are based on Butler et al. (2001), those of the vibrationally excited states on Widicus Weaver et al. (2005).

Sgr B2(N): the parameters of glycolaldehyde are listed in Table 17. The 3 mm emission is weak and optically thin (τ_{max} = 0.017). The source size is not constrained and was set to the same value as ethylene glycol (Sect. 4.4.11). The detection relies on only five weak lines that are not or only weakly blended with emission from other species. The lower-level energies of the detected transitions range from 4 K (97.92 GHz) to 78 K (96.87 GHz). The temperature is not well constrained (toward

lower values). There is no evidence for the presence of several velocity components, but this may be due to the limited signal-to-noise ratios.

No transition from within the vibrationally excited state $v = 1$ is detected.

Sgr B2(M): glycolaldehyde is not detected.

4.4.13. Methylcyanoacetylene CH$_3$C$_3$N

We use the CDMS entry (tag 65 503 version 1) which is based on Bester et al. (1983).

Sgr B2(N): the parameters of methylcyanoacetylene are listed in Table 18. The 3 mm emission is optically thin ($\tau_{max} = 0.017$). The source size was arbitrarily set to 3″. The observed spectrum is well fitted with two velocity components, one emitted by each hot core. A temperature of 100 K gives a good fit. A somewhat higher temperature (150 K) would still give a reasonable fit but tends to produce too strong emission at 107.395 and 111.533 GHz.

Sgr B2(M): the parameters of methylcyanoacetylene are listed in Table 69. The molecule is detected in emission at several frequencies, e.g., at 82.63, 90.89, 99.15, 107.41, and 111.54 GHz, but the signal-to-noise ratio for each transition is low. The spectrum is somewhat better fitted with a temperature of 100 K than with 50 or 150 K, but this is uncertain. The emission is optically thin ($\tau_{max} = 0.028$) and the source size is not constrained.

4.4.14. Propyne CH$_3$CCH

We use the CDMS entry for the vibrational ground state (Cazzoli & Puzzarini 2008) and first excited state $v_{10} = 1$ (Müller et al. 2002) of the main isotopologue (tag 40 502 version 3, 40 504 version 1), and the JPL entries for the ^{13}C isotopologues (tags 41 002, 41 003, and 41 004, all version 1) which are based on Dubrulle et al. (1978)[11].

Sgr B2(N): the parameters of all entries related to propyne are listed in Table 19. The 3 mm emission is optically thin ($\tau_{max} = 0.23$). Two groups of transitions with lower-level energies E_1/k ranging from 8 to 128 K are detected, which constrains the temperature relatively well. A source size of 10″ was arbitrarily chosen but we note that a large-scale map obtained with Mopra shows emission extended over several arc minutes (see Fig. 7 of Jones et al. 2008). No transition from within the vibrationally excited state $v_{10} = 1$ is detected.

The ^{13}C isotopologues were modeled with the same parameters as the main isotopologue, assuming an isotopic ratio of 20. The synthetic model is consistent with the observations, with one line of ^{13}CH$_3$CCH (83.13 GHz), one weak line of CH$_3$^{13}CCH (85.41 GHz), and one line of CH$_3$C^{13}CH (99.48 GHz) detected with no or little contamination.

Sgr B2(M): the parameters of all entries related to propyne are listed in Table 70. Two groups of transitions (around 85.45 and 102.54 GHz) are detected. Their lower-level energies E_1/k range from 8 to 128 K and constrain the temperature to about 70 K.

The source size has in turn to be larger than the beam at 1.3 mm to fit the transitions detected around 205.05 GHz. For a smaller size, the synthetic model becomes too strong (but remember the caveats about the modeling at 1.3 mm). With the current parameters, the transitions are all optically thin at 3 mm ($\tau_{max} = 0.045$). The ^{13}C isotopologues are detected with little contamination at 82.90, 99.48 (CH$_3$C^{13}CH), 99.75 (^{13}CH$_3$CCH), and 102.51 GHz (CH$_3$^{13}CCH).

4.4.15. Acetone CH$_3$C(O)CH$_3$

We use the JPL entry for the vibrational ground state (tag 58 003 version 3) which is based on Groner et al. (2002) with measurements in the range of our survey from Vacherand et al. (1986). An entry for the lowest $v_{12} = 1$ excited torsional state, based on an analysis presented by Groner et al. (2006), was provided by P. Groner. For both states, we use the partition function provided by the JPL catalog for entry 58 003. We note that this partition function has a strong kink at 75 K which looks suspicious even if it includes the contribution of low-lying vibrationally excited states. We suspect that some of the tabulated values are erroneous, which could then affect the derived column densities.

Sgr B2(N): the parameters of acetone are listed in Table 20. Most transitions at 3 mm are optically thin with $\tau < 0.3$, and only a few are marginally optically thin ($\tau_{max} \sim 0.8$). The source size was set arbitrarily. The detected transitions have lower-level energies E_1/k ranging from 8 K (at 98.30 GHz) to 194 K (at 92.93 GHz), which constrains the temperature relatively well. Several transitions are consistent with the presence of a second velocity component (see, e.g., at 90.29, 92.74, 99.42, and 101.45 GHz). Overall, the synthetic spectrum fits better the observed one with two velocity components.

We also detect emission from within the first torsionally excited state $v_{12} = 1$ (~78 cm^{-1}). Many lines are clearly detected at 3 mm, at, e.g., 92.65 ($E_1/k = 130$ K), 92.71 (130 K), 94.95 (123 K), 101.38 (133 K), 102.47 (135 K), and 106.39 GHz (227 K). All 3 mm transitions are optically thin, with $\tau_{max} \sim 0.35$. Two issues occur at 81.77 (124 K) and 90.50 GHz (155 K) but the discrepancies are certainly due to an overestimate of the baseline level. This is, to the best of our knowledge, the first report on the detection of torsionally excited acetone in space.

Sgr B2(M): the parameters of acetone are listed in Table 71. Acetone is clearly detected at several frequencies in the 3 mm window (e.g., groups of three transitions around 82.92, 92.74, and 111.25 GHz). The 1.3 mm range seems to constrain the temperature to low values. The source size is not constrained because all transitions detected at 3 mm are optically thin ($\tau_{max} \sim 0.16$).

4.4.16. Acetaldehyde CH$_3$CHO

We use the JPL entry (tag 44 003 version 3) and split it to model the ground state and the first torsionally excited state separately. The entry is based on Kleiner et al. (1996) with laboratory rest frequencies in the range of our survey taken from Bauder et al. (1976), Liang et al. (1986), Maes et al. (1987), Kleiner et al. (1991, 1992), Barclay et al. (1993), and Belov et al. (1993).

---

[11] The documentation in the JPL catalog quotes a wrong reference.

Sgr B2(N): the parameters of all entries related to acetaldehyde are listed in Table 21. The 3 mm emission is optically thin ($\tau_{max} \sim 0.7$). The source size was arbitrarily set. The detected transitions have lower-level energies ranging from 9 K (at 95.96 GHz) to 70 K (at 115.61 GHz). The temperature is not very well constrained. A temperature of 150 K yields a somewhat poorer fit than 100 K for the $J = 6-5$ multiplet around 115.6 GHz. A temperature of 60 K also fits the detected transitions relatively well. Two velocity components are clearly detected.

Transitions from within the torsionally excited state $v_t = 1$ (142 cm^{-1}) are clearly detected at, e.g., 95.65, 95.76, 96.80, 97.34, and 114.72 GHz. The column density parameter required to fit the torsionally excited state is a factor of two higher than for the ground state. With a temperature of 60 K, the discrepancy would be a factor of ten, which is why we favor a temperature of 100 K for both states. The higher column density parameter required to fit $v_t = 1$ suggests the presence of radiative pumping. Using Eq. (13) with the ground state as reference state, we derive a torsion temperature of 150 ± 20 K for $v_t = 1$. If a direct pumping mechanism exists, then it has to occur at ~70 μm. The torsional mode is sufficiently strong to facilitate direct infrared pumping. The presence of a second velocity component looks plausible. The only issue is at 95.76 GHz where the second component is not seen, but this could be due to an overstimate of the baseline level. This is, to the best of our knowledge, the first report on the detection of torsionally excited acetaldehyde.

Sgr B2(M): the parameters of acetaldehyde are listed in Table 72. Many transitions of acetaldehyde are detected in the 3 mm window, with lower-level energies ranging from 9 K (95.95 GHz) to 34 K (115.66 GHz). Higher energy transitions (up to ~70 K) are detected in the 2 and 1.3 mm ranges and constrain the temperature below 80 K and the source size above 20″. The line ratios around 96.35 GHz and around 115.65 GHz, and the detection at 205.15 GHz suggest a temperature higher than 20 K. All transitions detected at 3 mm are optically thin ($\tau_{max} \sim 0.016$). No transition from within the torsionally excited state $v_t = 1$ is detected.

4.4.17. Methyl cyanide CH$_3$CN

We use the CDMS entries for the vibrational ground state of the ^{12}C, ^{13}C, and ^{15}N isotopologues (tags 41 505, 42 508, 42 509, 42 510, and 43 513, all version 1), and the JPL entry for the vibrationally excited state $v_8 = 1$ of the main isotopologue (tag 41 010 version 1). The entries for the vibrationally excited state $v_8 = 1$ of the ^{13}C isotopologues and $v_8 = 2$ and $v_4 = 1$ of the main isotopologue were prepared by one of us (HSPM). The ground-state entries were all based on Müller et al. (2009), the $v_8 = 1$ entry was based on Bocquet et al. (1988), and the $v_8 = 2$ and $v_4 = 1$ on Müller et al. (2010a). The excited states of the ^{13}C isotopologues are based on unpublished work. Ground-state data in the range of our survey were taken from Cazzoli & Puzzarini (2006), Demaison et al. (1979), and Bauer et al. (1975) for the main, the ^{13}C, and the ^{15}N isotopologues, respectively. Bauer & Maes (1969), Bauer (1971), and Cosleou et al. (1991) provided corresponding data for the $v_8 = 1$, $v_8 = 2$, and $v_4 = 1$ states, respectively, of the main isotopic species.

The cyano C of methyl cyanide is rather close to the center of mass of the molecule. Therefore, transitions of CH$_3^{13}$CN and ^{13}CH$_3^{13}$CN occur close to those of the more abundant CH$_3$CN

and ^{13}CH$_3$CN, respectively, in particular at wavelengths as long as 3 mm.

Sgr B2(N): the parameters of all entries related to methyl cyanide are listed in Table 22. The model for the ground state of methyl cyanide ($\tau_{max} \sim 28$) was already reported in Sect. 4.4 of Belloche et al. (2009). The ^{13}C isotopologues are clearly detected ($\tau_{max} \sim 1.7$). The temperature is relatively well constrained by their K-ladders, and their few marginally optically thick lines also constrain the source size to some extent. Two velocity components are clearly detected. The derived parameters are used for the main isotopologue assuming an isotopic ratio of 20. The synthetic spectrum of the latter does not fit the shape of the observed spectrum very well because our radiative transfer method is too simplistic for such transitions with high optical depths. Like for ethyl cyanide (see Sect. 4.4.2), a third, redshifted, component is added to better fill the linewing. The ^{15}N isotopologue is not directly detected. Its transitions around 89.2 and 107.05 GHz are blended with deep absorption components of HCO$^+$ and emission lines of C$_2$H$_5^{13}$CN and SO$_2$, respectively. We still include this isotopologue in the complete model because it significantly improves the fit between 107.05 and 107.06 GHz, range over which it contributes to about 30% of the detected emission. Even if it is not clearly detected as such, the doubly-substituted ^{13}C isotopologue is also included in the complete model because it significantly contributes to the detected emission at 89.27 and 107.12 GHz.

We also detect emission lines from within three vibrationally excited states of the main isotopologue: $v_8 = 1$, $v_8 = 2$, and $v_4 = 1$ (365, 717, and 920 cm^{-1}, respectively), with $\tau_{max} \sim 5.5$, 0.65, and 0.15, respectively. The optically thick lines of $v_8 = 1$ require a source size a bit smaller than for the ground state[12]. The column density parameter needed to fit the emission of the excited states increases with their energy, suggesting that the vibration temperature is higher than the rotation temperature, probably because of radiative pumping. Using Eq. (13) with $v_8 = 1$ as reference state and only for the first velocity component, we derive vibration temperatures of 290 ± 20 and 340 ± 20 K for $v_8 = 2$ and $v_4 = 1$, respectively. The intensities of the infrared bands v_8, $2v_8$, and v_4 are possibly sufficient to permit direct infrared pumping. If such a direct pumping mechanism from the ground state exists for each of the three excited states $v_8 = 1$, $v_8 = 2$, and $v_4 = 1$, then it has to occur at ~27, 14, and 11 μm, respectively. The second velocity component is clearly detected for $v_8 = 1$ and $v_8 = 2$, and is consistent with the observed spectrum for $v_4 = 1$. The third, redshifted, component, is significantly detected for $v_8 = 1$ only. Emission lines from within the excited state $v_8 = 1$ of the ^{13}C isotopologues are also detected, e.g., at 89.52, 92.19, and 110.63 GHz. The column density ratio between the ^{12}C and ^{13}C isotopologues is only 14 for $v_8 = 1$. A few detected transitions of the ^{12}C isotopologue are optically thin (e.g., at 92.22 GHz with $\tau = 0.4$) so the deviation from the usual $\frac{^{12}C}{^{13}C}$ isotopic ratio of 20 does not seem to be related to an optical depth effect. The reason for this discrepancy is unclear.

Goldsmith et al. (1983) have detected transitions of the main isotopologue from within $v_8 = 1$ and Fortman et al. (2012) have very recently reported the detection of $v_8 = 2$ in Orion KL. Lines from within higher excited vibrational states as well as the $v_8 =$

---

[12] A model with the same source size as the ground state but a lower rotation temperature of 140 K still fits the optically thick lines reasonably well but not anymore the optically thin lines at 92.22 and 92.23 GHz.

1 lines of the ^{13}C isotopologues have been detected here for the first time.

Sgr B2(M): the parameters of all entries related to methyl cyanide are listed in Table 73. Following the results of de Vicente et al. (1997), we used two temperature components to model the vibrational ground state of the ^{12}C and ^{13}C isotopologues. However, the parameters are not well constrained, and the fit is not very satisfactory, especially for the main isotopologue. Like de Vicente et al. (1997), we detect the $J = K$ components of the $J = 5$–4 and 6–5 K-ladders in absorption. These authors accounted for these absorption features by adding a third component corresponding to a diffuse (10^3 cm^{-3}), hot (300 K), outer layer and computed their synthetic spectrum with a non-LTE model. This is beyond the scope of our simple, LTE modeling, which cannot reproduce these absorption features. The doubly-substituted ^{13}C isotopologue is not detected.

We detect emission lines from within two vibrationally excited states of the main isotopologue: $v_8 = 1$ and $v_8 = 2$. A model with the same source size and temperature as for the ground state (1.5″ and 200 K) fits the $v_8 = 1$ transitions at 3 mm as well as our model with 1″ and 300 K, but the former would require a column density twice as high to also fit the $v_8 = 2$ transitions while the latter fits both vibrationally excited states well with the same column density. If the presence of radiative pumping can explain the former model, then it is unclear which model is more realistic.

4.4.18. Acetamide CH$_3$C(O)NH$_2$

The entry for acetamide was provided by V. Ilyushin and is based on Ilyushin et al. (2004). We used partition functions for the A and E species considered as independent. They were computed and provided by V. Ilyushin (priv. comm.). The ground state and the first two torsionally excited states of each species were splitted into different entries in our catalog.

The first astronomical detection of acetamide was reported by Hollis et al. (2006) toward Sgr B2(N). Eight low-energy transitions (four from the A species and four from the E species) were detected with the GBT between 9 and 48 GHz, in absorption or in emission. The detected signals were interpreted as coming from a low-excitation (~8 K) halo surrounding both hot cores. Halfen et al. (2011) published a detailed analysis of the emission of acetamide based on their spectral survey of Sgr B2(N) performed with the ARO 12 m telescope ($HPBW \sim 60″$ at 100 GHz) and the SMT at 3, 2, and 1 mm. They claim the detection of 132 transitions of acetamide, the majority of them being "partially blended", and they identify two temperature components based on a rotation-diagram analysis (17 ± 4 and 171 ± 4 K, respectively).

Sgr B2(N): the parameters of all entries related to acetamide are listed in Table 23. In our spectrum, most of these transitions are significantly blended with emission from other species and only a few transitions can be reliably identified. The ground state of the A species is reasonably well detected at 87.63 ($E_1/k = 15$ K), 92.38 (109 K), 97.905 (19 K), 97.911 (19 K), and 97.94 GHz (20 K), and there are hints of detection at 87.72 (159 K), 88.08 (162 K), 90.91 (126 K), 101.28 (138 K), and 114.50 GHz (115 K), pointing to a high temperature. In comparison to the 12 m observations, our 30 m observations are relatively less sensitive to an extended, low-excitation component.

The temperature is however not very well constrained in our data and we set it to the value derived by Halfen et al. (2011) for their warm component, which is very close to the temperature we derive for formamide (see Sect. 4.4.37). We arbitrarily set the source size to the one that we derive for formamide (see Sect. 4.4.37). Two transitions at 108.21 (23 K) and 108.26 GHz (24 K) are overestimated by the model, by a factor of two for the latter. We do not think that it invalidates the detection because nearby transitions of ethyl cyanide (at 108.21 and 108.23 GHz) suffer from the same issue. Since the detection of ethyl cyanide is robust and its emission is very well reproduced at other frequencies, the issue around 108.2 GHz points to a calibration or pointing problem for that frequency range. The ground state of the E species is also reasonably well detected at 86.46 (279 K), 92.28 (174 K), 97.89 (19 K), 99.70 (152 K), 107.99 (23 K), and 108.19 GHz (24 K). We note however that the best fit yields a column density lower than for the A species by 25%.

We also include the contributions of the first two torsionally excited states of each species in the model. For the A species, transitions from within $v = 1$ are weakly detected at 92.34 (81 K) and 100.37 GHz (85 K) and from within $v = 2$ at 99.63 GHz (216 K), with the same parameters as for the ground state. The model for $v = 1$ overestimates the transition at 98.96 GHz (82.5 K) but we believe that it is due to the level of the baseline being overestimated. For the E species, transitions from within $v = 1$ are weakly detected at 97.40 (141 K), 99.19 (47 K), 101.61 (110 K), and 111.92 GHz (51 K) and from within $v = 2$ at 114.50 GHz (133 K), again with the same parameters as for the ground state. These detections are only very tentative per se, but we keep these entries in the complete model because their parameters are the same as for the ground states.

Sgr B2(M): acetamide is not detected.

4.4.19. Acetic acid CH$_3$COOH

We use entries provided by I. Kleiner for the ground state and the torsionally excited states $v_t = 1$ and $v_t = 2$. The entry was generated from Ilyushin et al. (2008). Ground state transition frequencies at 3 mm and also to a large extent in the higher frequency windows of our survey were published by Ilyushin et al. (2001). The partition function was computed including levels up to $J = 130$ and the first 11 torsionally excited states (V. Ilyushin, priv. comm.).

Sgr B2(N): the parameters of acetic acid are listed in Table 24. The 3 mm emission is optically thin ($\tau_{max} \sim 0.05$), so the source size is not constrained. The range of lower-energy levels of the detected transitions is very narrow, from 16 K (at 90.25 GHz) to 25 K (at 111.55 GHz), which is not sufficient to constrain the temperature. There is a hint of second velocity component at 100.86 GHz. The vibrationally excited states $v_t = 1$ and $v_t = 2$ are not detected.

Sgr B2(M): acetic acid is not detected.

4.4.20. Methylamine CH$_3$NH$_2$

We use the JPL entry (tag 31 008 version 1) which employed data summarized in Ilyushin et al. (2005). Additional data in the range of our survey were published by Kréglewski & Wlodarczak (1992).

Sgr B2(N): the parameters of methylamine are listed in Table 25. The 3 mm emission is optically thin ($\tau_{max} \sim 0.32$), so the source size is not constrained. The transitions detected in emission have lower-level energies E_1/k ranging from 6.4 K (at 89.08 GHz) to 286 K (at 97.48 GHz), which constrains the temperature relatively well. The presence of a second velocity component in emission is clearly seen. A few transitions are detected in absorption with two velocity components (e.g., at 84.31 GHz). One issue is that the transition at 89.96 GHz with $E_1/k = 2.1$ K is also expected in absorption but is not seen in the observed spectrum. This may be due to contamination by emission from another species that has not been identified so far. The emission being weak ($T_{mb} < 0.35$ K), no other isotopologue is expected to be detectable in our survey.

Sgr B2(M): the parameters of methylamine are listed in Table 74. A few transitions of methylamine are detected at 3 mm, both in emission (at, e.g., 83.98 and 84.31 GHz) and in absorption (at, e.g., 82.23 and 89.96 GHz). The lines detected in emission at 3 mm have lower-level energies ranging from 13 K (87.78 GHz) to 45 K (81.52 GHz), which does not constrain much the temperature. A model with 100 K fits the 3 mm spectrum reasonably well, but it produces too strong lines at 1.3 mm. 50 K is more consistent with the upper limits at 1.3 mm, but this is quite uncertain because of the dust-absorption and baseline-level issues mentioned earlier for this atmospheric window. In particular, there are still three low-energy transitions significantly overestimated by the 50 K synthetic spectrum in the 1.3 mm window, at 215.79, 247.08, and 254.61 GHz ($E_1/k = 7$, 26, and 17 K, respectively). The lines in emission at 3 mm are optically thin ($\tau_{max} \sim 0.07$), implying that the source size is not constrained. The absorption component is shifted by ~ 4 km s^{-1} in velocity compared to the emission component.

4.4.21. Dimethyl ether CH$_3$OCH$_3$

We use the CDMS entry for the ground state of the main isotopologue (tag 46 514 version 1). It is based on the very extensive analysis of Endres et al. (2009) and employed additional rest frequencies in the range of our survey from Lovas et al. (1979) and Neustock et al. (1990). The entries for the vibrationally excited states $v_{11} = 1$ and $v_{15} = 1$ were provided by C. Endres. The entry for the ground state of the ^{13}C isotopologue was provided by M. Koerber.

Sgr B2(N): the parameters of all entries related to dimethyl ether are listed in Table 26. The model for the ground state of dimethyl ether was already reported in Sect. 3.4 of Belloche et al. (2009). Some transitions detected in emission at 3 mm are marginally optically thick, others are optically thin ($\tau_{max} \sim 1.8$). The temperature is well constrained by the broad range of lower-energy levels of the optically thin transitions, from 5 K (at 99.32 GHz) to ~ 430 K (at 97.24 GHz). The source size is in turn constrained by the optically thick lines. The presence of a second velocity component is clearly seen. Assuming an isotopic ratio of 20, there are several hints of emission from the ^{13}C isotopologue at 81.81, 93.28, 108.20, and 114.14 GHz. There may be an issue at 86.87 GHz, but it is probably due to blending with velocity components of SiO in absorption that have not been included in the complete model.

We also detect emission lines from within two vibrationally excited states of the main isotopologue: $v_{11} = 1$ and $v_{15} = 1$ (199

and 241 cm^{-1}, respectively), with $\tau_{max} \sim 0.12$ and 0.08, respectively. We used the same model parameters as for the ground state. About ten transitions of $v_{11} = 1$ are weakly detected (e.g., 82.93, 111.93, and 113.02 GHz), and five for $v_{15} = 1$ (e.g., 81.83, 90.24, and 93.33 GHz). We note that the detection of numerous transitions from within both vibrationally excited states were recently reported toward G327.3-0.6 (Bisschop et al. 2013).

Sgr B2(M): the parameters of dimethyl ether are listed in Table 75. The transitions detected at 3 mm have lower-level energies ranging from 7 K (91.47 GHz) to 164 K (111.81 GHz), which yields a relatively well constrained temperature. The transitions at 3 mm are optically thin ($\tau_{max} \sim 0.045$) and do not constrain the source size. However the lines detected at 1.3 mm suggest a beam filling factor at 1.3 mm close to 1. A smaller source size, with a higher column density to still fit the 3 mm spectrum, tends to produce too strong lines at 1.3 mm. The ^{13}C isotopologue is not detected. The vibrationally excited states $v_{11} = 1$ and $v_{15} = 1$ of the main isotopologue are not detected either.

4.4.22. Methyl formate CH$_3$OCHO

We use the JPL entry (tag 60 003 version 2) which we have split into two entries to model the ground state and the first torsionally excited state separately. The entry is based on Ilyushin et al. (2009) with additional data from Karakawa et al. (2001).

Sgr B2(N): the parameters of all entries related to methyl formate are listed in Table 27. The model for the ground state of methyl formate was already reported in Sect. 3.4 of Belloche et al. (2009) but was slightly readjusted. Most detected transitions are (marginally) optically thin ($\tau_{max} \sim 1.3$). We refer to Belloche et al. (2009) for a comparison of our fit results to those obtained by Nummelin et al. (2000). The temperature is relatively well constrained while the source size is not. With a peak temperature of ~ 1.7 K at 3 mm for the main isotopologue, we expect the ^{13}C isotopologues to be detectable in our survey but we do not have a catalog file at our disposal yet.

We also detect emission lines from within the torsionally excited state $v_t = 1$ (132 cm^{-1}), with $\tau_{max} \sim 0.2$. Like for other species, the fit yields a column density parameter much higher than the one derived for the ground state, suggesting the presence of radiative pumping. Using Eq. (13) with the ground state as reference state and only for the first velocity component, we derive a torsional temperature of 120 ± 10 K for $v_t = 1$. If a direct pumping mechanism exists, then it has to occur at ~ 76 μm. However, the intensity of the methyl torsion is very low such that direct infrared pumping is very unlikely. The presence of a second velocity component is clearly seen at, e.g., 89.73, 95.24, and 100.22 GHz.

Sgr B2(M): the parameters of methyl formate are listed in Table 76. The transitions detected at 3 mm have lower-level energies ranging from 14 K (88.85 GHz) to 54 K (110.54 GHz) and are optically thin ($\tau_{max} \sim 0.26$). The temperature is somewhat constrained, but the source size is not. The first vibrationally excited state $v_t = 1$ is not unambiguously detected.

4.4.23. Methanol CH$_3$OH

The entry for the main isotopologue was taken from the JPL catalog (tag 32 003, version 3) and the one for the ^{13}C isotopologue

from the CDMS (tag 33 502, version 1). These entries are from Xu et al. (2008) and Xu & Lovas (1997). The entry for the ^{18}O species was prepared by one of us (HSPM). Transitions in the range of our survey were taken mainly from Lees & Baker (1968), Pickett et al. (1981), Herbst et al. (1984), Sastry et al. (1984), Anderson et al. (1990a), Müller et al. (2004), and Xu et al. (2008) for the main isotopologue, from Haque et al. (1974), Blake et al. (1984), Kuriyama et al. (1986), Anderson et al. (1987), and Anderson et al. (1990b) for ^{13}CH$_3$OH, and from Ikeda et al. (1998) for CH$_3^{18}$OH.

Sgr B2(N): the parameters of all entries related to methanol are listed in Table 28. Many transitions are detected at 3 mm, up to at least 720 K. However, methanol is very difficult to model. We model its emission and absorption with six temperature/velocity components (with $\tau_{max} \sim 7.5$ for the main hot component and 1.7 for the 15 K component), but several issues remain (see discussion in Sect. 5.4): at 97.20 and 97.21 GHz, the synthetic lines (with $E_1/k = 947$ K) have no counterpart in the observed spectrum; at 107.01 and 108.89 GHz ($E_1/k = 23$ and 8 K, respectively), the model predicts lines in emission while the observed spectrum is mostly in absorption; the model largely underestimates the emission of the transition detected at 84.52 GHz, which is known to be a maser line (see Sect. 5.4 and Müller et al. 2004). The starting parameters for the cold component (15 K) were taken from our model of Sgr B2(M). This component is mostly (but poorly) constrained by the transitions at 95.91, 96.74, and 97.58 GHz (E_1/k in the range 2.3 to 17 K). The two absorption components at $v_{off} \sim -170$ km s^{-1} were taken from our model toward Sgr B2(M). They are (weakly) detected close to 96.8 GHz only. The 3 mm emission of the ^{13}C isotopologue is clearly detected and is optically thin ($\tau_{max} \sim 0.34$ and 0.08 for the hot and cold components, respectively) and is dominated by the hot component for the transitions with $E_1/k > 20$ K. The lower-level energies of the detected transitions range from 2.3 K (at 94.41 GHz) to 470 K (at 90.86 GHz), which constrains the temperature of the hot component relatively well. The source size is in turn constrained by the optically thick lines of the main isotopologue. The 3 mm emission of the ^{18}O isotopologue is (barely) detected at 112.95 and 114.18 GHz ($\tau_{max} \sim 0.02$). The cold component is not constrained for this isotopologue.

We also detect emission lines from within two torsionally excited states of the main isotopologue: $v_t = 1$ and $v_t = 2$ (204.2 cm^{-1} for $J = K = 1$ of E symmetry and 353.2 cm^{-1} for $J = K = 0$ of A symmetry, respectively), with $\tau_{max} \sim 0.9$ and 0.2, respectively. About 15 transitions are detected at 3 mm for $v_t = 1$, but only three transitions are detected for $v_t = 2$, at 96.38, 96.55, and 102.42 GHz. The first one is partially blended with emission from CH$_3$CHO, the second one from CH$_3$OCHO and C$_2$H$_5$CN, $v_{13} + v_{21} = 1$, and the third one is weak. We had to reduce the source size compared to the model of the ground state in order to fit both the optically thin lines of $v_t = 1$ and those with an opacity close to 1. The presence of a second velocity component is clearly seen for $v_t = 1$ (e.g. 96.49 GHz). Finally, we also detect the ^{13}C isotopologue in its torsionally excited state $v_t = 1$ (e.g., 93.44, 102.71, and 110.73 GHz).

Sgr B2(M): the parameters of all entries related to methanol are listed in Table 77. Transitions with lower-level energies ranging from 2.3 K (96.74 GHz) to 489 K (81.65 GHz) are detected at 3 mm. There is a clear indication of at least two temperature components (see also Sutton et al. 1991). We use a temperature of 15 K for the cold component, similar to the values

found for methanol by Sutton et al. (1991) toward Sgr B2(M) at higher frequency and by Requena-Torres et al. (2006) toward Galactic-center clouds without hot cores. Our model largely underestimates the transitions at 84.52 GHz ($E_1/k = 36$ K) and 95.17 GHz (79 K), which are both known to be maser lines (see Sect. 5.4 and Müller et al. 2004). One component in absorption is added to fit the self-absorption seen at 96.74 GHz ($E_1/k = 2.3$ and 8 K) and 205.79 GHz (7 K), but it does not account well for the self-absorption seen at 107.01 GHz (23.2 K) and 108.89 GHz (8 K), where the model is much too strong (see discussion in Sect. 5.4). An additional cold component is added to account for the redshifted wing emission seen at, e.g., 84.52 (36 K), 95.91 (17 K), and 97.58 GHz (17 K). Several diffuse-cloud components are detected in absorption at 96.8 GHz. A hot component is necessary to account for the detected transitions with higher energies. Its temperature is relatively well constrained. The source size was determined by the optically thick transitions at 1.3 mm. At 3 mm, the hot component has a maximum opacity $\tau_{max} \sim 1.5$, similar to the maximum opacity of the main cold component (1.6). The ^{13}C isotopologue is clearly detected, especially at 94.41 GHz. Only the cold components in emission are detected at 3 mm. The hot component is tentatively detected in the 1.3 mm window at 235.9 and 236.0 GHz. The ^{18}O isotopologue is not detected.

We also detect emission lines from within the torsionally excited state $v_t = 1$. Only two transitions at 99.73 and 102.96 GHz are clearly seen at 3 mm, with $\tau_{max} = 0.19$.

4.4.24. Methyl mercaptan CH$_3$SH

The entries for the ground state, first and second torsionally excited states of methyl mercaptan were provided by L.-H. Xu prior to the publication of the recent extensive analysis (Xu et al. 2012). Transition frequencies in the range of our survey were taken mainly from Lees & Mohammadi (1980) and Sastry et al. (1986).

Sgr B2(N): the parameters of methyl mercaptan are listed in Table 29. Many lines of methyl mercaptan are blended with emission of other species, but four transitions are clearly detected at 101.14, 101.16, 101.96, and 102.20 GHz (E_1/k from 7 to 48 K) with two velocity components. The emission is weak ($T_{mb} < 0.6$ K) and optically thin ($\tau_{max} \sim 0.3$). The source size is not constrained and the temperature not very well either. The ^{13}C and ^{34}S isotopologues are not expected to be detectable in our survey. No transition from within the torsionally excited state $v_t = 1$ is unambiguously detected.

Sgr B2(M): the parameters of methyl mercaptan are listed in Table 78. A group of transitions with E_1/k ranging from 7 to 48 K is clearly detected around 101.2 GHz, which somewhat constrains the temperature. A temperature of 30 K yields a better fit to the $E_1/k = 60$ K transitions at 1.3 mm than 40 K. The lines are optically thin at 3 mm ($\tau_{max} = 0.33$), so the source size is not constrained. No transition from within the torsionally excited state $v_t = 1$ is detected.

4.4.25. Cyanide radical CN

We use the CDMS entries for the ^{12}C, ^{13}C, and ^{15}N isotopologues (tags 26 504, 27 505, and 27 506, all version 1). The predictions are based on a combined fit involving several isotopologues which is similar to the one in Saleck et al. (1994). Rest

frequencies for $C^{15}N$ from astronomical observations were also published in that work. Ground state data for ^{13}CN were published by Bogey et al. (1984). Unpublished data from C. Gottlieb were employed for the main isotopologue.

Sgr B2(N): the parameters of all entries related to the cyanide radical are listed in Table 30. The cyanide radical is essentially detected in absorption around 113.2 and 113.5 GHz and is modeled with 38 velocity components. The emission component on top of which the self-absorption and part of the diffuse-cloud absorption occur is very poorly constrained. The spectrum is not easy to model because of the hyperfine structure. The ^{13}C isotopologue is also detected in absorption around 108.40, 108.65, 108.78, and 109.22 GHz, mainly the self-absorption component but also a few diffuse-cloud components (e.g., at 108.84 GHz). We nevertheless keep the contribution of all diffuse-cloud components assuming the isotopic ratios listed in Table 2. There is a hint of detection of the ^{15}N isotopologue in absorption at 110.02 GHz, where the level of the baseline may have been underestimated. We only include the emission and self-absorption components in the model of this isotopologue.

Sgr B2(M): the parameters of all entries related to the cyanide radical are listed in Table 79. The model is constructed with 31 velocity components in a similar way as for Sgr B2(N). The emission component is poorly constrained. The ^{13}C isotopologue is clearly detected both at 3 and 1.3 mm, but may be affected by blends with emission lines. The ^{15}N isotopologue is weakly detected at 109.7 GHz, but clearly at 110.02 GHz (mainly the self-absorption component).

4.4.26. Carbon monoxide CO

We use the CDMS entries for CO, ^{13}CO, $C^{18}O$, $C^{17}O$, $^{13}C^{18}O$, and $^{13}C^{17}O$ (tags 28 503, 29 501, 30 502, 29 503, 31 502, and 30 503, all version 1 except version 2 for ^{13}CO). The entries are based on Winnewisser et al. (1997), Cazzoli et al. (2004), Klapper et al. (2001, 2003, 2000), and Klapper et al. (2003), respectively.

Sgr B2(N): the parameters of all entries related to carbon monoxide are listed in Table 31. Three isotopologues in addition to the main one are clearly detected (^{13}CO, $C^{18}O$, and $C^{17}O$). The emission of $^{13}C^{17}O$ is partially blended with emission from aminoacetonitrile and possibly another unidentified species. The emission of $^{13}C^{18}O$ is completely blended with emission from C_2H_3CN, $v_{11} = 1$, but it is still included in the full model because $^{13}C^{17}O$ is partially detected. The width and centroid velocity of the main emission component is constrained by the $C^{18}O$ and $C^{17}O$ spectra. The diffuse-cloud absorption components were first adjusted on ^{13}CO, then transfered to the other isotopologues assuming the isotopic ratios listed in Table 2. Two components were then readjusted on $C^{18}O$. They are in turn too deep in ^{13}CO. This may point to deviations from the assumed isotopic ratios or contamination of the ^{13}CO absorption components by emission from a species not included in the complete model. Apart for the self-absorption, absorption components with $v_{off} > -72$ km s^{-1} were not included in the model because they are blended with broad ^{13}CO emission, which implies too many degeneracies. The model for CO was derived from the ^{13}CO one, but it was not optimized further. Here again, the mixture of broad, multiple, emission and absorption

components cannot be modeled in a simple way. Finally, we note that the observed CO emission shows blueshifted components up to $V_{lsr} \sim 200$ km s^{-1} (see Fig. 6 of Menten et al. 2011, for Sgr B2(M)), but we did not include these components in the model.

Sgr B2(M): the parameters of all entries related to carbon monoxide are listed in Table 80. All isotopologues but $^{13}C^{17}O$ are clearly detected. $^{13}C^{17}O$ has a low signal-to-noise ratio at 3 mm but is well detected at 1.3 mm. The optically thick CO transition requires a temperature of at least 58 K. This transition is complex, with many emission and absorption components, and it is not well fitted. The linewidth of the main emission component was fitted on $C^{18}O$. The diffuse-cloud absorption components were first fitted on $C^{18}O$, then transfered to ^{13}CO for which additional components were added. All absorption components were then propagated to the other isotopologues assuming the isotopic ratios listed in Table 2. The diffuse-cloud absorption components are not detected in $^{13}C^{18}O$ and $^{13}C^{17}O$. Like for Sgr B2(N), the observed CO (and likely ^{13}CO too) emission shows blueshifted components up to $V_{lsr} \sim 200$ km s^{-1}, but we did not include these components in the model.

4.4.27. Carbon monosulfide CS

We use the CDMS entries for CS, ^{13}CS, $C^{34}S$, $C^{33}S$, and $^{13}C^{34}S$ (tags 44 501, 45 501, 46 501, 45 502, and 47 501, all version 2). The spectroscopic parameters were taken from Müller et al. (2005). Ground state transition frequencies in the range of our survey were taken from Gottlieb et al. (2003) for CS and $C^{34}S$, Bogey et al. (1982a) for ^{13}CS, and Bogey et al. (1981) for $C^{33}S$ and $^{13}C^{34}S$.

Sgr B2(N): the parameters of all entries related to carbon monosulfide are listed in Table 32. Three isotopologues are clearly detected in addition to the main one (^{13}CS, $C^{34}S$, and $C^{33}S$). $^{13}C^{34}S$ is not directly detected but it contributes to about 30% of the peak temperature at 90.92 GHz so we include it in the complete model. The emission of ^{13}CS and $C^{34}S$ at 1.3 mm and $C^{33}S$ at 3 mm cannot be simultaneously reproduced with a cold component only. A hot component is needed in addition to the cold component in emission to match the three lines. Its parameters are however not very well constrained. The diffuse-cloud absorption components were first adjusted on CS, then transfered to ^{13}CS and $C^{34}S$ and readjusted, and then transfered back to CS and $C^{33}S$, assuming the isotopic ratios listed in Table 2. Most absorption components of ^{13}CS and some of $C^{34}S$ are blended with emission of identified species. The complete model takes this into account but, since it is not perfectly matching the emission lines, some uncertainty remains for some of the absorption components. Several absorption components are too deep for CS. The reason may be blending with emission of still unidentified species or blueshifted wing emission of CS not included in the model, or an underestimate of the excitation temperature, or erroneous isotopic ratios.

Sgr B2(M): the parameters of all entries related to carbon monosulfide are listed in Table 81. Four isotopologues are clearly detected in addition to the main one (^{13}CS, $C^{34}S$, $C^{33}S$, and $^{13}C^{34}S$). $C^{34}S$ 5–4 is twice as strong as ^{13}CS 5–4, which is not expected given that both isotopologues should have roughly the same column density. This may be an isotopic anomaly, or

contamination by an unknown species. Contrary to Sgr B2(N), no warm component is needed to fit both the 3 and 1.3 mm transitions. The diffuse-cloud absorption components were modeled in the same way as for Sgr B2(N). None of them is detected in $^{13}C^{34}S$.

4.4.28. Ethenone CH$_2$CO

We use the CDMS entries for the ^{12}C and ^{13}C isotopologues (tags 42 501 version 2, 43 505, and 43 506, both version 1). The entry for the main isotopic species is based on Johns et al. (1992) with additional measurements in the range of our survey from Guarnieri & Huckauf (2003). The ^{13}C isotopologue entries are based on Guarnieri & Huckauf (2003). Predictions for excited states were generated by one of us (HSPM) from an unpublished fit based on the infrared analysis from Nemes et al. (2000) with rotational transitions in the range of our survey from Hinze et al. (1996).

The carbonyl C of ethenone is very close to the center of mass of the molecule. Therefore, the transitions of CH$_2$^{13}CO are frequently overlapped by those of the main species, in particular at wavelengths as long as 3 mm.

Sgr B2(N): the parameters of all entries related to ethenone are listed in Table 33. The 3 mm emission is marginally optically thick for most transitions ($\tau_{max} \sim 2.2$), but some are optically thin (e.g., at 80.82 GHz). Altogether, the source size and temperature are both partially constrained. The presence of a second velocity component is clearly seen. Most transitions of the ^{13}C isotopologues are close to transitions of the main isotopologue and partly hidden in their blueshifted wings, which prevents a firm identification. Two transitions of $^{13}CH_2CO$ (at 96.95 and 97.80 GHz) are not in this situation. Both look shifted by about 3 MHz compared to the features detected in the observed spectrum. While the discrepancy could be related to the uncertain level of the baseline in the first case, this seems to be unlikely for the second case. We do not have any good explanation for this discrepancy. The model is not very well constrained for the ^{13}C isotopologues and is simply a scaled version of the model of the main isotopologue. No transition from within the vibrationally excited states $v_5 = 1$, $v_6 = 1$, and $v_9 = 1$ is detected.

Sgr B2(M): the parameters of all entries related to ethenone are listed in Table 82. Two temperature components are needed to fit both the 3 and 1.3 mm ranges. At 3 mm, the detected transitions have lower-level energies ranging from 6 K (80.83 GHz) to 127 K (101.00 GHz) and are all optically thin ($\tau_{max} = 0.4$ for the hot component, 0.02 for the cold component). The transitions detected at 1.3 mm are dominated by the warm component and are slightly optically thick ($\tau_{max} = 2.4$). They partially constrain the source size and temperature, especially around 202.0 GHz where several transitions with different lower-level energies (from 43 to 252 K) are detected. The ^{13}C isotopologues are not detected at 3 mm but there are hints of detection at 213.26, 217.15, and 232.64 GHz for $^{13}CH_2CO$.

4.4.29. Formaldehyde H$_2$CO

We use the CDMS entries for the ^{12}C, ^{13}C, and ^{18}O isotopologues (tags 30 501 version 2, 31 503, and 32 503, both version 1). The entries are based on Brünken et al. (2003), Müller et al. (2000c,b), respectively, with additional measurements in

the range of our survey from Cornet & Winnewisser (1980) for all three isotopologues and from Johnson et al. (1972) and Dangoisse et al. (1978) for the main and ^{13}C species.

Sgr B2(N): the parameters of all entries related to formaldehyde are listed in Table 34. They are not very well constrained. The absorption components were introduced to fit the transition at 211.21 GHz. Only one transition is detected in the 3 mm window (at 101.33 GHz). The ^{13}C isotopologue is also detected with only one transition at 3 mm (at 96.38 GHz), but several at 1.3 mm. The ^{18}O isotopologue is not detected.

Sgr B2(M): the parameters of all entries related to formaldehyde are listed in Table 83. Only one transition of the main isotopologue is detected at 3 mm (at 101.33 GHz), and two at 1.3 mm. The model parameters are not well constrained. The ^{13}C isotopologue is detected at 1.3 mm only, but the model is a bit too strong (or the level of the baselines overestimated). The ^{18}O isotopologue is detected at 214.78 GHz.

4.4.30. Thioformaldehyde H$_2$CS

We use the CDMS entries for the ^{12}C, ^{13}C, and ^{34}S isotopologues (tags 46 509 version 2, 47 505, and 48 508, both version 1). The entry for the main species is based on the extensive account by Maeda et al. (2008). A small number of transition frequencies in the 3 mm range were taken from Beers et al. (1972). The entry for the ^{34}S isotopologue was based on McNaughton & Bruget (1993) with some higher order parameters derived from those of the main species in that study. The parameters for the ^{13}C isotopologue were also derived from those of the main species. The very limited data from Brown et al. (1987) and references therein permitted only a very small number of spectroscopic parameters to be determined.

Sgr B2(N): the parameters of all entries related to thioformaldehyde are listed in Table 35. Two velocity components are clearly detected. A combination of hot and cold components is required to fit the transitions both in the 3 and 1.3 mm windows, but their parameters are not very well constrained. The ^{34}S isotopologue is detected at 102.81 GHz, and significantly contributes to the "wing" of the emission detected at 99.77 GHz. The ^{13}C isotopologue is not unambiguously detected, but it is included in the complete model because it contributes to the emission detected at 97.63 and 100.53 GHz significantly (>50%). The ^{33}S isotopologue is not detected.

Sgr B2(M): the parameters of all entries related to thioformaldehyde are listed in Table 84. The main isotopologue is detected both at 3 and 1.3 mm. The higher-energy transitions in the 1.3 mm window are shifted in velocity compared to the lower-energy ones in the 3 mm window. This is a clear indication of two components. At 3 mm, both components are optically thin, with $\tau_{max} = 0.08$ for the cold one and 0.4 for the warm one. Some transitions of the latter are slightly optically thick at 1.3 mm ($\tau_{max} \sim 2$), but others are optically thin. As a result, both the temperature and the source size are somewhat constrained, but may be affected by the uncertainties of the baseline level. The third component accounts for the wing emission seen mainly for the low-energy transitions at 3 mm. Its source size is not constrained. Only one transition of the ^{34}S isotopologue

is detected, at 232.75 GHz. The ^{13}C isotopologue is tentatively detected at 97.63 and 227.76 GHz. It is included in the complete model.

4.4.31. Aminoacetonitrile NH$_2$CH$_2$CN

We use the CDMS entry (tag 56 507 version 1) which is based on spectroscopic parameters from Belloche et al. (2008). Transition frequencies in the range of our survey were published by Bogey et al. (1990).

Sgr B2(N): the parameters of aminoacetonitrile are listed in Table 36. The detection of this complex organic molecule was reported in Belloche et al. (2008). It has only been detected in Sgr B2(N) so far, and a correction of the column density for the contribution of vibrational modes to the partition function was reported by Braakman et al. (2010).

Sgr B2(M): aminoacetonitrile is not detected.

4.4.32. Hydrogen sulfide H$_2$S

We use the CDMS entries for the ^{32}S, ^{34}S, and ^{33}S isotopologues (tags 34 502, 36 504, and 35 503, all version 1). The entry for the main species is based on a modification of results in Belov et al. (1995). The entries for the ^{34}S and ^{33}S isotopologues are based on Saleck et al. (1995a). The frequencies for the only observed transition were published by Huiszoon (1971) for the ^{32}S and ^{34}S isotopologues.

Sgr B2(N): the parameters of hydrogen sulfide are listed in Table 37. Only one transition is detected in the 1.3 mm window. It is very strong (23 K). The model parameters are not constrained. The transitions of the ^{34}S and ^{33}S isotopologues are too heavily blended with emission from other species to be included in the complete model.

Sgr B2(M): the parameters of all entries related to hydrogen sulfide are listed in Table 85. Like toward Sgr B2(N), only one transition of the main isotopologue is detected at 216.71 GHz ($E_1/k = 74$ K). It is very strong (20.6 K), and thus requires a high temperature. The corresponding ^{34}S transition is detected at 214.38 GHz with a peak temperature of 2.8 K, indicating that the transition of the main isotopologue is optically thick. Even with this indication, we do not have enough constraints to derive the temperature and source size independently. Two additional components are added to the model to account for the wing emission. We arbitrarily use the same temperature and source size as for the main component. The ^{33}S isotopologue is blended with other species but it contributes significantly (about 50%) to the observed emission at 215.51 GHz, which led us to include it in the complete model.

4.4.33. Cyanoacetylene HC$_3$N

We use the CDMS entries for all isotopologues and vibrationally excited states, all version 1 except version 2 for the states $v_6 = v_7 = 1$ and $v_4 = 1$ of the main isotopologue. Most entries for the main isotopologue are based on Thorwirth et al. (2000a). Entries of the interacting $v_4 = 1/v_7 = 4/v_5 = v_7 = 1/v_6 = 2$ states were generated by extension and modification

of Yamada & Creswell (1986). The $v_3 = 1$ and $v_2 = 1$ entries are based on Sanz et al. (2005). The ^{13}C entries, including the doubly substituted ones, are based on Thorwirth et al. (2001), and those of HC$_3$^{15}N on Fayt et al. (2004). Additional measurements in the range of our survey were taken from Creswell et al. (1977) for the ground vibrational states of the main as well as singly substituted ^{13}C and ^{15}N entries, from Yamada et al. (1995) for $v = 0$ of the main species, Yamada & Creswell (1986) and Mbosei et al. (2000) for several excited states of the main isotopologue, and Thorwirth et al. (2001) for the HC$_3$^{15}N entries.

The resonant interactions between $v_7 = 4$ and $v_5 = v_7 = 1$ have been approached by the measurements of Yamada & Creswell (1986) and Mbosei et al. (2000), but not reached. Therefore, predicted transition frequencies involving these resonances may differ from the actual frequencies by amounts exceeding three times the predicted uncertainties. The interacting levels in the frequency range of our survey are $J = 10$ of $v_7 = 4$, $l = 2^-$, and $v_5 = v_7 = 1$, $l = 0^-$ and possibly $J = 26$ of $v_7 = 4$, $l = 2^+$, and $v_5 = v_7 = 1$, $l = 2^+$ as well as $J = 27$ of $v_7 = 4$, $l = 2^-$, and $v_5 = v_7 = 1$, $l = 2^-$.

Sgr B2(N): the parameters of all entries related to cyanoacetylene are listed in Table 38. Cyanoacetylene is difficult to model because it is widespread in the Sgr B2 molecular cloud (see, e.g., Fig. 4 of Jones et al. 2008) and the emission at 3 mm is optically thick ($\tau_{max} \sim 4.5$). We model the emission with four velocity components: one component for each hot core, and one blueshifted and one redshifted components to account for the line wings. The components associated with the hot cores have to be moderately compact to match the opacities directly derived from the ratio of the ^{12}C and ^{13}C detected transitions. The temperature has in turn to be higher than 50 K otherwise the optically thick lines saturate too much and do not match the observed spectrum. The ^{13}C isotopologues are clearly detected at 3 mm, with optically thin transitions ($\tau_{max} \sim 0.24$), but the range of lower-level energies is too narrow (15 to 33 K) to constrain the temperature well. The ^{15}N isotopologue is clearly detected at 106.00 GHz (with little contamination from CH$_3$SH and C$_2$H$_5$CN, $v_{13}+v_{21} = 1$), and it significantly contributes to the emission detected at other frequencies. One doubly-substituted ^{13}C isotopologue is detected at 105.33 GHz (H^{13}CC^{13}CN) and it, as well as the two other doubly-substituted ^{13}C isotopologues, significantly contributes to the emission detected at other frequencies. This justifies their inclusion in the complete model. The model for the wing components of the ^{13}C isotopologues has a $\frac{^{12}C}{^{13}C}$ isotopic ratio lower than 20, but this is rather a shortcoming of our simple radiative transfer method than a true indication that the isotopic ratio is lower than 20. The lineshape of the main isotopologue is indeed not very well reproduced. HCC^{13}C^{15}N is not detected.

We also detect emission lines from within ten vibrationally excited states of the main isotopologue: $v_7 = 1$, $v_7 = 2$, $v_6 = 1$, $v_7 = 3$, $v_5 = 1$, $v_6 = v_7 = 1$, $v_4 = 1$, $v_7 = 4$, $v_5 = v_7 = 1$, and $v_6 = 2$ (223, 446, 499, 663, 663, 721, 864, 883, 886, and 1013 cm^{-1}, respectively), with $\tau_{max} \sim 5$, 4, 3, 4, 4, 1.7, 0.6, 0.8, 0.8, and 0.6, respectively. Transitions of some of the ^{13}C isotopologues from within the first six states are also detected (for one, two or three of them, depending on the state) and are all optically thin. This is, to the best of our knowledge, the first detection in space of the ^{13}C isotopologues in their $v_7 = 3$ (HCC^{13}CN), $v_5 = 1$ (H^{13}CCCN), and $v_6 = v_7 = 1$ (HC^{13}CCN and HCC^{13}CN, and H^{13}CCCN tentatively) excited

states[13]. Our previous interferometric detection of transitions of HC$_3$N, $v_7 = 1$, HC$_3$N, $v_4 = 1$, and HC^{13}CCN, $v_7 = 1$ indicates that most of the emission detected with the 30 m telescope is very compact (see Fig. 5 of Belloche et al. 2008). Source sizes were estimated from the interferometric maps: $\sim 2.5''$ for the northern hot core for HC$_3$N, $v_7 = 1$; $\sim 1.5''$ for the components detected in each wing for HC$_3$N, $v_7 = 1$; $\sim 1.6''$ for the main (southern) hot core for HC^{13}CCN, $v_7 = 1$; $\sim 1.4''$ for the main hot core for HC$_3$N, $v_4 = 1$. These sizes were used as guidelines to model the 30 m emission of all states. A temperature of ~ 200 K was derived from the optically thick lines of $v_6 = v_7 = 1$ assuming the source size measured for $v_4 = 1$. This temperature was used for (nearly) all other states and the column densities were adjusted with the ^{13}C isotopologues if detected, or the optically thin lines of the main isotopologue if not. Like for methyl cyanide (Sect. 4.4.17), the column density parameter needed to fit the emission of the excited states increases with their energy, suggesting that the vibration temperature is higher than the rotation temperature, probably because of radiative pumping[14]. Given that the LTE modeling yields different sizes and rotation temperatures for the different states, we do not attempt to estimate any vibration temperature. There is no clear indication for wing emission for $v_7 = 3$ and the states further above, hence these states are modeled with only two components. No transition from $v_4 = v_7 = 1$, $(v_4 = 1, v_7 = 2)$, $v_5 = 2$, $v_3 = 1$ (2079 cm^{-1}), and $v_2 = 1$ (2274 cm^{-1}) of the main isotopologue is detected, neither from $v_4 = 1$ of the ^{13}C isotopologues and from $v_7 = 1$ of the ^{15}N isotopologue.

We note one minor issue: the transition of the entry $v_7 = 4/v_5 = v_7 = 1$ of HC$_3$N at 100.431 GHz would fit better the observed spectrum if its frequency was 2 or 3 MHz higher. Its uncertainty (0.3 MHz) is much higher than for the other nearby transitions which are well fitted. This discrepancy may be related to resonant interactions between $v_7 = 4$ and $v_5 = v_7 = 1$ as mentioned above.

Sgr B2(M): the parameters of all entries related to cyanoacetylene are listed in Table 86. The emission is modeled with three velocity components: one main component and two components to account for the linewing emission. The line ratios between the ^{12}C and ^{13}C isotopologues indicate that all transitions are optically thin. The source size is not constrained. A temperature of 60 K fits relatively well all detected transitions. The transitions detected in the 2 mm window seem to indicate a lower temperature for the wing components. The ^{15}N isotopologue is not detected.

We also detect emission lines from within seven vibrationally excited states of the main isotopologue: $v_7 = 1$, $v_7 = 2$, $v_6 = 1$, $v_7 = 3$, $v_5 = 1$, $v_6 = v_7 = 1$, and $v_4 = 1$. Transitions from within the first three vibrationally excited states of the ^{13}C isotopologues are also detected. The interferometric observations of de Vicente et al. (2000) indicate that the source size of these excited states is smaller than $3'' \times 5''$. We find that the transitions

---

from within $v_7 = 1$ of the main isotopologue are optically thick, while all transitions from within the higher excited states are optically thin. A source size of $1.3''$ and a temperature of 200 K fit the optically thick transitions of $v_7 = 1$ both at 3 and 1.3 mm relatively well, as well as the ^{13}C optically thin transitions of $v_7 = 1$. We keep these parameters for all other states. Like for Sgr B2(N), the column density parameter needed to fit the emission of the excited states increases with their energy. We did not find a good fit to the observed spectra when we added to the model of the ground state a hot component similar to the one used for the vibrationally excited states. Such a component produces in particular too strong ^{13}C lines at 1.3 mm, although this may be partly due to an overestimate of the level of the baseline in some places. A more detailed analysis would be necessary to resolve this inconsistency.

4.4.34. Cyanodiacetylene HC$_5$N

We use the CDMS entries for the ground state and the first vibrationally excited state $v_{11} = 1$ (tags 75 503 and 75 504, both version 1, Yamada et al. 2004).

Sgr B2(N): cyanodiacetylene is not detected.

Sgr B2(M): the parameters of all entries related to cyanodiacetylene are listed in Table 87. Simultaneously fitting the transitions detected at 3 and 1.3 mm requires two temperature components. All transitions are optically thin ($\tau_{max} = 0.11$). The ^{13}C isotopologues are not detected.

We also detect emission lines from within the vibrationally excited state $v_{11} = 1$ (106.8 cm^{-1}), but with a low signal-to-noise ratio. These transitions are well fitted with the hot component used for the ground state.

4.4.35. Ethynyl isocyanide HCCNC

We use the JPL entry 51 004 (version 1, Guarnieri et al. 1992).

Sgr B2(N): the parameters of ethynyl isocyanide are listed in Table 39. The detection relies on only two transitions, one uncontaminated at 99.35 GHz and one blended with the second component of CH$_3$OCHO at 109.29 GHz where, depending on the true level of the baseline, they may be in conflict. This detection should therefore be viewed as very tentative. If confirmed, it would be the first detection of HCCNC in a hot core (see Kawaguchi et al. 1992; Gensheimer 1997, for detections toward TMC1 and IRC+10216, respectively). We assumed the same source size and temperature as for the main component of HC$_3$N. The ^{13}C and ^{15}N isotopologues are not detected. No transition from within the vibrationally excited states $v_7 = 1$, $v_6 = 1$, and $v_4 = 1$ of the main isotopologue is detected.

Sgr B2(M): ethynyl isocyanide is not detected.

4.4.36. Hydrogen cyanide HCN

We use the CDMS entries for all isotopologues and vibrationally excited states (version 4 for HCN, version 2 for HCN, $v_2 = 1$ and H^{13}CN, and version 1 for all other entries). The HCN, $v_2 = 0$ and $v_2 = 1$ entries are based mainly on Thorwirth et al. (2003), those for higher excited states mainly on Zelinger et al. (2003).

---

[13] Pardo et al. (2007) report the detection of one transition of H^{13}CCCN in its $v_7 = 3$ state toward the protoplanetary nebula CRL 618. Transitions from within the $v_7 = 1$, $v_7 = 2$, and $v_6 = 1$ states were reported by Wyrowski et al. (1999) toward the hot core G10.47+0.03.

[14] If a direct pumping mechanism from the ground state exists for each of the ten excited states listed above, then it has to occur at ~ 45, 22, 20, 15, 15, 14, 12, 11, 11, and 10 μm, respectively. Direct infrared pumping should be possible for $v_6 = 1$, $v_5 = 1$, $v_6 = v_7 = 1$, and maybe for $v_7 = 1$. The intensities of $2v_7$ and v_4 are probably too low to support direct infrared pumping for $v_7 = 2$ and $v_4 = 1$.

Among the transitions observed in the current survey, $v_2 = 0$ data were taken from de Lucia & Gordy (1969), and for several of the higher excited transitions from de Lucia & Helminger (1977). The H^{13}CN entries are mostly based on Fuchs et al. (2004) and Cazzoli & Puzzarini (2005) for $v_2 = 1$ and $v_2 = 0$, respectively. The entries for the ground vibrational states of HC^{15}N, H^{13}C^{15}N, and DCN were based largely on Cazzoli et al. (2005), Fuchs et al. (2004), and Brünken et al. (2004), respectively.

Sgr B2(N): the parameters of all entries related to hydrogen cyanide are listed in Table 40. The molecule is detected at 3 mm both in emission and absorption. Its ^{13}C isotopologue is detected at 3, 2, and 1.3 mm and its ^{15}N isotopologue at 3 and 1.3 mm. H^{13}C^{15}N is detected at 83.73 GHz, to our knowledge for the first time in space. The parameters of the emission components are not well constrained. The diffuse-cloud absorption components were modeled first on the ^{13}C isotopologue, then transfered to the main isotopologue and readjusted when they were too weak, and finally transfered back to the ^{13}C and ^{15}N isotopologues. Only a few diffuse-cloud components are detected for the latter, but the two self-absorption components are prominent. Some absorption components are too deep for the main isotopologue. The possible reasons for this discrepancy are the same as for CS (see Sect. 4.4.27).

Following the detection and modeling of several transitions from within vibrationally excited states of HCN toward Sgr B2 by Rolffs et al. (2011), we include $v_2 = 1$ (712.0 cm^{-1}) and $v_2 = 2$ (1411.4 cm^{-1}) in our model, with the source size and rotation temperature derived by these authors. Four transitions from within $v_2 = 1$ are detected at 3 mm, only one from within $v_2 = 2$. There is no detection for $v_2 = 3$, $v_1 = 1$, and $v_3 = 1$. One transition of the ^{13}C isotopologue from within $v_2 = 1$ is detected at 2 mm.

Sgr B2(M): the parameters of all entries related to hydrogen cyanide are listed in Table 88. Like for Sgr B2(N), the parameters of the emission components are not well constrained. We followed the same strategy as for Sgr B2(N) to model the diffuse-cloud absorption components. Only a few of them are detected in HC^{15}N. The H^{13}C^{15}N isotopologue is tentatively detected in absorption at 83.73 GHz. We also detect DCN at 1.3 mm, but this detection is based on only one transition, so it is uncertain.

We included $v_2 = 1$ and $v_2 = 2$ in our model with the same temperature as for Sgr B2(N). We reduced the source size to limit the strength of the transition of $v_2 = 2$ in the 1.3 mm window, but its lineshape is not good (too much saturation). The vibrational states $v_2 = 3$, $v_3 = 1$, and $v_1 = 1$ are likely detected at 3 mm too, but the LTE model that fits them predicts much too strong lines at 1.3 mm, so we did not include them in the complete model. The vibrational state $v_2 = 1$ of the ^{13}C isotopologue may be detected at 172.63 GHz, but the assignment is uncertain and we do not include it in the complete model.

4.4.37. Formamide NH$_2$CHO

We use the CDMS entries for the vibrational ground state of the ^{12}C and ^{13}C isotopologues (tags 45 512 and 46 512, both version 2) as well as for $v_{12} = 1$ of the main species (tag 45 516 version 1). These entries have been updated or created in the review process of this article. They are based largely on Motiyenko et al. (2012), but also contain additional data. Laboratory data in the range of our survey were published by Kryvda et al. (2009).

The entry for $v_{12} = 1$ of the ^{13}C isotopologue was prepared by one of us (HSPM) based on data from Stubgaard (1978).

Sgr B2(N): the parameters of all entries related to formamide are listed in Table 41. The strongest transitions detected at 3 mm are optically thick ($\tau_{max} \sim 7.5$). Transitions with $E_1/k < 10$ K are seen both in emission and in absorption (with a velocity offset of 19 km s^{-1}, see, e.g., at 81.69, 84.54, and 87.85 GHz). The ^{13}C isotopologue is detected at 3 mm with optically thin ($\tau_{max} \sim 0.38$) transitions of lower-level energy up to 57 K (at 105.95 GHz). The temperature is somewhat better constrained with the weak transitions of the main isotopologue that are optically thin like, e.g., at 101.30, 104.18, and 108.33 GHz ($E_1/k = 185$, 385, and 150 K, respectively). The source size is in turn constrained by the optically thick lines. The presence of a second velocity component from the northern hot core is clearly seen. The ^{15}N and ^{18}O isotopologues are not detected at 3 mm because of blends with emission from other species.

We also detect emission lines from within the vibrationally excited state $v_{12} = 1$ of the main isotopologue (289 cm^{-1}). They are optically thin ($\tau_{max} \sim 0.75$) and two velocity components are clearly detected. Transitions of the ^{13}C isotopologue from within $v_{12} = 1$ are predicted to be weak. A few of them contribute significantly (>30%) to the detected emission, and one is potentially detected at 84.33 GHz, which justifies including this entry in the complete model. Transitions pertaining to $v_{12} = 1$ of the main isotopologue have been reported in the ISM very recently only (Motiyenko et al. 2012). In addition, it is worthwhile mentioning that ten unidentified lines observed toward Sgr B2(N) by Nummelin et al. (2000) can be assigned, at least in part, to formamide in its $v_{12} = 1$ excited vibrational state.

Sgr B2(M): the parameters of all entries related to formamide are listed in Table 89. Transitions of formamide are detected at 3 mm with lower-level energies ranging from 6 K (84.54 GHz) to 58 K (106.11 GHz). At 1.3 mm, they range up to 256 K (212.25 GHz). Two components, a cold one and a warm one, are necessary to fit the 3 and 1.3 mm transitions simultaneously. All transitions are optically thin ($\tau_{max} = 0.12$ and 0.035 for the cold and warm components at 3 mm, respectively, and 0.07 and 0.17 at 1.3 mm). The source sizes are thus not constrained. Two additional components in absorption are added to the model to account for the self-absorption seen at, e.g., 84.54 and 87.85 GHz.

4.4.38. Formyl cation HCO$^+$

We use the CDMS entries for the ^{12}C, ^{13}C, ^{18}O, and ^{17}O isotopologues (tags 29 507, 30 504, both version 2, and 31 506, 30 505, both version 1). The entries are based on Tinti et al. (2007), Lattanzi et al. (2007), Schmid-Burgk et al. (2004), and Dore et al. (2001a), respectively. The $J = 1$–0 transitions were taken from Buffa et al. (1994) for HCO$^+$, Schmid-Burgk et al. (2004) for the ^{13}C and ^{18}O isotopologues, and from Dore et al. (2001b) for the ^{17}O isotopologue.

Sgr B2(N): the parameters of all entries related to the formyl cation are listed in Table 42. The model for this ion and its isotopologues is based on the model constructed for Sgr B2(M) and already reported in Menten et al. (2011). The components in emission are very poorly constrained. The parameters for the diffuse-cloud absorption components were essentially optimized for the ^{13}C isotopologue and then transfered to the other

isotopologues assuming the isotopic ratios listed in Table 2. Both self-absorption components (at $v_{\rm off} \sim 0$ and 16 km s^{-1}) are prominent for the ^{18}O and ^{17}O isotopologues. A few diffuse-cloud components appear to be too weak for the former, but this could be due to an improper estimate of the level of the baseline. The main isotopologue suffers from the opposite effect: many diffuse-cloud components appear to be too deep (see Sect. 4.4.27 for possible explanations).

Sgr B2(M): the parameters of all entries related to the formyl cation are listed in Table 90. The model was already reported in Menten et al. (2011). The emission components are poorly constrained. Some diffuse-cloud absorption components seem to be detected in the ^{17}O isotopologue, but the uncertain level of the baseline prevents an accurate analysis.

4.4.39. Thiomethylium HCS$^+$

We use the CDMS entry (tag 45 506) which is based on frequencies summarized by Margulès et al. (2003). Measurements in the range of our survey were reported by Gudeman et al. (1981) and Tang & Saito (1995).

Sgr B2(N): the parameters of thiomethylium are listed in Table 43. The 5–4 transition of HCS$^+$ is clearly detected at 213.36 GHz. However the 2–1 transition at 85.35 GHz is blended with a diffuse-cloud absorption component of c-C$_3$H$_2$ and we see no evidence for emission at that frequency. Our LTE modeling yields an acceptable fit at both frequencies only if we assume a compact source ($FWHM < 10''$) and a temperature higher than ~50 K. A more extended source would produce emission at 85.35 GHz that would not be consistent with our spectrum. Given that HCS$^+$ was also claimed to be detected toward Sgr B2(N) at 256.03 GHz by Nummelin et al. (1998), we consider the detection as reliable, even if we detect only one line in our survey. However, the parameters of our model are very uncertain.

Sgr B2(M): the parameters of thiomethylium are listed in Table 91. The situation is very similar to the case of Sgr B2(N). In addition, we exclude that the column density of the overlapping absorption component of c-C$_3$H$_2$ is underestimated (which would allow for a more extended HCS$^+$ emission) because it fits the absorption feature at 82.10 GHz reasonably well. Nummelin et al. (1998) and Sutton et al. (1991) report the detection of HCS$^+$ at 256.03 and 341.35 GHz, respectively, toward Sgr B2(M), which again gives us confidence in the identification of this molecule in our survey.

4.4.40. Singly deuterated water HDO

We use the JPL entry (tag 19 002 version 3). The entry is based on Johns (1985), and rest frequencies of transitions at 3 mm were taken in particular from Erlandsson & Cox (1956) and de Lucia et al. (1971).

Sgr B2(N): the parameters of singly deuterated water are listed in Table 44. Only one line is detected at 80.58 GHz ($E_1/k = 43$ K) with two velocity components. The temperature has to be lower than 300 K to be consistent with the upper limit derived for another transition with $E_1/k = 826$ K at 87.96 GHz.

The detection of other, higher-frequency transitions of HDO toward Sgr B2(N) and (M) gives us confidence that the detection at 3 mm can be trusted (see, e.g., Comito et al. 2003, 2010). However, our model parameters based on the 3 mm window only are not constrained, except for the upper limit on the temperature mentioned above.

Sgr B2(M): the parameters of singly deuterated water are listed in Table 92. The situation is the same as for Sgr B2(N).

4.4.41. Hydrogen isocyanide HNC

We use the CDMS entries for the ^{12}C and ^{13}C isotopologues (tags 27 502 and 28 515, versions 2 and 1, respectively), and the JPL entry for the ^{15}N isotopologue (tag 28 006 version 1). The entries are based on results from Thorwirth et al. (2000b), van der Tak et al. (2009), and Pearson et al. (1976), respectively. The $J = 1$–0 transition of the main isotopologue was taken from Saykally et al. (1976).

Sgr B2(N): the parameters of all entries related to hydrogen isocyanide are listed in Table 45. The emission and absorption components of hydrogen isocyanide were modeled following the same strategy as for hydrogen cyanide (Sect. 4.4.36). Both the ^{13}C and ^{15}N isotopologues are detected, mainly the two self-absorption components. A few diffuse-cloud components are also detected for the ^{13}C isotopologue. The other ones are too weak or blended with emission from other species.

Sgr B2(M): the parameters of all entries related to hydrogen isocyanide are listed in Table 93. The model was prepared following the same strategy as for Sgr B2(N). The poor baseline quality around 88.9 GHz prevents the secure detection of diffuse-cloud absorption components for the ^{15}N isotopologue.

4.4.42. Isocyanic acid HNCO

We use the CDMS entries for the vibrational ground state of the ^{12}C isotopologue (tag 43 511 version 1) by Lapinov et al. (2007) with additional measurements in the range of our survey by Hocking et al. (1975), the JPL entries for the ^{13}C and ^{18}O isotopologues (tags 44 008 and 45 006, both version 1, Hocking et al. 1975), and private entries for the vibrationally excited states $v_5 = 1$, $v_6 = 1$, and $v_4 = 1$ of the main isotopologue, prepared by one of us (HSPM) based on a preliminary, unpublished analysis of the ground and the four lowest excited states. The excited states data were summarized in Niedenhoff et al. (1996). Transition frequencies in the range of our survey were published by Yamada & Winnewisser (1977) and Yamada (1977).

The C atom of HNCO is close to the center of mass of the molecule. Therefore, the transitions of HN^{13}CO are frequently overlapped by those of the main species, especially at low frequencies.

Sgr B2(N): the parameters of all entries related to isocyanic acid are listed in Table 46. Our model for the vibrational ground state of isocyanic acid was already reported in Brünken et al. (2010). The model for the ^{13}C isotopologue is difficult to constrain because its transitions are always blended with the emission of the blueshifted wing of the main isotopologue. We simply

used a scaled version of the model of the latter. The ^{18}O isotopologue is detected at only one frequency (83.19 GHz).

We also detect emission lines from within three vibrationally excited states of the main isotopologue: $v_5 = 1$, $v_6 = 1$, and $v_4 = 1$ (577, 656, and 777 cm^{-1}, respectively). The detected transitions are all optically thin ($\tau_{max} \sim 0.17, 0.18$, and 0.26, respectively), and the presence of a second velocity component is plausible for $v_5 = 1$. The column density parameters required to fit the vibrationally excited states are higher than for the ground state. This may be due to radiative pumping. Using Eq. (13) with the ground state as reference state and only for the velocity component with a source size of 2.4″, we derive vibration temperatures of 310 ± 20, 290 ± 10, and 390 ± 20 K for $v_5 = 1$, $v_6 = 1$, and $v_4 = 1$, respectively. If a direct pumping mechanism from the ground state exists for each of the three excited states listed above, then it has to occur at ~17, 15, and 13 μm, respectively. Direct infrared pumping is likely for $v_5 = 1$ and $v_6 = 1$. The larger effect seen for $v_4 = 1$ is compatible with the higher intensity of the infrared band ν_4.

Sgr B2(M): the parameters of all entries related to isocyanic acid are listed in Table 94. The model was already reported in Brünken et al. (2010), except that we added a third component to account for the wing emission, which is prominent for the low-energy transitions only, indicating that it has a low excitation temperature. Like for Sgr B2(N), the emission of the ^{13}C isotopologue is always blended with the main isotopologue. The ^{18}O isotopologue is not detected.

4.4.43. Isothiocyanic acid HNCS

We use the CDMS entry (tag 59 503 version 1). The rest frequencies were summarized in Niedenhoff et al. (1995), those in the range of our survey were taken from Yamada et al. (1979).

Sgr B2(N): the parameters of isothiocyanic acid are listed in Table 47. Our survey alone does not provide a secure detection of this molecule: the three lines potentially detected at 3 mm are all partially blended (with absorption components of c-C_3H_2, unidentified lines, and CH_3OCH_3, respectively). However, the detection by Halfen et al. (2009) at a position about 10″ offset from Sgr B2(N) looks secure enough to include this molecule in our complete model. We assumed a rotation temperature of 20 K, consistent with the temperature derived by these authors (18 ± 3 K), and a beam filling factor of unity, consistent with the extent of the emission (at least $3' \times 6'$) seen in maps of Adande et al. (2010). All three lines are optically thin ($\tau_{max} \sim 0.014$). The column density derived from our modeling is about three times higher than the value obtained by Halfen et al. (2009) from an excitation diagram analysis. The position offset between both datasets is small compared to the large beam of the ARO 12 m telescope. If the emission is extended and relatively uniform, this should not affect the column density estimates. We note that we assumed a linewidth smaller than the one measured by Halfen et al. (2009) (20 versus 25 km s^{-1}), but using a higher value would increase the discrepancy even further. The reason for this discrepancy is still unclear.

Sgr B2(M): the parameters of isothiocyanic acid are listed in Table 95. The emission of this molecule is less blended than toward Sgr B2(N). It is detected at 93.83 and 105.56 GHz. We

model the emission with the same parameters as HSCN, apart for the column density (see Sect. 4.4.47).

4.4.44. Cyanic acid HOCN

We use the CDMS entry (tag 43 510 version 1, Brünken et al. 2009a).

Sgr B2(N): the parameters of cyanic acid are listed in Table 48. Our model for the vibrational ground state of cyanic acid was already reported in Brünken et al. (2010). It has been slightly updated and we removed the two high-temperature components that were not really constrained. One line is clearly detected at 83.90 GHz but the other main transition in the 3 mm window (at 104.87 GHz) is blended with emission from C_2H_3CN, $v_{11} = 1/v_{15} = 1$ and $^{13}CH_3CH_2CN$. Our complete model overestimates the observed intensity of this blended feature, but this is likely due to an overestimate of the baseline level. The transitions are optically thin ($\tau_{max} \sim 0.028$).

Sgr B2(M): the parameters of cyanic acid are listed in Table 96. The model was already reported in Brünken et al. (2010).

4.4.45. Protonated carbon dioxide HOCO$^+$

We use the JPL entry (tag 45 010 version 1, Bogey et al. 1988).

Sgr B2(N): the parameters of protonated carbon dioxide are listed in Table 49. Two transitions are detected at 3 mm, one at 85.53 GHz ($E_1/k = 6.2$ K) blended with C_2H_3CN, $v_{15} = 1$, and one at 106.91 GHz ($E_1/k = 10$ K) partially blended with an unidentified line. The emission at 85.53 GHz looks extended in the large-scale maps of Jones et al. (2008) so we assumed a beam-filling factor of unity. The peak-temperature ratio of both lines plus the upper limit for a transition at 85.85 GHz ($E_1/k = 44$ K) constrain the temperature to be lower than 20 K, provided the LTE assumption is valid. The transitions are all optically thin ($\tau_{max} \sim 0.017$).

Sgr B2(M): the parameters of protonated carbon dioxide are listed in Table 97. The same transitions as toward Sgr B2(N) are detected. They are also optically thin ($\tau_{max} \sim 0.026$).

4.4.46. Hydroxymethylidynium HOC$^+$

We use the CDMS entry (tag 29 504 version 1). Rest frequencies for the ground and first excited bending mode were published by Amano & Maeda (2000), 3 mm data were taken from Gudeman & Woods (1982).

Sgr B2(N): the parameters of hydroxymethylidynium are listed in Table 50. Only one transition is detected at 3 mm, both in emission and absorption. We assumed a beam-filling factor of unity and a temperature of 20 K for the emission component. The ^{13}C isotopologue is not detected. We do not detect any transition from within the vibrationally excited state $v_2 = 1$ of the main isotopologue either.

Sgr B2(M): the parameters of hydroxymethylidynium are listed in Table 98. Only one line is detected, mostly in absorption. The parameters are very poorly constrained.

4.4.47. Thiocyanic acid HSCN

We use the CDMS entry (tag 59 505 version 1, Brünken et al. 2009b).

Sgr B2(N): the parameters of thiocyanic acid are listed in Table 51. Our survey alone is not sufficient to secure the detection of this molecule but, like for isothiocyanic acid (see Sect. 4.4.43), we include it in our complete model because it was rather convincingly detected by Halfen et al. (2009). We assumed the same size and temperature as for HNCS, which is consistent with the findings of these authors (extended emission and $T_{rot} = 19 \pm 2$ K). All transitions in the 3 mm window are at least partially blended with emission from other species. At 91.75 GHz, the synthetic spectrum accounts for only ~50% of the intensity of the detected feature, suggesting that the HSCN emission is blended with a still unidentified line. All transitions are optically thin ($\tau_{max} \sim 0.014$).

Sgr B2(M): the parameters of thiocyanic acid are listed in Table 99. The molecule is clearly detected at 91.75 and 103.22 GHz. The other transitions at 3 mm are too weak or blended with other species. We model the emission with a beam filling factor of unity because the map of Adande et al. (2010) shows that it is extended over several arcminutes. We use a temperature close to the one measured by Halfen et al. (2009) toward Sgr B2(N). A higher temperature produces too strong $K = 1$ transitions. All transitions are optically thin ($\tau_{max} \sim 0.009$).

4.4.48. Diazenylium N_2H^+

We use the CDMS entries with hyperfine structure for the ^{14}N and ^{15}N isotopologues (tags 29 506 version 3, 30 507 and 30 508, both version 2). Predictions for the main isotopologue were generated from an unpublished analysis using hyperfine-free center frequencies mainly from Amano et al. (2005) and Pagani et al. (2009). The ^{14}N hyperfine splitting values were taken from Caselli et al. (1995). Entries for the ^{15}N isotopologues were generated from results published by Dore et al. (2009). The $J = 1$–0 transitions were taken from Gudeman (1982).

Sgr B2(N): the parameters of diazenylium are listed in Table 52. The 1–0 transition of diazenylium is detected both in emission and in multiple absorption components produced by spiral-arm diffuse clouds along the line of sight. The hyperfine structure of the emission component is not resolved but it is for some of the absorption components. The shape of the emission and self-absorption components is relatively well reproduced, but the model parameters are certainly not unique. Fifteen diffuse-cloud components were needed to fit the absorption part. Some of them are blended with emission from other species, which implies that their parameters are model-dependent and thus more uncertain. The ^{15}N isotopologues are not (and cannot be) detected because their transitions are heavily blended with emission from $^{13}CH_3OH$ and HC_3N, $v_7 = 1$.

Sgr B2(M): the parameters of all entries related to diazenylium are listed in Table 100. Diazenylium is detected in emission and in absorption. We fit the diffuse-cloud absorption with 9 components. $^{15}NNH^+$ is detected in absorption at 90.26 GHz, but $N^{15}NH^+$ is blended at 91.20 GHz with a transition from within the vibrationally excited state $v_7 = 1$ of HC_3N, which prevents a firm identification.

4.4.49. Cyanamide NH_2CN

We use the JPL entry for the ^{12}C isotopologue (tag 42 003 version 1), based on Birk et al. (1993) with measurements in the frequency range of our survey from Johnson et al. (1976) and Read et al. (1986), and the CDMS entry for the ^{13}C isotopologue (tag 43 515 version 1) based on Kraśnicki et al. (2011b).

The C atom of cyanamide is very close to the center of mass of the molecule. Therefore, the transitions of $NH_2^{13}CN$ are frequently overlapped by those of the main species, in particular at long wavelengths.

Sgr B2(N): the parameters of all entries related to cyanamide are listed in Table 53. About ten transitions of cyanamide are detected at 3 mm, with lower-level energies ranging from 9.6 K (at 99.97 GHz) to 136 K (80.06 GHz). A fit with two temperature components yields a better result than with only one. The presence of a low-excitation, extended component is strongly suggested by the large-scale map of Jones et al. (2008, see their Fig. 9). Although not fully certain, the presence of a second (warm) velocity component is plausible. The emission corresponding to the warm component is optically thin for a source size of 2″ ($\tau_{max} \sim 0.9$), but this size is not constrained. The ^{13}C isotopologues were included in the complete model assuming a $^{12}C/^{13}C$ isotopic ratio of 20 because there is a hint of weak detection at 100.59 GHz and their emission is consistent with the observed spectrum at other frequencies, but the detection is not secure in itself.

Sgr B2(M): the parameters of cyanamide are listed in Table 101. We detect four transitions with lower-level energies ranging from 10 K (99.97 GHz) to 24 K (99.31 GHz). We see no evidence at 3 and 1.3 mm for the presence of a warm component (e.g., upper limit of a transition with $E_1/k = 81$ K at 99.89 GHz). The ^{13}C isotopologue is not detected.

4.4.50. Singly deuterated ammonia NH_2D

We use the CDMS entry (tag 18 501 version 1). The spectroscopic parameters were taken from Müller et al. (2010b). That work employed transition frequencies in the range of our survey from de Lucia & Helminger (1975) and Cohen & Pickett (1982).

Sgr B2(N): the parameters of singly deuterated ammonia are listed in Table 54. Only one transition is clearly detected at 99.12 GHz ($E_1/k = 257$ K), with two velocity components. Another transition (with $E_1/k = 29$ K) significantly contributes (~30%) to a feature detected at 85.93 GHz, the rest of the emission coming from C_2H_3CN, $v_{11} = 2$ and CH_3OCHO. The temperature is not well constrained. The emission is optically thin ($\tau_{max} \sim 0.17$).

Sgr B2(M): singly deuterated ammonia is not detected.

4.4.51. Nitrogen sulfide radical NS

We use the CDMS entry (tag 46 515 version 1). Predictions were generated from a combined fit of several isotopic species, similar to the one from Saleck et al. (1995b). The data for the main isotopologue were contributed by Lee et al. (1995).

Sgr B2(N): the parameters of the nitrogen sulfide radical are listed in Table 55. All transitions detected at 3 mm have the same lower-level energy (4.5 K). However, several higher-energy transitions are detected in our 1.3 mm survey, implying a temperature of 20 K at least. An additional self-absorption component is needed to reproduce the shape of the lines detected at 3 mm. No minor isotopologue is detected.

Sgr B2(M): the parameters of nitrogen sulfide radical are listed in Table 102. The model is constructed in a similar way as for Sgr B2(N). The emission component underestimates the transitions around 115.57 GHz while those around 115.16 GHz, with the same lower-level energy, are well fitted.

4.4.52. Carbonyl sulfide OCS

We use the CDMS entries for the vibrational ground state of the ^{12}C (Golubiatnikov et al. 2005), ^{13}C (Dubrulle et al. 1980), ^{34}S (Vanek et al. 1989), ^{33}S, and ^{18}O (Burenin et al. 1981) isotopologues and for the vibrationally excited state $v_2 = 1$ of the main isotopologue (Morino et al. 2000) (tags 60 503 version 2, 61 502, 62 505, 61 503, 62 506, and 60 504, all version 1). (Additional) transition frequencies in the range of our survey were contributed by Dubrulle et al. (1980) for all species, by Winton & Gordy (1970) and van Dijk & Dymanus (1974) for the main isotopologue in its ground vibrational state, and by Larsen & Winnewisser (1974) for the ^{13}C isotopologue and for $v_2 = 1$ of the main species.

Sgr B2(N): the parameters of all entries related to carbonyl sulfide are listed in Table 56. The ^{13}C, ^{34}S, and ^{33}S isotopologues are clearly detected at 3 mm with two velocity components. The flux of the ^{34}S isotopologue detected by Friedel et al. (2004) at 106.79 GHz with BIMA with a beam of $23'' \times 5''$ toward Sgr B2(N) agrees within 25% with the flux that they detected with the NRAO 12 m telescope, which means that the emission is dominated by a compact component. However, the large-scale Mopra maps of Jones et al. (2008) also show some extended emission from the main isotopologue (see their Fig. 6). The range of lower-level energies of the transitions detected at 3 mm is limited, so the temperature is not well constrained by the minor isotopologues. However, the transitions of the main isotopologue are optically thick ($\tau_{max} \sim 4$) and thus constrain the product of the source size and temperature. We arbitrarily assumed a source size of $8''$, then implying a temperature of ~ 60 K. Two additional components are needed to account for the line wings of the main isotopologue. Their parameters are poorly constrained. This wing emission is barely detected in the ^{13}C isotopologue, and is too weak (or blended with emission from other species) in the other isotopologues. The shape of the core of the lines detected in the main isotopologue is not well reproduced with the two velocity components. This may be due to the high optical depths and the presence of a colder, optically thick (?), foreground component as suggested by the Mopra maps but not accounted for by our simple model. The ^{18}O isotopologue may

be detected at 102.68 GHz. It is included in the complete model assuming the isotopic ratio given in Table 2, but a ^{16}O/^{18}O ratio twice lower would still be consistent with the data. The emission of the other isotopologues is too weak to be detected.

We also detect several transitions from within the vibrationally excited state $v_2 = 1$ of the main isotopologue (e.g., 97.42, 97.52, and 109.71 GHz), but the model parameters are not constrained. The wings detected in the ground-state transitions are not seen for these transitions.

Transitions belonging to the $v_2 = 1$ and $v_3 = 1$ vibrationally excited states of the main isotopologue were reported toward Orion KL by Tercero et al. (2010).

Sgr B2(M): the parameters of all entries related to carbonyl sulfide are listed in Table 103. We detect transitions from the main isotopologue and the ^{34}S isotopologue at 3 and 1.3 mm. The ^{13}C isotopologue is detected at 3 and 2 mm, and requires two temperature components to be well fitted. A third component is detected in the redshifted wing of the low-energy transitions of the main isotopologue at 3 mm, but not for the higher-energy transitions at 1.3 mm, indicating a low temperature. The other isotopologues are not detected.

4.4.53. Phosphorus nitride PN

We use the CDMS entry with hyperfine structure (tag 45 511 version 1) based on Cazzoli et al. (2006). The hyperfine parameters were taken from Raymonda & Klemperer (1971).

Sgr B2(N): the parameters of phosphorus nitride are listed in Table 57. The detection is uncertain because it relies on only one feature seen in absorption with two velocity components at 93.98 GHz. Nevertheless, we include it in the complete model because phosphorus nitride was already detected (in emission) toward Orion-KL and Sgr B2(OH) (Ziurys 1987), and more recently toward two shocked regions related to the outflow of the protostar IRAS 20 386+6751 in L 1157 (Yamaguchi et al. 2011)

Sgr B2(M): the parameters of phosphorus nitride are listed in Table 104. The case is the same as for Sgr B2(N).

4.4.54. Silicon monoxide SiO

We use the CDMS entries for SiO and its ^{29}Si, ^{30}Si, and ^{18}O isotopologues (tags 44 505, 45 504, 46 502, and 46 503, all version 1). The predictions are based on an unpublished isotope-invariant fit employing rest frequencies in the range of our survey from Lowry Manson et al. (1977) and Mollaaghababa et al. (1991) for the main isotopic species and from Cho & Saito (1998). Isotopic information on the ^{29}SiO and ^{30}SiO isotopologues come mainly from Törring (1968).

Sgr B2(N): the parameters of all entries related to silicon monoxide are listed in Table 58. Silicon monoxide is detected both in emission and absorption in the 3 mm window. The absorption consists of self-absorption, which we decompose into four components based on the detection in the ^{29}Si and ^{30}Si isotopologues, and spiral-arm diffuse-cloud components, which are detected only in the main isotopologue. Two blueshifted and red-shifted components are also added in emission to account for wing emission in the main isotopologue. The parameters of the

three components in emission are poorly constrained. Part of the self-absorption components of the ^{30}Si isotopologue is blended with emission features of NH_2CHO, $v_{12} = 1$ and CH_3OH. The ^{18}O isotopologue is not detected because of a blend with C_2H_5CN, $v_{13} + v_{21} = 1$.

Sgr B2(M): the parameters of all entries related to silicon monoxide are listed in Table 105. The main isotopologue is detected at 3 and 1.3 mm, while the ^{29}Si, ^{30}Si, and ^{18}O are detected at 3 mm only, the latter only in absorption. Three components in emission are used to reproduce the core of the lines of the main isotopologue and their wings. Their temperature has to be lower than 20 K to fit both the 3 and 1.3 mm transitions. Self-absorption is detected for all isotopologues, with two velocity components. Diffuse-cloud absorption components are detected for the main isotopologue, but the baseline level is apparently overestimated, which in turn leads to an overestimate of the column densities of these components and makes the identification of weak absorption components unreliable. The parameters of the diffuse-cloud absorption components are therefore very uncertain. The ^{29}Si isotopologue may also show the signature of a few diffuse-cloud components, but it suffers from the same baseline issue as the main isotopologue. The ^{30}Si and ^{18}O isotopologues are too weak for the diffuse-cloud components to be detected.

4.4.55. Sulfur dioxide SO$_2$

We use the CDMS entries for the vibrational ground state of all isotopologues and for the vibrationally excited state $v_2 = 1$ of the main isotopologue (tags 64 502 version 2, 66 501, 65 501, 66 502, and 65 502, all version 1, and 64 503 version 2). The entries for the ground and first vibrationally excited states of the main isotopologue are based on Müller & Brünken (2005), those for $^{34}SO_2$ and $SO^{18}O$ on Belov et al. (1998), and those for $^{33}SO_2$ and $SO^{17}O$ on Müller et al. (2000a). Important additional data for the ground and first vibrationally excited states of the main isotopologue as well as for $^{34}SO_2$ in the range of our survey were taken from Alekseev et al. (1996).

Sgr B2(N): the parameters of all entries related to sulfur dioxide are listed in Table 59. Many transitions of sulfur dioxide are detected in the 3 mm window, with lower-level energies ranging from 2.8 K (at 104.03 GHz) to 545 K (at 84.32 GHz). A complex mixture of velocity and temperature components is needed to reproduce the features detected in emission and absorption. Three hot velocity components are required by the high-energy transitions (e.g., 82.95 GHz). An additional redshifted component is necessary to reproduce the wing emission of the low-energy transitions (e.g., 83.69 and 104.03 GHz). The low-excitation component in emission close to the systemic velocity is needed to fit the transition at 83.69 GHz. The absorption components account for the self-absorption detected at 104.03 GHz. The ^{34}S isotopologue is detected at 83.04, 102.03, and 104.39 GHz. The ^{33}S, ^{18}O, and ^{17}O isotopologues are not detected. No transition from within the vibrationally excited state $v_2 = 1$ is detected.

Sgr B2(M): the parameters of all entries related to sulfur dioxide are listed in Table 106. Numerous transitions of the main isotopologue are detected in all bands. At 3 mm, the lower-level energies range from 2.8 K (104.03 GHz) to 1151 K (90.00 GHz), and we need two temperature components to fit all the detected transitions. The colder component is in particular necessary for the transitions at 83.69, 104.03, and 104.24 GHz ($E_1/k = 33$, 2.8, and 50 K). The detected transitions are a mixture of optically thin and thick transitions ($\tau_{max} = 19$ for the hot component, and 0.08 for the colder component), which simultaneously allows an estimate of the temperature and the source size. The ^{34}S isotopologue is also detected with many transitions ($\tau_{max} = 0.8$ for the hot component, and 0.0033 for the colder one). The ^{33}S isotopologue is weak but clearly detected, e.g., at 83.35 and 103.00 GHz, but the model tends to underestimate the emission. The ^{18}O isotopologue is weak. It is clearly detected at 267.04 GHz and maybe at 109.64 GHz (but underestimated by the model?). The ^{17}O isotopologue is not detected at 3 mm, but it is likely detected at 216.67 and 217.02 GHz and was for this reason included in the complete model.

We also detect many transitions from within the vibrationally excited state $v_2 = 1$ of the main isotopologue. A few lines are optically thick at 3 mm ($\tau_{max} = 1.8$), but the majority is optically thin. A very small size is needed to limit the strength of the (optically thick) lines at 1.3 mm.

4.4.56. Sulfur monoxide SO

We use the CDMS entries for the main isotopologue and its ^{34}S, ^{33}S, and ^{18}O isotopologues (tags 48 501, 50 501, 49 501, and 50 502, all version 1). The entry for the main isotopologue is based on Bogey et al. (1997), the remaining entries on Klaus et al. (1996). Data in the range of our survey were taken mainly from Tiemann (1982) for the main, ^{34}S, and ^{18}O isotopologues and from Bogey et al. (1982b) for the ^{34}S and ^{18}O species.

Sgr B2(N): the parameters of all entries related to sulfur monoxide are listed in Table 60. Four transitions of sulfur monoxide are detected at 3 mm, one of them both in emission and absorption, with two self-absorption components (at 99.30 GHz). The flux density of the transition at 86.09 GHz ($E_1/k = 15$ K) represents about 75% of the flux density detected with the NRAO 12 m telescope (Friedel et al. 2004). Since the 12 m flux density is partly contaminated by Sgr B2(M) which emits more than Sgr B2(N) in this transition, the contribution of Sgr B2(N) to the emission detected with the 12 m telescope is mainly confined to the 30 m beam. In addition, the 30 m flux density at that frequency is about twice the flux density detected with BIMA with an angular resolution of $27.2'' \times 6.6''$ (Friedel et al. 2004), which implies that at least half of the 30 m flux density is emitted by a region more extended than the minor size of the BIMA beam, but also that there is at least one additional component more compact than the BIMA beam. Since both SO and SO$_2$ are shock tracers, we expect that they should trace similar regions and we constructed a model for SO similar to the one for SO$_2$, the latter being better constrained thanks to the wider range of lower-level energies of its detected transitions. Two transitions of the ^{34}S isotopologue are clearly detected at 3 mm, the other two being blended with emission from other species, in particular from a recombination line of hydrogen close to 106.74 GHz. The ^{33}S isotopologue is not unambiguously detected, but its transitions around 98.49 GHz contribute to nearly 50% of the observed features so we include it in the complete model. The other isotopologues (^{18}O, ^{17}O, ^{36}S) are not detected. No transition from within the vibrationally excited state $v = 1$ is detected.

Sgr B2(M): the parameters of all entries related to sulfur monoxide are listed in Table 107. Sulfur monoxide is detected with four lines at 3 mm and four lines at 1 mm. The transition at 99.30 GHz ($E_1/k = 4$ K) is detected both in emission and absorption, even from spiral-arm diffuse clouds. The emission is modeled with three components, one for the core of the lines and two for the wings. The Mopra maps of Jones et al. (2008) show that there is a component extended over several arcminutes (mainly seen at 99.30 GHz), but also a more compact component peaking toward Sgr B2(M). The ^{34}S isotopologue is clearly detected in emission at 3 and 1.3 mm (e.g., 97.72 and 211.01 GHz), but the diffuse-cloud absorption components are not detected. The ^{33}S and ^{18}O isotopologues are clearly detected in emission at 3 mm (e.g., 98.49 and 93.27 GHz). Assuming the isotopic ratios listed in Table 2, a size of the main cold emission component similar to the beam at 3 mm gives a reasonable fit to all isotopologues. The 3 mm lines are dominated by the main cold component of the model (with $\tau_{max} = 0.9$), while the warm component ($\tau_{max} = 6$ at 3 mm) contributes mainly at 214.36 GHz ($E_1/k = 71$ K) and less than 50% for the other 1.3 mm transitions. We note however that the transition at 100.03 GHz ($E_1/k = 34$ K) is underestimated by the model. Finally, one transition of the vibrationally excited state $v = 1$ of the main isotopologue may be detected at 213.50 GHz, but it requires a column density ten times higher than the one of the warm component of the ground state, so the detection is highly uncertain and this state is not included in the complete model.

4.4.57. Formic acid t-HCOOH

We use the CDMS entry (tag 46 506 version 1) which is based on Winnewisser et al. (2002), with additional data in the range of our survey mainly from Bellet et al. (1971).

Sgr B2(N): the parameters of formic acid in the *trans* form are listed in Table 61. This model was already reported in Sect. 3.4 of Belloche et al. (2009). The detected transitions are all optically thin ($\tau_{max} \sim 0.14$). The ^{13}C isotopologue is not detected.

Sgr B2(M): formic acid is not detected.

4.5. Non-detections

Upper limits to the column densities of glycine (NH$_2$CH$_2$COOH), methoxyacetonitrile (CH$_3$OCH$_2$CN), 2-cyanoethanol (HOCH$_2$CH$_2$CN), 2-aminopropionitrile (CH$_3$CH(NH$_2$)CN), and *n*-butyl cyanide (*n*-C$_4$H$_9$CN) based on our spectral survey of Sgr B2(N) were reported elsewhere (Belloche et al. 2008; Braakman et al. 2010; Møllendal et al. 2012; Ordu et al. 2012). In this section, we list a few additional upper limits derived from our survey for species that were either claimed to be detected toward Sgr B2(N) by other authors, or that are of some interest for astrochemistry.

4.5.1. Vinyl alcohol CH$_2$CHOH

We use the CDMS entries (tags 44 506 and 44 507, both version 1) for the *syn* and *anti* conformers of vinyl alcohol. They are based on the measurements performed by Saito (1976) and Rodler (1983) for the former, and Rodler (1985) for the latter.

Turner & Apponi (2001) report the detection of vinyl alcohol toward Sgr B2(N) with the Kitt Peak 12 m telescope at 3

and 2 mm. They claim the detection of five transitions of the *anti* conformer and two transitions of the *syn* conformer, with linewidths (FWHM) in the range 8–16 km s^{-1}. With a beam filling factor of unity, they derive an excitation temperature of $11.6^{+13.5}_{-4.7}$ K and a column density of $(2.4 \pm 0.6) \times 10^{13}$ cm^{-2} for the former and a column density of 2.0×10^{14} cm^{-2} for the latter, assuming the same temperature. The observation of the high-lying *anti* conformer together with the low rotation temperature suggests, assuming the detection of vinyl alcohol is correct, that the molecule resides in the extended part of Sgr B2, which often shows large deviations from LTE. Since the beam in our survey is much smaller, our survey is relatively less sensitive to such an extended, low-excitation component.

With a beam filling factor of unity, a linewidth of 9 km s^{-1}, and a temperature of 11.6 K, we derive an upper limit of 2×10^{14} cm^{-2} for the *anti* conformer, which is less constraining than the detection reported by Turner & Apponi (2001). Our upper limit is mainly set by the non-detection of the transition at 84.83 GHz. On the other hand, if we assume a source size (3″), temperature (100 K), and linewidth (7 km s^{-1}) similar to the values used for its isomer ethylene oxide (c-C$_2$H$_4$O, see Sect. 4.4.6), then we obtain an upper limit of 1.5×10^{16} cm^{-2}, i.e. a ratio of *anti*-vinyl alcohol to ethylene oxide column densities lower than 0.4. Assuming the same parameters as for acetaldehyde (CH$_3$CHO, 5″, 60 K, and 8 km s^{-1}, see Sect. 4.4.16), we obtain an upper limit of 3×10^{15} cm^{-2}, i.e. a ratio of *anti*-vinyl alcohol to acetaldehyde column densities lower than 0.1. For the *syn* form, we find an upper limit of 2×10^{14} cm^{-2} for a low-excitation, extended component, marginally consistent with the detection of Turner & Apponi (2001). For a 100 K, compact component, the upper limit is 3×10^{16} cm^{-2}, implying a *syn*-vinyl alcohol to ethylene oxide column densities lower than 0.8. For a 60 K, compact component, the upper limit is 8×10^{15} cm^{-2}, i.e. a ratio of *syn*-vinyl alcohol to acetaldehyde column densities lower than 0.3.

4.5.2. Ketenimine CH$_2$CNH

We use the CDMS entry (tag 41 503 version 1) which is based on measurements performed by Rodler et al. (1984, 1986).

The first detection of ketenimine was claimed by Lovas et al. (2006) toward Sgr B2(N) based on GBT observations of three lines in absorption, with lower-level energies ranging from 33 to 50 K. Assuming a source size of 5″, they derive an excitation temperature of 65 K and a column density of $\sim 1.5 \times 10^{16}$ cm^{-2}, with an uncertainty of a factor of two. Assuming the same source size and temperature and a linewidth (FWHM) of 20 km s^{-1}, our spectral survey at 3 mm yields a column-density upper limit of 2×10^{16} cm^{-2} toward Sgr B2(N), which is less constraining than the detection reported by Lovas et al. (2006).

4.5.3. *trans* methyl formate CH$_3$OCHO

The entry for the *trans* conformer of methyl formate (only the *A* species) was provided by B. H. Pate in March 2010, prior to publication (Neill et al. 2012).

A tentative detection of the *trans* conformer of methyl formate, both the *A* and *E* species, was reported in absorption toward Sgr B2(N) by Neill et al. (2012) based on low-frequency observations with the GBT. They derive an excitation temperature of 7.6 ± 1.5 K and estimate the column density to be $1.2^{+1.2}_{-0.6} \times 10^{13}$ cm^{-2}. These authors also report that the *cis* conformer is detected in emission in the GBT survey and conclude

that the two conformers have a different spatial distribution, the *trans* conformer coming from a colder, more extended region.

The *trans* conformer of methyl formate is not unambiguously detected in our 3 mm survey toward Sgr B2(N). Using the same source size and temperature as we derived for the *cis* conformer (4″ and 80 K, see Sect. 4.4.22), we obtain an upper limit of 8×10^{14} cm^{-2} for the column density of the *trans* conformer for the main hot core with $V_{lsr} = 64$ km s^{-1}. Hints of emission may be seen at 82.15 ($E_1/k \sim 41$–61 K), 91.28 (45–65 K), and 109.54 GHz (74 K), but they are not sufficient to claim a detection. As a result, we obtain an upper limit to the ratio of the *trans* to *cis* column densities of 0.2%. For comparison, the thermal-equilibrium value would be $\sim 10^{-16}$ at 80 K (see Neill et al. 2012). If we assume an emission more extended than the beam and an excitation temperature of 7.6 K, we derive an upper limit of 2×10^{13} cm^{-2} for a linewidth of 7 km s^{-1}, which is less constraining than the tentative detection of the *A* species by Neill et al. (2012).

4.5.4. Propanal C$_2$H$_5$CHO, propenal C$_2$H$_3$CHO, and propynal CHCCHO

We use the CDMS entry (tag 58 505 version 1) for the *syn* form of propanal, the JPL entry (tag 56 008 version 1, with the partition function values updated in October 2012) for propenal, and the CDMS entry (tag 54 510 version 1) for propynal. The entry for propanal is based on measurements reported by Hardy et al. (1982) and Demaison et al. (1987). The part of the entry dealing with the *trans* conformer of propenal is mostly based on measurements reported by Winnewisser et al. (1975). The *cis* conformer is much higher in energy (~ 594 cm^{-1}). The entry for propynal is based on measurements performed mainly by Costain & Morton (1959) and Winnewisser (1973).

Hollis et al. (2004) report the detection of six transitions of propanal, two transitions of propenal, and one transition of propynal toward Sgr B2(N) with the GBT ($HPBW = 28$–40″), with a mixture of emission and absorption in several velocity components that prevented them to derive reliable column densities. Propynal was reported for the first time in space toward TMC1 by Irvine et al. (1988). Assuming a beam filling factor of unity, a linewidth of 8 km s^{-1}, and a temperature of 50 K, our 3 mm survey of Sgr B2(N) yields column-density upper limits of 1.5×10^{14} cm^{-2} for the *syn* form of propanal, 3×10^{13} cm^{-2} for propenal, and 3×10^{13} cm^{-2} for propynal. For a temperature of 15 K, the upper limits become 1.0×10^{14}, 2×10^{13}, and 2×10^{13} cm^{-2}, respectively.

4.5.5. Silicon monosulfide SiS

We use the CDMS entry (tag 60 506 version 1, see Müller et al. 2007).

Silicon monosulfide was reported toward Sgr B2(OH) at 3 mm by Cummins et al. (1986) and Turner (1989, 1991). Both detections are somewhat uncertain as they rely on only one transition at 90.77 GHz with a low signal-to-noise ratio. The 5–4 and 6–5 transitions fall into the range of our survey at 3 mm. At both frequencies (90.77 and 108.92 GHz), there is emission detected toward Sgr B2(N) and (M) with a peak temperature of ~ 0.2 and 0.1 K but this emission is broad and likely results from the overlap of several lines. Therefore we are not able to firmly identify SiS in our spectra. With an excitation temperature of 25 K, a linewidth of 18 km s^{-1}, and a beam filling factor of unity, as assumed by Turner (1991), we derive column

density upper limits of 4.5×10^{13} and 3×10^{13} cm^{-2} toward Sgr B2(N) and (M), respectively. The line tentatively reported toward Sgr B2(OH), which also includes Sgr B2(M) given the large beam of the NRAO 12 m telescope, yields a column density of 1.2×10^{13} cm^{-2} (Turner 1991). We note that Dickinson & Kuiper (1981) report the detection of both transitions at 3 mm toward Sgr B2(OH) at a velocity of 56–58 km s^{-1}. They derive a column density of 1–2×10^{13} cm^{-2} assuming a temperature of 20 K.

4.5.6. Glycine NH$_2$CH$_2$COOH

Upper limits to the column density of glycine based on our survey toward Sgr B2(N) were already published in Belloche et al. (2008). More stringent constraints were reported by Jones et al. (2007) and Cunningham et al. (2007).

4.5.7. Deuterated methanol CH$_2$DOH

We use the JPL entry (tag 33 004, version 1).

Using the same parameters as for ^{13}CH$_3$OH (see Sect. 4.4.23), we derive an upper limit of 1.0×10^{17} or 1.0×10^{14} cm^{-2} for the column density of a warm or cold component, respectively, toward Sgr B2(N). This yields an upper limit to the deuterium fractionation of methanol of 0.7% or 0.3%, respectively. Following the same procedure, we find an upper limit to the deuterium fractionation of 7% or 0.4% for a warm or cold component toward Sgr B2(M), respectively. These upper limits are consistent with the low levels of deuterium fractionation measured toward Sgr B2 for, e.g., water, ammonia, and HCO$^+$ (1.6×10^{-3}, 1.1×10^{-3}, and 2×10^{-4}, see Jacq et al. 1990; Peng et al. 1993; Jacq et al. 1999, respectively).

4.5.8. Deuterated formamide

We use the CDMS entries for the three isotopologues NH$_2$CDO, *c*-NHDCHO, and *t*-NHDCHO (tags 46 520, 46 521, and 46 522, all version 1). They are based on Kutsenko et al. (2013) with additional data from Nielsen (1973).

Using the same parameters as for NH$_2$CHO (see Sect. 4.4.37), we derive upper limits of 8.0×10^{15}, 8.0×10^{15}, and 1.2×10^{16} cm^{-2} for the column densities of NH$_2$CDO, *c*-NHDCHO, and *t*-NHDCHO, respectively, toward Sgr B2(N). This yields upper limits to the deuterium fractionation of formamide of 0.6%, 0.6%, and 0.9%, respectively. These upper limits are consistent with the low levels of deuterium fractionation mentioned in Sect. 4.5.7.

4.5.9. Vibrationally excited CN and SiO

Data for both excited vibrational states are contained in the entries dealing with the ground states. Laboratory data for CN were taken from Dixon & Woods (1977), those for SiO from Mollaaghababa et al. (1991).

The only CN transitions from within $v = 1$ covered by our survey are at ~ 112.1 and 112.4 GHz. Assuming the same source size (0.9″) and temperature (500 K) as for HCN, $v_2 = 1$ (see Sect. 4.4.36), we obtain an upper limit on the column density parameter of $\sim 5 \times 10^{19}$ cm^{-2} for a linewidth of 7 km s^{-1}.

No transition of SiO from within $v = 1$ is detected. The most stringent constraint is obtained at 86.243370 GHz. Assuming again the same source size, temperature, and

Table 108. Frequencies of unidentified lines in the 3 mm line survey of Sgr B2(N) with a peak temperature higher than 0.3 K in main-beam temperature scale (about 13σ).

Frequency (GHz)	Frequency (GHz)	Frequency (GHz)	Frequency (GHz)
85 528.4	103 120.0	109 091.1	112 396.1
89 768.9	103 281.6	109 160.4	112 560.1
94 415.2	103 589.3	109 223.5	112 803.5
95 745.3	103 999.0	109 235.7	112 926.9
95 894.0	104 197.7	109 721.0	112 936.2
96 253.4	104 479.3	110 098.0	113 722.4
98 650.2	104 532.9	110 144.0	113 781.7
98 726.6	104 842.8	110 157.7	113 793.7
99 826.7	104 850.6	110 160.6	113 796.0
99 968.6	104 856.3	110 216.4	113 872.0
100 522.7	104 999.4	110 222.4	114 039.7
100 527.1	105 004.8	110 224.6	114 126.2
100 867.3	105 030.3	110 900.9	114 481.2
101 176.2	105 133.1	111 394.9	114 673.7
101 211.1	105 514.8	111 525.6	114 687.2
101 240.2	106 353.6	111 634.6	114 872.4
101 340.8	107 404.2	111 708.9	115 089.4
101 659.2	107 690.2	112 112.1★	115 093.3
102 380.4	107 693.7	112 115.8	115 413.9
102 912.3	107 705.1	112 121.8★	115 652.2
103 022.7	108 879.8	112 384.4	

Notes. The typical uncertainty is on the order of 1 MHz but could also be higher in some cases. The rest frequencies assume a systemic velocity of 64 km s^{-1}. Frequencies marked with a star indicate lines which are likely contamination from the image band (CO 1–0).

Table 109. Frequencies of unidentified lines in the 3 mm line survey of Sgr B2(M) with a peak temperature higher than 0.3 K in main-beam temperature scale (about 13σ).

Frequency (GHz)	Frequency (GHz)	Frequency (GHz)	Frequency (GHz)
95 145.3	110 154.5	112 110.9★	112 124.3★
95 948.9	110 157.7	112 115.2	115 806.4
95 964.6	110 164.1		

Notes. The typical uncertainty is on the order of 1 MHz but could also be higher in some cases. The rest frequencies assume a systemic velocity of 62 km s^{-1}. Frequencies marked with a star indicate lines which are likely contamination from the image band (CO 1–0).

linewidth (12 km s^{-1}) as for HCN, $v_2 = 1$, we obtain an upper limit on the column density parameter of $\sim 5 \times 10^{17}$ cm^{-2}.

4.6. Strong unidentified lines

Tables 108 and 109 list the frequencies of the 83 and 10 unidentified lines that have a peak temperature higher than 0.3 K (i.e. about 13σ) in the 3 mm surveys of Sgr B2(N) and (M), respectively. In some cases, these frequencies are uncertain because of blends with other lines. For Sgr B2(N), some of them may also correspond to the second velocity component of a line at higher (by ∼2.7–3.9 MHz) frequency. For both sources, a few unidentified lines may also correspond to contamination by CO 1–0 from the image band.

Table 110. Molecules and their isotopologues detected in the present survey and comparison to previous surveys of Sgr B2.

Species	B13[a]		C86[b]	T89[c]	S91[d]		N98[e]		F04[f]
	N	M	OH	OH	N	M	N	M	N
(1)	(2)	(3)	(4)	(5)	(6)	(7)	(8)	(9)	(10)
C_2H_3CN	+	+	+	+	−	−	+	+	+
$CH_2CH^{13}CN$★	+	−	−	−	−	−	−	−	−
$CH_2^{13}CHCN$★	+	−	−	−	−	−	−	−	−
$^{13}CH_2CHCN$★	+	−	−	−	−	−	−	−	−
C_2H_5CN	+	+	+	+	−	−	+	+	+
$C_2H_5^{13}CN$	+	−	−	−	−	−	−	−	−
$CH_3^{13}CH_2CN$	+	−	−	−	−	−	−	−	−
$^{13}CH_3CH_2CN$	+	−	−	−	−	−	−	−	−
C_2H_5OCHO★	+	−	−	−	−	−	−	−	−
C_2H_5OH	+	+	+	+	−	+	+	+	+
$CH_3^{13}CH_2OH$	m	−	−	−	−	−	−	−	−
$^{13}CH_3CH_2OH$	m	−	−	−	−	−	−	−	−
n-C_3H_7CN★	+	−	−	−	−	−	−	−	−
c-C_2H_4O	+	−	−	−	−	−	+	−	−
c-C_3H_2	+	+	+	+	+	+	+	+	−
c-$H^{13}CCCH$	+	+	−	−	−	−	−	−	−
c-$HC^{13}CCH$	m	+	−	−	−	−	−	−	−
CCH	+	+	+	+	−	+	+	+	−
^{13}CCH	+	+	−	−	−	−	−	−	−
$C^{13}CH$	?	+	−	−	−	−	−	−	−
CCS	+	+	−	+	−	−	−	−	+
CH_2NH	+	+	−	+	−	+	+	+	−
a-$(CH_2OH)_2$	+	−	−	−	−	−	−	−	−
$CH_2(OH)CHO$	+	−	−	−	−	−	−	−	−
CH_3C_3N	+	+	−	−	−	−	−	−	−
CH_3CCH	+	+	+	+	−	+	+	+	−
$CH_3C^{13}CH$	+	+	−	−	−	−	−	−	−
$CH_3^{13}CCH$	m	+	−	−	−	−	−	−	−
$^{13}CH_3CCH$	+	+	−	−	−	−	m	−	−
$CH_3C(O)CH_3$	+	+	−	−	−	−	−	−	−
CH_3CHO	+	+	+	+	−	−	+	+	−
CH_3CN	+	+	+	+	+	+	+	+	+
$^{13}CH_3CN$	+	+	+	+	−	−	+	+	−
$CH_3^{13}CN$	+	+	+	+	−	−	+	+	+
$^{13}CH_3^{13}CN$	m	−	−	−	−	−	−	−	−
$CH_3C^{15}N$	m	−	−	−	−	−	m	−	−
$CH_3C(O)NH_2$	+	−	−	−	−	−	−	−	−
CH_3COOH	+	−	−	−	−	−	−	−	−
CH_3NH_2	+	+	+	+	−	−	+	−	−
CH_3OCH_3	+	+	+	+	+	+	+	+	+
$CH_3O^{13}CH_3$	m	−	−	−	−	−	−	−	−
CH_3OCHO	+	+	+	+	−	−	+	+	+
CH_3OH	+	+	+	+	+	+	+	+	+
$^{13}CH_3OH$	+	+	+	+	−	−	+	+	−
$CH_3^{18}OH$	+	−	−	−	−	−	m	m	−
CH_3SH	+	+	+	+	−	−	+	+	−

Notes. Detections and non-detections are marked with + and − symbols, respectively. Potential detections are marked with "m". First detections in space based on our survey are indicated with a ★ symbol after the name of the species. [a] This survey, toward Sgr B2(N) and (M); [b] Cummins et al. (1986) toward Sgr B2(OH); [c] Turner (1989) toward Sgr B2(OH); [d] Sutton et al. (1991) toward Sgr B2(N) and (M); [e] Nummelin et al. (1998) toward Sgr B2(N) and (M); [f] Friedel et al. (2004) toward Sgr B2(N).

5. Discussion

5.1. Comparison to previous surveys

The molecules and their isotopologues detected in the present survey of Sgr B2(N) and (M) are listed in Table 110. Their

Table 110. continued.

Species	B13[a]		C86[b]	T89[c]	S91[d]		N98[e]		F04[f]
	N	M	OH	OH	N	M	N	M	N
(1)	(2)	(3)	(4)	(5)	(6)	(7)	(8)	(9)	(10)
CN	+	+	+	+	–	+	+	+	–
^{13}CN	+	+	+	+	–	–	–	–	+
C^{15}N	m	+	–	–	–	–	–	–	–
CO	+	+	+	–	+	+	+	+	–
^{13}CO	+	+	+	+	–	+	+	+	+
C^{18}O	+	+	+	+	–	–	+	+	–
C^{17}O	+	+	+	+	–	+	+	+	–
^{13}C^{18}O	?	+	+	+	–	–	–	–	–
^{13}C^{17}O	m	m	–	–	–	–	–	–	–
CS	+	+	+	+	+	+	+	+	–
^{13}CS	+	+	–	+	–	+	+	+	–
C^{34}S	+	+	–	+	–	+	+	+	–
C^{33}S	+	+	+	+	–	+	+	+	–
^{13}C^{34}S	m	+	–	–	m	m	+	+	–
CH$_2$CO	+	+	+	+	–	+	+	+	–
^{13}CH$_2$CO	m	m	–	–	–	–	–	–	–
CH$_2$^{13}CO	m	–	–	–	–	–	–	–	–
H$_2$CO	+	+	+	+	–	+	+	+	–
H$_2$^{13}CO	+	+	–	–	–	+	+	+	–
H$_2$C^{18}O	–	+	–	–	–	–	–	–	–
H$_2$CS	+	+	+	+	+	+	+	+	–
H$_2$^{13}CS	m	m	–	–	–	–	–	–	–
H$_2$C^{34}S	+	m	–	+	–	–	–	–	–
NH$_2$CH$_2$CN*	+	–	–	–	–	–	–	–	–
H$_2$S	+	+	–	–	–	–	–	–	–
H$_2$^{34}S	–	+	–	–	–	–	–	–	–
H$_2$^{33}S	–	–	–	–	–	–	–	–	–
HC$_3$N	+	+	+	+	+	+	+	+	+
H^{13}CCCN	+	+	+	+	–	–	+	+	+
HC^{13}CCN	+	+	+	+	–	–	+	+	+
HCC^{13}CN	+	+	+	+	–	–	+	+	+
HC$_3$^{15}N	+	–	–	+	–	–	–	–	–
H^{13}CC^{13}CN*	+	–	–	–	–	–	–	–	–
HC^{13}C^{13}CN	m	–	–	–	–	–	–	–	–
H^{13}C^{13}CCN	m	–	–	–	–	–	–	–	–
HC$_5$N	–	+	+	+	–	–	–	–	+
HCCNC	m	–	–	–	–	–	–	–	–
HCN	+	+	+	+	–	+	–	–	–
H^{13}CN	+	+	+	+	+	+	+	+	+
HC^{15}N	+	+	+	+	+	+	+	+	+
H^{13}C^{15}N*	+	m	–	–	–	–	–	–	–
DCN	–	m	–	+	–	–	–	–	–
NH$_2$CHO	+	+	+	+	+	–	+	+	+
NH$_2$^{13}CHO	+	–	–	–	–	–	–	–	–
HCO$^+$	+	+	+	+	–	–	–	–	–
H^{13}CO$^+$	+	+	+	+	+	+	+	+	+
HC^{18}O$^+$	+	+	+	+	–	+	+	+	–
HC^{17}O$^+$	+	+	+	+	–	–	–	+	+

Table 110. continued.

Species	B13[a]		C86[b]	T89[c]	S91[d]		N98[e]		F04[f]
	N	M	OH	OH	N	M	N	M	N
(1)	(2)	(3)	(4)	(5)	(6)	(7)	(8)	(9)	(10)
HCS$^+$	+	+	+	+	+	–	+	+	–
HDO	+	+	–	–	–	–	+	+	–
HNC	+	+	+	+	–	–	–	–	–
HN^{13}C	+	+	+	+	–	+	+	+	+
H^{15}NC	+	+	–	–	–	–	–	–	–
HNCO	+	+	+	+	m	+	+	+	+
HN^{13}CO	m	m	m	–	–	–	–	–	–
HNC^{18}O	m	–	–	–	–	–	–	–	–
HNCS	+	+	+	+	–	–	–	–	–
HOCN	+	+	–	–	–	–	–	–	–
HOCO$^+$	+	+	–	+	–	–	+	+	–
HOC$^+$	+	+	–	–	–	+	–	–	–
HSCN	+	+	–	–	–	–	–	–	–
N$_2$H$^+$	+	+	–	+	–	–	–	–	–
^{15}NNH$^+$	–	m	–	–	–	–	–	–	+
N^{15}NH$^+$	–	–	–	–	–	–	–	–	–
NH$_2$CN	+	+	+	+	–	–	+	+	–
NH$_2$^{13}CN	m	–	–	–	–	–	–	–	–
NH$_2$D	+	–	+	+	–	–	–	–	+
NS	+	+	+	+	–	–	+	+	–
OCS	+	+	+	+	–	+	+	+	–
O^{13}CS	+	+	+	+	m	–	+	+	–
OC^{34}S	+	+	+	+	m	–	+	+	+
OC^{33}S	+	–	–	–	–	–	–	–	–
^{18}OCS	m	–	–	–	–	–	m	–	–
PN	m	m	–	+	–	–	–	–	–
SiO	+	+	+	+	+	+	+	+	+
^{29}SiO	+	+	+	+	–	–	–	+	–
^{30}SiO	+	+	+	+	–	–	–	+	–
Si^{18}O	–	+	–	–	–	–	–	–	–
SO$_2$	+	+	+	+	+	+	+	+	–
^{34}SO$_2$	+	+	+	+	+	+	+	+	+
^{33}SO$_2$	–	+	–	+	–	–	–	+	–
SO^{18}O	–	+	–	–	–	–	–	+	–
SO^{17}O	–	m	–	–	–	–	–	–	–
SO	+	+	+	+	+	+	+	+	+
^{34}SO	+	+	+	+	m	+	+	+	+
^{33}SO	m	+	–	–	–	+	–	+	–
S^{18}O	–	+	–	–	–	+	–	+	–
t-HCOOH	+	–	+	+	m	–	+	–	+

detection or non-detection in previous spectral surveys of Sgr B2 (either N, M, or OH) is also indicated. The statistics of the present survey are compared to these previous surveys in Table 111. With respect to the 3 mm survey of Turner (1989), the density of detected lines has increased by 70% for Sgr B2(M). Surprisingly enough, the density of *identified* lines has increased by about 20% only, while we could have expected a larger improvement given the growth of the CDMS and JPL spectroscopic databases over the years. While we set our identification threshold to 50% of the detected level of emission/absorption (see Sect. 4.2), the criterion used by Turner (1989, 1991) to mark a line as identified may have been less stringent and their number

of identified lines was in turn perhaps overestimated. Another explanation may be that Turner's survey is a priori less sensitive to hot-core species: its angular resolution is poorer by a factor 3 and its target, Sgr B2(OH), is located ~25″ south of Sgr B2(M).

In contrast, our survey toward Sgr B2(N) shows a much clearer improvement (factor 2) both in terms of line detection and identification compared to previous surveys. Further progress in reducing the fraction of unidentified lines in our survey of Sgr B2(N) is expected when spectroscopic predictions for vibrationally or torsionally excited states of known species will become available. For instance, we expect about 300 additional lines of ethyl cyanide to be detectable in our survey, and about ten for vinyl cyanide (see Sects. 4.4.2 and 4.4.1, respectively). The ^{13}C isotopologues of methyl formate in their vibrational ground state may also contribute two dozens of lines (see Sect. 4.4.22). Provided these estimates are correct, these entries missing in our catalog would already reduce the number of unidentified lines to ~750 and increase the fraction of identified lines to ~80%.

Table 111. Number of detected lines and fraction of identified lines compared to previous surveys of Sgr B2.

Survey[a] (1)	Telescope (2)	Source (3)	Coverage[b] (4)	N_{det}[c] (5)	N_{id}[d] (6)	n_{det}[e] (7)	n_{id}[f] (8)	n_u[g] (9)	f_{id}[h] (10)
C86	BTL 7 m	OH	72–144 (49)	457	426	9.3	8.7	0.6	0.93
T89	NRAO 11 m	OH	70–115 (45)	641	470	14.2	10.4	3.8	0.73
S91	CSO 10.4 m	M	330–355 (25)	128	127	5.1	5.1	0.0	0.99
N98	SEST 15 m	M	218–264 (45)	660	609	14.7	13.5	1.2	0.92
B13	IRAM 30 m	M	80–116 (36)	945	444	26.3	12.3	14.0	0.47
N98	SEST 15 m	N	218–264 (45)	1730	1393	38.4	31.0	7.4	0.81
F04	BIMA	N	86–113 (3.6)	218	98	60.6	27.2	33.4	0.45
B13	IRAM 30 m	N	80–116 (36)	3675	2573	102.1	71.5	30.6	0.70

Notes. [a] See footnote of Table 110. The large telescope beams of the C86 and T89 surveys pointed toward Sgr B2(OH) include Sgr B2(M) (see Fig. 1 of Friedel et al. 2004). [b] The edges of the observed band are given in GHz. Since the band was not always fully covered, the effective bandwidth is given in parentheses. [c] Total number of detected lines. [d] Total number of identified lines. [e] Average number of detected lines per GHz. [f] Average number of identified lines per GHz. [g] Average number of unidentified lines per GHz. [h] Fraction of identified lines.

Finally, we emphasize that, although the fraction of identified lines in our survey of Sgr B(M) may appear surprisingly low compared to Sgr B2(N) (see Col. 10 of Table 111), the density of unidentified lines per unit frequency is actually a factor of two higher for the latter (see Col. 9 of Table 111).

5.2. First detections in space

The high sensitivity of our survey toward Sgr B2(N) and/or the recent availability of spectroscopic predictions for new molecules, rare isotopologues, and vibrationally or torsionally excited states of already known molecules, allowed us to identify a number of such species/entries for the first time in space. Our detections of three new molecules – aminoacetonitrile, ethyl formate, and *n*-propyl cyanide – were already reported in Belloche et al. (2008, 2009), and the detection of the ^{13}C isotopologues of vinyl cyanide in Müller et al. (2008). Here, we report the first detection of two other rare isotopologues, $H^{13}C^{15}N$ and $H^{13}CC^{13}CN$ (see Sects. 4.4.36 and 4.4.33, respectively). We also report the first detection of transitions from within twelve new vibrationally or torsionally excited states of known molecules: four states of vinyl cyanide, one state of acetone, one state of acetaldehyde, one state of methyl cyanide, one state of the ^{13}C isotopologues of methyl cyanide, and four states of the ^{13}C isotopologues of cyanoacetylene (see Sects. 4.4.1, 4.4.15, 4.4.16, 4.4.17, 4.4.17 and 4.4.33 respectively).

While the line density and the line intensity of typical hot-core molecules increase with frequency from the 3 mm atmospheric window to the 1 mm window, we would like to stress the fact that the 3 mm range appears to be best suited in our survey for the detection of new molecules toward Sgr B2(N). The line confusion at 2 and 1 mm is such that the weak emission of rare molecules is most of the time hidden below the stronger emission of more abundant species. In addition, the frequent overlap between transitions from different species and the significant opacity of the continuum emission makes the modeling more difficult and the line identification in turn less reliable at 2 and 1 mm. We note that quite a number of interstellar complex organic molecules were first detected toward Sgr B2 at the beginnings of molecular radio astronomy, surprisingly, at long centimeter wavelengths, namely methanol, formic acid, formamide, acetaldehyde, methanimine, methylamine, vinyl cyanide, and methyl formate (for a historical perspective and references, see Menten 2004). More recently, propanal, acetamide, and cyanoformaldehyde were added

(Hollis et al. 2004, 2006; Remijan et al. 2008). These frequency ranges have an even lower level of line confusion than the 3 mm range, which in some cases facilitates the line identification. They seem, however, to trace extended emission with low excitation rather than the high-temperature/high-density emission of the embedded hot cores that is traced at 3 mm and at higher frequencies. Moreover, the cm observations indicate that the populations of the low-lying energy levels giving rise to lines at these wavelengths are far from LTE. This causes some lines to become inverted, causing low gain amplification of the strong extended radio continuum emission and absorption against that emission in others (see Menten 2004).

The large number of unidentified lines in our survey of Sgr B2(N) may still allow future identifications of new molecules. We expect however a high fraction of these unidentified lines to be emitted by transitions from within vibrationally or torsionally excited states of known molecules for which spectroscopic predictions are currently missing. In particular, ethyl cyanide is expected to be a major contributor (see Sect. 5.1).

5.3. Implications for interstellar chemistry

The implications for the interstellar chemistry of the detection of the three molecules found for the first time in space in the course of this project (aminoacetonitrile, propyl cyanide, and ethyl formate) were already discussed by Belloche et al. (2009) based on a comparison to predictions of a numerical, gas-grain, chemical model. The main conclusion is that the abundance ratios in the chemical classes of interstellar esters and alkyl cyanides ($HCOOH/CH_3OCHO/C_2H_5OCHO$ and $CH_3CN/C_2H_5CN/C_3H_7CN$) can be relatively well reproduced if the main mechanism leading to the formation of these complex organic molecules occurs on the grain surfaces as a piecewise construction from their constituent functional-group radicals. In particular, the hydrogenation of less saturated species appears to be much less significant for the formation of alkyl cyanides than this piecewise formation mode.

The detection of aminoacetonitrile (NH_2CH_2CN) allowed us to predict a very low column density for glycine (NH_2CH_2COOH), based on the measured ratio of acetic acid to methyl cyanide column densities ([CH_3CN]/[CH_3COOH] ~ 200). If both pairs of molecules (carboxylic acid/cyanide) share similar formation routes, then we expect glycine to be about 200 times less abundant than aminoacetronitrile (Belloche et al. 2008). The detection of glycine in Sgr B2(N), and by extension

in the interstellar medium, will therefore likely have to wait for the full completion of ALMA.

Our first detection of the ^{13}C isotopologues of vinyl cyanide led us to conclude that the northern hot core in Sgr B2(N) is in a different evolutionary stage than the main hot core, based on a comparison of the measured ratio of vinyl cyanide to ethyl cyanide column densities ([C$_2$H$_3$CN]/[C$_2$H$_5$CN]) to predictions of older chemical models (see Müller et al. 2008, and references therein). We were, however, not able to determine which source is the youngest one. A more detailed comparison based on several sets of molecules should help braking the degeneracy.

Although the results reported in the present article could allow for a more detailed comparison to predictions of chemical models, the lack of angular resolution implies ambiguities that cannot be solved easily with the current dataset and may lead to erroneous conclusions. Even if we do constrain the size of the emitting region for some species that have both optically thick and thin lines in our single-dish survey, nothing guarantees that two species with the same source size are emitted from the same region. A very good counter-example can be seen in the interferometric maps shown in Fig. 5 of Belloche et al. (2008): the emission peak of methyl formate (panel n) is displaced by about 1.7″ compared to the emission peaks of aminoacetonitrile (panels a to e) and ethyl cyanide (panel h). Since we currently have an ongoing project with ALMA to complete a line survey of Sgr B2(N) in the 3 mm window with an improvement by 1.5 orders of magnitude in both signal-to-noise ratio and angular resolution (P.I.: Belloche), we plan to discuss the implications in terms of interstellar chemistry in more details based on this coming new dataset, taking advantage of the line identification already performed for this article.

5.4. Peculiar case of methanol

That our LTE model significantly underpredicts the emission in the 84.52 and 95.17 GHz transitions *and* underpredicts or does not predict absorption in the transitions at 107.01 and 108.89 GHz can both be understood from excitation peculiarities of the methanol molecule. As described by Menten (1991a,b), in the absence of a dominating far infrared field, the combination of (1) a propensity for $\Delta k = 0$ collisions over $|\Delta k| = 1$ collisions and (2) the fact that spontaneous transitions out of the $k = -1$ ladder are much slower than $J_{k=-1} - (J - 1)_{k=-1}$ transitions, the molecules funnel down the $k = -1$ ladder relative to levels of the neighboring k ladders, overpopulating the levels in that ladder. For $J_{-1} - J_0$ transitions, the upper energy levels are in the $k = -1$ ladder for $J \gtrsim 4$, while for $J = 3, 2$, and 1 this is true for the lower energy levels. This leads to inversion (and so called class I) methanol maser emission in the $4_{-1}-3_0$ E and $5_{-1}-4_0$ E lines at 36.17 and 84.52 GHz, respectively, and to anti-inversion (over-cooling) in the 2_0-3_{-1} E, 1_0-2_{-1} E, and 0_0-1_{-1} E lines at 12.18, 60.53, and 108.89 GHz, respectively.

For A-type methanol, analogously, the levels in the $K = 0$ ladder are overpopulated relative to levels in the $K = 1$ ladder. This causes inversion in the 7_0-6_1 A^+ and 8_0-7_1 A^+ transitions at 44.07 and 95.17 GHz, and anti-inversion in, e.g., the 5_1-6_0 A^+, 4_1-5_0 A^+, and 3_1-4_0 A^+ transitions at 6.67, 57.03, and 107.01 GHz, respectively, and also lower J A-type lines.

The above explains the excitation anomalies we observe in the 84.52 and 95.17 GHz lines (both inverted) and the 107.01 and 108.89 GHz lines (both anti-inverted). In addition deep absorption has been observed (with large beam widths) in the 6.68 and 12.18 GHz lines (Whiteoak et al. 1988; Menten 1991b). We note that the above scenario only holds for a range of densities

and temperatures that are more moderate than encountered in hot cores proper. Under hot core proper conditions, $\gtrsim$150 K, $n \gtrsim 10^7$ cm^{-3}, the levels in the transitions discussed above are thermalized and the maser action and over-cooling is quenched. In fact the FIR emission in many, but not all, hot cores leads to inversion in the 6.67 GHz 5_1-6_0 A^+ and the 12.18 GHz 2_0-3_{-1} E transitions, which are the strongest class II methanol maser transitions. Therefore, the observed emission and absorption discussed above must arise, in both Sgr B2(M) and (N), from material surrounding the hot cores. In contrast, class II methanol maser emission has been found from 12 sites scattered over the greater Sgr B2 region (Caswell 1996). None of these is closer than several arc seconds to any of the compact submillimeter sources/hot cores imaged by Qin et al. (2011).

6. Conclusions

We performed a complete and sensitive spectral line survey toward Sgr B2(N) and (M) with the IRAM 30 m telescope in the 3 mm atmospheric window as well as partial surveys at 2 and 1.3 mm in order to search for new complex organic molecules in the interstellar medium. The spectra were analyzed under the assumption of local thermodynamic equilibrium. Optical depth effects and the finite angular resolution of the telescope were taken into account. We made extensive use of the CDMS and JPL spectroscopic databases to identify the detected lines. The main results of this project are the following:

1. About 3675 and 945 spectral lines are detected at 3 mm with a peak signal-to-noise ratio higher than 4 toward Sgr B2(N) and (M), respectively. This yields densities of 102 and 26 lines per GHz, respectively, i.e. an increase by about a factor of two over previous surveys of Sgr B2.

2. About 70% and 47% of the lines detected toward Sgr B2(N) and (M) at 3 mm are identified and assigned to 56 and 46 distinct molecules as well as 66 and 54 less abundant isotopologues of these molecules, respectively. In addition, transitions from 59 and 24 catalog entries corresponding to vibrationally or torsionally excited states of some of these molecules were detected toward Sgr B2(N) and (M), respectively, up to a vibration energy of 1400 cm^{-1} (2000 K). The density of unidentified lines per unit frequency is a factor of two higher for Sgr B2(N) than for (M).

3. The line confusion and the significant opacity of the continuum emission at 2 and 1.3 mm make the modeling more difficult and the line identification process less reliable. The 3 mm window turns out to be the best suited to search for weak emission of rare hot-core species in our survey.

4. Absorption features produced by diffuse clouds along the line of sight are detected in transitions with low rotation quantum numbers of many simple molecules and are modeled with ~30–40 velocity components with typical linewidths of ~3–5 km s^{-1}.

5. Three complex organic molecules – aminoacetonitrile, ethyl formate, and *n*-propyl cyanide – and five rare isotopologues – the ^{13}C isotopologues of vinyl cyanide, H^{13}C^{15}N, and H^{13}CC^{13}CN – were detected for the first time in space. The detection of transitions from within twelve new vibrationally or torsionally excited states of known molecules is also reported for the first time.

6. Although the large number of unidentified lines may still allow future identifications of new molecules, we expect most of these lines to belong to vibrationally or torsionally excited states or to rare isotopologues of known molecules for which

spectroscopic predictions are currently missing. In particular, ethyl cyanide (mainly), vinyl cyanide, and the ^{13}C isotopologues of methyl formate could account for about 30% of the unidentified lines toward Sgr B2(N).

7. Excitation temperatures, column densities, systemic velocities, and linewidths were derived for each detected species under the LTE approximation, sometimes with large uncertainties however. They should be used with caution. Most complex species detected toward Sgr B2(N) have two velocity components corresponding to the two unresolved hot cores embedded in this source.

8. The 3 mm observed and synthetic spectra of each source are made publicly available to allow potentially interested readers to search for their favorite molecules, either on their own or on a collaborative basis.

The size of the often unresolved emitting region(s) could be to some extent derived for the species emitting both optically thick and optically thin lines. They are, however, somewhat uncertain and, as was shown interferometrically elsewhere, two species with the same source size are not necessarily located in the very same region. Therefore, we did not attempt to compare the derived column densities of all detected species to predictions of state-of-the-art chemical models in a systematic way. Interferometric observations will be necessary to break the remaining degeneracies. This is one of the main goals of our ongoing unbiased spectral line survey toward Sgr B2(N) at 3 mm with ALMA in its cycles 0 and 1 (P.I.: Belloche). With an improvement in angular resolution and sensitivity by more than one order of magnitude compared to our single-dish survey, we expect to set tighter constraints on the location, origin, and abundance of complex organic molecules and to detect a few, or maybe even a dozen of, new species. We are therefore confident that the field of astrochemistry will, in the near future, largely benefit from the tremendous opportunities offered by this new, powerful interferometer.

Appendix A: Star formation rate of Sgr B2

Combining their results with those of Mehringer et al. (1993), Gaume et al. (1995) report that there are at least 57 H II regions in the whole Sgr B2 complex, 41 of which being ultracompact (UC) with diameters less than 0.1 pc. These 41 UCH II regions correspond to OB stars with spectral types ranging from B0.5 to O5 (see Table 3 of Gaume et al. 1995). We use Table 1 of Panagia (1973) to convert the spectral types into stellar luminosities. We then compute the stellar masses with the equation $\frac{L}{L_\odot} = 2.3 \times \left(\frac{M}{M_\odot}\right)^{3.51}$, valid for $M > 5\,M_\odot$ (Griffiths et al. 1988). We obtain a total stellar mass of 675 $M_\odot$ for the 41 UCH II regions detected in Sgr B2.

The spectral type B0.5 corresponds to a stellar mass of ~11 $M_\odot$ with the equation above. Given an initial mass function (IMF), we call f_{11} the ratio of the mass of all stars with a mass between 11 and 120 $M_\odot$ to the mass of all stars with a mass between 0.01 and 120 $M_\odot$. We find $f_{11} = 0.179$ for the IMF of Chabrier (2005), 0.174 for the IMF of Kroupa (2001), and 0.242 for the Orion IMF of Muench et al. (2002) modified like in Murray & Rahman (2010). The total stellar mass of Sgr B2 based on the detected UCH II regions and corrected for the IMF with the extrapolation factor computed above is therefore ~3800, 3900, and 2800 $M_\odot$ for the three IMFs listed above, respectively.

As a consistency check, we also compute the total luminosity of the 49 H II regions detected by Gaume et al. (1995). We find $4.7 \times 10^6\,L_\odot$. We use Eq. (4) of Griffiths et al. (1988) to evaluate the contribution $f_{L,11}$ of all stars with a mass between 11 and 120 $M_\odot$ to the total luminosity of all stars with a mass between 0.01 and 120 $M_\odot$. We find $f_{L,11} = 99.4\%$, 99.5%, and 99.6% for the three IMFs listed above, respectively. We deduce a total stellar luminosity of $4.7 \times 10^6\,L_\odot$ for Sgr B2. This is within a factor of two consistent with the luminosity of ~$8.5 \times 10^6\,L_\odot$ derived for Sgr B2(N) and (M) by Goldsmith et al. (1992) from the modeling of the far-infrared continuum emission[15].

The lifetime of the UCH II regions detected in Sgr B2 is uncertain. With a lifetime of 10^5 yr (see Peters et al. 2010), we obtain a star formation rate of 0.028–0.039 $M_\odot$ yr^{-1} averaged over 10^5 yr for the Sgr B2 complex. This rate represents about 2–3% of the global star formation rate of the Galaxy (1.2±0.2 $M_\odot$ yr^{-1}, see Lee et al. 2012).

If the current star formation rate of Sgr B2 could be sustained over a longer period, it would take 130–360 Myr to consume the total mass of the complex (5–$10 \times 10^6\,M_\odot$, Lis & Goldsmith 1990). This timescale is about two orders of magnitude shorter than the Hubble time and 2.5 orders of magnitude shorter than the timescale of 69 Gyr obtained for the whole Galaxy with the star formation rate mentioned above and a mass of $8.3 \times 10^{10}\,M_\odot$ (without the dark halo, Sofue et al. 2009). This qualifies Sgr B2 as a ministarburst region.

References

Adande, G. R., Halfen, D. T., Ziurys, L. M., Quan, D., & Herbst, E. 2010, ApJ, 725, 561

Alekseev, E., Dyubko, S. F., Ilyushin, V. V., & Podnos, S. V. 1996, J. Mol. Spectrosc., 176, 316

Amano, T., & Maeda, A. 2000, J. Mol. Spectrosc., 203, 140

Amano, T., Hirao, T., & Takano, J. 2005, J. Mol. Spectrosc., 234, 170

Anderson, T., Herbst, E., & De Lucia, F. C. 1987, ApJS, 64, 703

Anderson, T., De Lucia, & Herbst, E. 1990a, ApJS, 72, 797

Anderson, T., Herbst, E., & De Lucia, F. C. 1990b, ApJS, 74, 647

Barclay, W. L., Jr., Anderson, M. A., Ziurys, L. M., Kleiner, I., & Hougen, J. T. 1993, ApJS, 89, 221

Baskakov, O., Dyubko, S. F. Ilyushin, V. V., et al. 1996, J. Mol. Spectrosc., 179, 94

Bauder, A., Lovas, F. J., & Johnson, D. R. 1976, J. Phys. Chem. Ref. Data, 5, 53

Bauer, A. 1971, J. Mol. Spectrosc., 40, 183

Bauer, A., & Maes, S. 1969, J. Phys. France, 30, 169

Bauer, A., Tarrago, G., & Remy, A. 1975, J. Mol. Spectrosc., 58, 111

Beers, Y., Klein, G. P., Kirchhoff, W. H., & Johnson, D. R. 1972, J. Mol. Spectrosc., 44, 553

Bellet, J., Samson, C., Steenbeckliers, G., & Wertheimer, R. 1971, J. Mol. Struct., 9, 49

---

[15] Goldsmith et al. (1992) assumed a distance of 8.5 kpc, while we use 7.9 kpc in this article. However, we do not correct the luminosity of Goldsmith et al. (1992) for the distance in this appendix because we compare it with the luminosity derived from the emission of UCH II regions that was analyzed by Gaume et al. (1995) who assumed the same distance as Goldsmith et al. (1992).

Belloche, A., Menten, K. M., Comito, C., et al. 2008, A&A, 482, 179; Erratum A&A, 492, 769

Belloche, A., Garrod, R. T., Müller, H. S. P., et al. 2009, A&A, 499, 215

Belov, S. P., Tretyakov, M. Y., Kleiner, I., & Hougen, J. T. 1993, J. Mol. Spectrosc., 160, 61

Belov, S., Yamada, K. M. T., Winnewisser, G., et al. 1995, J. Mol. Spectrosc., 173, 380

Belov, S. P., Tretyakov, M. Y., Kozin, I. N., et al. 1998, J. Mol. Spectrosc., 191, 17

Bernstein, M. P., Dworkin, J. P., Sandford, S. A., Cooper, G. W., & Allamandola, L. J. 2002, Nature, 416, 401

Bester, M., Tanimoto, M., Vowinkel, B., Winnewisser, G., & Yamada, K. 1983, Z. Naturforsch. A, 38, 64

Birk, M., Winnewisser, M., & Cohen, E. A. 1993, J. Mol. Spectrosc., 159, 69

Bisschop, S. E., Schilke, P., Wyrowski, F., et al. 2013, A&A, 552, A122

Blake, G. A., Sutton, E. C., Masson, C. R., et al. 1984, ApJ, 286, 586

Bocquet, R., Wlodarczak, G., Bauer, A., & Demaison, J. 1988, J. Mol. Spectrosc., 127, 382

Bogey, M., Demuynck, C., & Destombes, J. L. 1981, Chem. Phys. Lett., 81, 256

Bogey, M., Demuynck, C., & Destombes, J. L. 1982a, J. Mol. Spectrosc., 95, 35

Bogey, M., Demuynck, C., & Destombes, J. L. 1982b, Chem. Phys., 66, 99

Bogey, M., Demuynck, C., & Destombes, J. L. 1984, Can. J. Phys., 62, 1248

Bogey, M., Demuynck, C., & Destombes, J. L. 1986, Chem. Phys. Lett., 125, 383

Bogey, M., Demuynck, C., Destombes, J. L., & Dubus, H. 1987, J. Mol. Spectrosc., 122, 313

Bogey, M., Demuynck, C., Destombes, J., & Krupnov, A. 1988, J. Mol. Struct., 190, 465

Bogey, M., Dubus, H., & Guillemin, J. C. 1990, J. Mol. Spectrosc., 143, 180

Bogey, M., Civiš, S., Delcroix, B., et al. 1997, J. Mol. Spectrosc., 182, 85

Bouchez, A., Walters, A., Müller, H. S. P., et al. 2012, J. Quant. Spec. Radiat. Transf., 113, 1148

Braakman, R., Belloche, A., Blake, G. A., & Menten, K. M. 2010, ApJ, 724, 994

Brauer, C. S., Pearson, J. C., Drouin, B. J., & Yu, S. 2009, ApJS, 184, 133

Brown, R. D., Godfrey, P. D., McNaughton, D., & Yamanouchi, K. 1987, Mol. Phys., 62, 1429

Brünken, S., Müller, H. S. P., Lewen, F., & Winnewisser, G. 2003, Phys. Chem. Chem. Phys., 5, 1515

Brünken, S., Fuchs, U., Lewen, F., et al. 2004, J. Mol. Spectrosc., 225, 152

Brünken, S., Gottlieb, C. A., McCarthy, M. C., & Thaddeus, P. 2009a, ApJ, 697, 880

Brünken, S., Yu, Z., Gottlieb, C. A., McCarthy, M. C., & Thaddeus, P. 2009b, ApJ, 706, 1588

Brünken, S., Belloche, A., Martín, S., Verheyen, L., & Menten, K. M. 2010, A&A, 516, A109

Buffa, G., Tarrini, O., Cazzoli, G., & Dore, L. 1994, Phys. Rev. A, 49, 3557

Burenin, A. V., Val'Dov, A. N., Karyakin, E. N., Krupnov, A. F., & Shapin, S. M. 1981, J. Mol. Spectrosc., 87, 312

Butler, R. A. H., De Lucia, F. C., Petkie, D. T., et al. 2001, ApJS, 134, 319

Caselli, P., Myers, P. C., & Thaddeus, P. 1995, ApJ, 455, L77

Caswell, J. L. 1996, MNRAS, 283, 606

Cazzoli, G., & Kisiel, Z. 1988, J. Mol Spectrosc., 130, 303

Cazzoli, G., & Puzzarini, C. 2005, J. Mol. Spectrosc., 233, 280

Cazzoli, G., & Puzzarini, C. 2006, J. Mol. Spectrosc., 240, 153

Cazzoli, G., & Puzzarini, C. 2008, A&A, 487, 1197

Cazzoli, G., Puzzarini, C., & Lapinov, A. V. 2004, ApJ, 611, 615

Cazzoli, G., Puzzarini, C., & Gauss, J. 2005, ApJS, 159, 181

Cazzoli, G., Cludi, L., & Puzzarini, C. 2006, J. Mol. Struct., 780, 260

Chabrier, G. 2005, in The Initial Mass Function 50 Years Later, eds. E. Corbelli, F. Palla, & H. Zinnecker, Astrophys (Dordrecht: Springer), Space Sci. Library, 327, 41

Cho, S.-H., & Saito, S. 1998, ApJ, 496, L51

Christen, D., & Müller, H. S. P. 2003, Phys. Chem. Chem. Phys., 5, 3600

Cohen, E. A., & Pickett, H. M. 1982, J. Mol. Spectrosc., 93, 83

Cole, A. R. H., & Green, A. A. 1973, J. Mol. Spectrosc., 48, 246

Colmont, J. M., Wlodarczak, G., Priem, D., et al. 1997, J. Mol. Spectrosc., 181, 330

Comito, C., Schilke, P., Gerin, M., et al. 2003, A&A, 402, 635

Comito, C., Schilke, P., Phillips, T. G., et al. 2005, ApJS, 156, 127

Comito, C., Schilke, P., Rolffs, R., et al. 2010, A&A, 521, L38

Cornet, R. A., & Winnewisser, G. 1980, J. Mol. Spectrosc., 80, 438

Cosleou, J., Wlodarczak, G., Boucher, D., & Demaison, J. 1991, J. Mol. Spectrosc., 146, 49

Costain, C. C., & Morton, J. R. 1959, J. Chem. Phys., 31, 389

Creswell, R. A., Winnewisser, G., & Gerry, M. C. L. 1977, J. Mol. Spectrosc., 65, 420

Cummins, S. E., Linke, R. A., & Thaddeus, P. 1986, ApJS, 60, 819

Cunningham, M. R., Jones, P. A., Godfrey, P. D., et al. 2007, MNRAS, 376, 1201

Dahmen, G., Wilson, T. L., & Matteucci, F. 1995, A&A, 295, 194

Daly, A. M., Bermúdez, C., López, A., et al. 2013, ApJ, 768, 81

Dangoisse, D., Willemot, E., & Bellet, J. 1978, J. Mol. Spectrosc., 71, 414

de Lucia, F., & Gordy, W. 1969, Phys. Rev., 187, 58

de Lucia, F. C., & Helminger, P. 1975, J. Mol. Spectrosc., 54, 200

de Lucia, F. C., & Helminger, P. A. 1977, J. Chem. Phys., 67, 4262

de Lucia, F. C., Cook, R. L., Helminger, P., & Gordy, W. 1971, J. Chem. Phys., 55, 5334

Demaison, J., Dubrulle, A., Boucher, D., Burie, J., & Typke, V. 1979, J. Mol. Spectrosc., 76, 1

Demaison, J., Maes, H., van Eijck, B. P., Wlodarczak, G., & Lasne, M. C. 1987, J. Mol. Spectrosc., 125, 214

Demaison, J., Cosléou, J., Bocquet, R., & Lesarri, A. G. 1994, J. Mol. Spectrosc., 167, 400

de Pree, C. G., Goss, W. M., & Gaume, R. A. 1998, ApJ, 500, 847

de Vicente, P., Martin-Pintado, J., & Wilson, T. L. 1997, A&A, 320, 957

de Vicente, P., Martín-Pintado, J., Neri, R., & Colom, P. 2000, A&A, 361, 1058

Dickinson, D. F., & Kuiper, E. N. R. 1981, ApJ, 247, 112

Dixon, T. A., & Woods, R. C. 1977, J. Chem. Phys., 67, 3956

Dore, L., Puzzarini, C., & Cazzoli, G. 2001a, Can. J. Phys., 79, 359

Dore, L., Cazzoli, G., & Caselli, P. 2001b, A&A, 368, 712

Dore, L., Bizzocchi, L., Degli Esposti, C., & Tinti, F. 2009, A&A, 496, 275

Dore, L., Bizzocchi, L., Degli Esposti, C., & Gauss, J. 2010, J. Mol. Spectrosc., 263, 44

Dore, L., Bizzocchi, L., & Degli Esposti, C. 2012, A&A, 544, A19

Dubernet, M. L., Boudon, V., Culhane, J. L., et al. 2010, J. Quant. Spec. Radiat. Transf., 111, 2151

Dubrulle, A., Boucher, D., Burie, J., & Demaison, J. 1978, J. Mol. Spectrosc., 72, 158

Dubrulle, A., Demaison, J., Burie, J., & Boucher, D. 1980, Z. Naturforsch. A, 35, 471

Ehrenfreund, P., Glavin, D. P., Botta, O., Cooper, G., & Bada, J. L. 2001, Proc. Nat. Acad. Sci., 98, 2138

Elsila, J. E., Dworkin, J. P., Bernstein, M. P., Martin, M. P., & Sandford, S. A. 2007, ApJ, 660, 911

Elsila, J. E., Glavin, D. P., & Dworkin, J. P. 2009, Meteorit. Planet. Sci., 44, 1323

Endres, C. P., Drouin, B. J., Pearson, J. C., et al. 2009, A&A, 504, 635

Erlandsson, G., & Cox, J. 1956, J. Chem. Phys., 25, 778

Fayt, A., Vigouroux, C., Willaert, F., et al. 2004, J. Mol. Struct., 695, 295

Fortman, S. M., McMillan, J. P., Neese, C. F., et al. 2012, J. Mol. Spectrosc., 280, 11

Friedel, D. N., Snyder, L. E., Turner, B. E., & Remijan, A. 2004, ApJ, 600, 234

Fuchs, U., Brünken, S., Fuchs, G. W., et al. 2004, Z. Naturforsch. A, 59, 861

Fukuyama, Y., Odashima, H., Takagi, K., & Tsunekawa, S. 1996, ApJS, 104, 329

Fukuyama, Y., Omori, K., Odashima, H., Takagi, K., & Tsunekawa, S. 1999, J. Mol. Spectrosc., 193, 72

Furuya, R. S., Walmsley, C. M., Nakanishi, K., Schilke, P., & Bachiller, R. 2003, A&A, 409, L21

Gaume, R. A., & Claussen, M. J. 1990, ApJ, 351, 538

Gaume, R. A., Claussen, M. J., de Pree, C. G., Goss, W. M., & Mehringer, D. M. 1995, ApJ, 449, 663

Gensheimer, P. D. 1997, ApJ, 479, L75

Gerry, M. C. L., & Winnewisser, G. 1973, J. Mol. Spectrosc., 48, 1

Gibb, E., Nummelin, A., Irvine, W. M., Whittet, D. C. B., & Bergman, P. 2000, ApJ, 545, 309

Goldsmith, P. F., Krotkov, R., Snell, R. L., Brown, R. D., & Godfrey, P. 1983, ApJ, 274, 184

Goldsmith, P. F., Lis, D. C., Lester, D. F., & Harvey, P. M. 1992, ApJ, 389, 338

Golubiatnikov, G. Y., Lapinov, A. V., Guarnieri, A., & Knöchel, R. 2005, J. Mol. Spectrosc., 234, 190

Gottlieb, C. A., Myers, P. C., & Thaddeus, P. 2003, ApJ, 588, 655

Griffiths, S. C., Hicks, R. B., & Milone, E. F. 1988, JRASC, 82, 1

Groner, P., Albert, S., Herbst, E., et al. 2002, ApJS, 142, 145

Groner, P., Herbst, E., De Lucia, F. C., Drouin, B. J., & Mäder, H. 2006, J. Mol. Struct., 795, 173

Guarnieri, A., & Huckauf, A. 2003, Z. Naturforsch. A, 58, 272

Guarnieri, A., Hinze, R., Krüger, M., et al. 1992, J. Mol. Spectrosc., 156, 39

Gudeman, C. S. 1982, Ph.D. Thesis, University of Wisconsin, Madison, WI, USA

Gudeman, C. S., & Woods, R. C. 1982, Phys. Rev. Lett., 48, 1344

Gudeman, C. S., Haese, N. N., Piltch, N. D., & Woods, R. C. 1981, ApJ, 246, L47

Halfen, D. T., Ziurys, L. M., Brünken, S., et al. 2009, ApJ, 702, L124

Halfen, D. T., Ilyushin, V., & Ziurys, L. M. 2011, ApJ, 743, 60

Haque, S. S., Lees, R. M., Saint Clair, J. M., Beers, Y., & Johnson, D. R. 1974, ApJ, 187, L15

Hardy, J. A., Cox, A. P., Fliege, E., & Dreizler, H. 1982, Z. Naturforsch., 37, 1035
Herbst, E., & van Dishoeck, E. F. 2009, ARA&A, 47, 427
Herbst, E., Messer, J. K., de Lucia, F. C., & Helminger, P. 1984, J. Mol. Spectrosc., 108, 42
Hieret, C. O. 2005, Absorption studies along the line of sight towards Sgr B2(M), Diplomarbeit in Physik, Mathematisch-Naturwissenschaftlichen Fakultät der Rheinischen Friedrich-Wilhelms-Universität Bonn, Germany
Hinze, R., Zerbe-Foese, H. Doose, J., & Guarnieri, A. 1996, J. Mol. Spectrosc., 176, 133
Hirose, C. 1974, ApJ, 189, L145
Hocking, W. H., Gerry, M. C. L., & Winnewisser, G. 1975, Can. J. Phys., 53, 1869
Hollis, J. M., Lovas, F. J., & Jewell, P. R. 2000, ApJ, 540, L107
Hollis, J. M., Lovas, F. J., Jewell, P. R., & Coudert, L. H. 2002, ApJ, 571, L59
Hollis, J. M., Pedelty, J. A., Boboltz, D. A., et al. 2003, ApJ, 596, L235
Hollis, J. M., Jewell, P. R., Lovas, F. J., Remijan, A., & Møllendal, H. 2004, ApJ, 610, L21
Hollis, J. M., Lovas, F. J., Remijan, A. J., et al. 2006, ApJ, 643, L25
Huiszoon, C. 1971, Rev. Sci. Instrum., 42, 477
Ikeda, M., Duan, Y.-B., Tsunekawa, S., & Takagi, K. 1998, ApJS, 117, 249
Ilyushin, V. V., Alekseev, E. A., Dyubko, S. F., et al. 2001, J. Mol. Spectrosc., 205, 286
Ilyushin, V. V., Alekseev, E. A., Dyubko, S. F., Kleiner, I., & Hougen, J. T. 2004, J. Mol. Spectrosc., 227, 115
Ilyushin, V. V., Alekseev, E. A., Dyubko, S. F., Motiyenko, R. A., & Hougen, J. T. 2005, J. Mol. Spectrosc., 229, 170
Ilyushin, V., Kleiner, I., & Lovas, F. J. 2008, J. Phys. Chem. Ref. Data, 37, 97
Ilyushin, V., Kryvda, A., & Alekseev, E. 2009, J. Mol. Spectrosc., 255, 32
Irvine, W. M., Brown, R. D., Cragg, D. M., et al. 1988, ApJ, 335, L89
Jacq, T., Walmsley, C. M., Henkel, C., et al. 1990, A&A, 228, 447
Jacq, T., Baudry, A., Walmsley, C. M., & Caselli, P. 1999, A&A, 347, 957
Johns, J. W. C. 1985, J. Opt. Soc. Am. B, 2, 1340
Johns, J. W. C., Nemes, L., Yamada, K. M. T., et al. 1992, J. Mol. Spectrosc., 156, 501
Johnson, D. R., Lovas, F. J., & Kirchhoff, W. H. 1972, J. Phys. Chem. Ref. Data, 1, 1011
Johnson, D. R., Suenram, R. D., & Lafferty, W. J. 1976, ApJ, 208, 245
Jones, P. A., Cunningham, M. R., Godfrey, P. D., & Cragg, D. M. 2007, MNRAS, 374, 579
Jones, P. A., Burton, M. G., Cunningham, M. R., et al. 2008, MNRAS, 386, 117
Kalenskii, S. V., & Johansson, L. E. B. 2010, Astron. Rep., 54, 1084
Karakawa, Y., Oka, K., Odashima, H., Takagi, K., & Tsunekawa, S. 2001, J. Mol. Spectrosc., 210, 196
Kawaguchi, K., Ohishi, M., Ishikawa, S.-I., & Kaifu, N. 1992, ApJ, 386, L51
Kisiel, Z., Pszczółkowski, L., Drouin, B. J., et al. 2009, J. Mol. Spectrosc., 258, 26
Kisiel, Z., Pszczółkowski, L., Drouin, B. J., et al. 2012, J. Mol. Spectrosc., 280, 134
Klapper, G., Lewen, F., Belov, S. P., & Winnewisser, G. 2000, Z. Naturforsch. A, 55, 441
Klapper, G., Lewen, F., Gendriesch, R., Belov, S. P., & Winnewisser, G. 2001, Z. Naturforsch. A, 56, 329
Klapper, G., Surin, L., Lewen, F., et al. 2003, ApJ, 582, 262
Klaus, T., Saleck, A. H., Belov, S. P., et al. 1996, J. Mol. Spectrosc., 180, 197
Kleiner, I., Hougen, J. T., Suenram, R. D., Lovas, F. J., & Godefroid, M. 1991, J. Mol. Spectrosc., 148, 38
Kleiner, I., Hougen, J. T., Suenram, R. D., Lovas, F. J., & Godefroid, M. 1992, J. Mol. Spectrosc., 153, 578
Kleiner, I., Lovas, F. J., & Godefroid, M. 1996, J. Phys. Chem. Ref. Data, 25, 1113
Kraśnicki, A., & Kisiel, Z. 2011, J. Mol. Spectrosc., 270, 83
Kraśnicki, A., Kisiel, Z., Drouin, B. J., & Pearson, J. C. 2011a, J. Mol. Struct., 1006, 20
Kraśnicki, A., Kisiel, Z., Jabs, W., Winnewisser, B. P., & Winnewisser, M. 2011b, J. Mol. Spectrosc., 267, 144
Kréglewski, M., & Wlodarczak, G. 1992, J. Mol. Spectrosc., 156, 383
Kroupa, P. 2001, MNRAS, 322, 231
Kryvda, A. V., Gerasimov, V. G., Dyubko, S. F., Alekseev, E. A., & Motiyenko, R. A. 2009, J. Mol. Spectrosc., 254, 28
Kuan, Y.-J., Mehringer, D. M., & Snyder, L. E. 1996, ApJ, 459, 619
Kuriyama, H., Takagi, K., Takeo, H., & Matsumura, C. 1986, ApJ, 311, 1073
Kutsenko, A. S., Motiyenko, R. A., Margulès, L., & Guillemin, J.-C. 2013, A&A, 549, A128
Lapinov, A. V., Golubiatnikov, G. Y., Markov, V. N., & Guarnieri, A. 2007, Astron. Lett., 33, 121
Larsen, N. W., & Winnewisser, B. P. 1974, Z. Naturforsch. A, 29, 1213
Lattanzi, V., Walters, A., Drouin, B. J., & Pearson, J. C. 2007, ApJ, 662, 771

Lee, E. J., Murray, N., & Rahman, M. 2012, ApJ, 752, 146
Lee, S. K., Ozeki, H., & Saito, S. 1995, ApJS, 98, 351
Lees, R. M., & Baker, J. G. 1968, J. Chem. Phys., 48, 5299
Lees, R. M., & Mohammadi, M. A. 1980, Can. J. Phys., 58, 1640
Liang, W., Baker, J. G., Herbst, E., Booker, R. A., & de Lucia, F. C. 1986, J. Mol. Spectrosc., 120, 298
Lis, D. C., & Goldsmith, P. F. 1990, ApJ, 356, 195
Lis, D. C., Goldsmith, P. F., Carlstrom, J. E., & Scoville, N. Z. 1993, ApJ, 402, 238
Liu, S., & Snyder, L. E. 1999, ApJ, 523, 683
Lovas, F. J., Lutz, H., & Dreizler, H. 1979, J. Phys. Chem. Ref. Data, 8, 1051
Lovas, F. J., Hollis, J. M., Remijan, A. J., & Jewell, P. R. 2006, ApJ, 645, L137
Lowry Manson, E., Jr., Clark, W. W., De Lucia, F. C., & Gordy, W. 1977, Phys. Rev. A, 15, 223
Maeda, A., Medvedev, I. R., Winnewisser, M., et al. 2008, ApJS, 176, 543
Maes, H., Wlodarczak, G., Boucher, D., & Demaison, J. 1987, Z. Naturforsch. A, 42, 97
Margulès, L., Lewen, F., Winnewisser, G., Botschwina, P., & Müller, H. S. P. 2003, Phys. Chem. Chem. Phys., 5, 2770
Margulès, L., Motiyenko, R., Demyk, K., et al. 2009, A&A, 493, 565
Mbosei, L., Fayt, A., Dréan, P., & Cosléou, J. 2000, J. Mol. Struct., 517, 271
McCarthy, M. C., Gottlieb, C. A., & Thaddeus, P. 1995, J. Mol. Spectrosc., 173, 303
McNaughton, D., & Bruget, D. N. 1993, J. Mol. Spectrosc., 159, 340
Medcraft, C., Thompson, C. D., Robertson, E. G., Appadoo, D. R. T., & McNaughton, D. 2012, ApJ, 753, 18
Medvedev, I. R., De Lucia, F. C., & Herbst, E. 2009, ApJS, 181, 433
Mehringer, D. M., Palmer, P., Goss, W. M., & Yusef-Zadeh, F. 1993, ApJ, 412, 684
Mehringer, D. M., Snyder, L. E., Miao, Y., & Lovas, F. J. 1997, ApJ, 480, L71
Mehringer, D. M., Pearson, J. C., Keene, J., & Phillips, T. G. 2004, ApJ, 608, 306
Menten, K. M. 1991a, in Atoms, Ions and Molecules: New Results in Spectral Line Astrophysics, eds. A. D. Haschick & P. T. P. Ho, ASP Conf. Ser. (San Francisco, CA: ASP), 16, 119
Menten, K. M. 1991b, ApJ, 380, L75
Menten, K. M. 2004, in The Dense Interstellar Medium in Galaxies, eds. Pfalzner, Kramer, Staubmeier & Heithausen, Springer Proc. physics (Berlin, Heidelberg: Springer), 91, 69
Menten, K. M., Wyrowski, F., Belloche, A., et al. 2011, A&A, 525, A77
Milam, S. N., Savage, C., Brewster, M. A., Ziurys, L. M., & Wyckoff, S. 2005, ApJ, 634, 1126
Mollaaghababa, R., Gottlieb, C. A., Vrtilek, J. M., & Thaddeus, P. 1991, ApJ, 368, L19
Møllendal, H., Margulès, L., Belloche, A., et al. 2012, A&A, 538, A51
Morino, I., Yamada, K. M. T., & Maki, A. G. 2000, J. Mol. Spectrosc., 200, 145
Motiyenko, R. A., Tercero, B., Cernicharo, J., & Margulès, L. 2012, A&A, 548, A71
Muench, A. A., Lada, E. A., Lada, C. J., & Alves, J. 2002, ApJ, 573, 366
Müller, H. S. P., & Brünken, S. 2005, J. Mol. Spectrosc., 232, 213
Müller, H. S. P., & Christen, D. 2004, J. Mol. Spectrosc., 228, 298
Müller, H. S. P., Farhoomand, J., Cohen, E. A., et al. 2000a, J. Mol. Spectrosc., 201, 1
Müller, H. S. P., Gendriesch, R., Lewen, F., & Winnewisser, G. 2000b, Z. Naturforsch. A, 55, 486
Müller, H. S. P., Gendriesch, R., Margulès, L., et al. 2000c, Phys. Chem. Chem. Phys., 2, 3401
Müller, H. S. P., Thorwirth, S., Roth, D. A., & Winnewisser, G. 2001, A&A, 370, L49
Müller, H. S. P., Pracna, P., & Horneman, V.-M. 2002, J. Mol. Spectrosc., 216, 397
Müller, H. S. P., Menten, K. M., & Mäder, H. 2004, A&A, 428, 1019
Müller, H. S. P., Schlöder, F., Stutzki, J., & Winnewisser, G. 2005, J. Mol. Struct., 742, 215
Müller, H. S. P., McCarthy, M. C., Bizzocchi, L., et al. 2007, Phys. Chem. Chem. Phys., 9, 1579
Müller, H. S. P., Belloche, A., Menten, K. M., Comito, C., & Schilke, P. 2008, J. Mol. Spectrosc., 251, 319
Müller, H. S. P., Drouin, B. J., & Pearson, J. C. 2009, A&A, 506, 1487
Müller, H. S. P., Drouin, B. J., Pearson, J. C., et al. 2010a, contribution RC12, 65th International Symposium On Molecular Spectroscopy, Columbus, OH, USA
Müller, H. S. P., Dong, F., Nesbitt, D. J., Furuya, T., & Saito, S. 2010b, Phys. Chem. Chem. Phys., 12, 8362
Murray, N., & Rahman, M. 2010, ApJ, 709, 424
Neill, J. L., Muckle, M. T., Zaleski, D. P., et al. 2012, ApJ, 755, 153
Nemes, L., Luckhaus, D., Quack, M., & Johns, J. W. C. 2000, J. Mol. Struct., 517, 217

Neustock, W., Guarnieri, A., Demaison, J., & Wlodarczak, G. 1990, Z. Naturforsch. A, 45, 702

Niedenhoff, M., Winnewisser, G., Yamada, K. M. T., & Belov, S. P. 1995, J. Mol. Spectrosc., 169, 224

Niedenhoff, M., Yamada, K. M. T., & Winnewisser, G. 1996, J. Mol. Spectrosc., 176, 342

Nielsen, C. J. 1973, Ph.D. Thesis, Københavns Universitet, Denmark

Nummelin, A., & Bergman, P. 1999, A&A, 341, L59

Nummelin, A., Bergman, P., Hjalmarson, Å., et al. 1998, ApJS, 117, 427

Nummelin, A., Bergman, P., Hjalmarson, Å., et al. 2000, ApJS, 128, 213

Ordu, M. H., Müller, H. S. P., Walters, A., et al. 2012, A&A, 541, A121

Padovani, M., Walmsley, C. M., Tafalla, M., Galli, D., & Müller, H. S. P. 2009, A&A, 505, 1199

Pagani, L., Daniel, F., & Dubernet, M.-L. 2009, A&A, 494, 719

Pan, J., Albert, S., Sastry, K. V. L. N., Herbst, E., & De Lucia, F. C. 1998, ApJ, 499, 517

Panagia, N. 1973, AJ, 78, 929

Pardo, J. R., Cernicharo, J., Goicoechea, J. R., Guélin, M., & Asensio Ramos, A. 2007, ApJ, 661, 250

Pearson, E. F., Creswell, R. A., Winnewisser, M., & Winnewisser, G. 1976, Z. Naturforsch. A, 31, 1394

Pearson, J. C., Sastry, K. V. L. N., Winnewisser, M., Herbst, E., & de Lucia, F. C. 1995, J. Phys. Chem. Ref. Data, 24, 1

Pearson, J. C., Sastry, K. V. L. N., Herbst, E., & De Lucia, F. C. 1996, J. Mol. Spectrosc., 175, 246

Pearson, J. C., Sastry, K. V. L. N., Herbst, E., & De Lucia, F. C. 1997, ApJ, 480, 420

Pearson, J. C., Brauer, C. S., & Drouin, B. J. 2008, J. Mol. Spectrosc., 251, 394

Pearson, J. C., Brauer, C. S., Yu, S., & Drouin, B. J. 2009, contribution WH13, 64th International Symposium On Molecular Spectroscopy, Columbus, OH, USA

Peng, Y., Vogel, S. N., & Carlstrom, J. E. 1993, ApJ, 418, 255

Penzias, A. A. 1981, ApJ, 249, 513

Peters, T., Mac Low, M.-M., Banerjee, R., Klessen, R. S., & Dullemond, C. P. 2010, ApJ, 719, 831

Pickett, H. M., Cohen, E. A., Brinza, D. E., & Schaefer, M. M. 1981, J. Mol. Spectrosc., 89, 542

Pickett, H. M., Poynter, R. L., Cohen, E. A., Delitsky, M. L., Pearson, J. C., & Müller, H. S. P. 1998, J. Quant. Spec. Radiat. Transf., 60, 883

Qin, S.-L., Schilke, P., Rolffs, R., et al. 2011, A&A, 530, L9

Raymonda, J., & Klemperer, W. 1971, J. Chem. Phys., 55, 232

Read, W. G., Cohen, E. A., & Pickett, H. M. 1986, J. Mol. Spectrosc., 115, 316

Reid, M. J., Menten, K. M., Zheng, X. W., Brunthaler, A., & Xu, Y. 2009, ApJ, 705, 1548

Remijan, A. J., Hollis, J. M., Lovas, F. J., et al. 2008, ApJ, 675, L85

Requena-Torres, M. A., Martín-Pintado, J., Rodríguez-Franco, A., et al. 2006, A&A, 455, 971

Richard, C., Margulès, L., Motiyenko, R. A., & Guillemin, J.-C. 2012, A&A, 543, A135

Rodler, M. 1983, Ph.D. Thesis, Eidgenössische Technische Hochschule, Zürich, Switzerland

Rodler, M. 1985, J. Mol. Spectrosc., 114, 23

Rodler, M., Brown, R. D., Godfrey, P. D., & Tack, L. M. 1984, Chem. Phys. Lett., 110, 447

Rodler, M., Brown, R. D., Godfrey, P. D., & Kleibömer, B. 1986, J. Mol. Spectrosc., 118, 267

Rodríguez-Fernández, N. J., Tafalla, M., Gueth, F., & Bachiller, R. 2010, A&A, 516, A98

Rolffs, R., Schilke, P., Wyrowski, F., et al. 2011, A&A, 529, A76

Saito, S. 1976, Chem. Phys. Lett., 42, 399

Saito, S., Kawaguchi, K., Yamamoto, S., et al. 1987, ApJ, 317, L115

Sakai, N., Saruwatari, O., Sakai, T., Takano, S., & Yamamoto, S. 2010, A&A, 512, A31

Saleck, A. H., Simon, R., & Winnewisser, G. 1994, ApJ, 436, 176

Saleck, A., Tanimoto, M., Belov, S. P., Klaus, T., & Winnewisser, G. 1995a, J. Mol. Spectrosc., 171, 481

Saleck, A. H., Ozeki, H., & Saito, S. 1995b, Chem. Phys. Lett., 244, 199

Sanz, M. E., McCarthy, M. C., & Thaddeus, P. 2005, J. Chem. Phys., 122, 194319

Sastry, K. V. L. N., Lees, R. M., & de Lucia, F. C. 1984, J. Mol. Spectrosc., 103, 486

Sastry, K. V. L. N., Herbst, E., Booker, R. A., & de Lucia, F. C. 1986, J. Mol. Spectrosc., 116, 120

Saykally, R. J., Szanto, P. G., Anderson, T. G., & Woods, R. C. 1976, ApJ, 204, L143

Schilke, P., Groesbeck, T. D., Blake, G. A., & Phillips, T. G. 1997, ApJS, 108, 301

Schilke, P., Phillips, T. G., & Mehringer, D. M. 1999, in The Physics and Chemistry of the Interstellar Medium, eds. V. Ossenkopf, J. Stutzki & G. Winnewisser (GCA-Verlag Herdecke), 330

Schmid-Burgk, J., Muders, D., Müller, H. S. P., & Brupbacher-Gatehouse, B. 2004, A&A, 419, 949

Scoville, N. Z., Solomon, P. M., & Penzias, A. A. 1975, ApJ, 201, 352

Snyder, L. E., Lovas, F. J., Hollis, J. M., Friedel, D. N., et al. 2005, ApJ, 619, 914

Sofue, Y., Honma, M., & Omodaka, T. 2009, PASJ, 61, 227

Spezzano, S., Tamassia, F., Thorwirth, S., et al. 2012, ApJS, 200, 1

Stubgaard, M. 1978, Ph.D. Thesis, Københavns Universitet, Denmark

Sutton, E. C., Jaminet, P. A., Danchi, W. C., & Blake, G. A. 1991, ApJS, 77, 255

Tafalla, M., Santiago-García, J., Hacar, A., & Bachiller, R. 2010, A&A, 522, A91

Tang, J., & Saito, S. 1995, ApJ, 451, L93

Tercero, B., Cernicharo, J., Pardo, J. R., & Goicoechea, J. R. 2010, A&A, 517, A96

Thorwirth, S., Müller, H. S. P., & Winnewisser, G. 2000a, J. Mol. Spectrosc., 204, 133

Thorwirth, S., Müller, H. S. P., Lewen, F., Gendriesch, R., & Winnewisser, G. 2000b, A&A, 363, L37

Thorwirth, S., Müller, H. S. P., & Winnewisser, G. 2001, Phys. Chem. Chem. Phys., 3, 1236

Thorwirth, S., Müller, H. S. P., Lewen, F., et al. 2003, ApJ, 585, L163

Tiemann, E. 1982, J. Mol. Spectrosc., 91, 60

Tinti, F., Bizzocchi, L., Degli Esposti, C., & Dore, L. 2007, ApJ, 669, L113

Törring, T. 1968, Z. Naturforsch. A, 23, 777

Turner, B. E. 1989, ApJS, 70, 539

Turner, B. E. 1991, ApJS, 76, 617

Turner, B. E., & Apponi, A. J. 2001, ApJ, 561, L207

Vacherand, J. M., van Eijck, B. P., Burie, J., & Demaison, J. 1986, J. Mol. Spectrosc., 118, 355

van der Tak, F. F. S., Müller, H. S. P., Harding, M. E., & Gauss, J. 2009, A&A, 507, 347

van Dijk, F., & Dymanus, A. 1974, Chem. Phys., 6, 474

Vanek, M. D., Jennings, D. A., Wells, J. S., & Maki, A. G. 1989, J. Mol. Spectrosc., 138, 79

Vrtílek, J. M., Gottlieb, C. A., & Thaddeus, P. 1987, ApJ, 314, 716

Whiteoak, J. B., Gardner, F. F., Caswell, J. L., et al. 1988, MNRAS, 235, 655

Widicus Weaver, S. L., Butler, R. A. H., Drouin, B. J., et al. 2005, ApJS, 158, 188

Wilson, T. L., & Rood, R. 1994, ARA&A, 32, 191

Winnewisser, G. 1973, J. Mol. Spectrosc., 46, 16

Winnewisser, G., Belov, S. P., Klaus, T., & Schieder, R. 1997, J. Mol. Spectrosc., 184, 468

Winnewisser, M., Winnewisser, G., Honda, T., & Hirota, E. 1975, Z. Naturforsch. A, 30, 1001

Winnewisser, M., Winnewisser, B. P., Stein, M., et al. 2002, J. Mol. Spectrosc., 216, 259

Winton, R. S., & Gordy, W. 1970, Phys. Lett. A, 32, 219

Wlodarczak, G., Martinache, L., Demaison, J., Marstokk, K.-M., & Møllendal, H. 1988, J. Mol. Spectrosc., 127, 178

Wouterloot, J. G. A., Henkel, C., Brand, J., & Davis, G. R. 2008, A&A, 487, 237

Wyrowski, F., Schilke, P., & Walmsley, C. M. 1999, A&A, 341, 882

Xu, L.-H., & Lovas, F. J. 1997, J. Phys. Chem. Ref. Data, 26, 17

Xu, L.-H., Fisher, J., Lees, R. M., et al. 2008, J. Mol. Spectrosc., 251, 305

Xu, L.-H., Lees, R. M., Crabbe, G. T., et al. 2012, J. Chem. Phys., 137, 104313

Yamada, K. 1977, J. Mol. Spectrosc., 68, 423

Yamada, K., & Winnewisser, M. 1977, J. Mol. Spectrosc., 68, 307

Yamada, K., Winnewisser, M., Winnewisser, G., Szalanski, L. B., & Gerry, M. C. L. 1979, J. Mol. Spectrosc., 78, 189

Yamada, K. M. T., & Creswell, R. A. 1986, J. Mol. Spectrosc., 116, 384

Yamada, K. M. T., Moravec, A., & Winnewisser, G. 1995, Z. Naturforsch. A, 50, 1179

Yamada, K. M. T., Degli Esposti, C., Botschwina, P., et al. 2004, A&A, 425, 767

Yamaguchi, T., Takano, S., Sakai, N., et al. 2011, PASJ, 63, L37

Zelinger, Z., Amano, T., Ahrens, V., et al. 2003, J. Mol. Spectrosc., 220, 223

Zernickel, A., Schilke, P., Schmiedeke, A., et al. 2012, A&A, 546, A87

Ziurys, L. M. 1987, ApJ, 321, L81
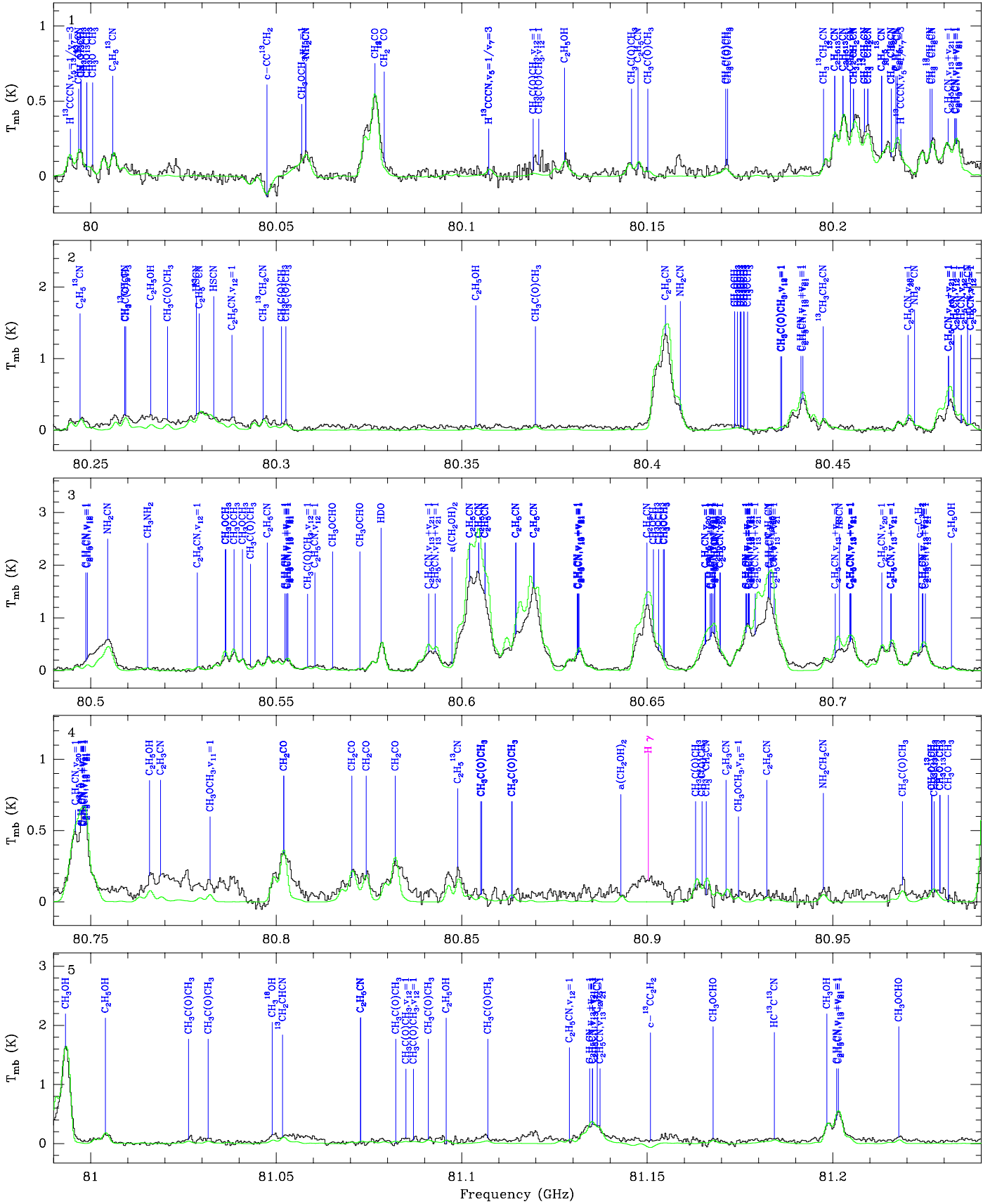
Fig. 2. Spectrum obtained toward Sgr B2(N) in the 3 mm window with the IRAM 30 m telescope in main-beam temperature scale. The synthetic model is overlaid in green and its relevant lines are labeled in blue. The frequencies of the hydrogen recombination lines are indicated with a pink label. The position of the lines with a peak temperature higher than 2 K in the image band and possibly contaminating the spectrum are marked with a red label indicating their rest frequency and their peak temperature in K in the image band.

Fig. 2. continued.
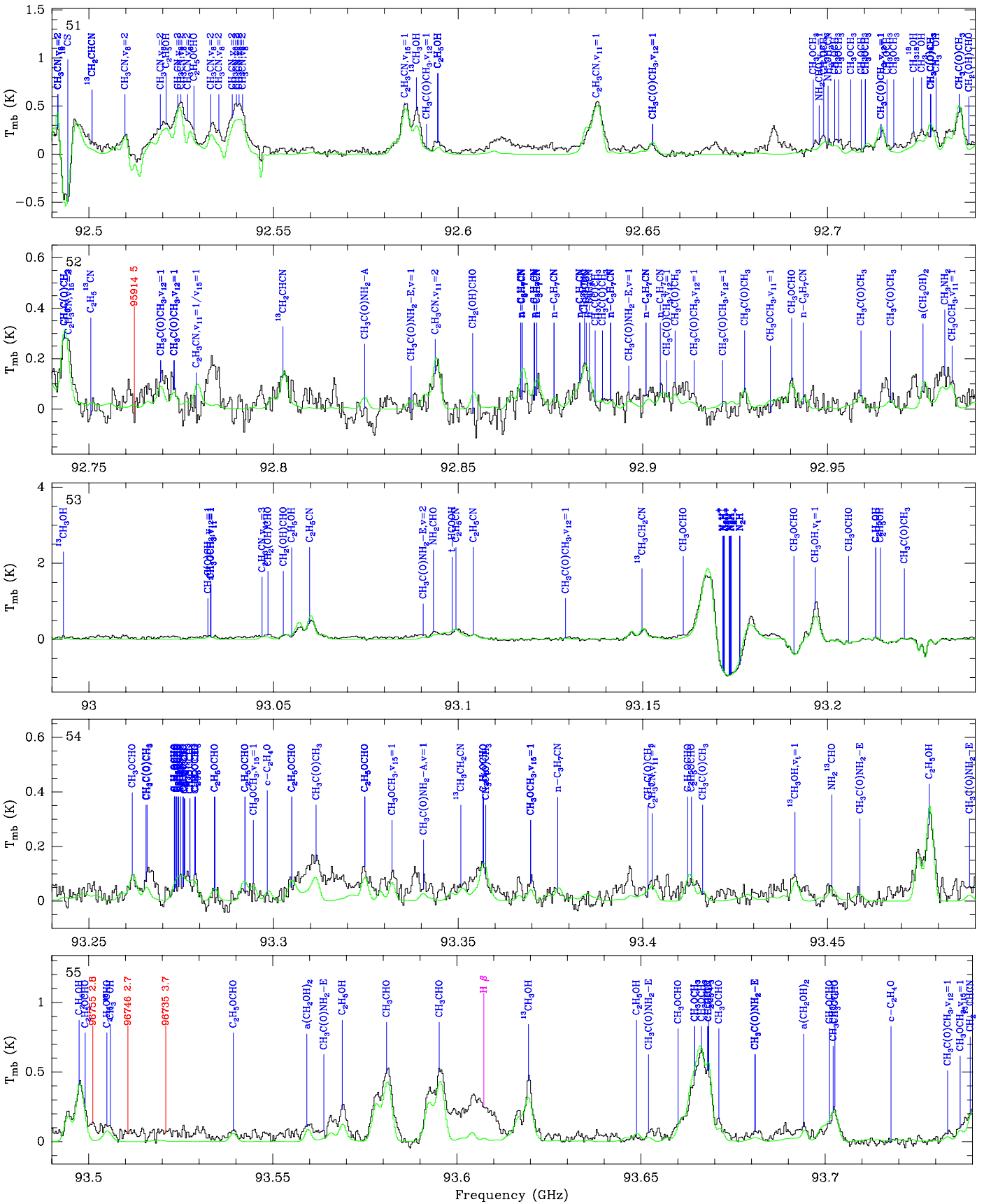
Fig. 2. continued.
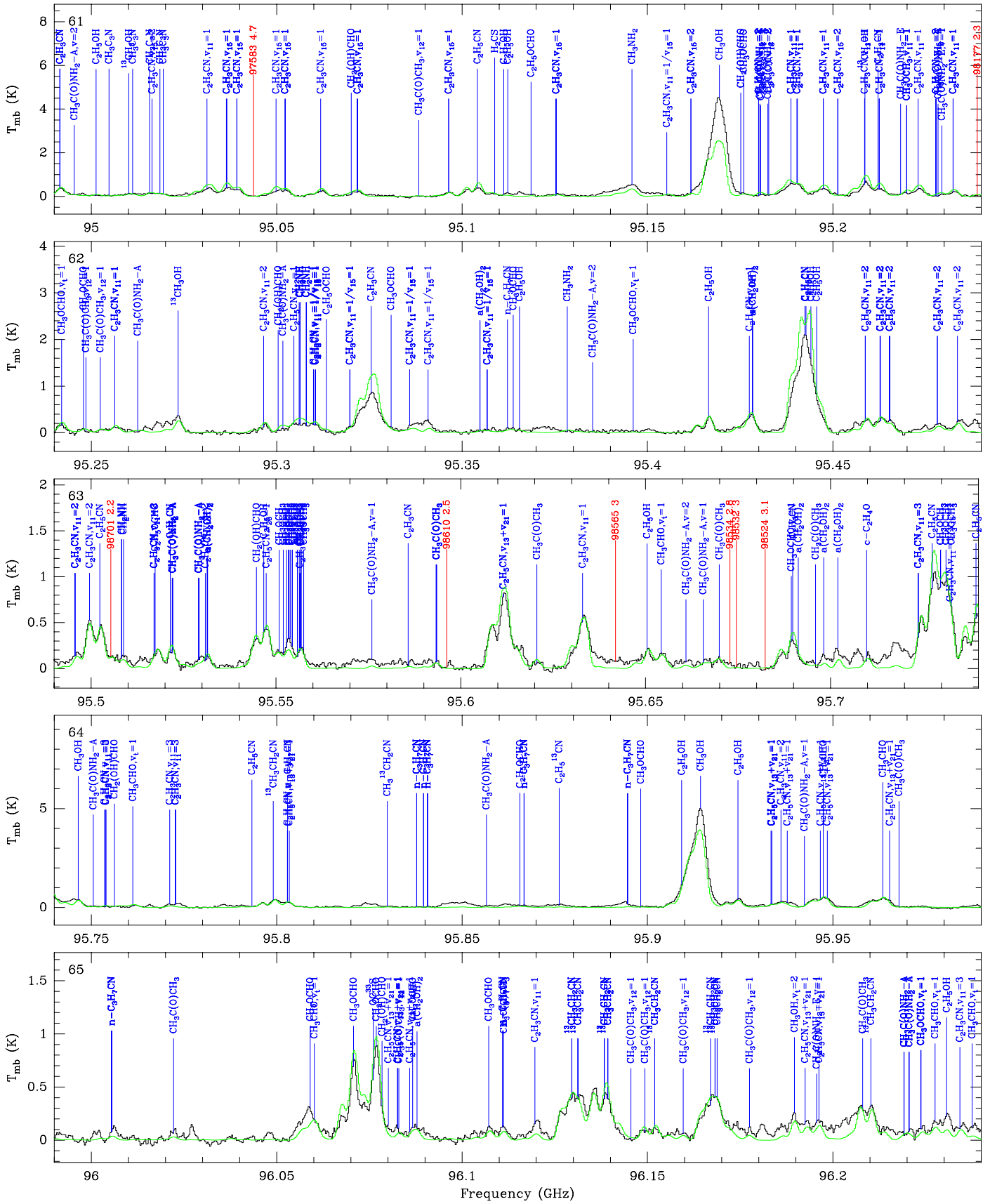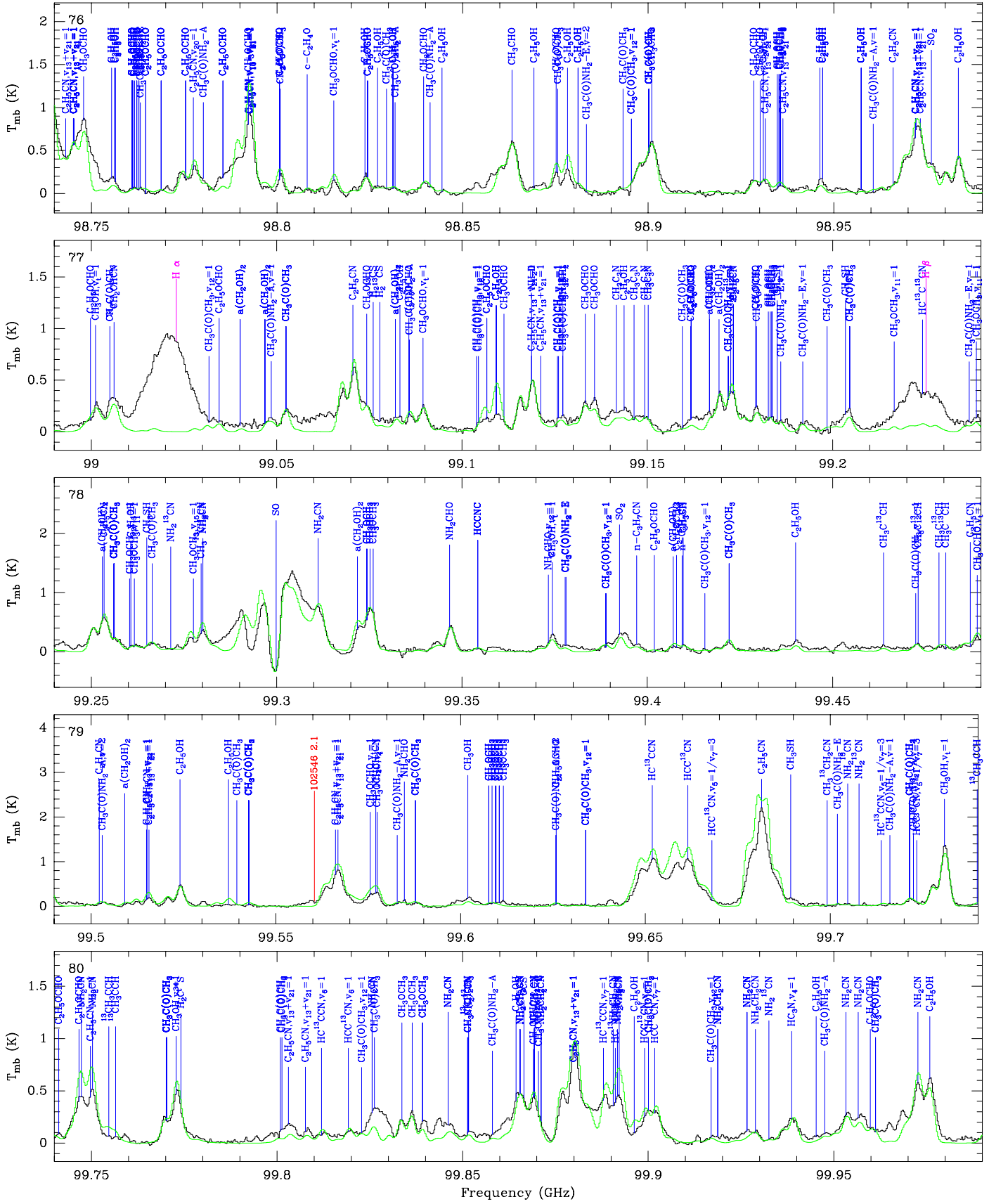
Fig. 2. continued.

Fig. 2. continued.

Fig. 2. continued.

Fig. 2. continued.

Fig. 2. continued.

Fig. 2. continued.

Fig. 2. continued.

Fig. 2. continued.

Fig. 2. continued.

Fig. 2. continued.

Fig. 2. continued.

Fig. 2. continued.

Fig. 2. continued.

Fig. 2. continued.

Fig. 2. continued.

Fig. 2. continued.

Fig. 2. continued.

Fig. 2. continued.

Fig. 2. continued.

Fig. 2. continued.
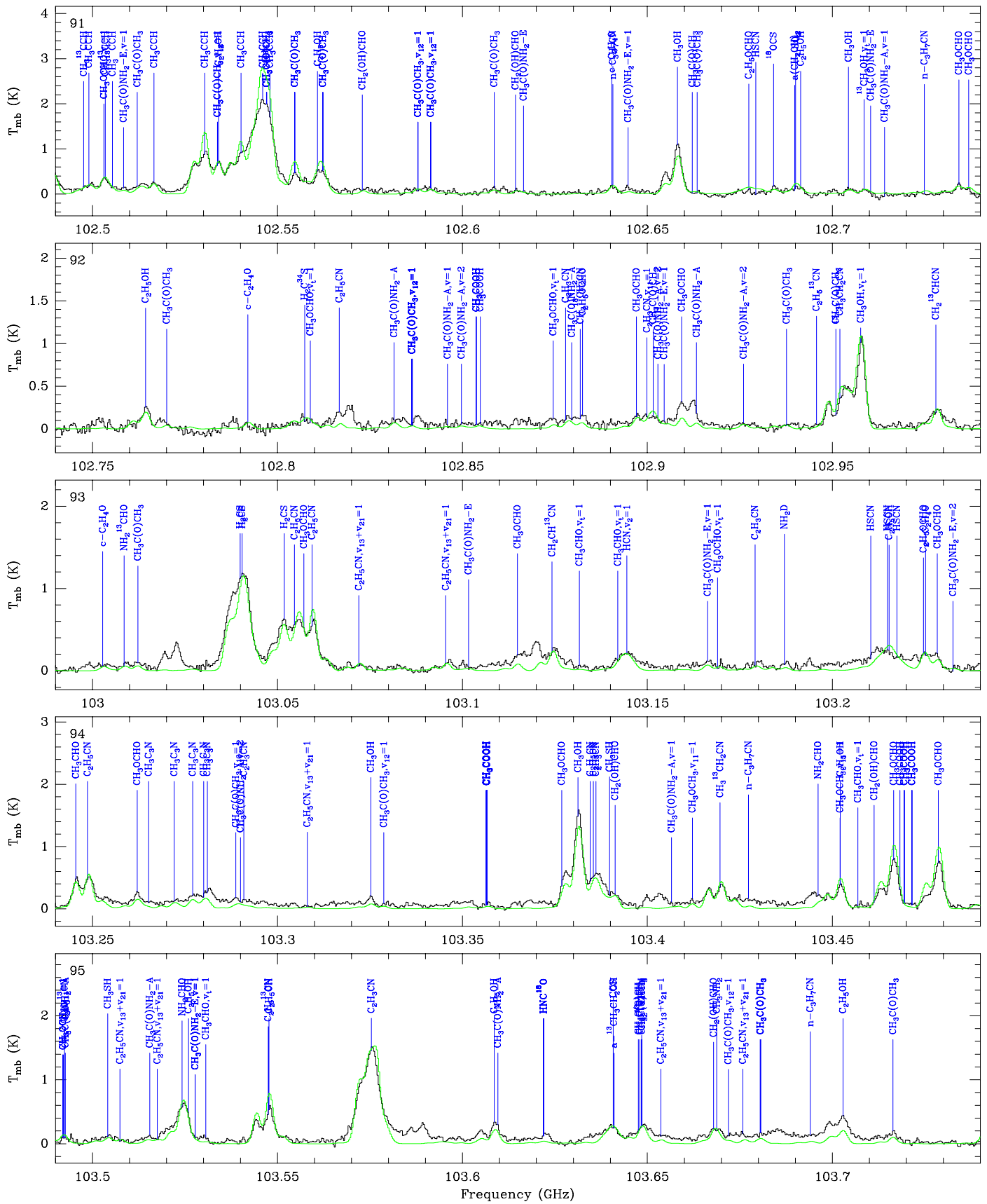
Fig. 2. continued.
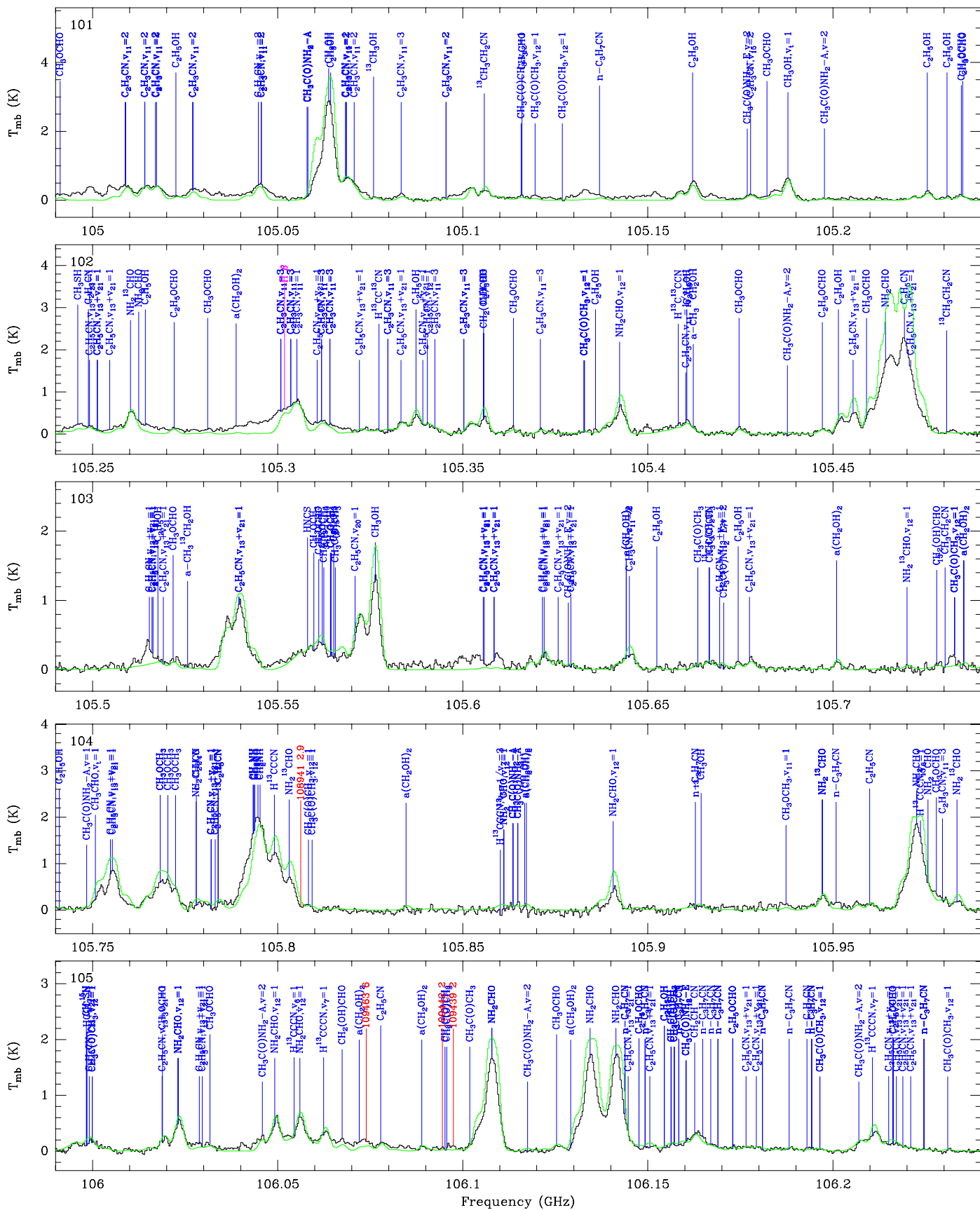
Fig. 2. continued.
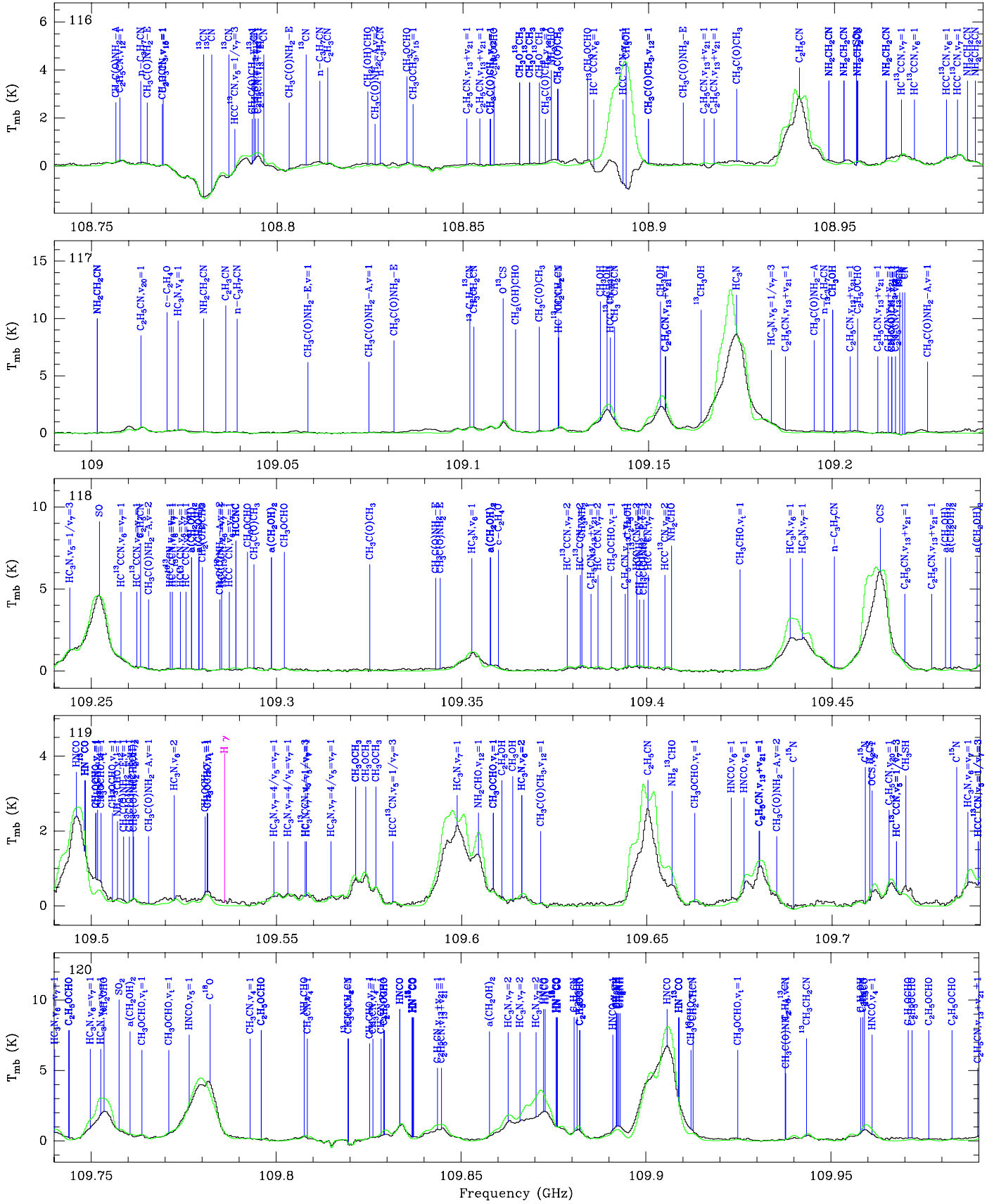
Fig. 2. continued.
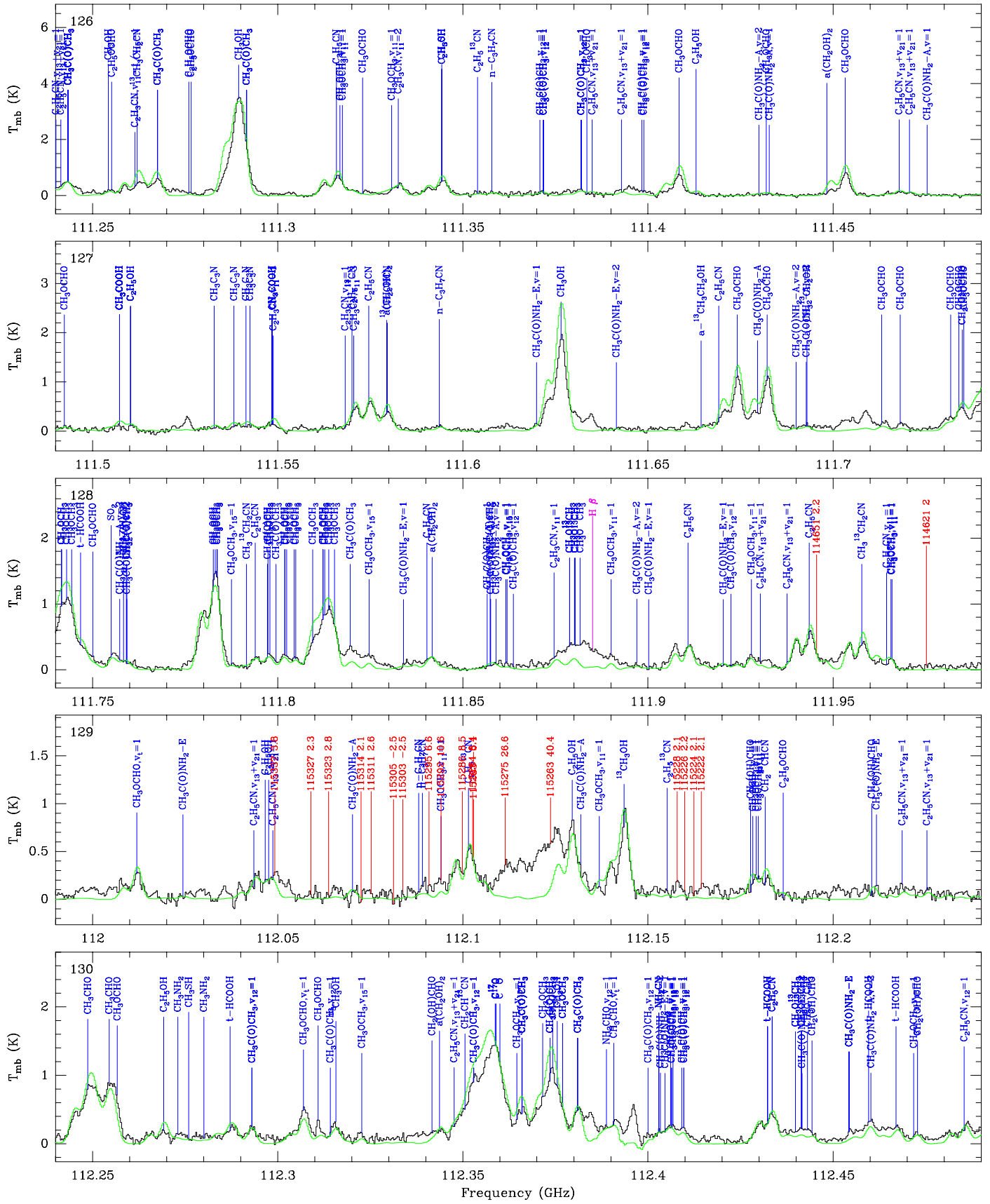
Fig. 2. continued.
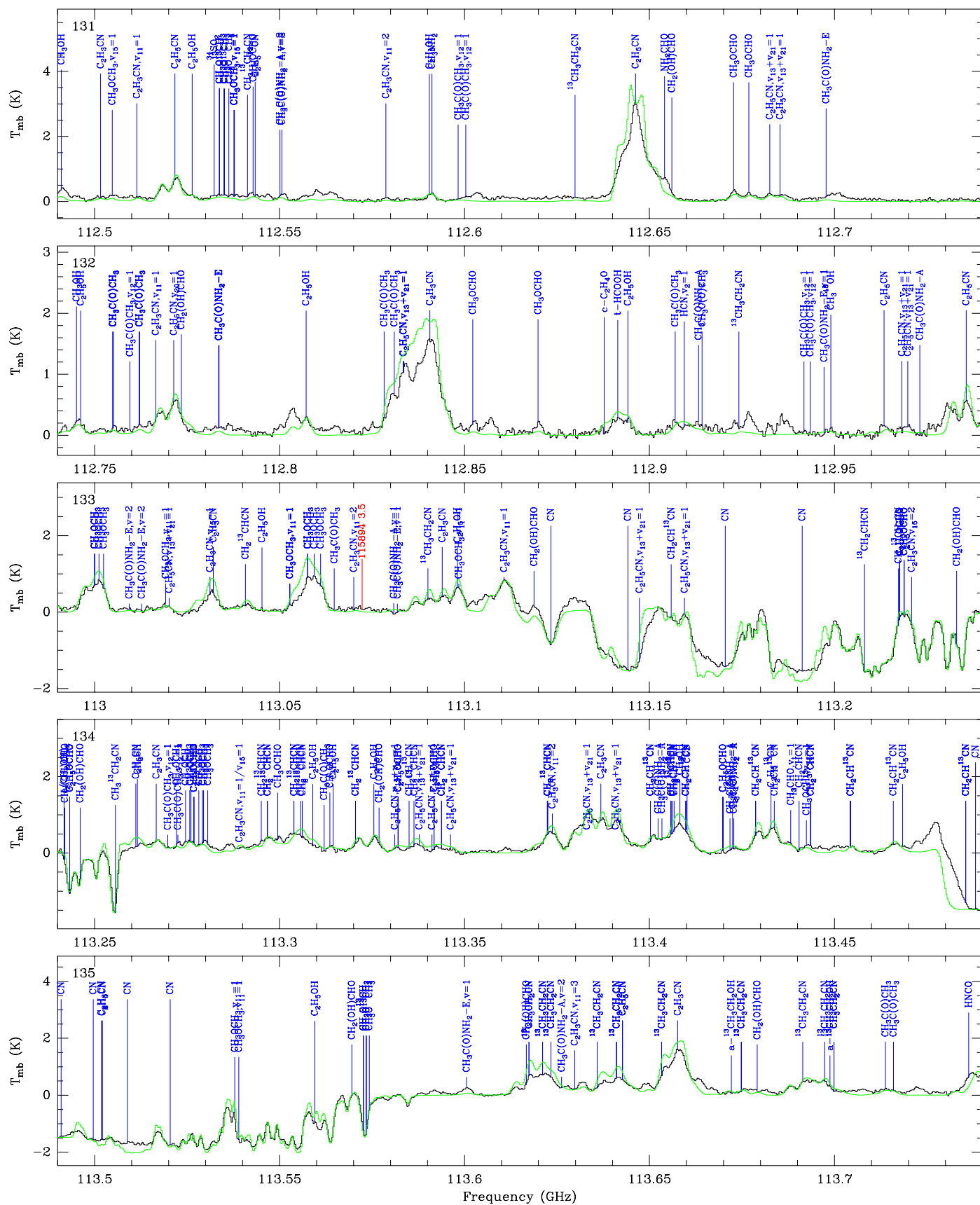
Fig. 2. continued.

Fig. 2. continued.
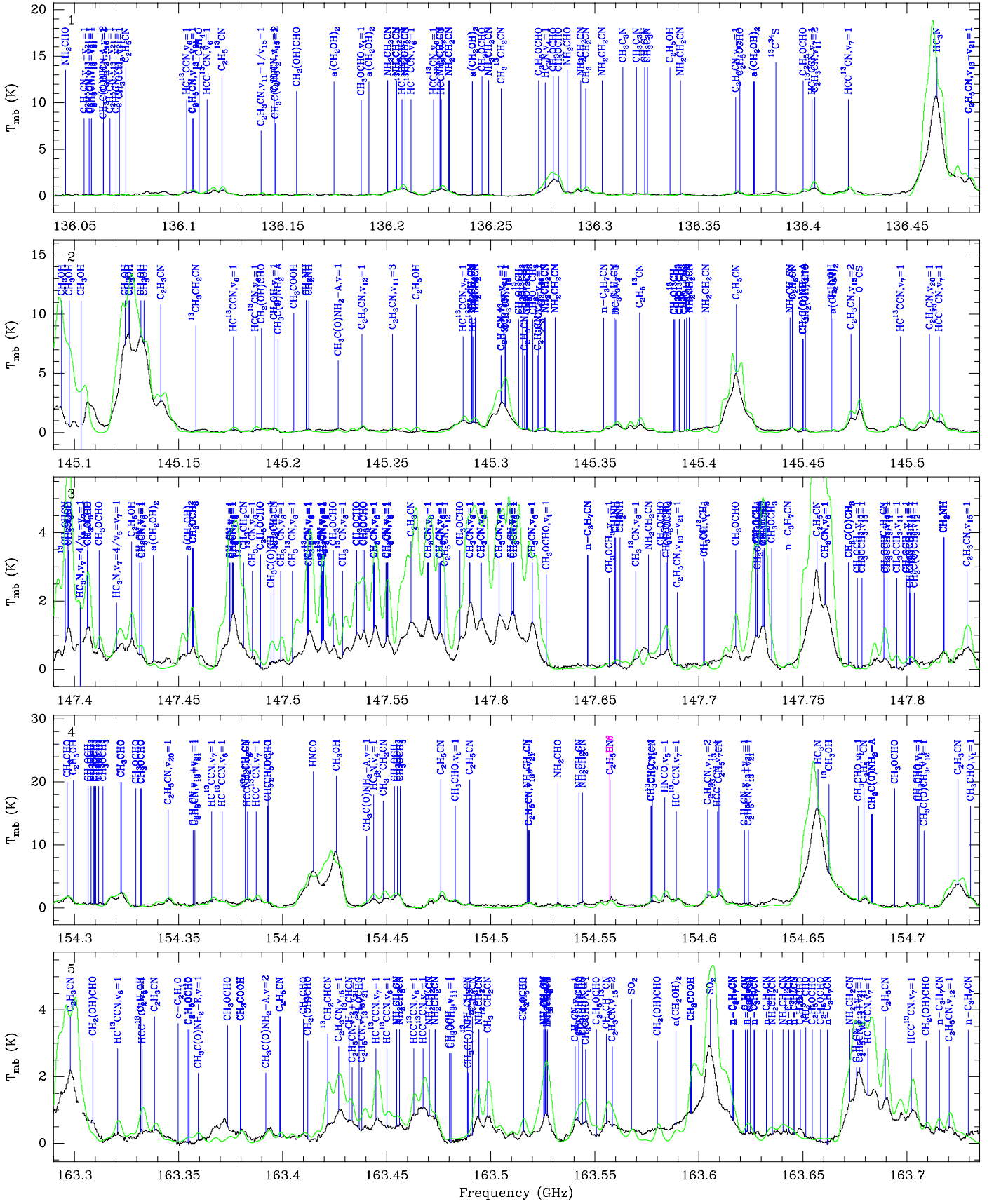
Fig. 3. Spectrum obtained toward Sgr B2(N) in the 2 mm window with the IRAM 30 m telescope in main-beam temperature scale. The synthetic model is overlaid in green and its relevant lines are labeled in blue. The frequencies of the hydrogen recombination lines are indicated with a pink label.

Fig. 3. continued.

Fig. 4. Spectrum obtained toward Sgr B2(N) in the 1 mm window with the IRAM 30 m telescope in main-beam temperature scale. The synthetic model is overlaid in green and its relevant lines are labeled in blue. The frequencies of the hydrogen recombination lines are indicated with a pink label.

Fig. 4. continued.

Fig. 4. continued.

Fig. 4. continued.

Fig. 4. continued.

Fig. 4. continued.

Fig. 4. continued.

Fig. 4. continued.

Fig. 4. continued.
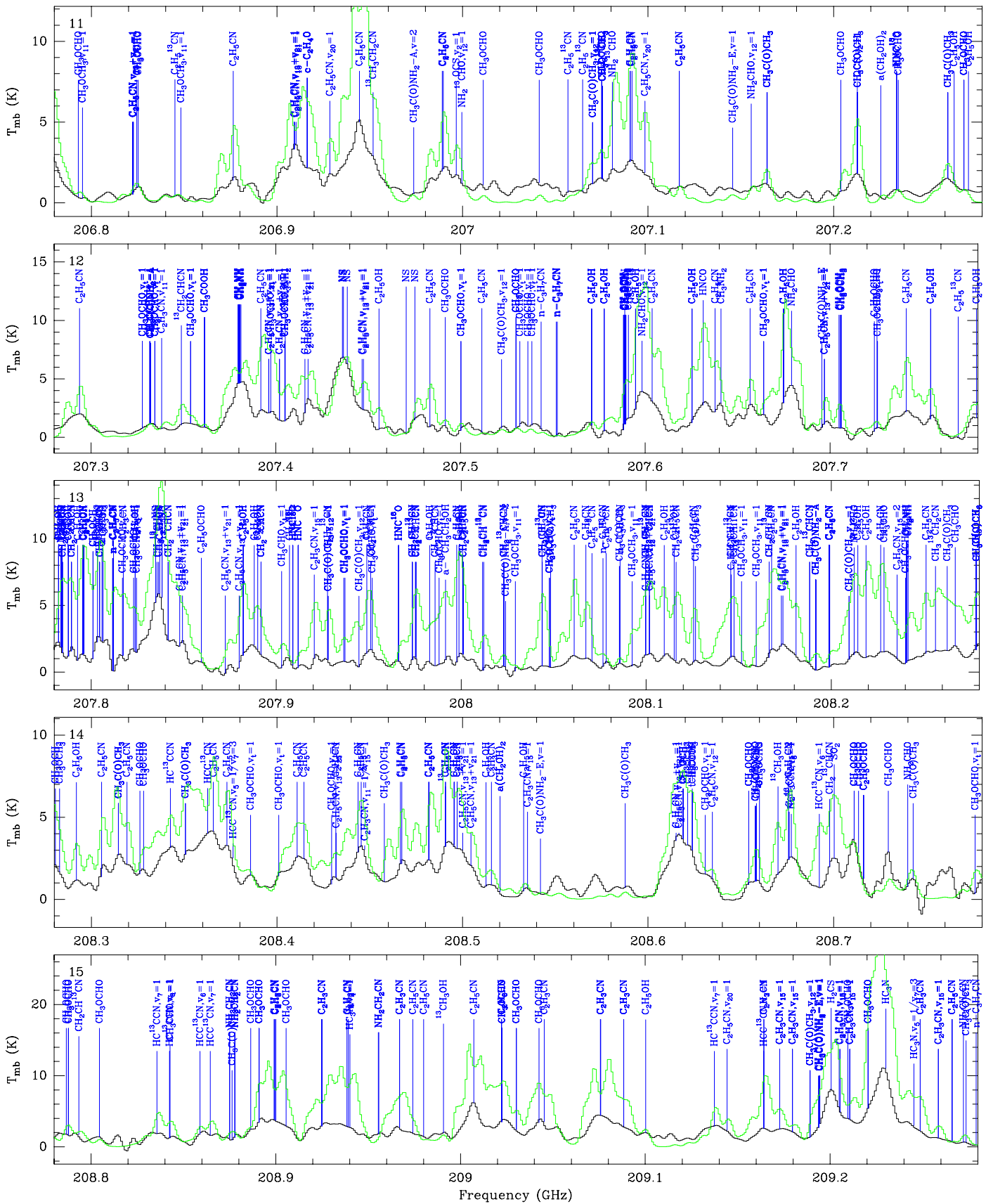
Fig. 4. continued.
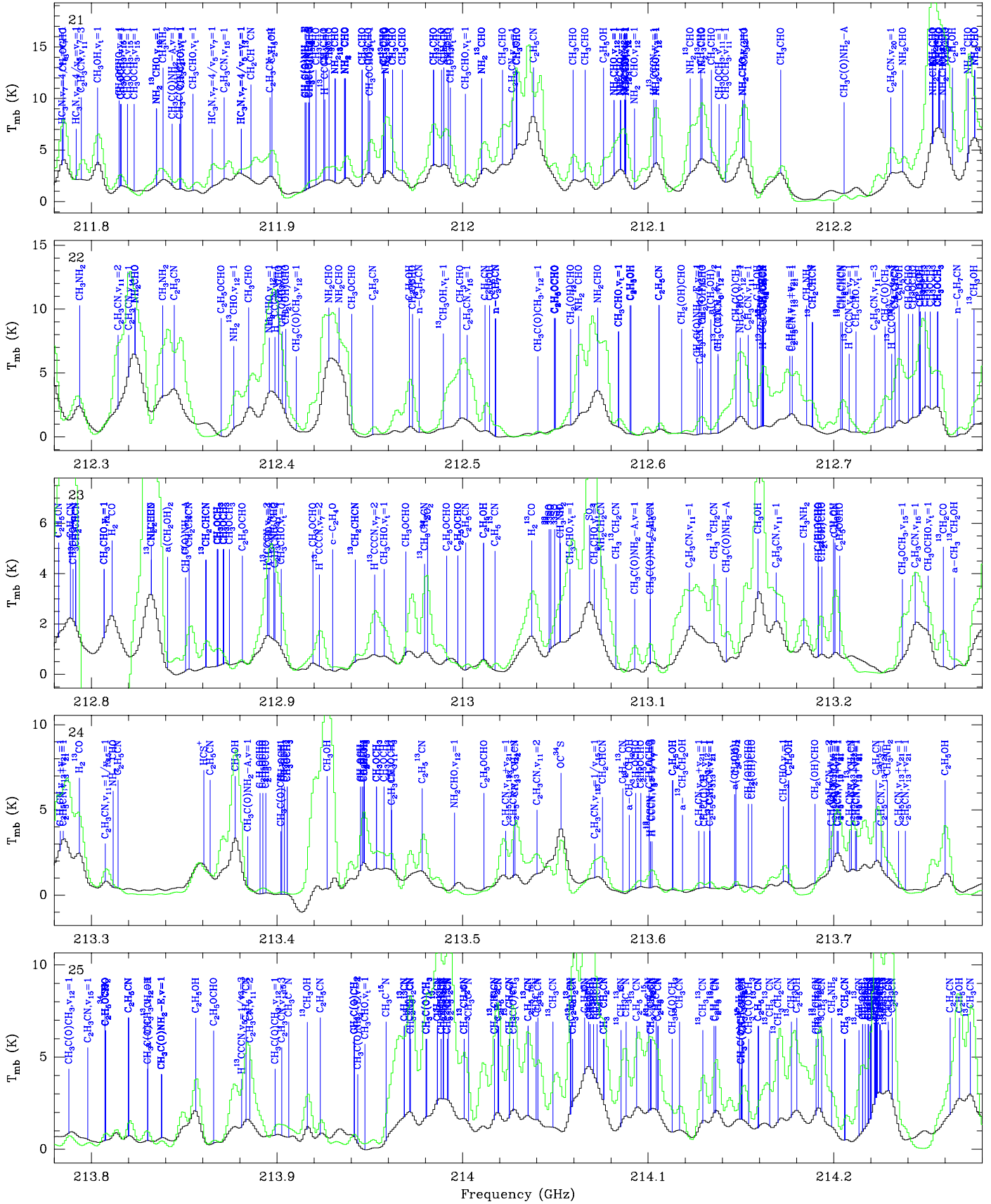
Fig. 4. continued.
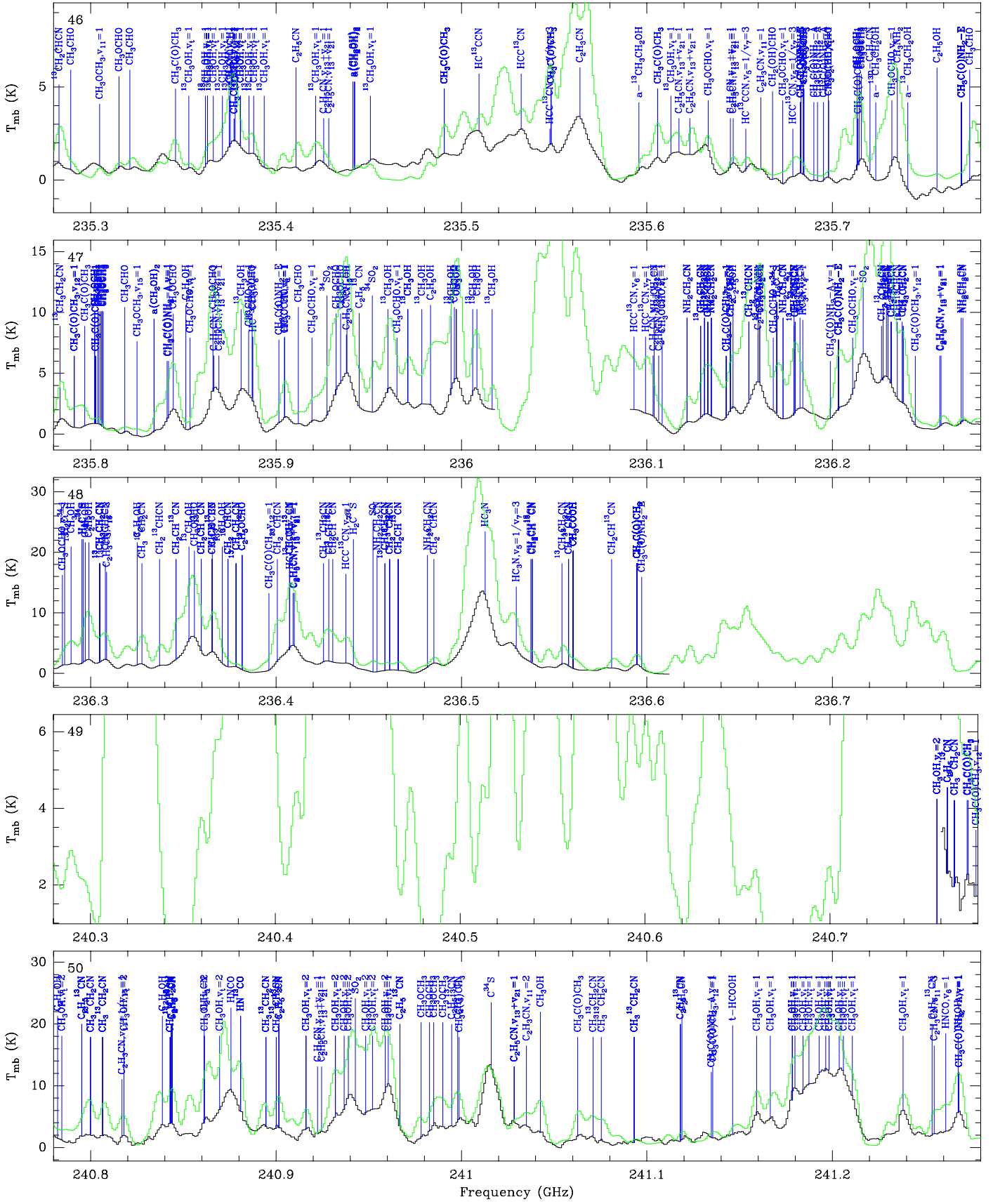
Fig. 4. continued.
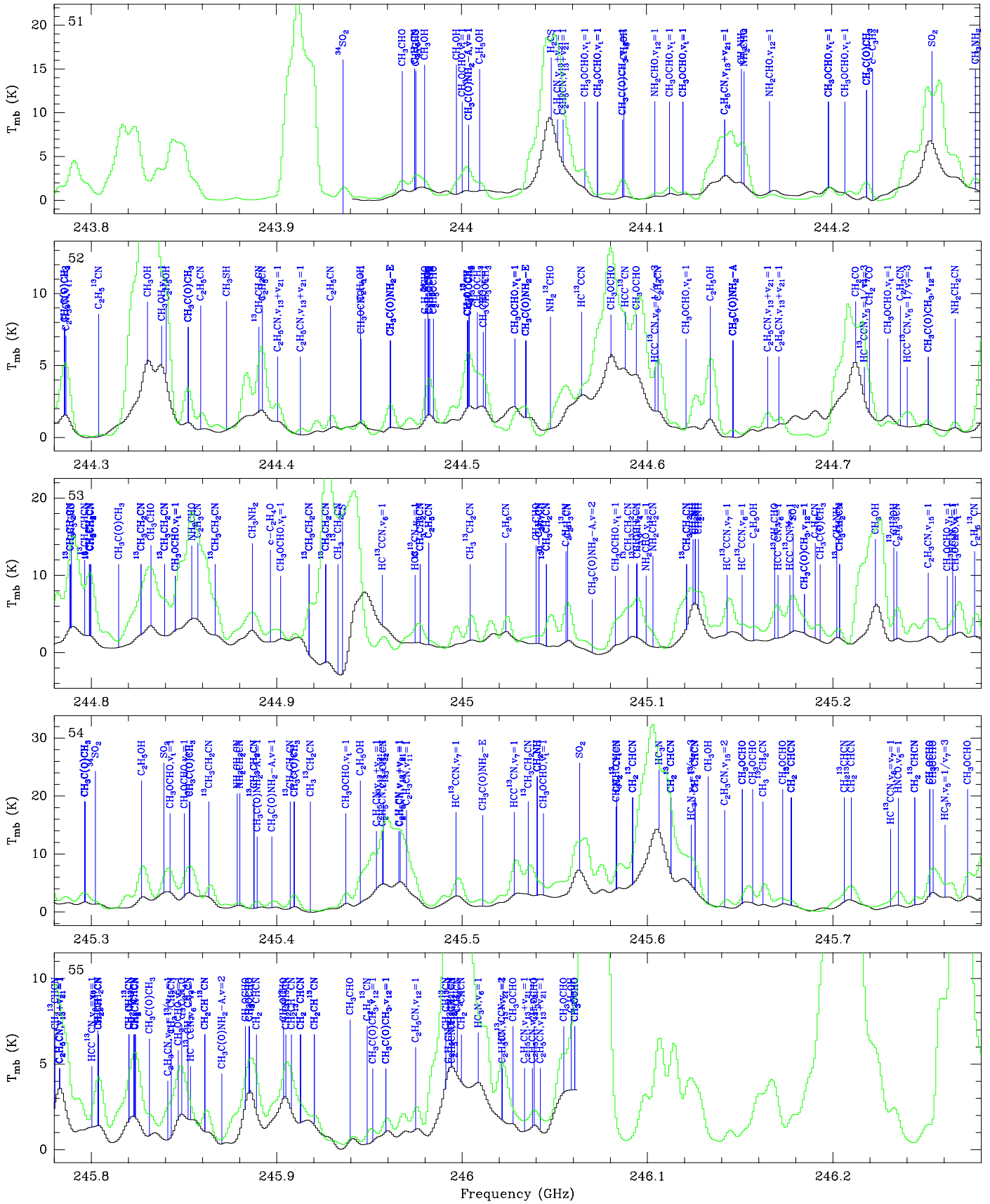
Fig. 4. continued.

Fig. 4. continued.
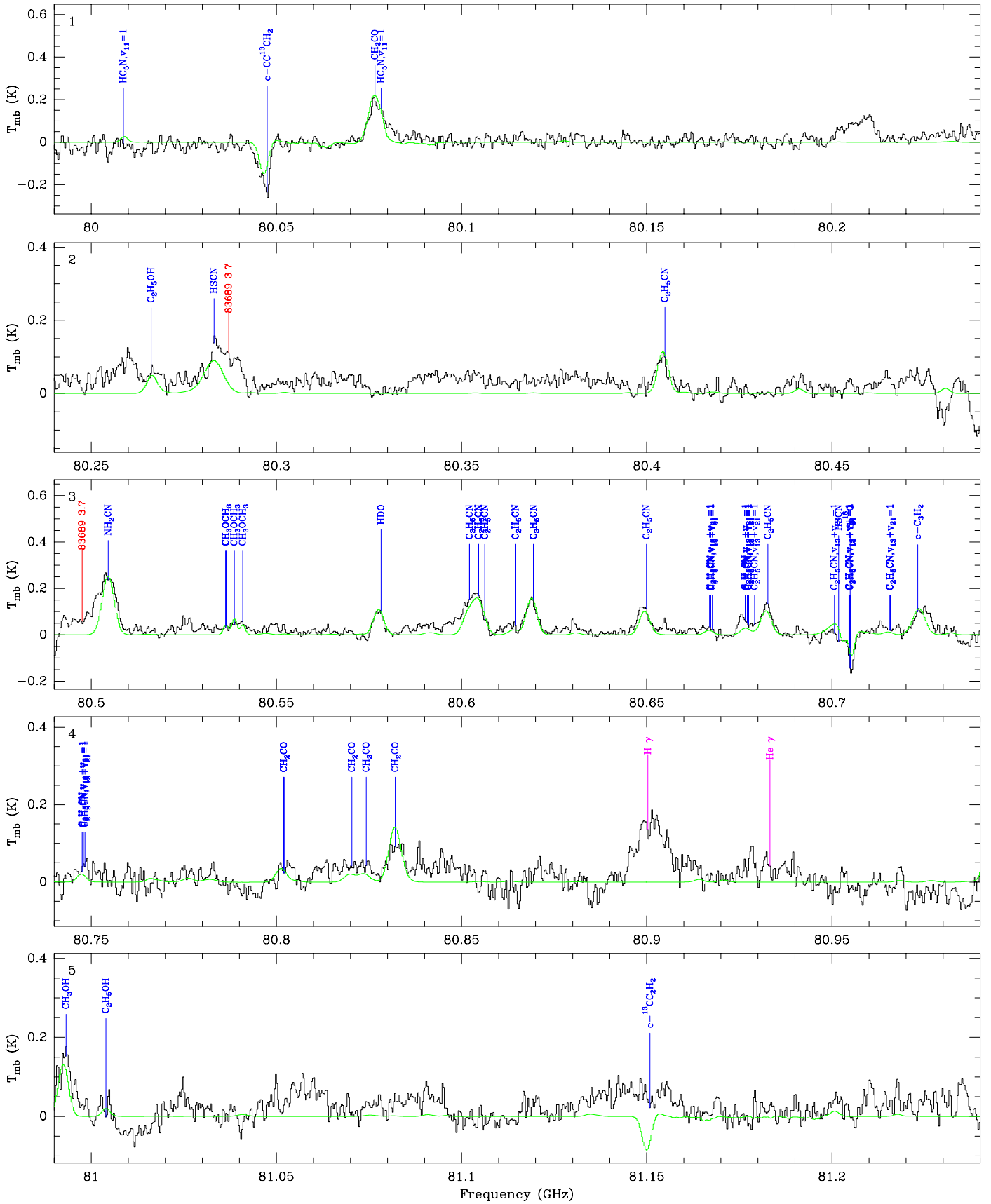
Fig. 5. Spectrum obtained toward Sgr B2(M) in the 3 mm window with the IRAM 30 m telescope in main-beam temperature scale. The synthetic model is overlaid in green and its relevant lines are labeled in blue. The frequencies of the hydrogen and helium recombination lines are indicated with a pink label. The position of the lines with a peak temperature higher than 2 K in the image band and possibly contaminating the spectrum are marked with a red label indicating their rest frequency and their peak temperature in K in the image band.

Fig. 5. continued.
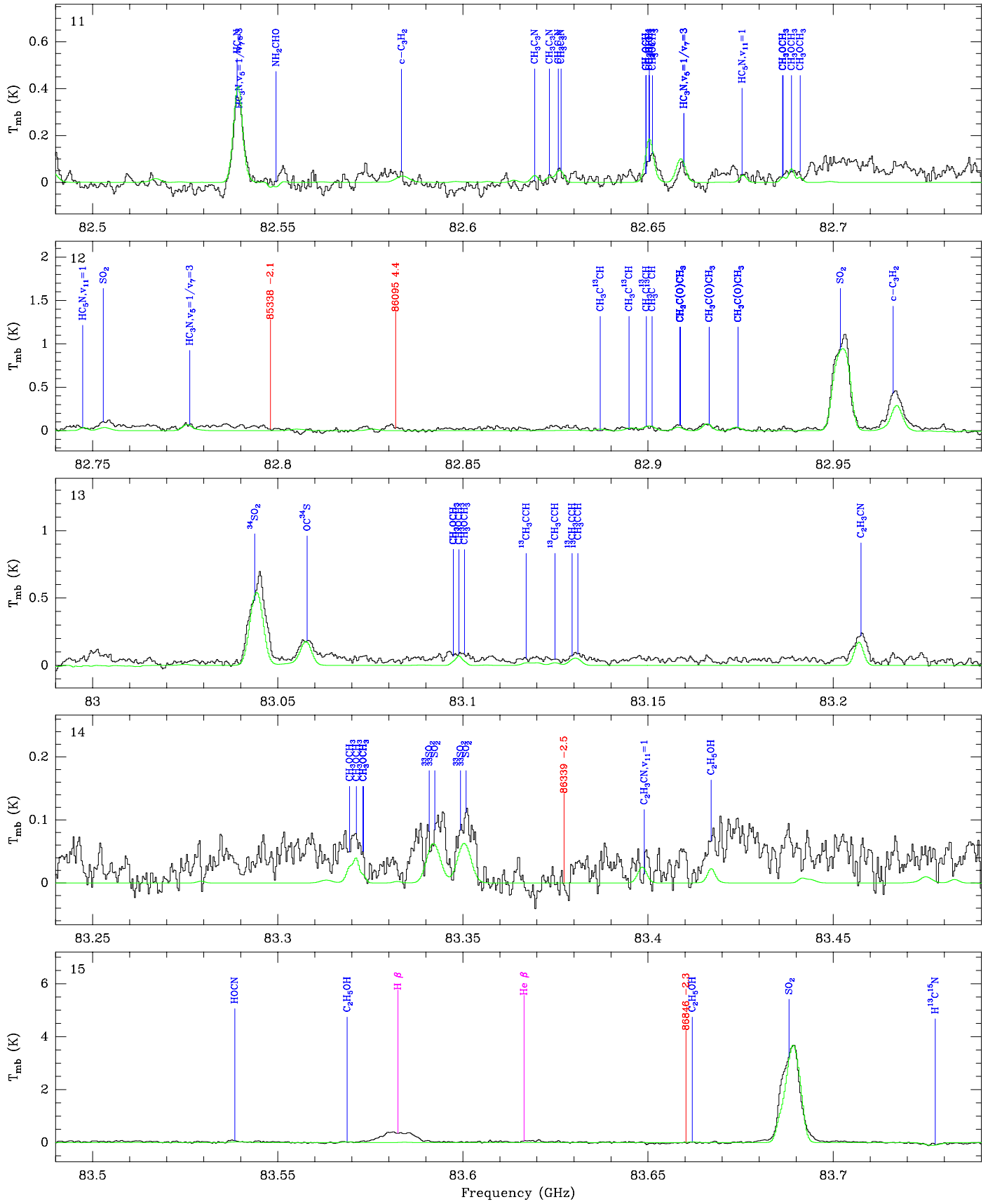
Fig. 5. continued.
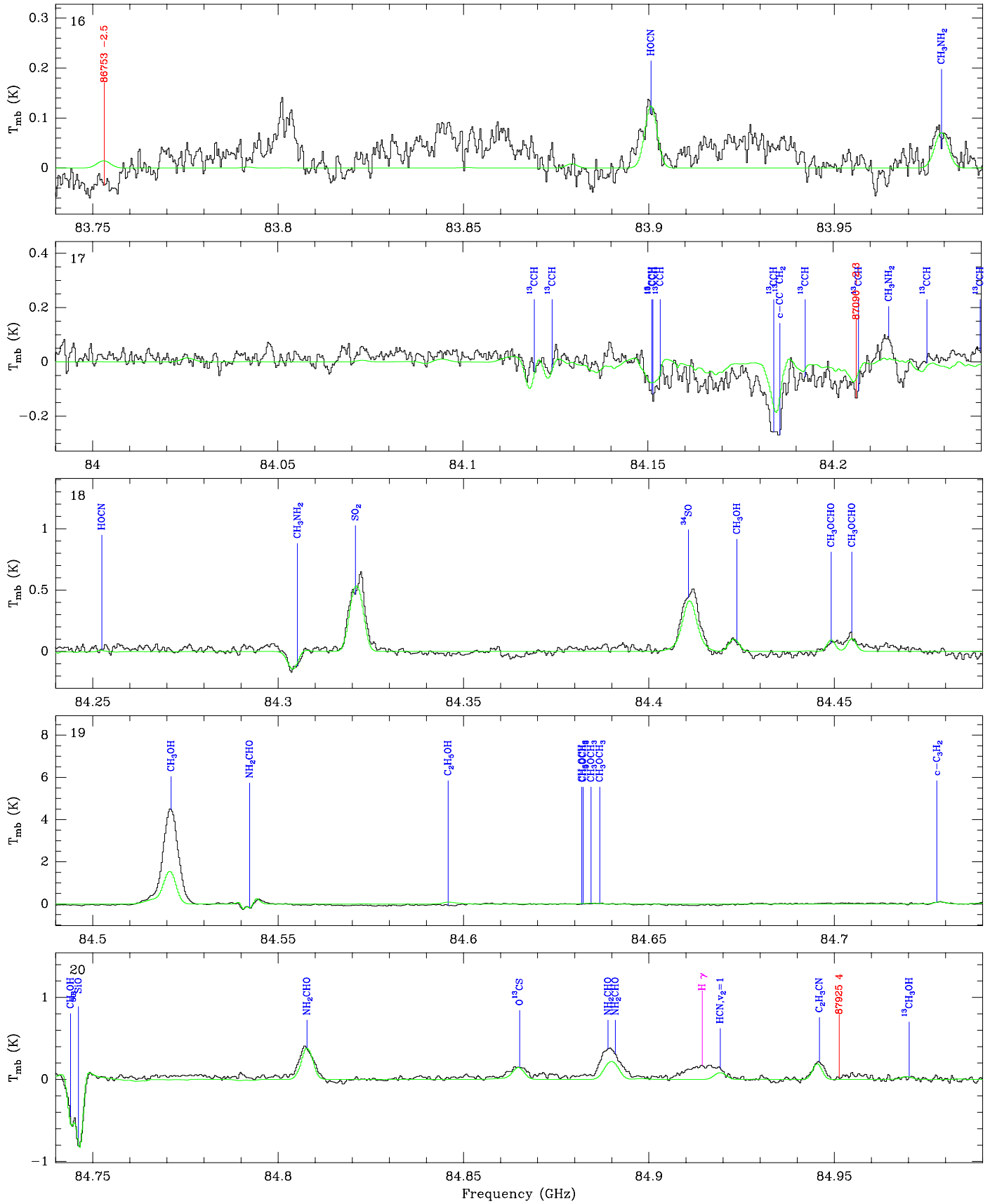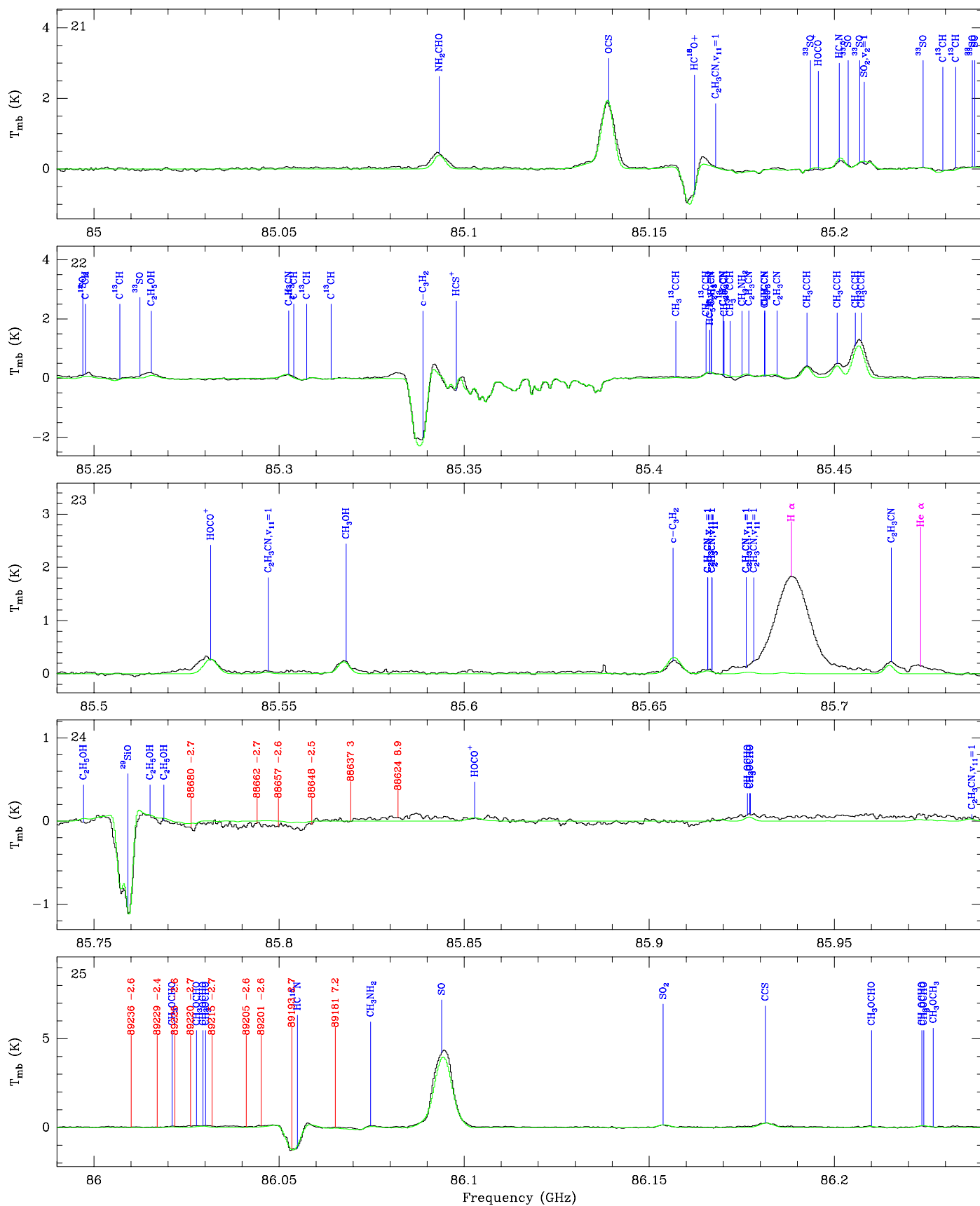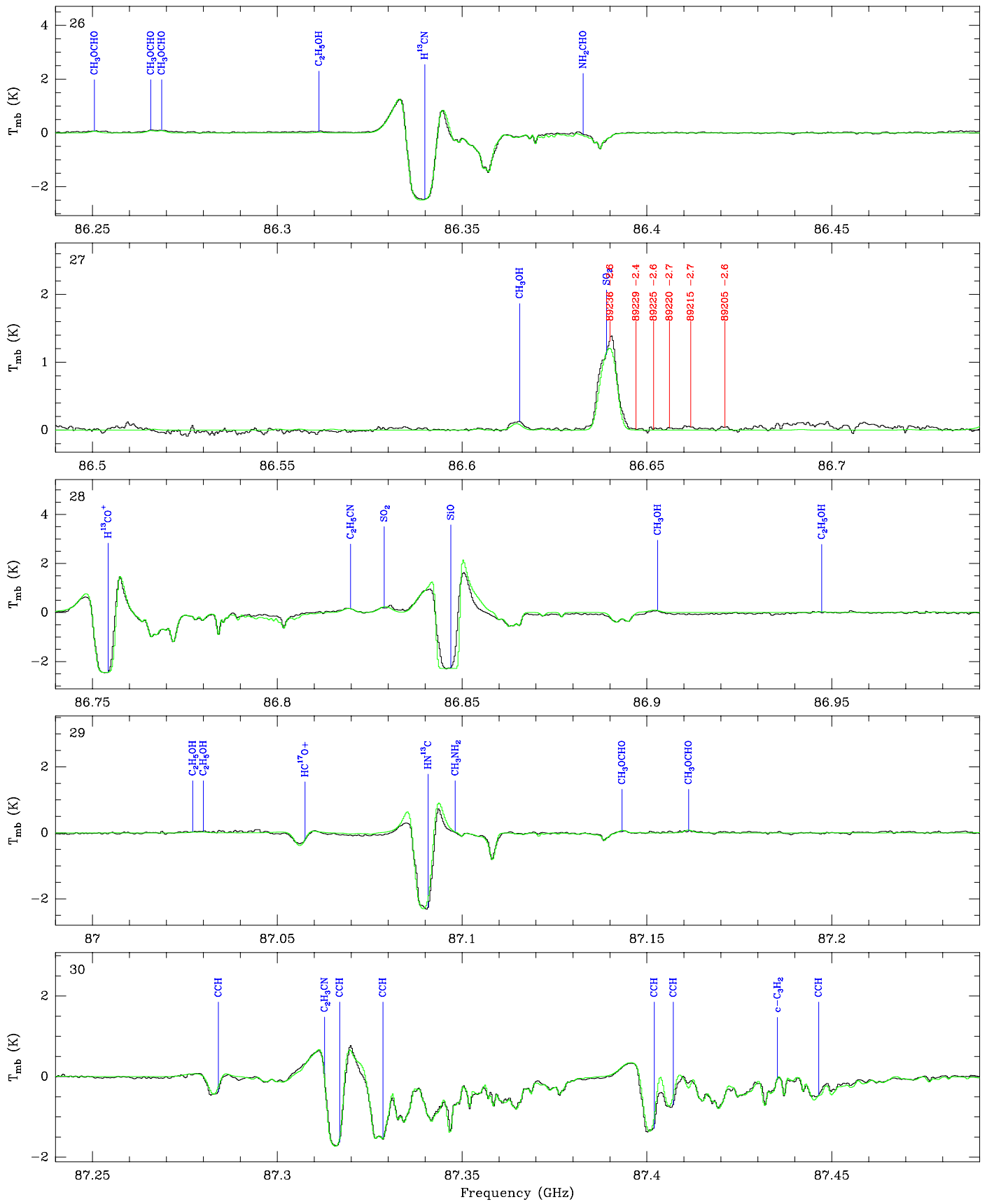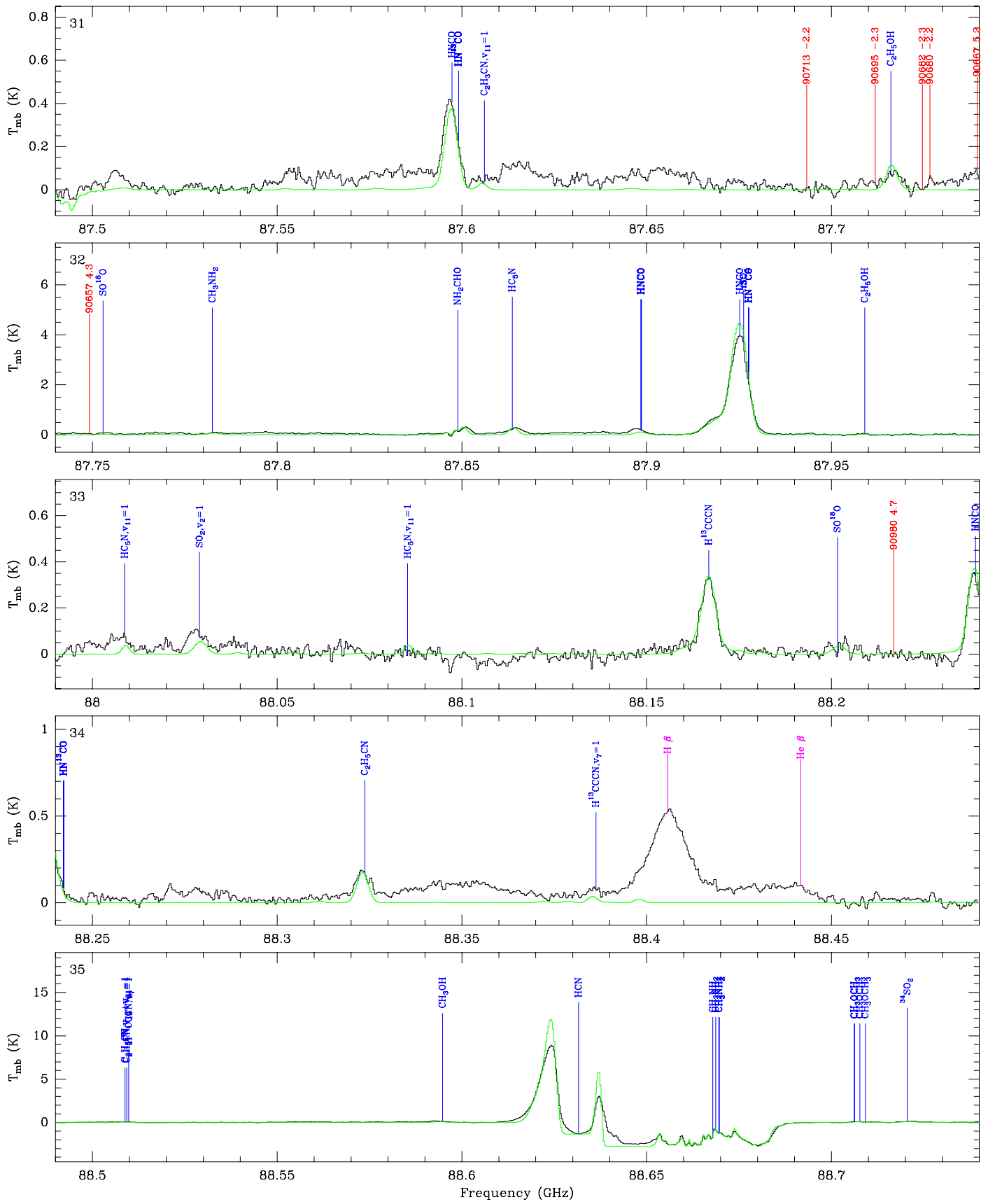
Fig. 5. continued.

Fig. 5. continued.

Fig. 5. continued.
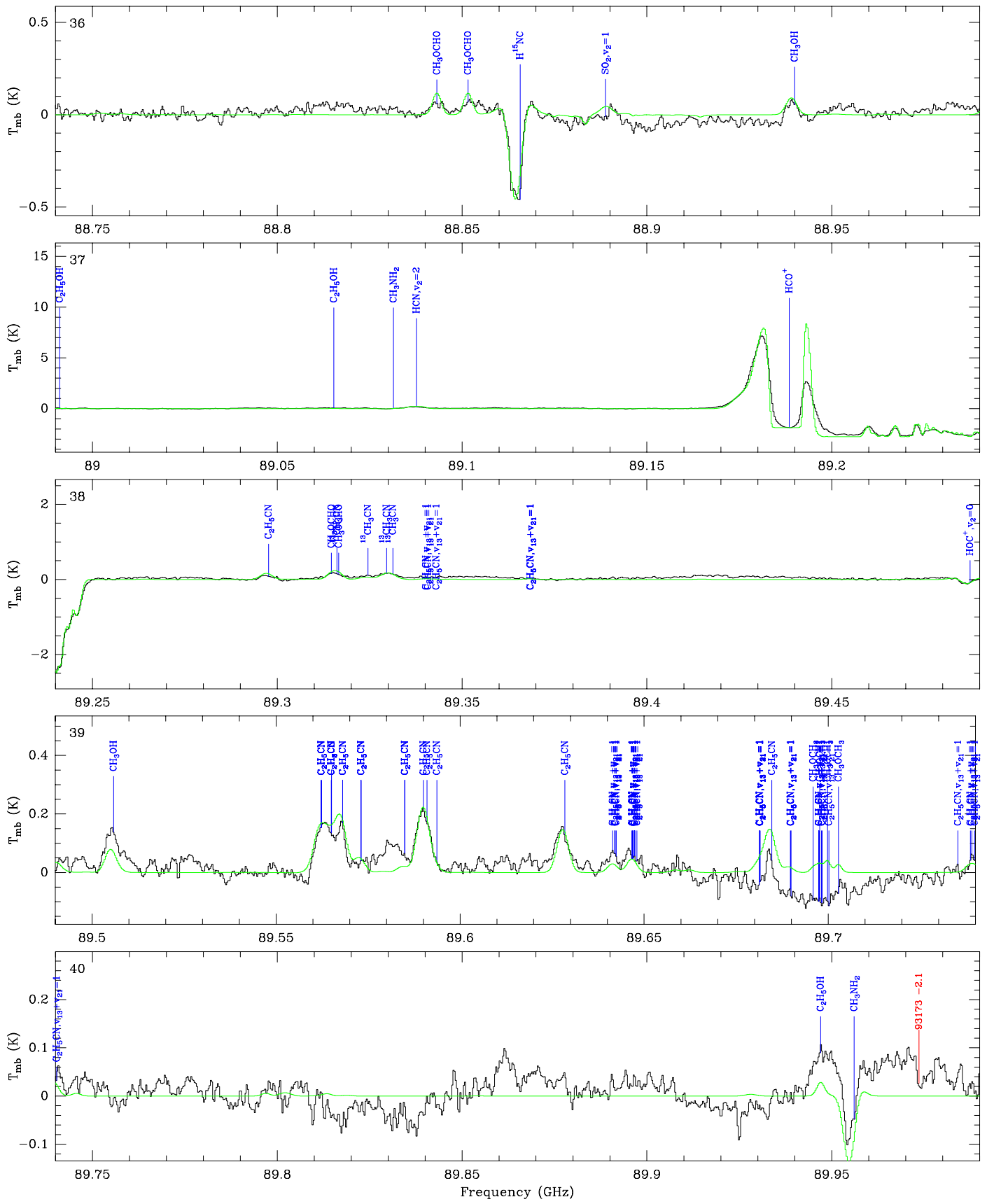
Fig. 5. continued.
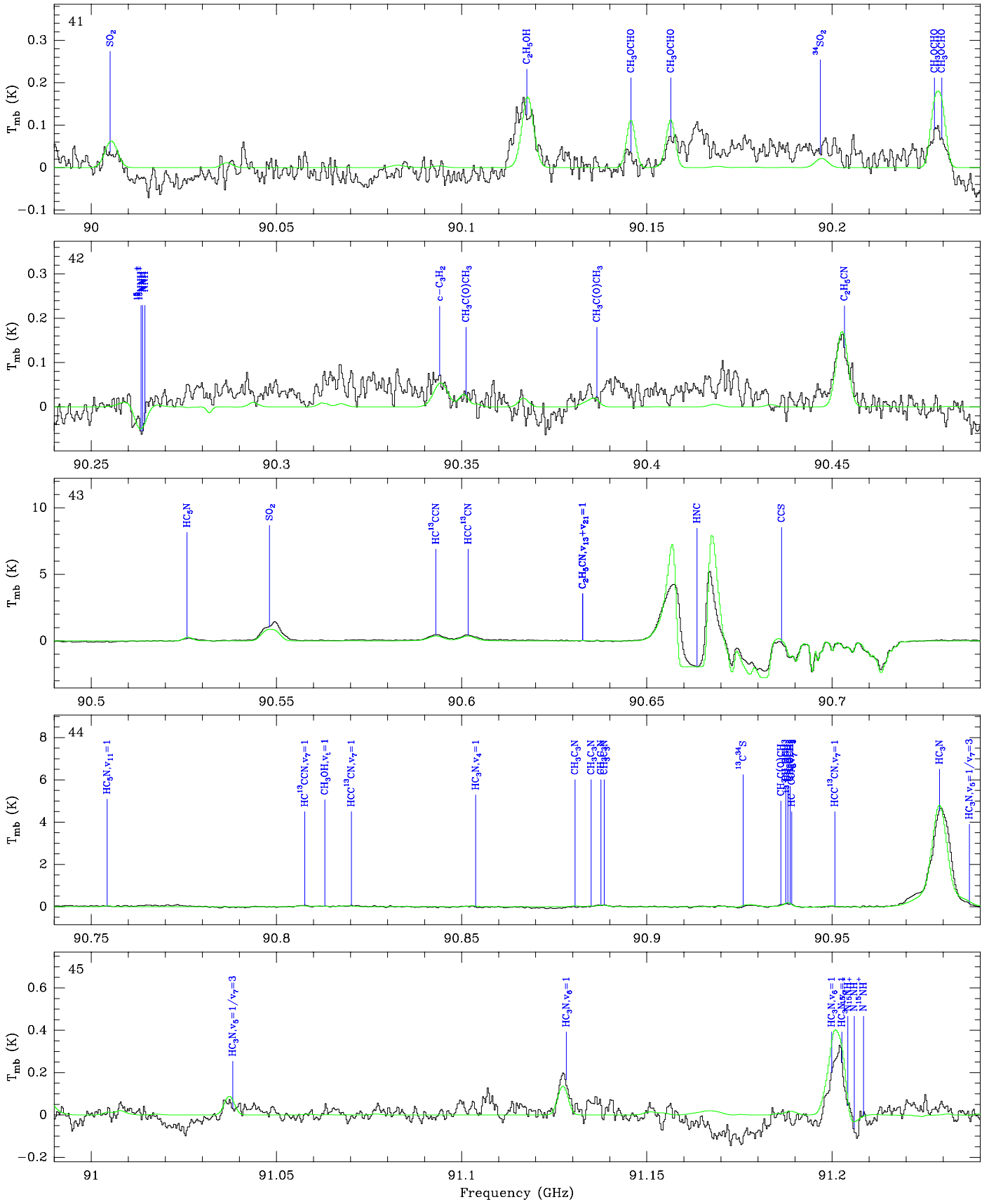
Fig. 5. continued.
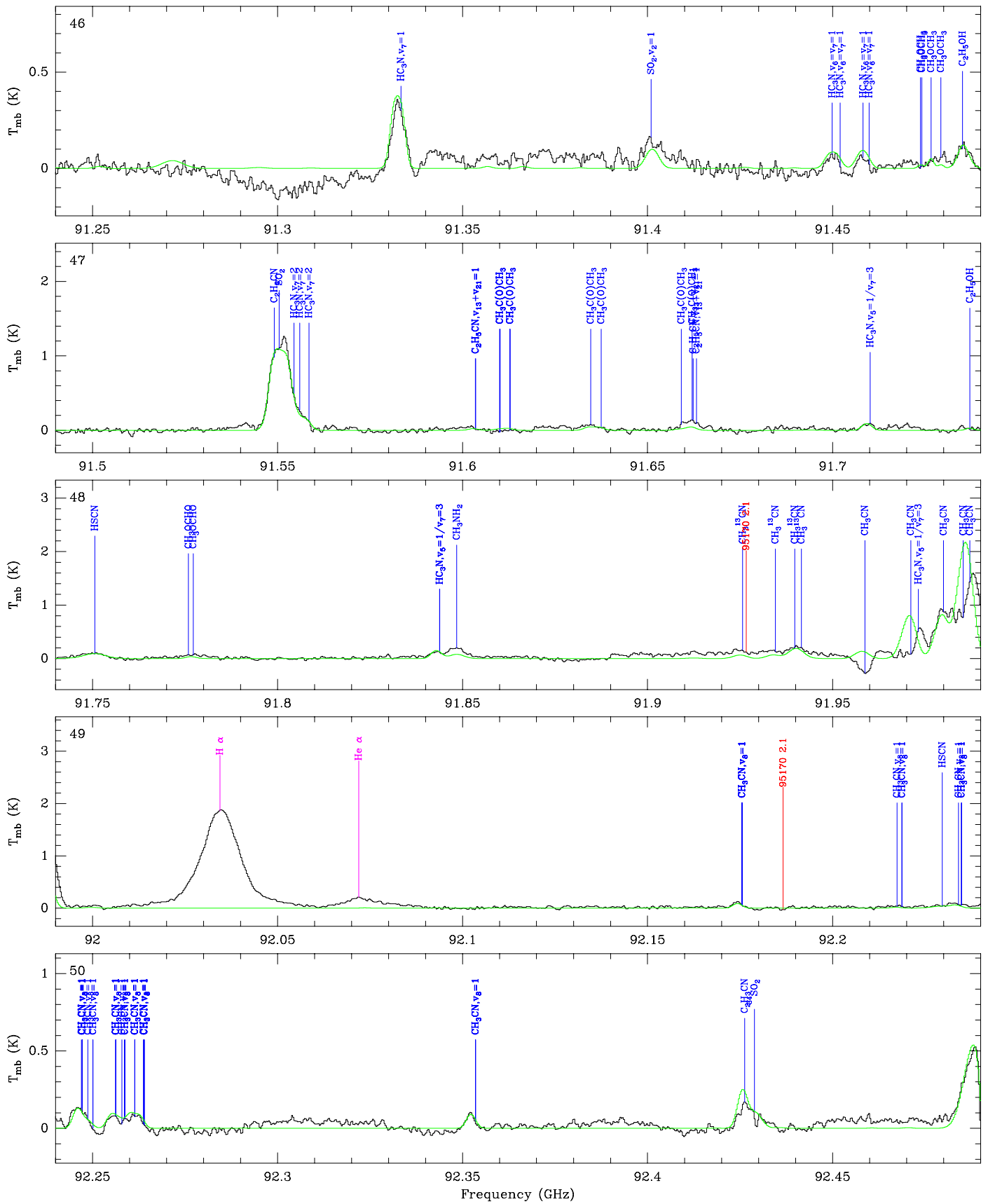
Fig. 5. continued.
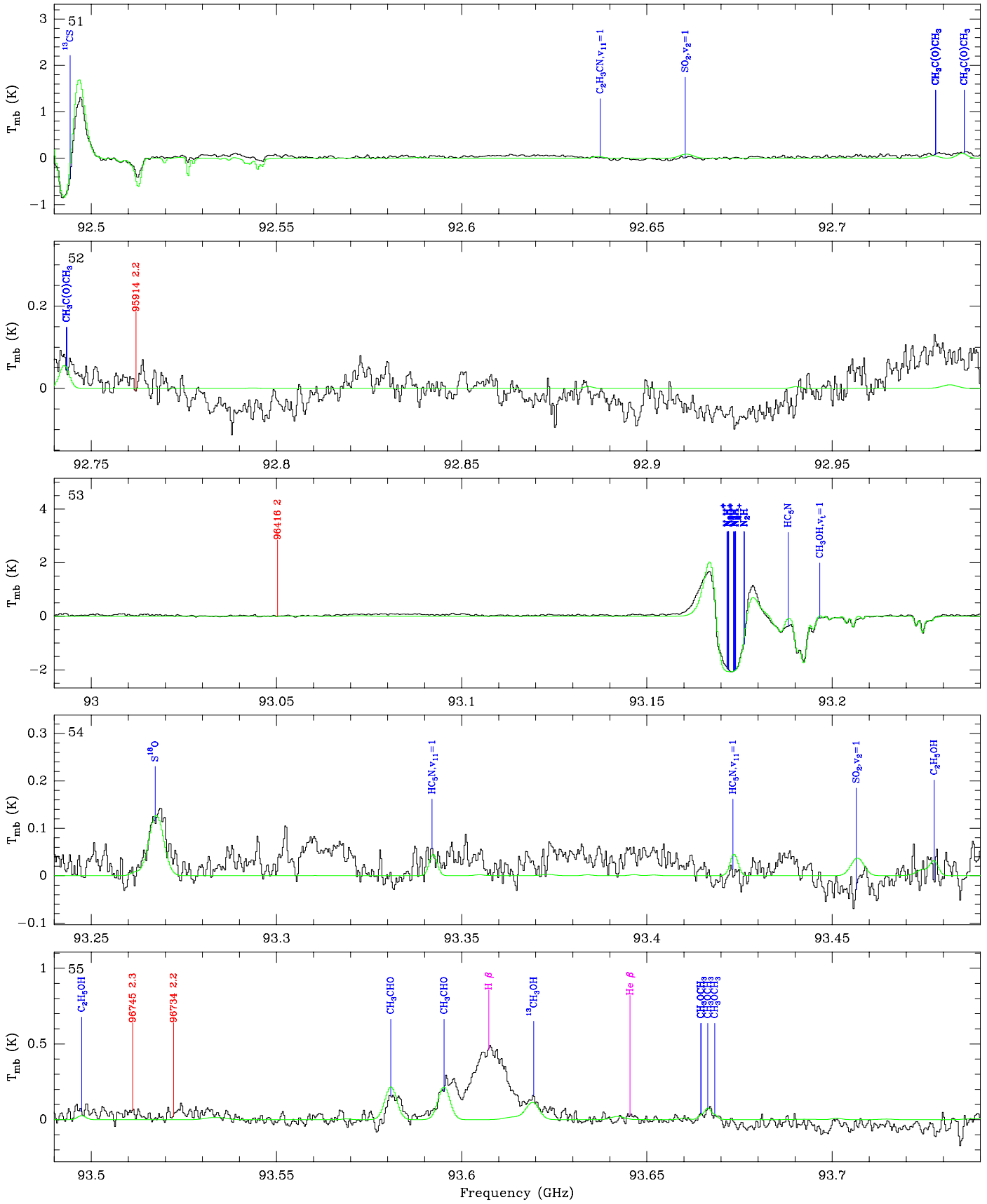
Fig. 5. continued.
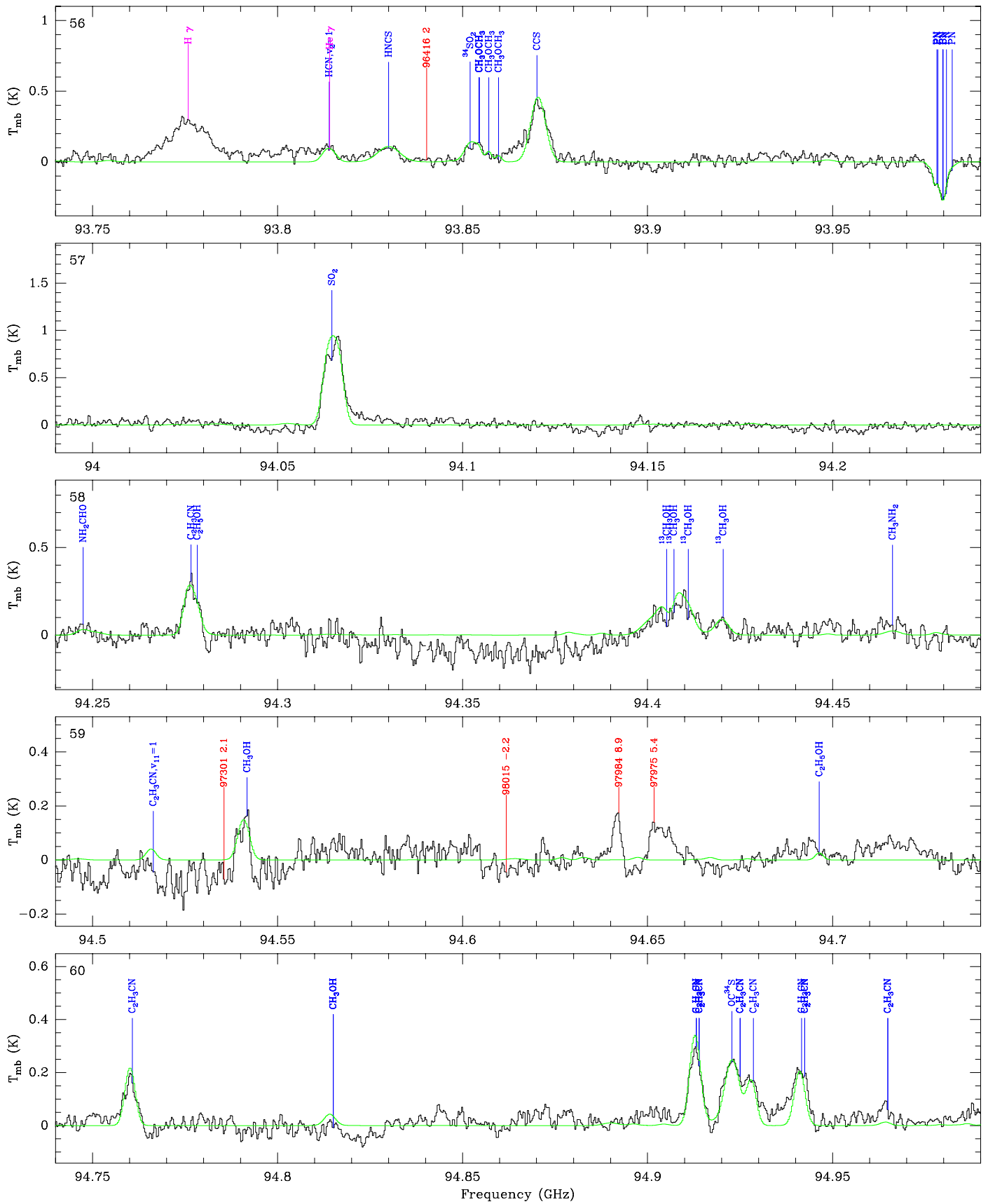
Fig. 5. continued.
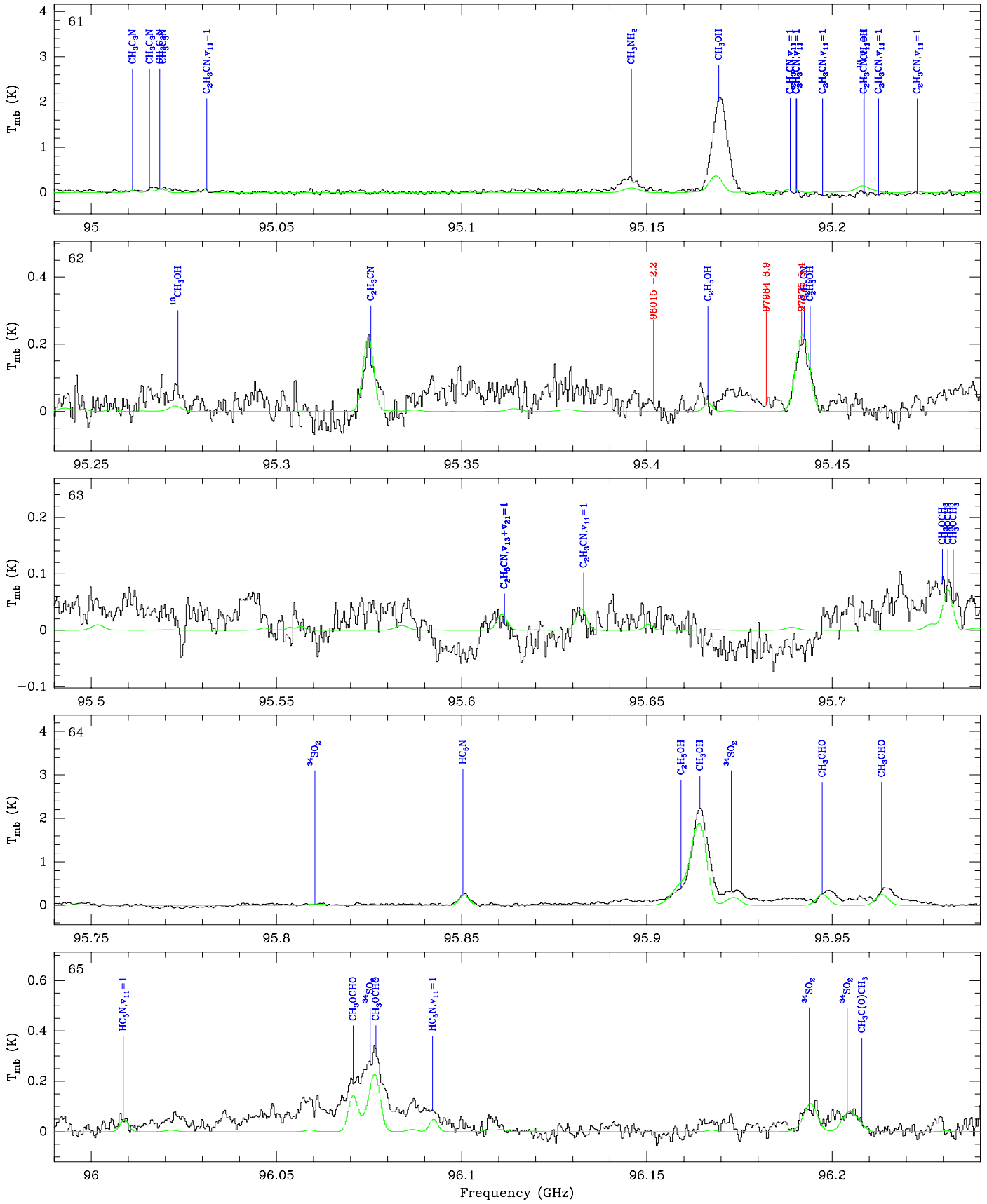
Fig. 5. continued.
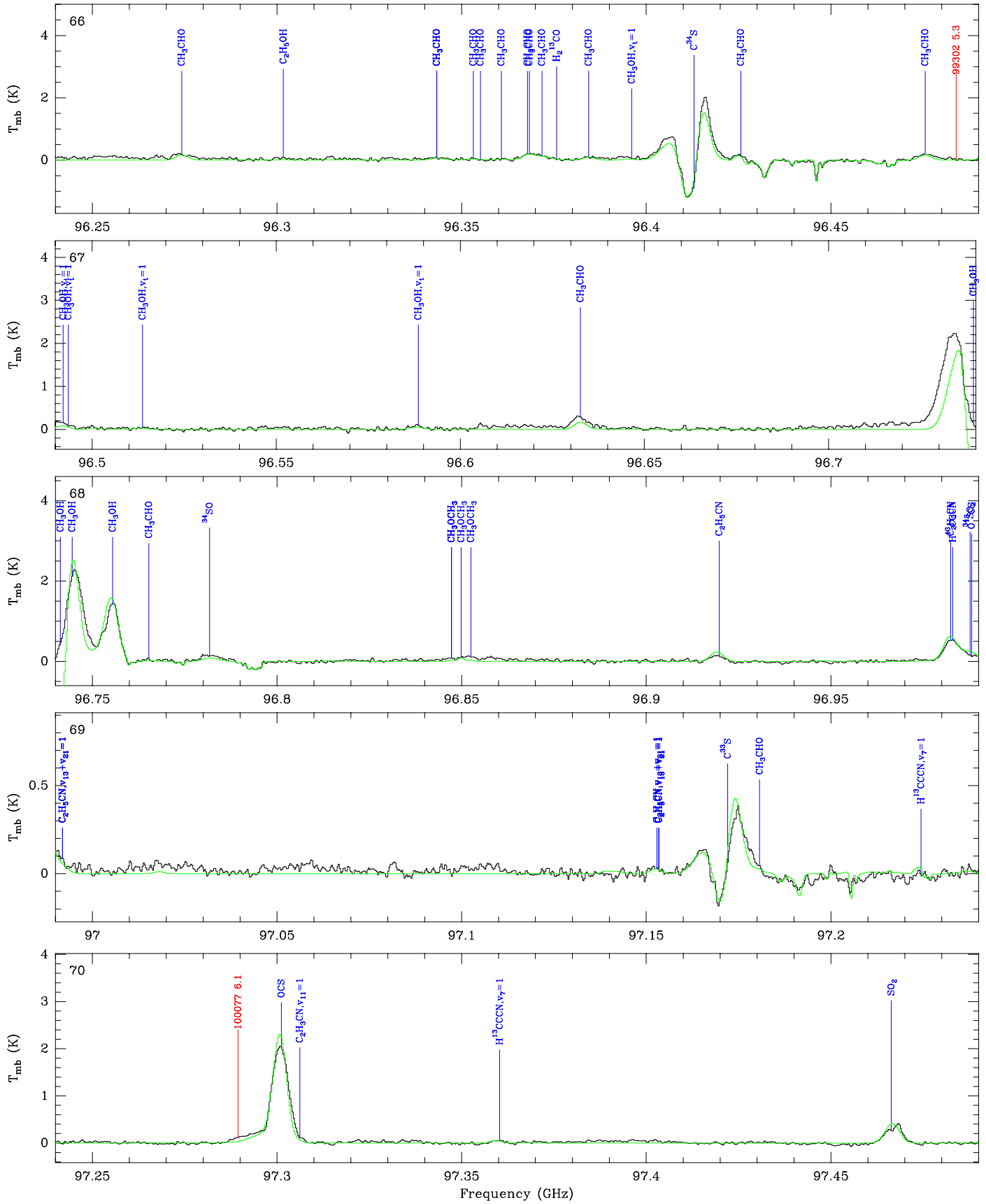
Fig. 5. continued.
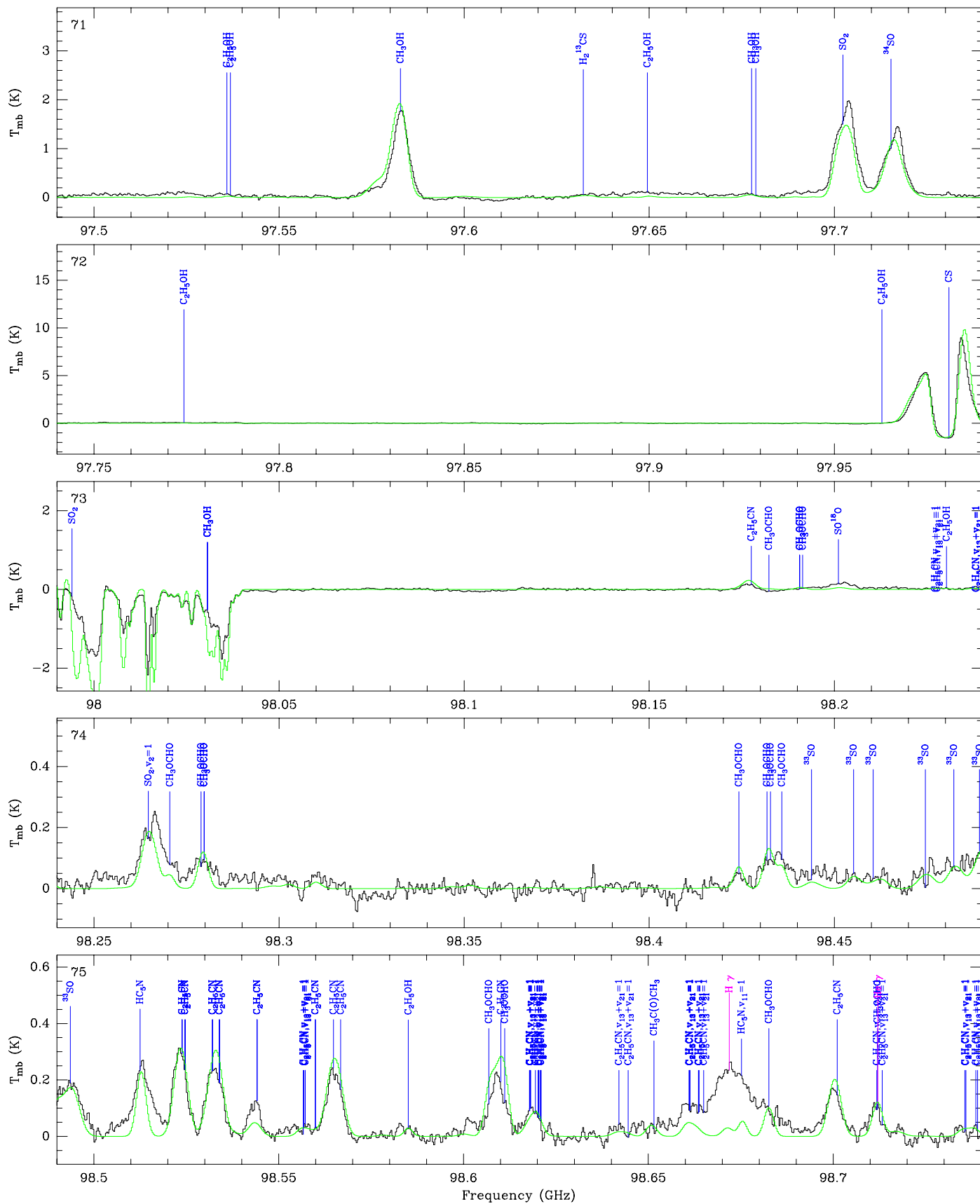
Fig. 5. continued.
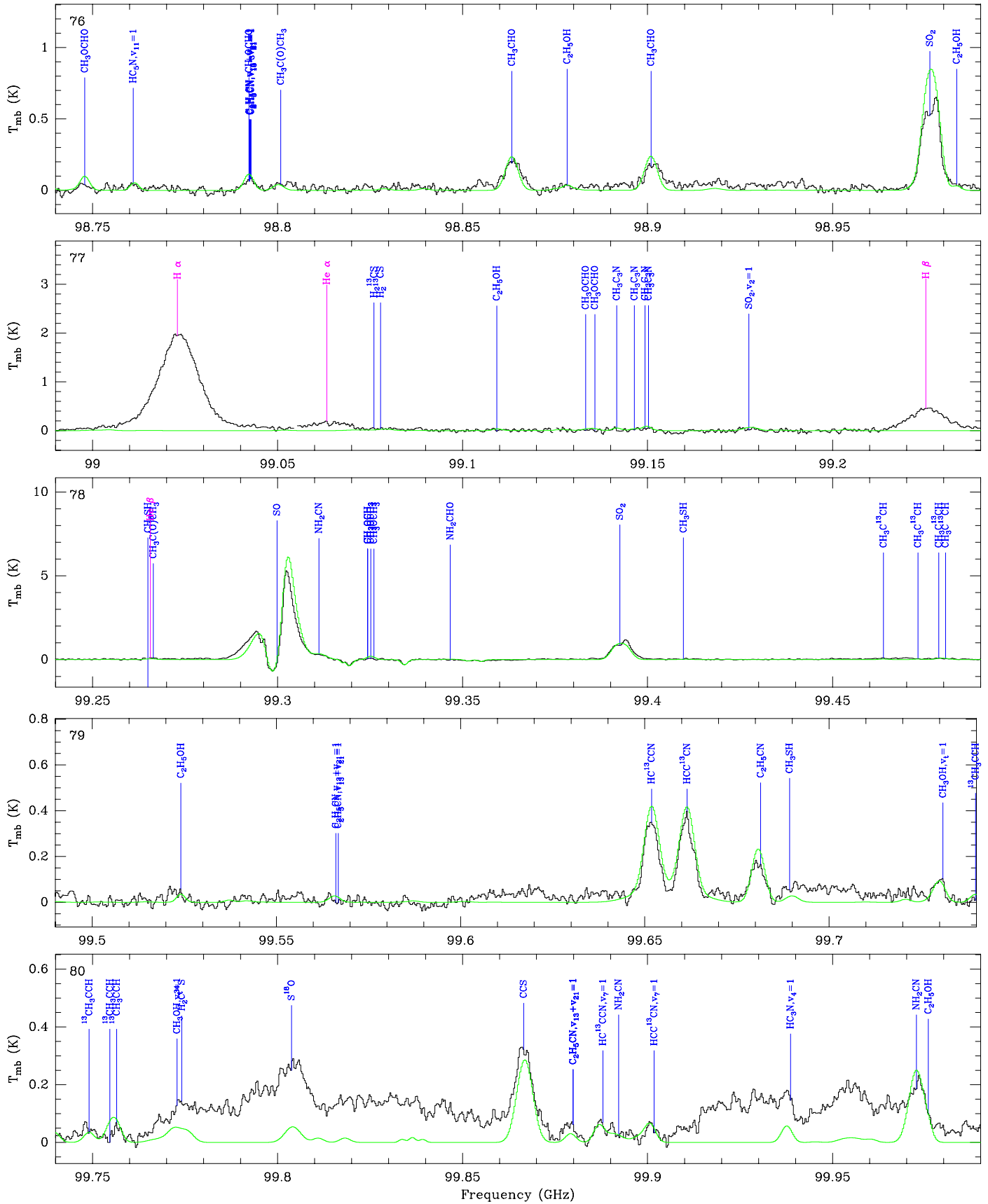
Fig. 5. continued.
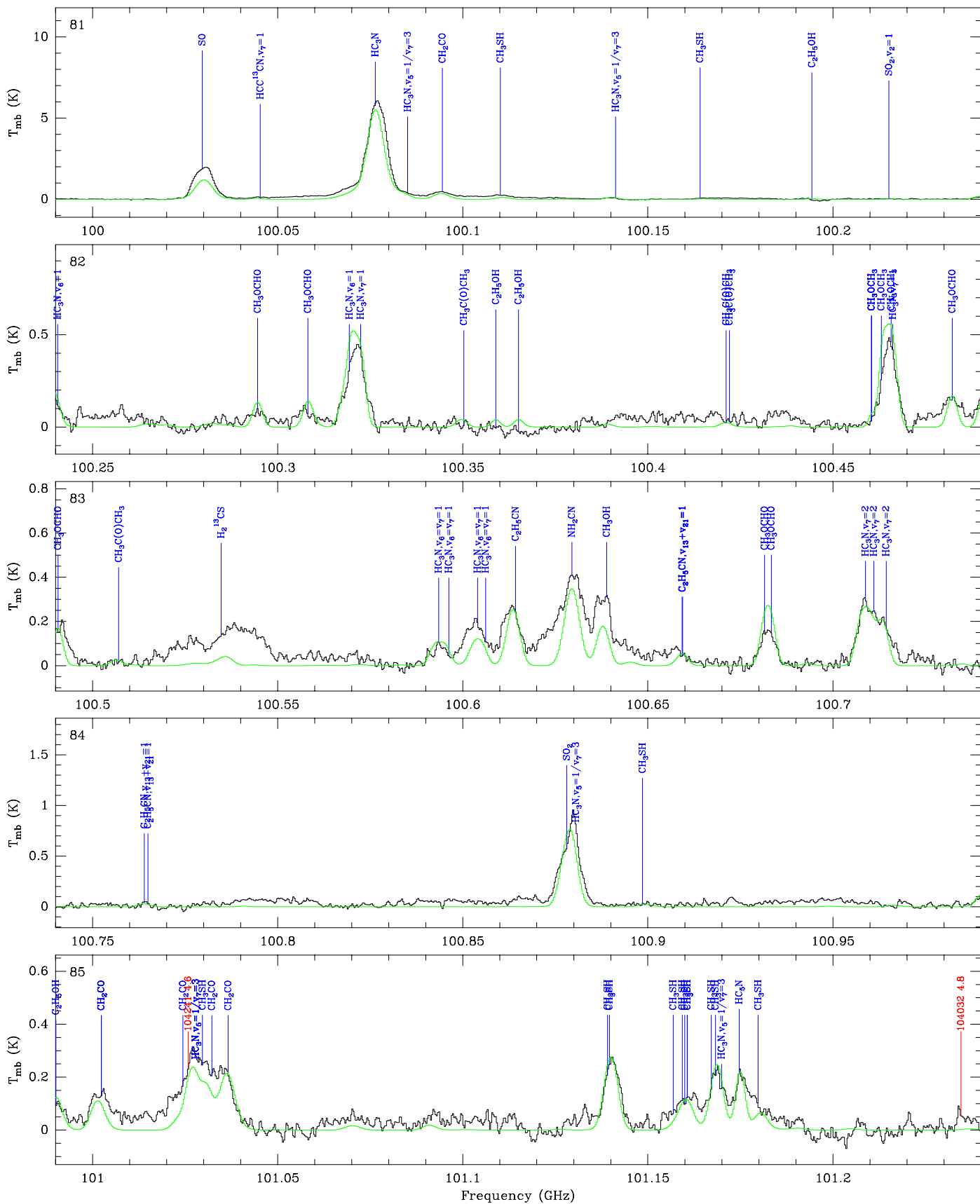
Fig. 5. continued.
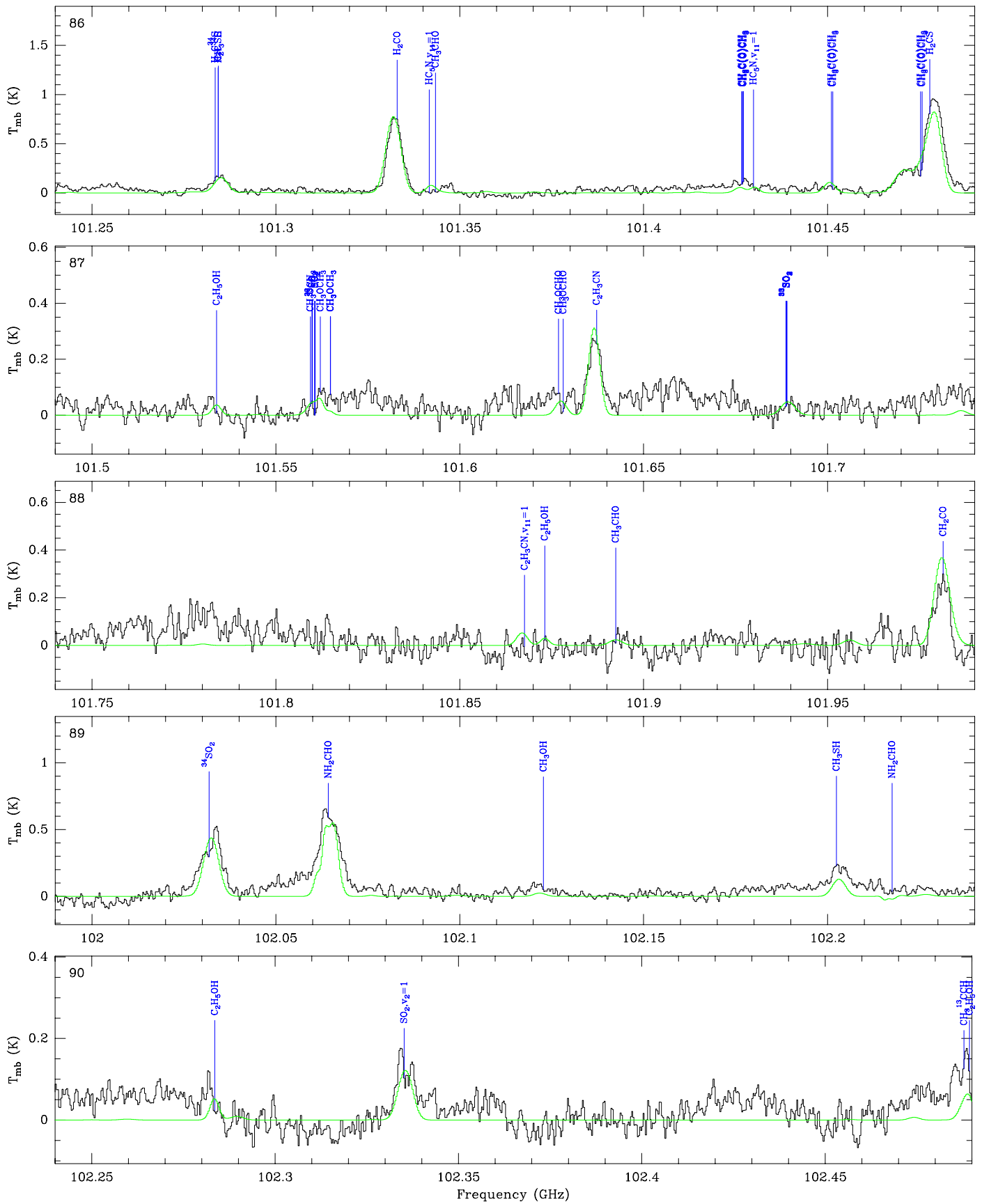
Fig. 5. continued.
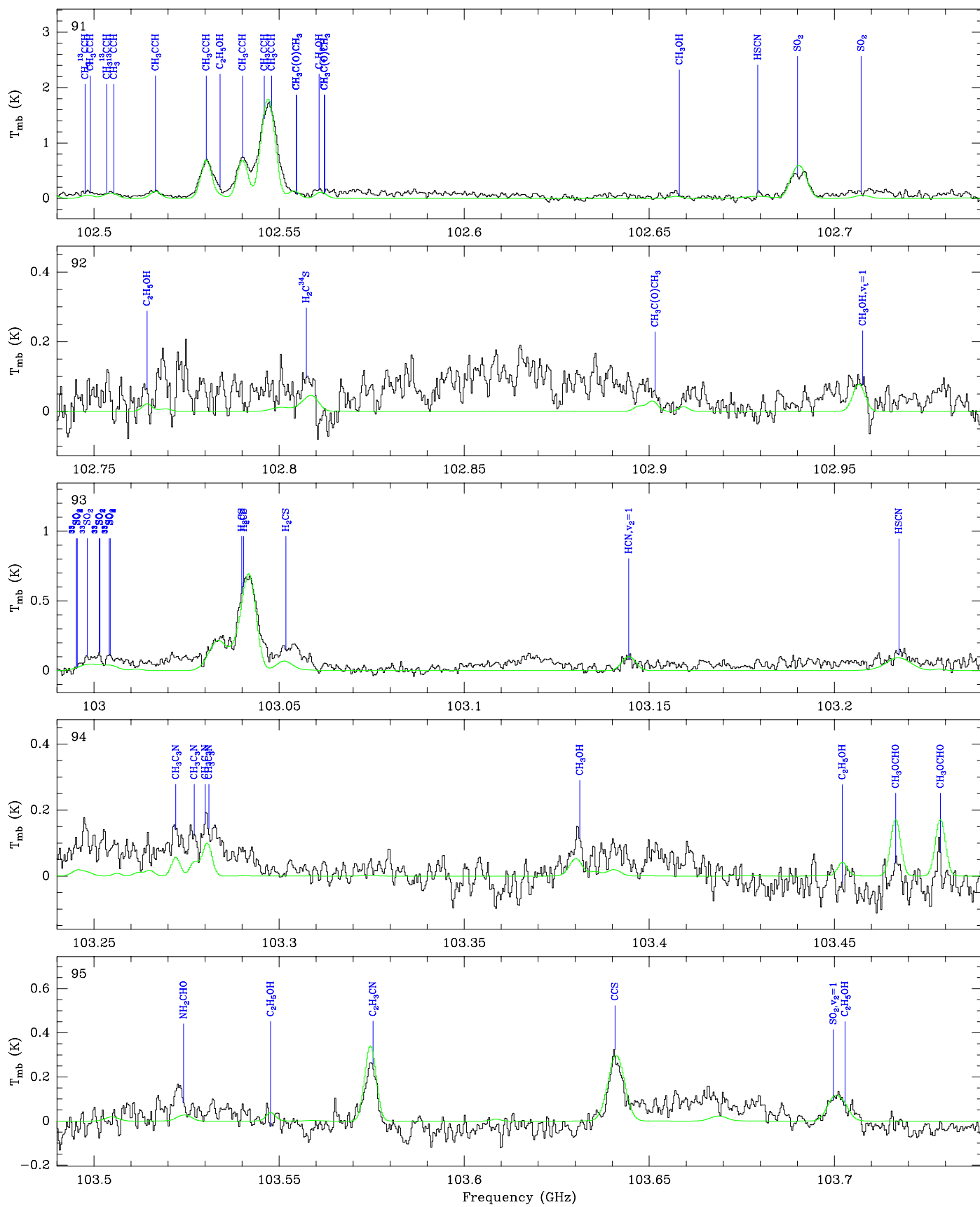
Fig. 5. continued.
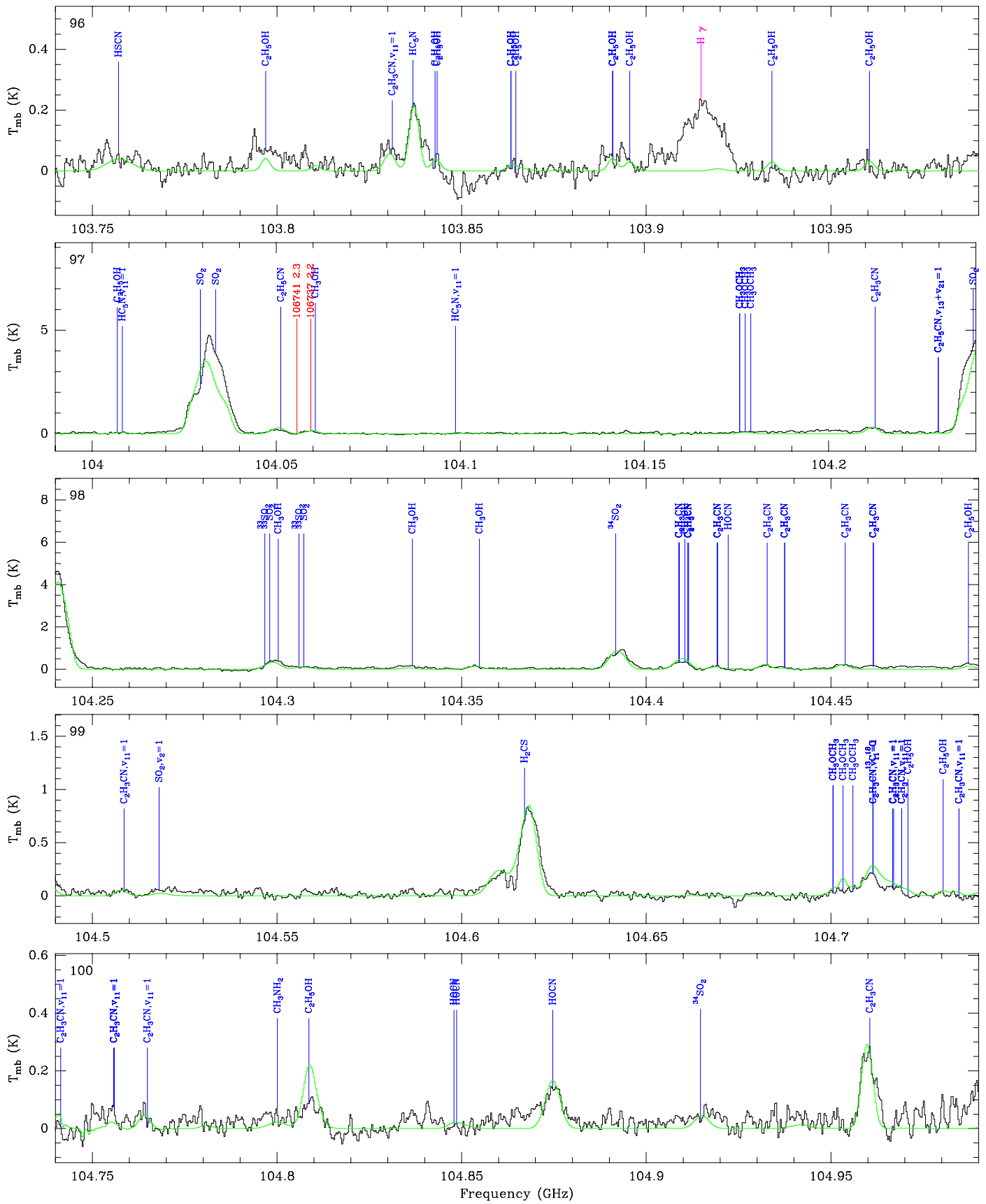
Fig. 5. continued.
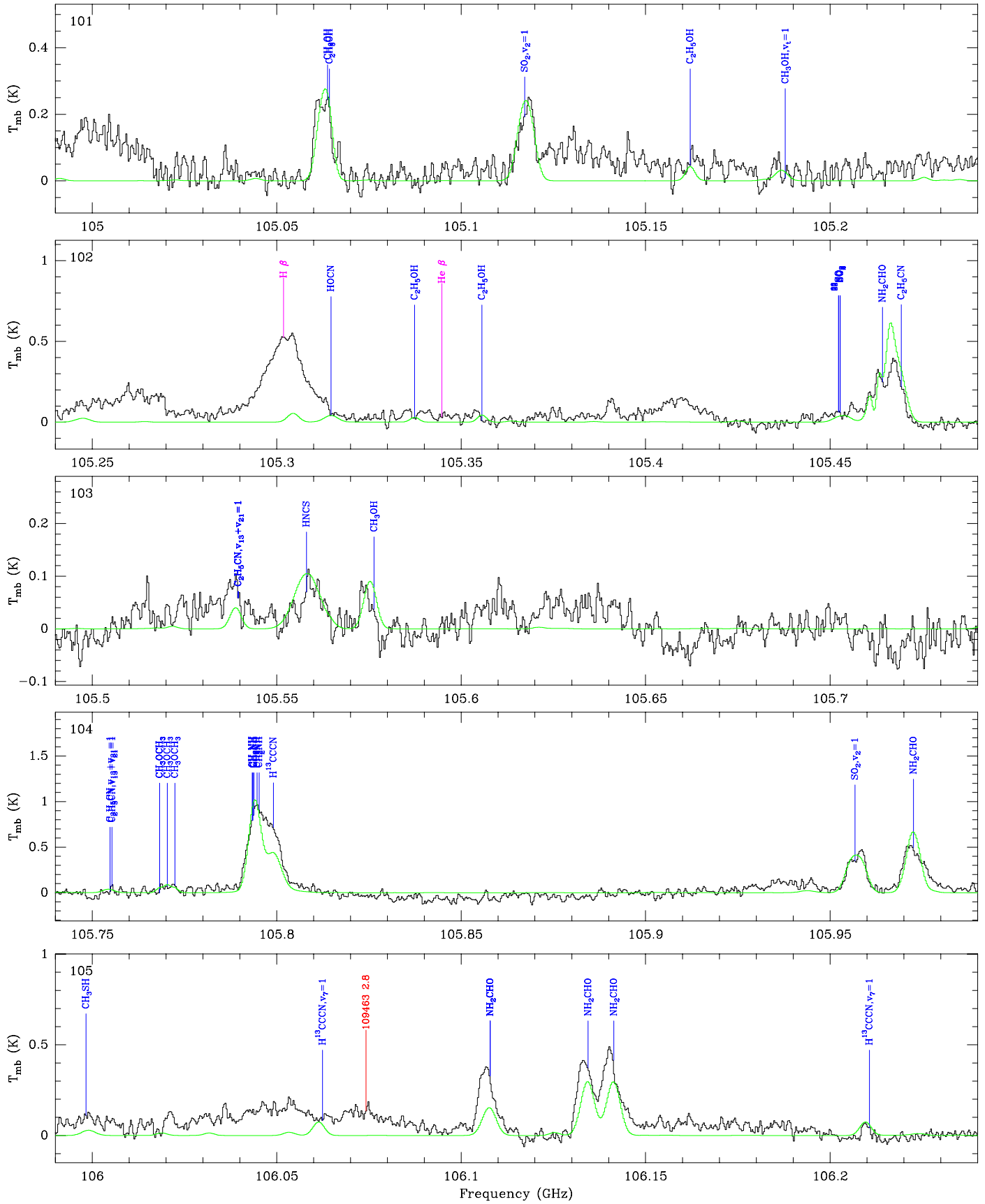
Fig. 5. continued.
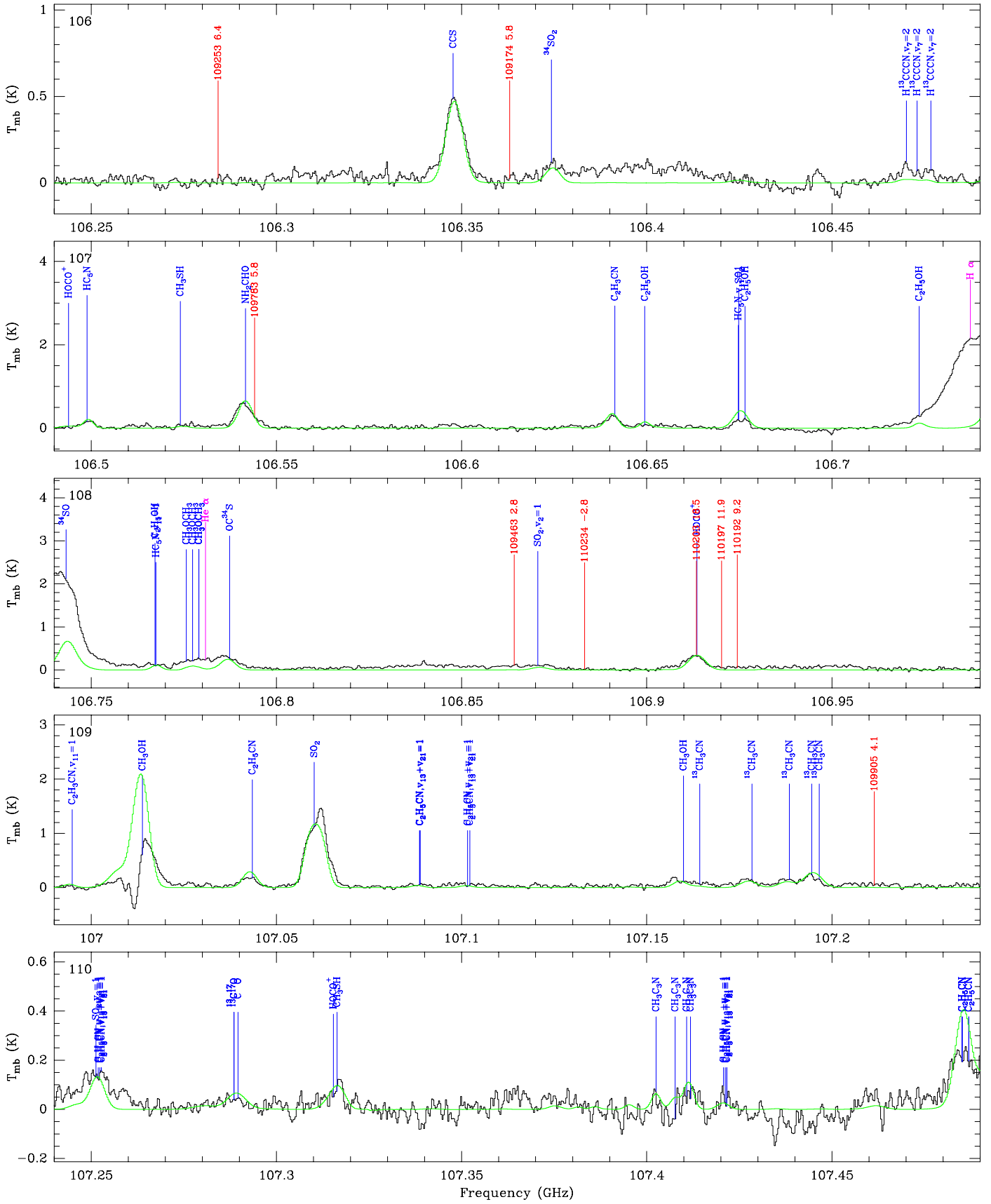
Fig. 5. continued.
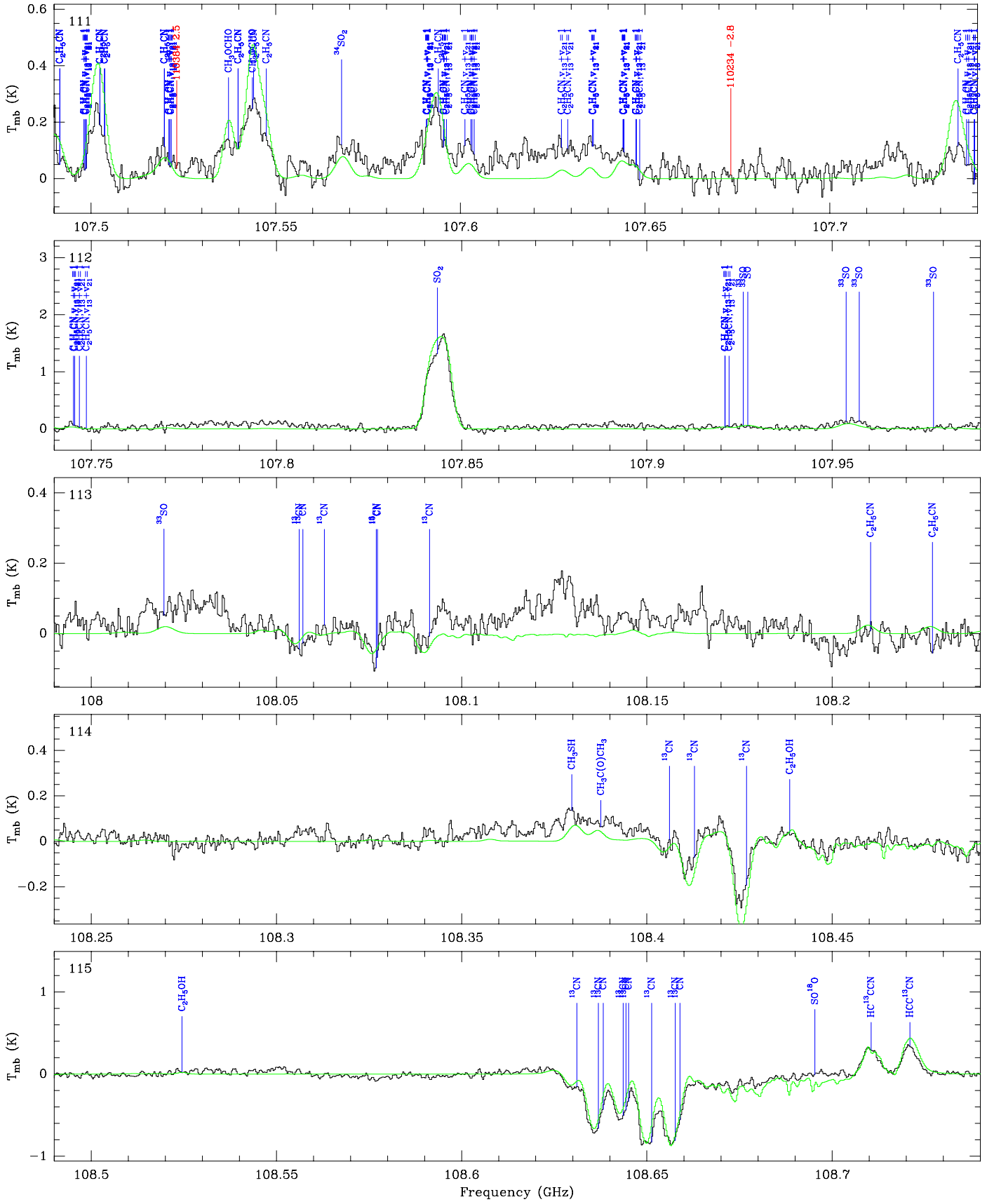
Fig. 5. continued.
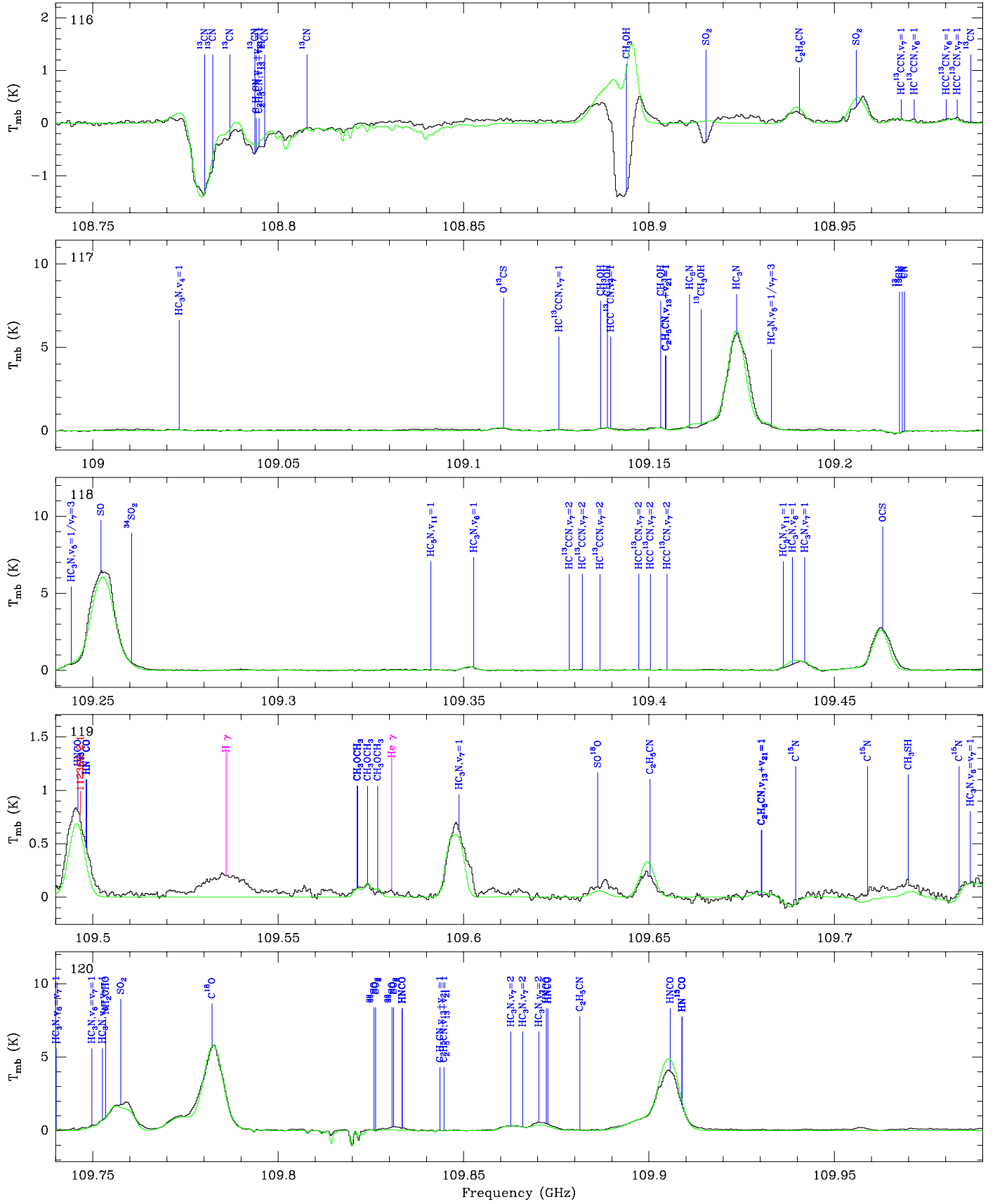
Fig. 5. continued.
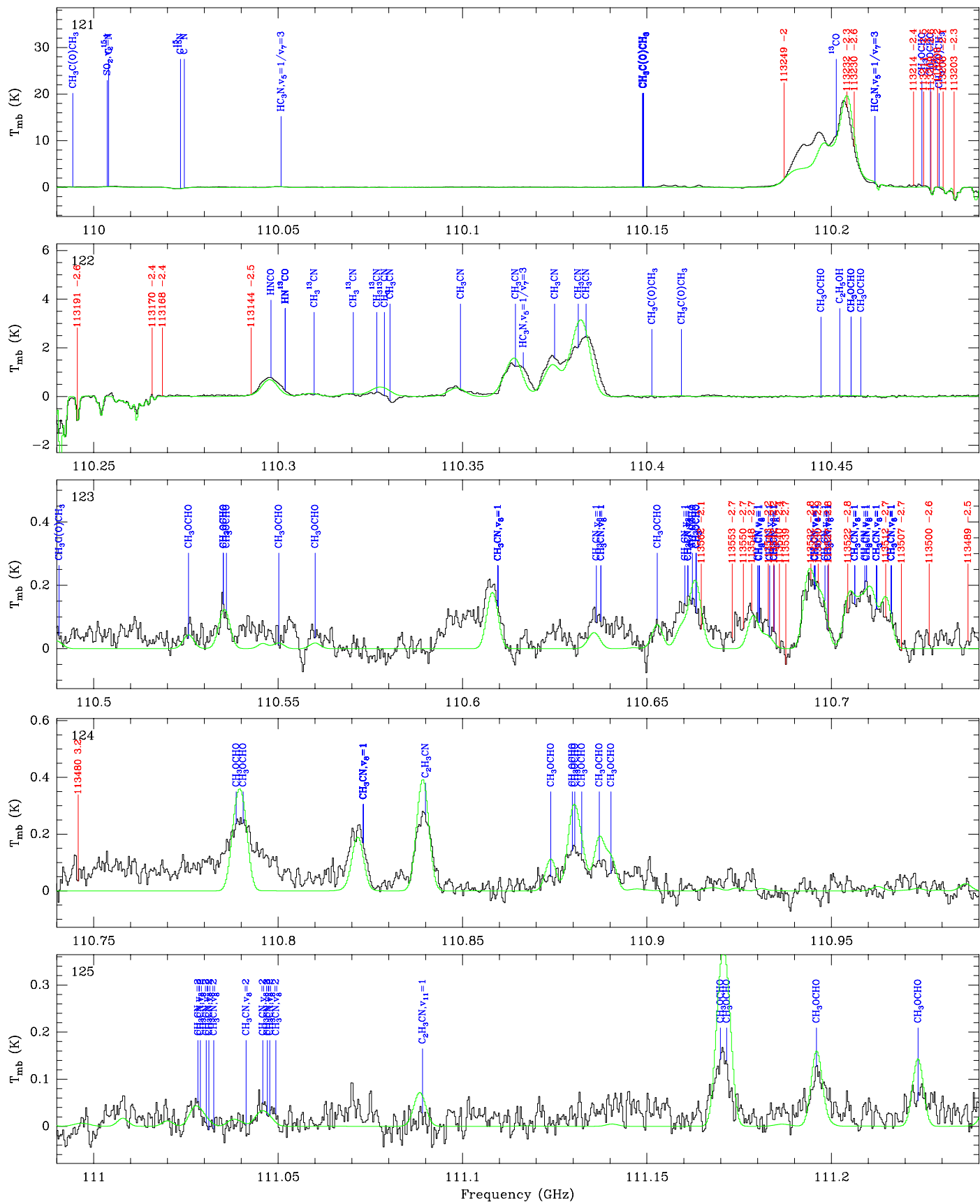
Fig. 5. continued.
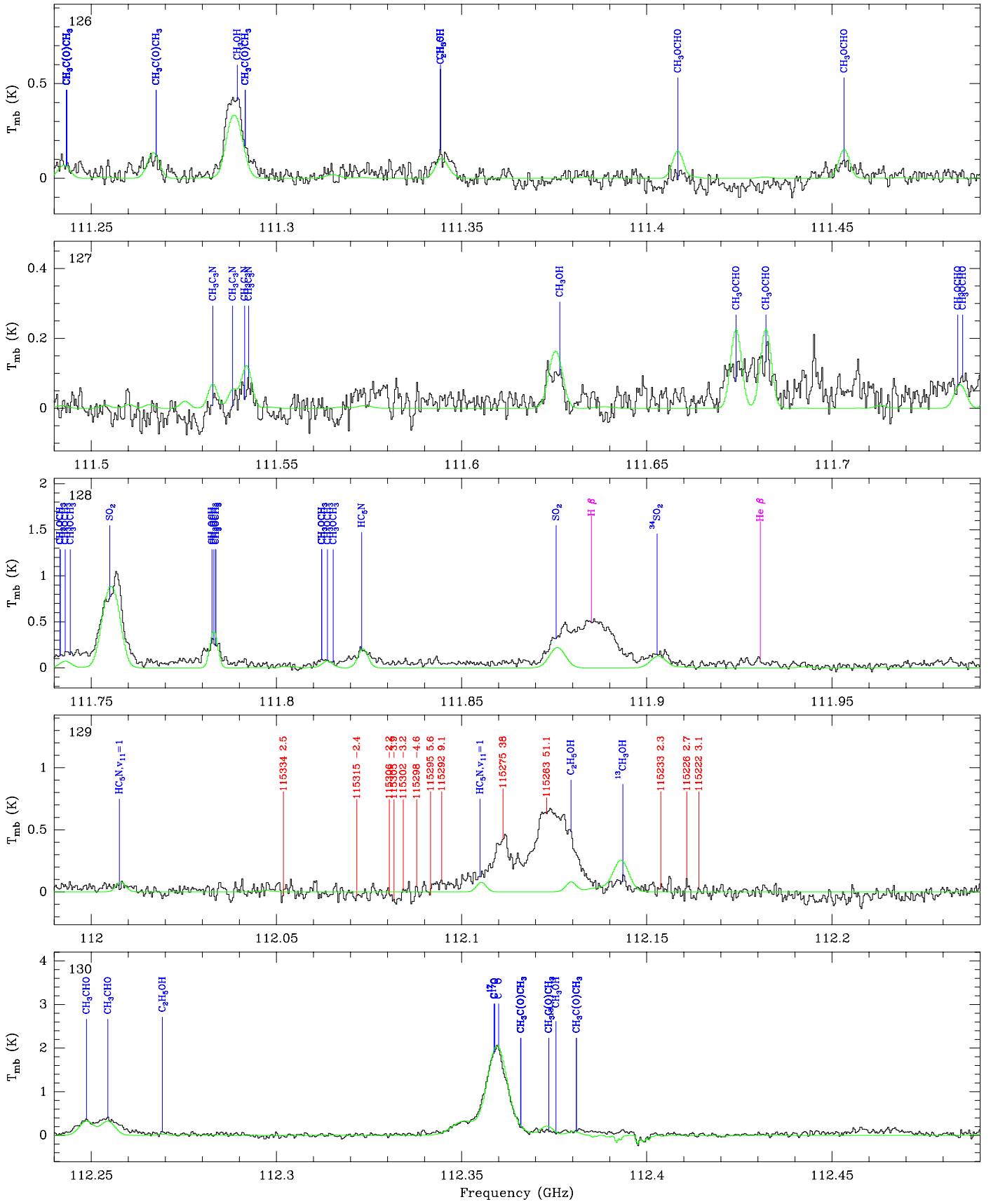
Fig. 5. continued.
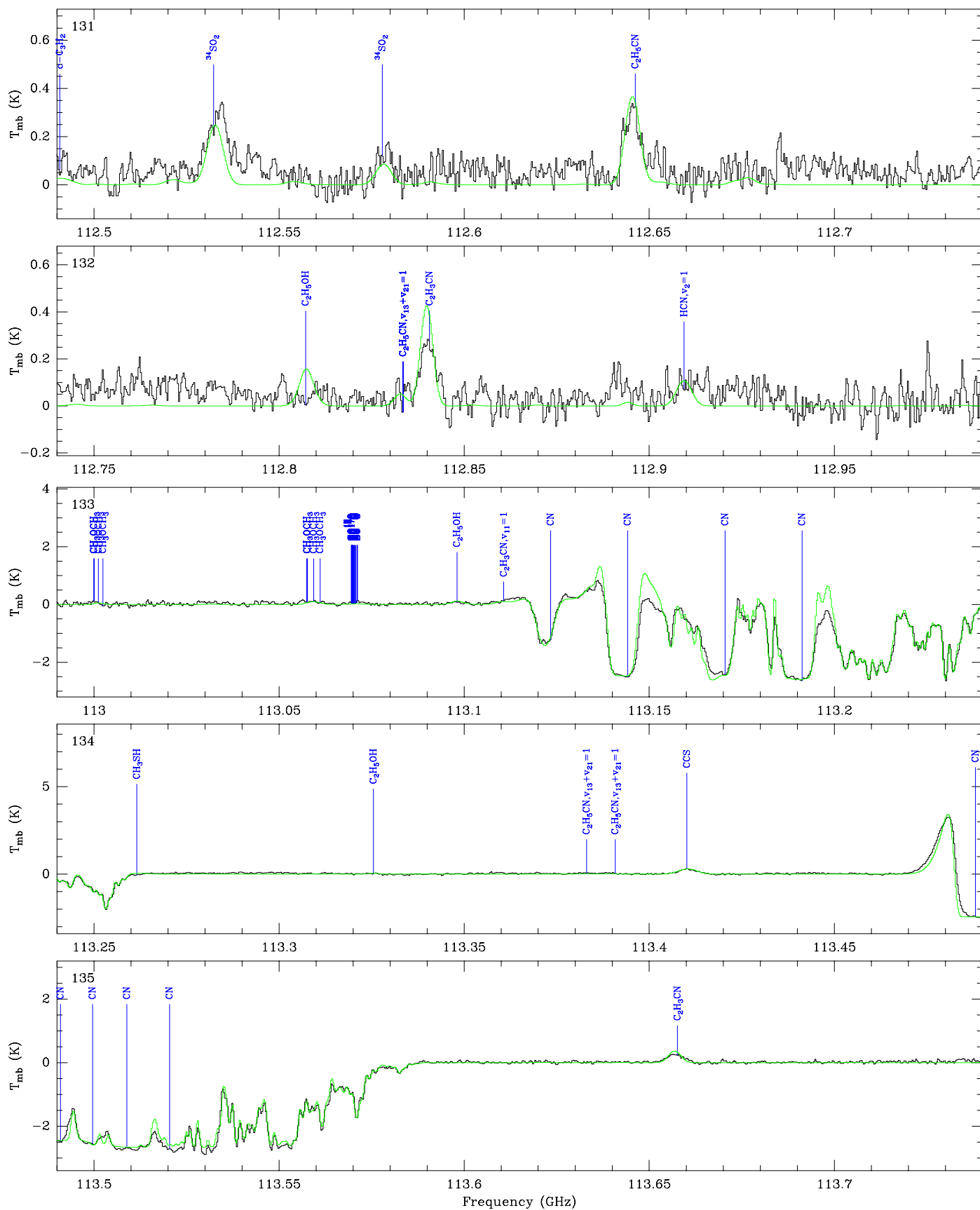
Fig. 5. continued.
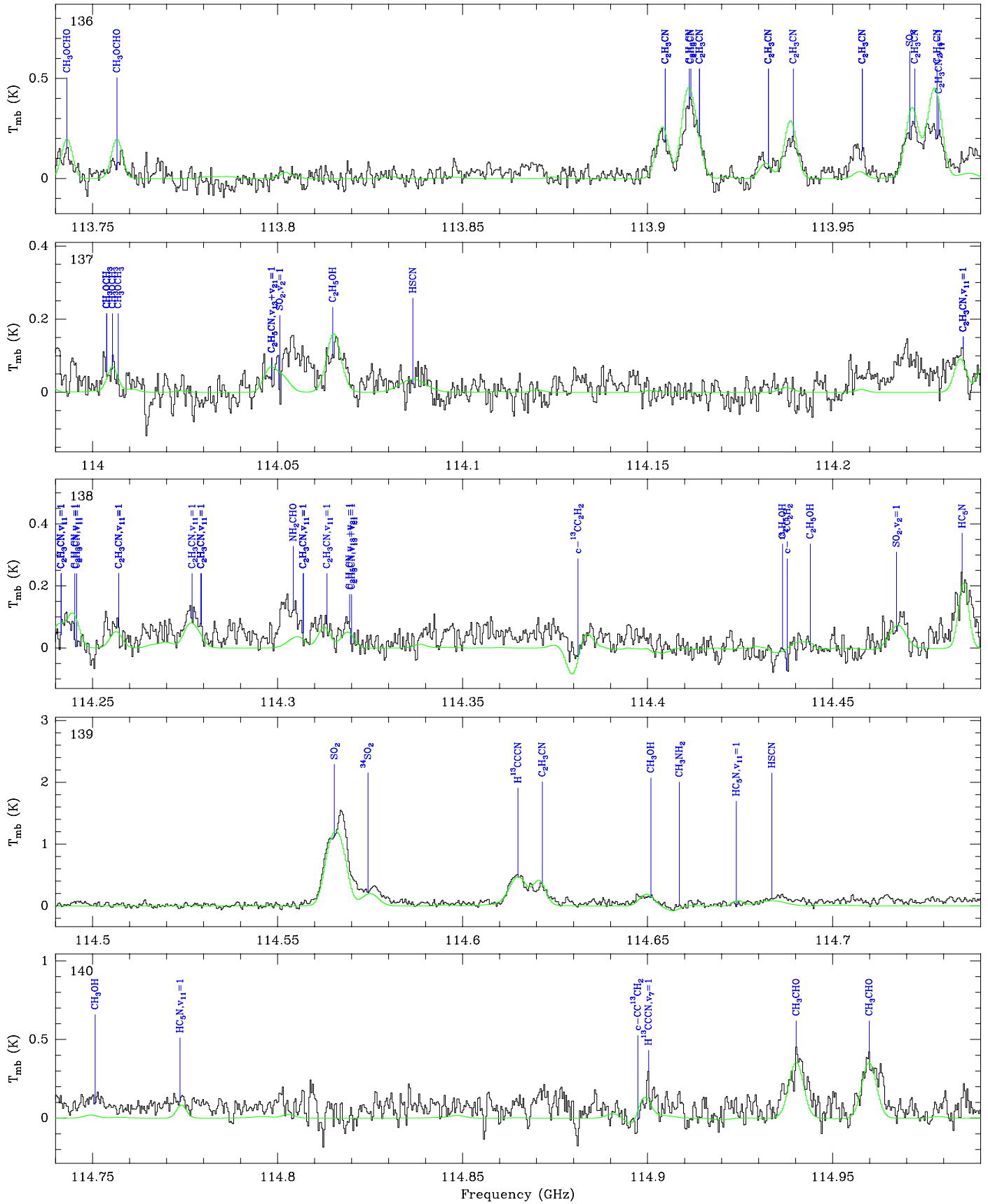
Fig. 5. continued.
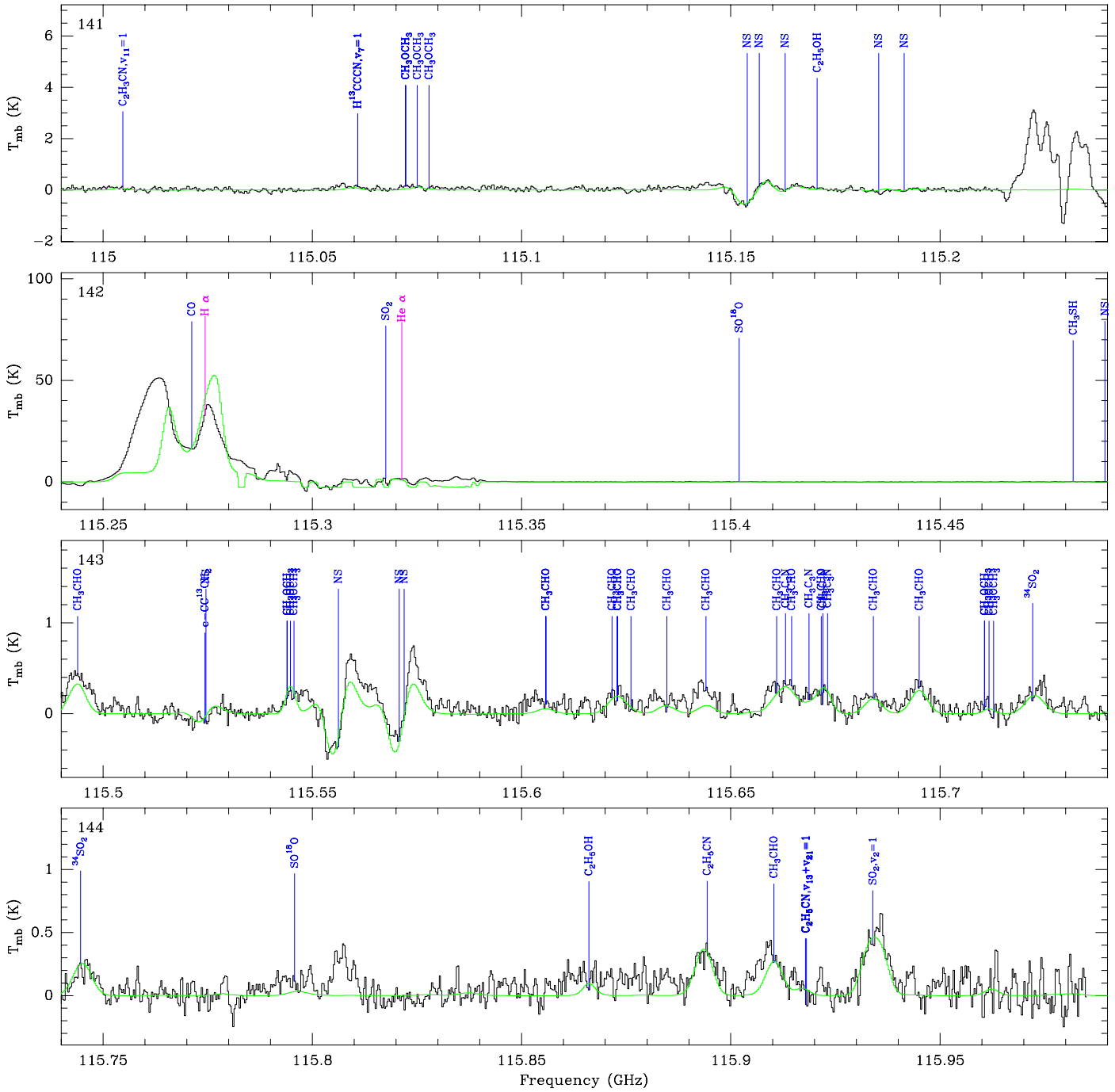
Fig. 5. continued.

Fig. 5. continued.
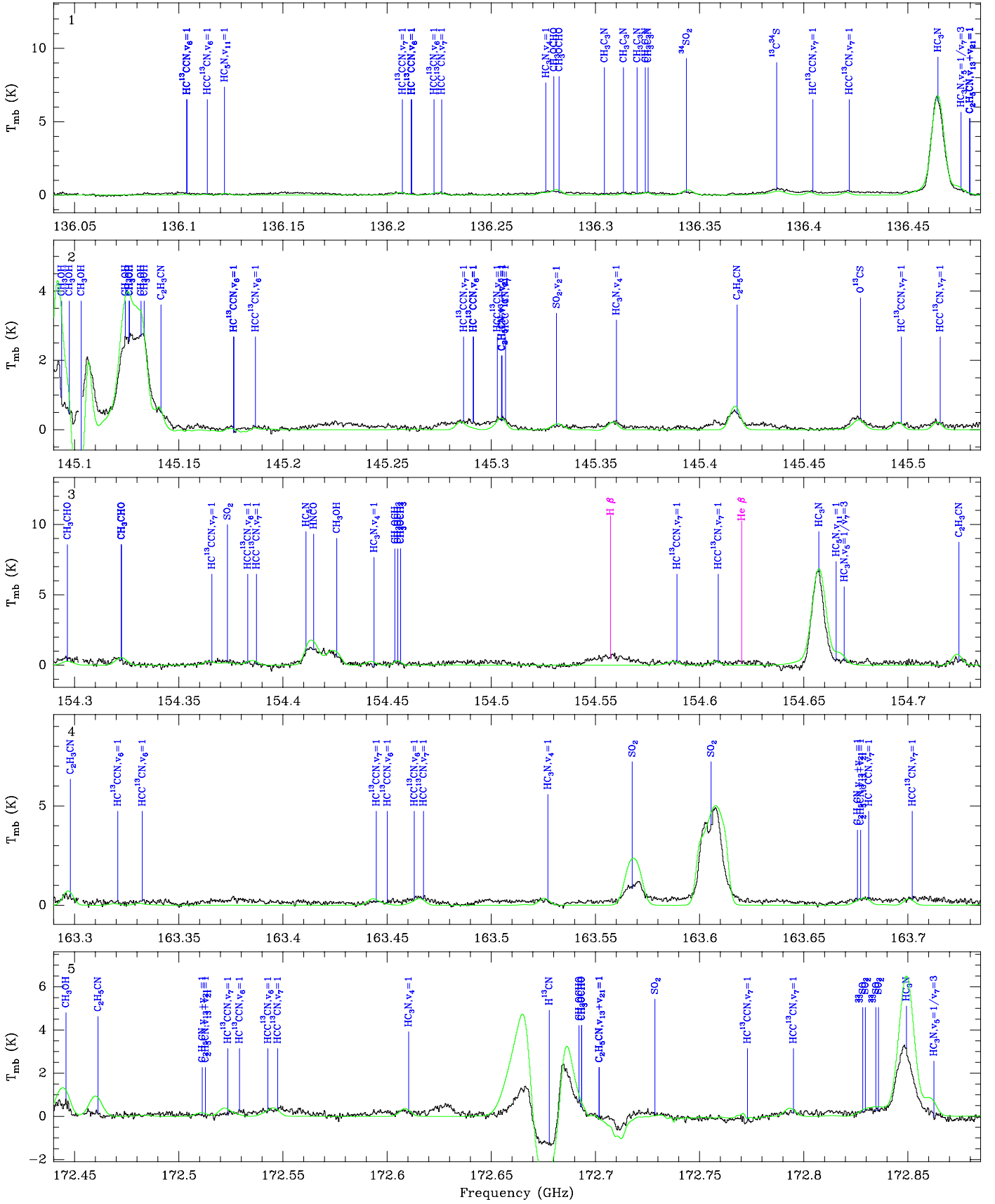
Fig. 6. Spectrum obtained toward Sgr B2(M) in the 2 mm window with the IRAM 30 m telescope in main-beam temperature scale. The synthetic model is overlaid in green and its relevant lines are labeled in blue. The frequencies of the hydrogen and helium recombination lines are indicated with a pink label.

Fig. 6. continued.
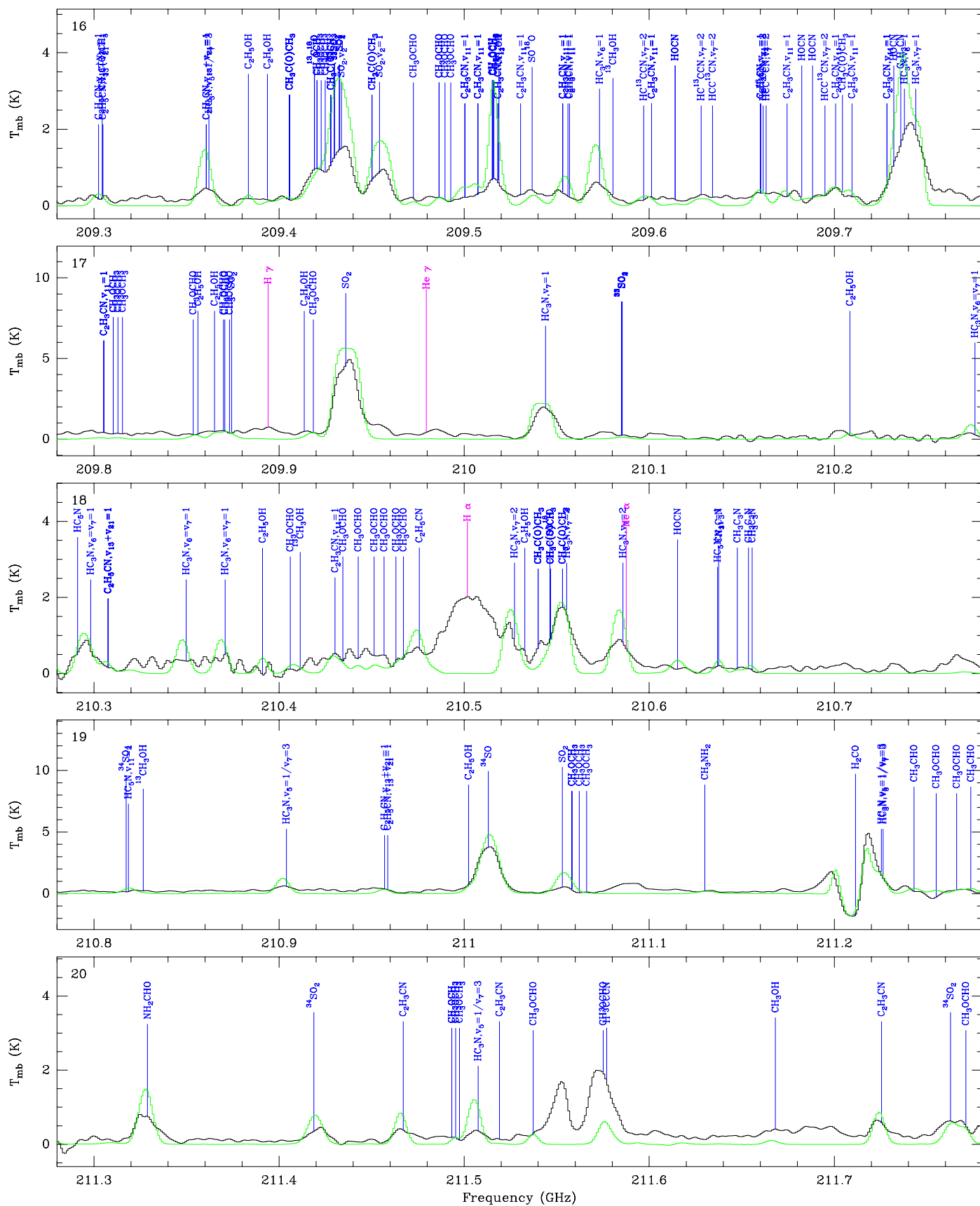
Fig. 7. Spectrum obtained toward Sgr B2(M) in the 1 mm window with the IRAM 30 m telescope in main-beam temperature scale. The synthetic model is overlaid in green and its relevant lines are labeled in blue. The frequencies of the hydrogen and helium recombination lines are indicated with a pink label.

Fig. 7. continued.

Fig. 7. continued.

Fig. 7. continued.

A47, page 120 of 187

Fig. 7. continued.

Fig. 7. continued.

Fig. 7. continued.

Fig. 7. continued.
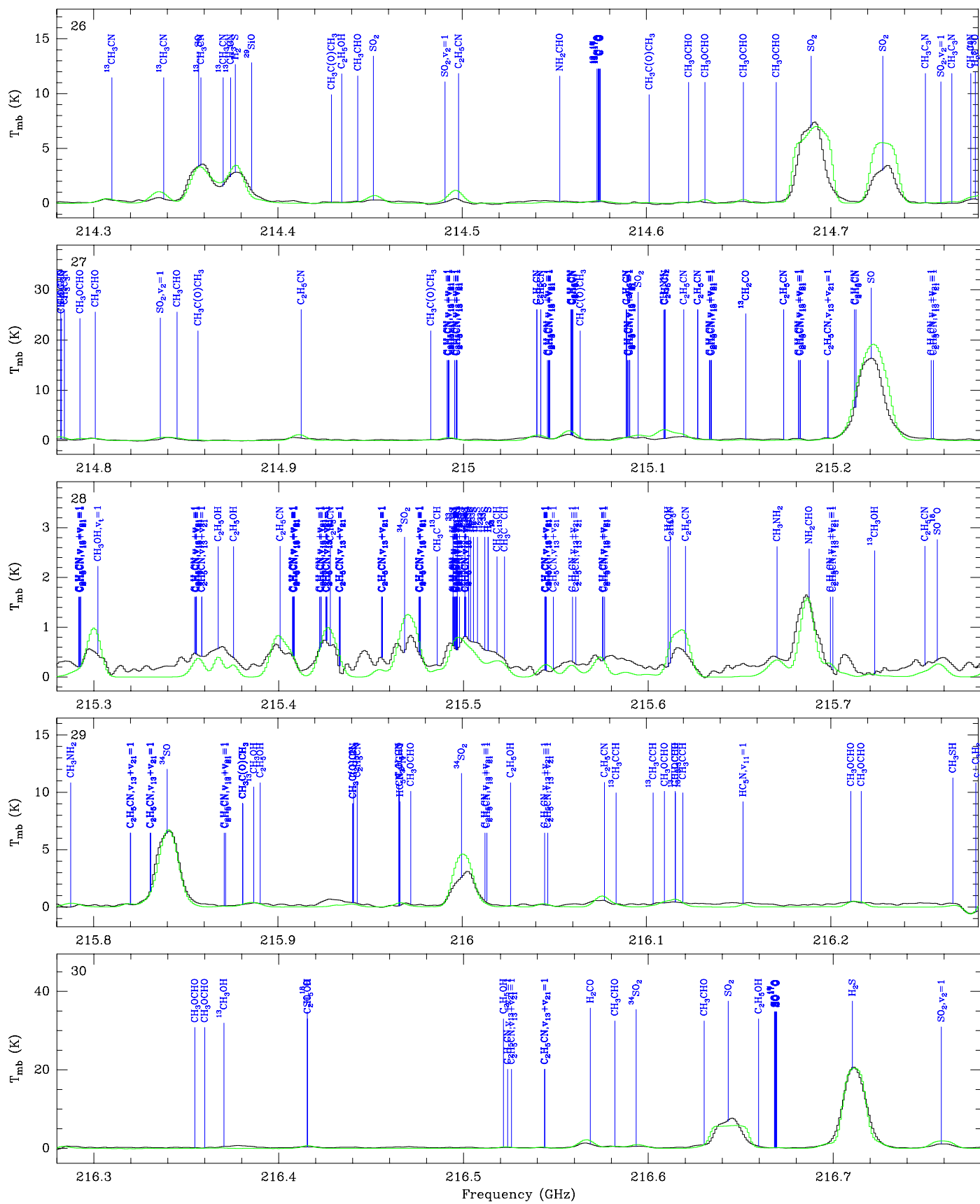
Fig. 7. continued.
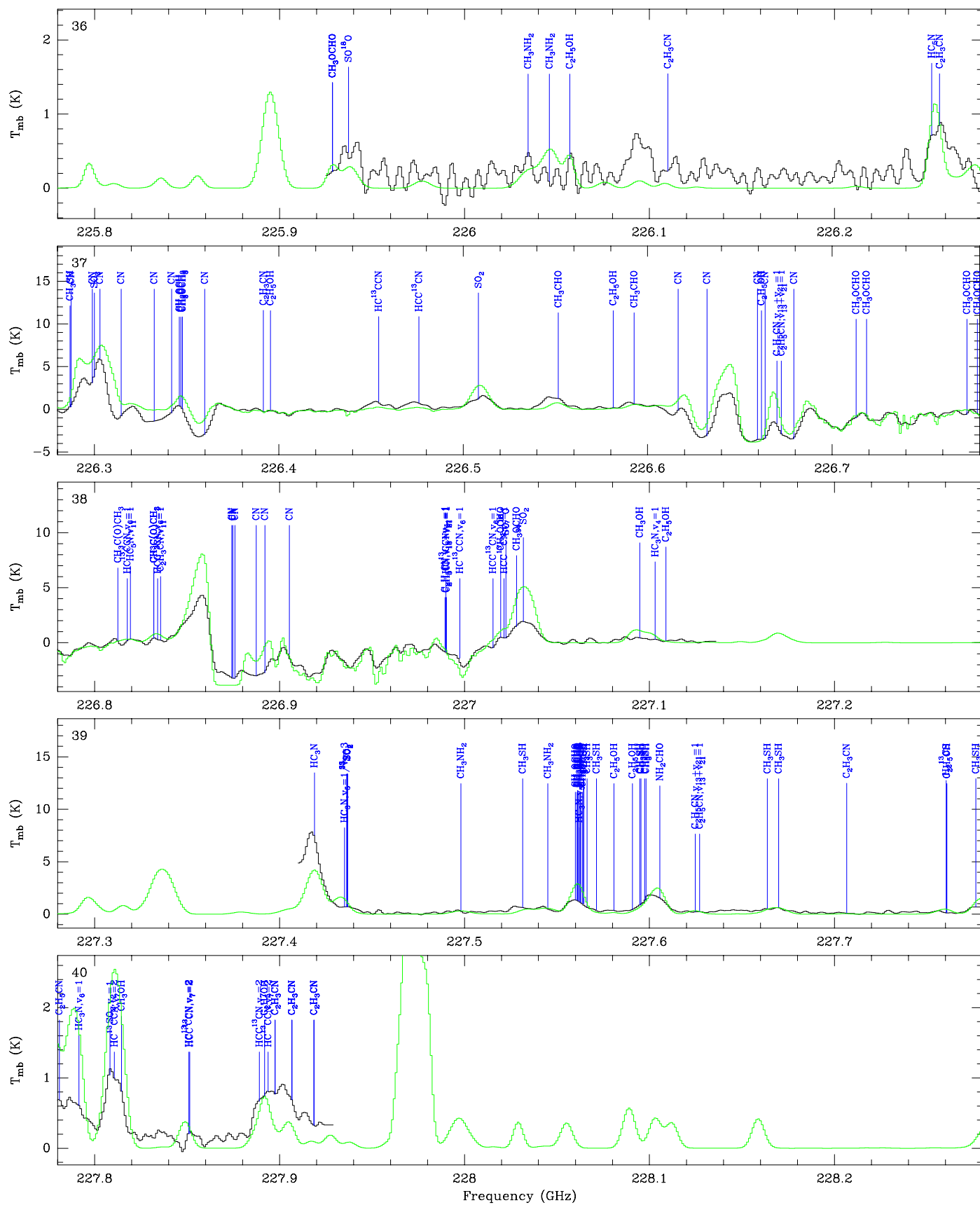
Fig. 7. continued.
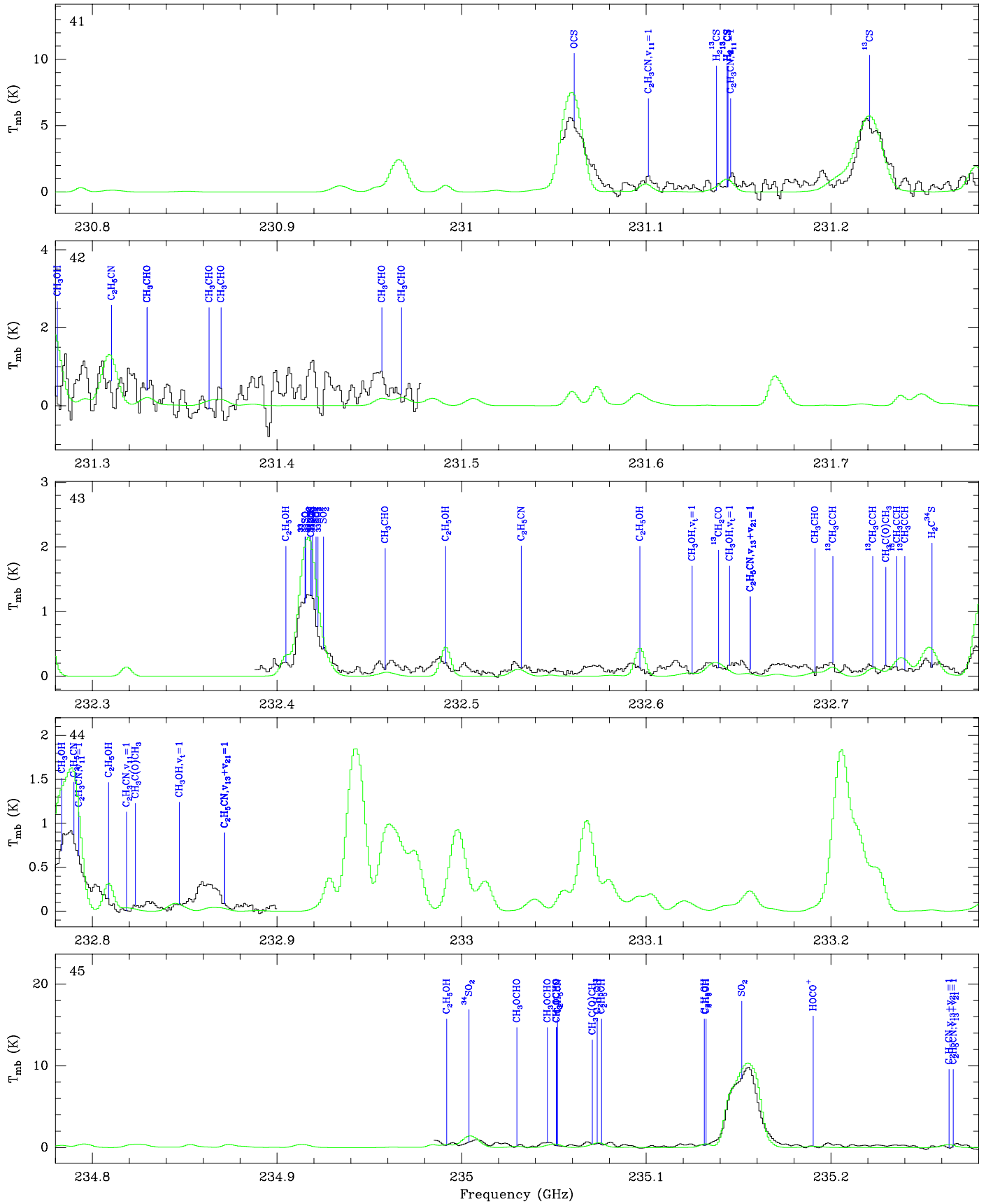
Fig. 7. continued.
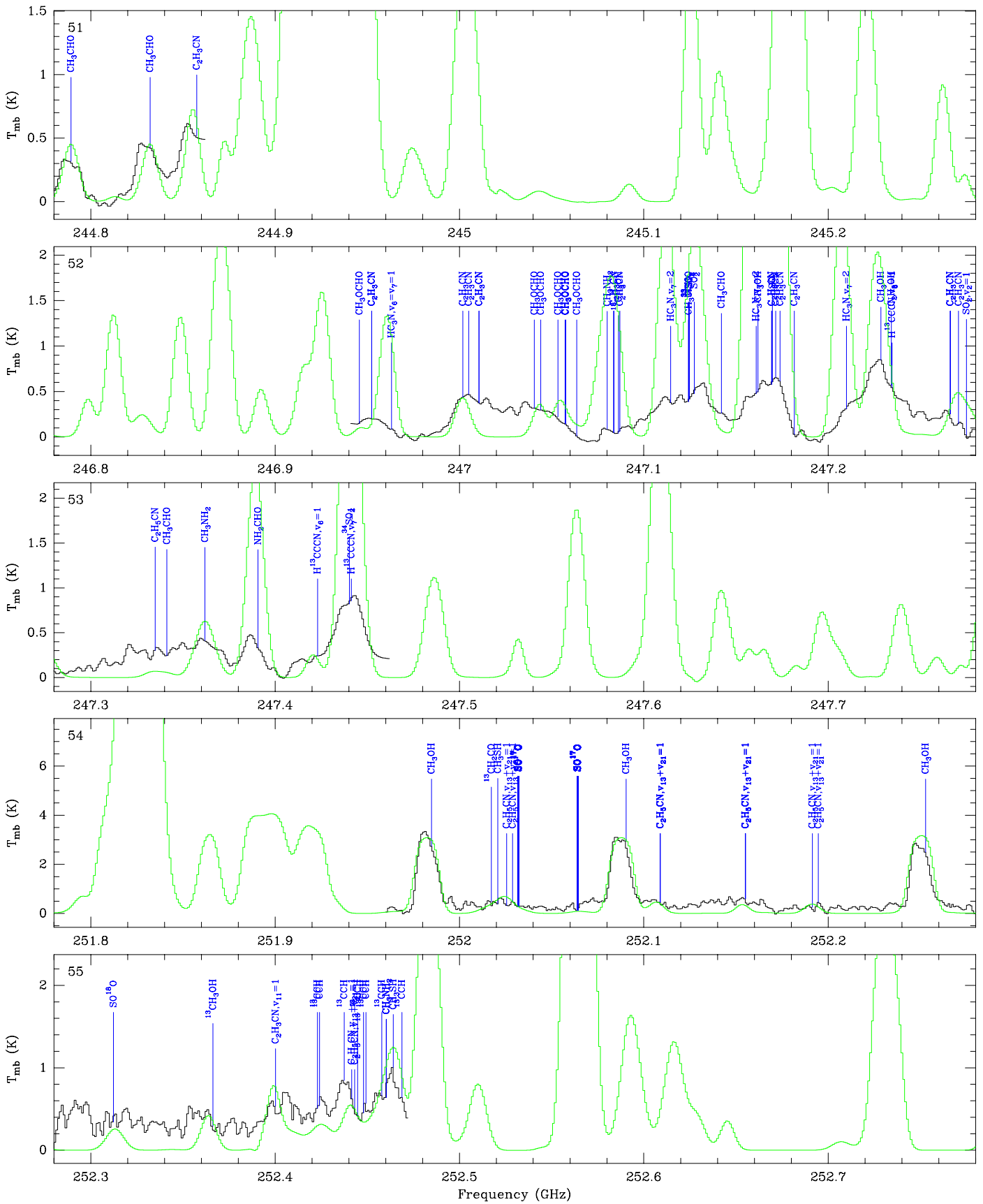
Fig. 7. continued.
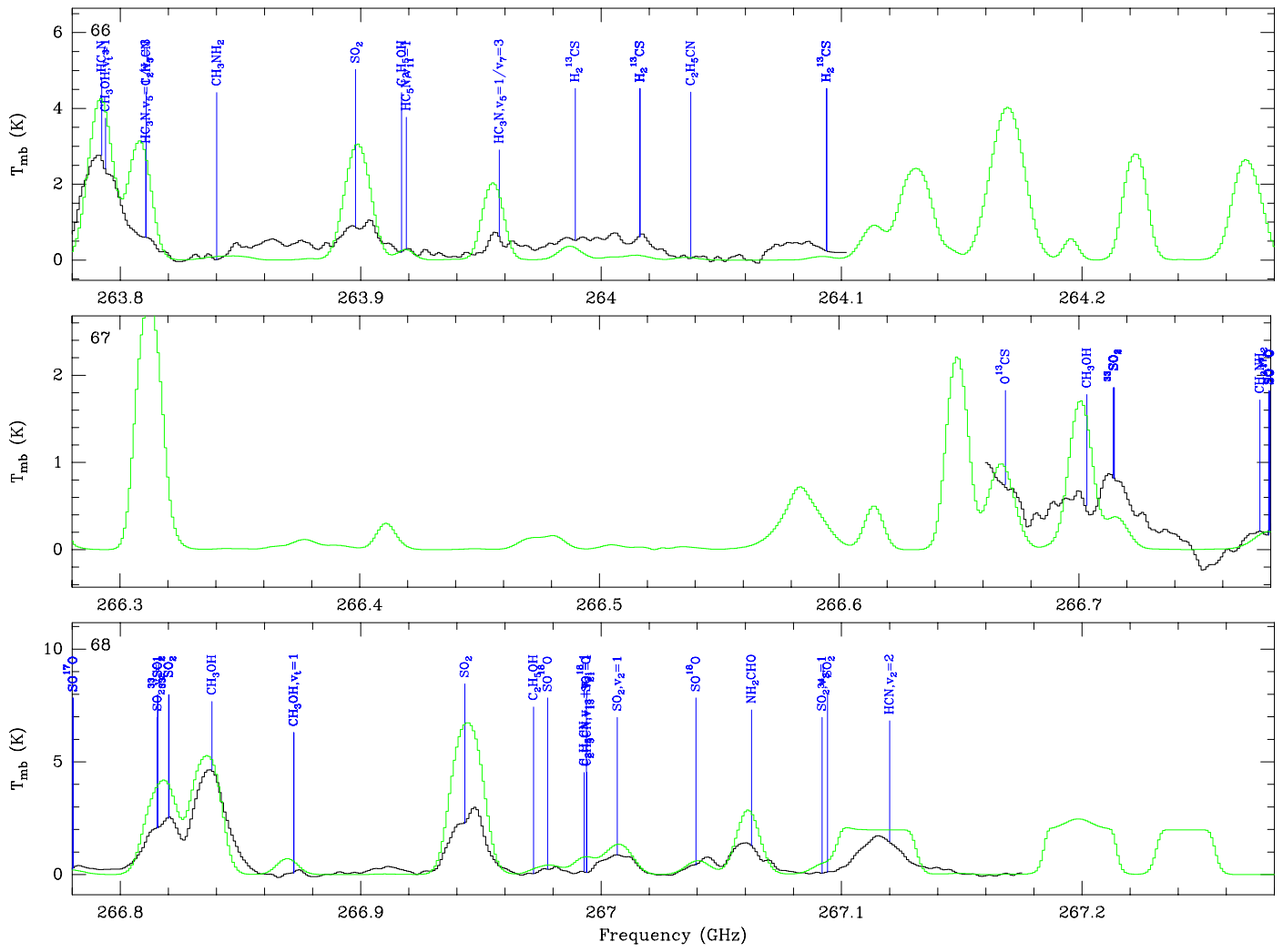
Fig. 7. continued.

Fig. 7. continued.

Table 6. Parameters of our best-fit model of C_2H_3CN toward Sgr B2(N).

Molecule[a]	Size[b] (″)	T_{rot}[c] (K)	N[d] (cm^{-2})	C_{int}[e]	C_{vib}[f]	C_N[g]	ΔV[h] (km s^{-1})	V_{off}[i] (km s^{-1})	F[j]
(1)	(2)	(3)	(4)	(5)	(6)	(7)	(8)	(9)	(10)
C_2H_3CN	2.3	170	7.38×10^{17}	0.92	1.00	0.92	7.0	−1.0	e
	2.3	170	2.21×10^{17}	0.92	1.00	0.92	7.0	9.0	e
	2.3	170	9.22×10^{16}	0.92	1.00	0.92	10.0	−9.0	e
$C_2H_3CN, v_{11} = 1$	1.6	170	3.69×10^{18}	0.92	1.00	0.92	7.0	−1.0	e
	1.6	170	9.22×10^{17}	0.92	1.00	0.92	7.0	9.0	e
$C_2H_3CN, v_{15} = 1$	1.6	170	4.61×10^{18}	0.92	1.00	0.92	7.0	−1.0	e
	1.6	170	1.11×10^{18}	0.92	1.00	0.92	7.0	9.0	e
$C_2H_3CN, v_{11} = 2$	1.6	170	5.53×10^{18}	0.92	1.00	0.92	7.0	−1.0	e
	1.6	170	1.38×10^{18}	0.92	1.00	0.92	7.0	9.0	e
$C_2H_3CN, v_{11} = 1/v_{15} = 1$	1.6	170	5.53×10^{18}	0.92	1.00	0.92	7.0	−1.0	e
	1.6	170	1.38×10^{18}	0.92	1.00	0.92	7.0	9.0	e
$C_2H_3CN, v_{15} = 2$	1.6	170	1.01×10^{19}	0.92	1.00	0.92	7.0	−1.0	e
$C_2H_3CN, v_{11} = 3$	1.6	170	1.20×10^{19}	0.92	1.00	0.92	7.0	−1.0	e
$CH_2CH^{13}CN$	2.3	170	3.77×10^{16}	1.00	1.26	1.26	7.0	−1.0	e
	2.3	170	1.13×10^{16}	1.00	1.26	1.26	7.0	9.0	e
	2.3	170	4.72×10^{15}	1.00	1.26	1.26	10.0	−9.0	e
$CH_2^{13}CHCN$	2.3	170	3.77×10^{16}	1.00	1.26	1.26	7.0	−1.0	e
	2.3	170	1.13×10^{16}	1.00	1.26	1.26	7.0	9.0	e
	2.3	170	4.72×10^{15}	1.00	1.26	1.26	10.0	−9.0	e
$^{13}CH_2CHCN$	2.3	170	3.77×10^{16}	1.00	1.26	1.26	7.0	−1.0	e
	2.3	170	1.13×10^{16}	1.00	1.26	1.26	7.0	9.0	e
	2.3	170	4.72×10^{15}	1.00	1.26	1.26	10.0	−9.0	e

Notes. [a] Torsionally or vibrationally excited states are indicated after the name of the molecule and are modeled as separate entries. Entries with only the name of the molecule correspond to the ground state. [b] Source diameter (FWHM). [c] Rotational temperature. [d] Column density. [e] Correction factor that was applied to the column density to account for the correction to the approximate interpolation performed by XCLASS to compute the partition function. [f] Correction factor that was applied to the column density to account for the contribution of vibrationally or torsionally excited states or other conformers to the partition function. [g] Global correction factor that was applied to the column density ($C_{int} \times C_{vib}$). [h] Linewidth (*FWHM*). [i] Velocity offset with respect to the systemic velocity of Sgr B2(N) $V_{lsr} = 64$ km s^{-1}. [j] Flag indicating if the component belongs to the "emission" (e) or "absorption" (a) group.

Table 7. Parameters of our best-fit model of C_2H_5CN toward Sgr B2(N).

Molecule[a]	Size[b] (″)	T_{rot}[c] (K)	N[d] (cm^{-2})	C_{int}[e]	C_{vib}[f]	C_N[g]	ΔV[h] (km s^{-1})	V_{off}[i]	F[j]
(1)	(2)	(3)	(4)	(5)	(6)	(7)	(8)	(9)	(10)
C_2H_5CN	3.0	170	1.84×10^{18}	1.00	1.53	1.53	6.5	−1.0	e
	2.3	170	2.14×10^{18}	1.00	1.53	1.53	6.5	9.0	e
	1.7	170	1.38×10^{18}	1.00	1.53	1.53	8.0	−11.0	e
C_2H_5CN, $v_{13} + v_{21} = 1$	2.0	170	1.07×10^{19}	1.00	1.53	1.53	6.5	-1.0	e
	1.5	170	9.19×10^{18}	1.00	1.53	1.53	6.5	9.0	e
	1.7	170	1.99×10^{18}	1.00	1.53	1.53	8.0	−11.0	e
C_2H_5CN, $v_{20} = 1$	2.0	170	4.59×10^{18}	1.00	1.53	1.53	6.5	−1.0	e
	1.5	170	4.59×10^{18}	1.00	1.53	1.53	6.5	9.0	e
	1.7	170	1.53×10^{18}	1.00	1.53	1.53	8.0	−11.0	e
C_2H_5CN, $v_{12} = 1$	2.0	170	1.38×10^{19}	1.00	1.53	1.53	6.5	−1.0	e
	1.5	170	1.38×10^{19}	1.00	1.53	1.53	6.5	9.0	e
	1.7	170	4.59×10^{18}	1.00	1.53	1.53	8.0	−11.0	e
$C_2H_5^{13}CN$	3.0	170	6.12×10^{16}	1.00	1.53	1.53	6.5	−1.0	e
	2.3	170	7.66×10^{16}	1.00	1.53	1.53	6.5	9.0	e
	1.7	170	6.12×10^{16}	1.00	1.53	1.53	8.0	−11.0	e
$CH_3^{13}CH_2CN$	3.0	170	6.12×10^{16}	1.00	1.53	1.53	6.5	−1.0	e
	2.3	170	7.66×10^{16}	1.00	1.53	1.53	6.5	9.0	e
	1.7	170	6.12×10^{16}	1.00	1.53	1.53	8.0	−11.0	e
$^{13}CH_3CH_2CN$	3.0	170	6.12×10^{16}	1.00	1.53	1.53	6.5	−1.0	e
	2.3	170	7.66×10^{16}	1.00	1.53	1.53	6.5	9.0	e
	1.7	170	6.12×10^{16}	1.00	1.53	1.53	8.0	−11.0	e

Notes. See notes of Table 6.

Table 8. Parameters of our best-fit model of C_2H_5OCHO toward Sgr B2(N).

Molecule[a]	Size[b] (″)	T_{rot}[c] (K)	N[d] (cm^{-2})	C_{int}[e]	C_{vib}[f]	C_N[g]	ΔV[h] (km s^{-1})	V_{off}[i]	F[j]
(1)	(2)	(3)	(4)	(5)	(6)	(7)	(8)	(9)	(10)
C_2H_5OCHO	3.0	100	5.41×10^{16}	1.00	1.00	1.00	7.0	0.0	e

Notes. See notes of Table 6.

Table 9. Parameters of our best-fit model of C_2H_5OH toward Sgr B2(N).

Molecule[a]	Size[b] (″)	T_{rot}[c] (K)	N[d] (cm^{-2})	C_{int}[e]	C_{vib}[f]	C_N[g]	ΔV[h] (km s^{-1})	V_{off}[i]	F[j]
(1)	(2)	(3)	(4)	(5)	(6)	(7)	(8)	(9)	(10)
C_2H_5OH	3.0	150	9.14×10^{17}	1.05	1.00	1.05	7.0	−0.5	e
	3.0	150	3.99×10^{17}	1.05	1.00	1.05	7.0	9.5	e
a-$CH_3^{13}CH_2OH$	3.0	150	4.34×10^{16}	1.00	2.39	2.39	7.0	−0.5	e
	3.0	150	1.90×10^{16}	1.00	2.39	2.39	7.0	9.5	e
a-$^{13}CH_3CH_2OH$	3.0	150	4.34×10^{16}	1.00	2.39	2.39	7.0	−0.5	e
	3.0	150	1.90×10^{16}	1.00	2.39	2.39	7.0	9.5	e

Notes. See notes of Table 6.

Table 10. Parameters of our best-fit model of n-C_3H_7CN toward Sgr B2(N).

Molecule[a]	Size[b] (″)	T_{rot}[c] (K)	N[d] (cm^{-2})	C_{int}[e]	C_{vib}[f]	C_N[g]	ΔV[h] (km s^{-1})	V_{off}[i]	F[j]
(1)	(2)	(3)	(4)	(5)	(6)	(7)	(8)	(9)	(10)
n-C_3H_7CN	3.0	150	1.54×10^{16}	1.02	1.00	1.02	7.0	−1.0	e
	3.0	150	6.76×10^{15}	1.02	1.00	1.02	7.0	9.0	e

Notes. See notes of Table 6.

Table 11. Parameters of our best-fit model of c-C_2H_4O toward Sgr B2(N).

Molecule[a]	Size[b] (″)	$T_{\rm rot}$[c] (K)	N[d] (cm^{-2})	$C_{\rm int}$[e]	$C_{\rm vib}$[f]	C_N[g]	ΔV[h]	$V_{\rm off}$[i] (km s^{-1})	F[j]
(1)	(2)	(3)	(4)	(5)	(6)	(7)	(8)	(9)	(10)
c-C_2H_4O	3.0	100	3.89×10^{16}	1.00	1.00	1.00	7.0	−1.0	e

Notes. See notes of Table 6.

Table 12. Parameters of our best-fit model of c-C_3H_2 toward Sgr B2(N).

Molecule[a]	Size[b] (″)	$T_{\rm rot}$[c] (K)	N[d] (cm^{-2})	$C_{\rm int}$[e]	$C_{\rm vib}$[f]	C_N[g]	ΔV[h]	$V_{\rm off}$[i] (km s^{-1})	F[j]
(1)	(2)	(3)	(4)	(5)	(6)	(7)	(8)	(9)	(10)
c-C_3H_2	200	14	2.50×10^{14}	1.00	1.00	1.00	15.0	3.0	e
	120	2.7	3.39×10^{13}	1.06	1.00	1.06	9.0	17.0	a
	120	2.7	1.27×10^{14}	1.06	1.00	1.06	10.5	0.5	a
	120	2.7	2.33×10^{12}	1.06	1.00	1.06	5.0	−32.0	a
	120	2.7	9.42×10^{11}	1.06	1.00	1.06	5.0	−42.0	a
	120	2.7	4.13×10^{12}	1.06	1.00	1.06	6.0	−46.0	a
	120	2.7	3.81×10^{12}	1.06	1.00	1.06	6.0	−52.0	a
	120	2.7	3.39×10^{12}	1.06	1.00	1.06	3.5	−55.6	a
	120	2.7	8.78×10^{12}	1.06	1.00	1.06	6.5	−61.0	a
	120	2.7	3.60×10^{12}	1.06	1.00	1.06	4.5	−66.5	a
	120	2.7	2.43×10^{12}	1.06	1.00	1.06	5.0	−83.5	a
	120	2.7	4.66×10^{12}	1.06	1.00	1.06	6.0	−89.0	a
	120	2.7	2.33×10^{12}	1.06	1.00	1.06	4.0	−93.5	a
	120	2.7	1.16×10^{12}	1.06	1.00	1.06	4.0	−99.5	a
	120	2.7	2.33×10^{12}	1.06	1.00	1.06	3.3	−104.7	a
	120	2.7	9.42×10^{11}	1.06	1.00	1.06	3.0	−109.7	a
	120	2.7	1.69×10^{12}	1.06	1.00	1.06	3.0	−113.0	a
	120	2.7	9.42×10^{11}	1.06	1.00	1.06	3.5	−122.5	a
	120	2.7	1.80×10^{12}	1.06	1.00	1.06	6.0	−133.8	a
	120	2.7	3.49×10^{12}	1.06	1.00	1.06	4.5	−139.0	a
	120	2.7	1.48×10^{12}	1.06	1.00	1.06	4.0	−144.1	a
	120	2.7	9.95×10^{11}	1.06	1.00	1.06	5.0	−148.3	a
	120	2.7	8.25×10^{11}	1.06	1.00	1.06	4.0	−152.5	a
	120	2.7	2.33×10^{12}	1.06	1.00	1.06	4.0	−157.0	a
	120	2.7	4.66×10^{11}	1.06	1.00	1.06	4.0	−161.5	a
	120	2.7	9.42×10^{11}	1.06	1.00	1.06	4.0	−165.8	a
	120	2.7	4.44×10^{12}	1.06	1.00	1.06	4.0	−170.2	a
c-$CC^{13}CH_2$	200	14	1.25×10^{13}	1.00	1.00	1.00	15.0	3.0	e
	120	2.7	3.00×10^{12}	1.07	1.00	1.07	9.0	17.0	a
	120	2.7	9.34×10^{12}	1.07	1.00	1.07	10.5	0.5	a
	120	2.7	5.90×10^{10}	1.07	1.00	1.07	5.0	−32.0	a
	120	2.7	1.59×10^{10}	1.07	1.00	1.07	5.0	−42.0	a
	120	2.7	6.97×10^{10}	1.07	1.00	1.07	6.0	−46.0	a
	120	2.7	6.44×10^{10}	1.07	1.00	1.07	6.0	−52.0	a
	120	2.7	1.72×10^{11}	1.07	1.00	1.07	3.5	−55.6	a
	120	2.7	4.45×10^{11}	1.07	1.00	1.07	6.5	−61.0	a
	120	2.7	1.82×10^{11}	1.07	1.00	1.07	4.5	−66.5	a
	120	2.7	6.17×10^{10}	1.07	1.00	1.07	5.0	−83.5	a
	120	2.7	1.18×10^{11}	1.07	1.00	1.07	6.0	−89.0	a
	120	2.7	5.90×10^{10}	1.07	1.00	1.07	4.0	−93.5	a
	120	2.7	2.95×10^{10}	1.07	1.00	1.07	4.0	−99.5	a
	120	2.7	5.90×10^{10}	1.07	1.00	1.07	3.3	−104.7	a
	120	2.7	2.39×10^{10}	1.07	1.00	1.07	3.0	−109.7	a
	120	2.7	4.29×10^{10}	1.07	1.00	1.07	3.0	−113.0	a
	120	2.7	4.77×10^{10}	1.07	1.00	1.07	3.5	−122.5	a
	120	2.7	9.12×10^{10}	1.07	1.00	1.07	6.0	−133.8	a
	120	2.7	1.77×10^{11}	1.07	1.00	1.07	4.5	−139.0	a
	120	2.7	7.51×10^{10}	1.07	1.00	1.07	4.0	−144.1	a
	120	2.7	5.04×10^{10}	1.07	1.00	1.07	5.0	−148.3	a

Notes. See notes of Table 6.

Table 12. continued.

Molecule[a]	Size[b] ('')	T_{rot}[c] (K)	N[d] (cm^{-2})	C_{int}[e]	C_{vib}[f]	C_N[g]	ΔV[h]	V_{off}[i] (km s^{-1})	F[j]
(1)	(2)	(3)	(4)	(5)	(6)	(7)	(8)	(9)	(10)
	120	2.7	4.18×10^{10}	1.07	1.00	1.07	4.0	−152.5	a
	120	2.7	1.18×10^{11}	1.07	1.00	1.07	4.0	−157.0	a
	120	2.7	2.36×10^{10}	1.07	1.00	1.07	4.0	−161.5	a
	120	2.7	4.77×10^{10}	1.07	1.00	1.07	4.0	−165.8	a
	120	2.7	2.25×10^{11}	1.07	1.00	1.07	4.0	−170.2	a
c-^{13}CC$_2$H$_2$	200	14	1.25×10^{13}	1.00	1.00	1.00	15.0	3.0	e
	120	2.7	2.96×10^{12}	1.06	1.00	1.06	9.0	17.0	a
	120	2.7	9.19×10^{12}	1.06	1.00	1.06	10.5	0.5	a
	120	2.7	5.81×10^{10}	1.06	1.00	1.06	5.0	−32.0	a
	120	2.7	1.56×10^{10}	1.06	1.00	1.06	5.0	−42.0	a
	120	2.7	6.86×10^{10}	1.06	1.00	1.06	6.0	−46.0	a
	120	2.7	6.34×10^{10}	1.06	1.00	1.06	6.0	−52.0	a
	120	2.7	1.69×10^{11}	1.06	1.00	1.06	3.5	−55.6	a
	120	2.7	4.38×10^{11}	1.06	1.00	1.06	6.5	−61.0	a
	120	2.7	1.80×10^{11}	1.06	1.00	1.06	4.5	−66.5	a
	120	2.7	6.07×10^{10}	1.06	1.00	1.06	5.0	−83.5	a
	120	2.7	1.16×10^{11}	1.06	1.00	1.06	6.0	−89.0	a
	120	2.7	5.81×10^{10}	1.06	1.00	1.06	4.0	−93.5	a
	120	2.7	2.90×10^{10}	1.06	1.00	1.06	4.0	−99.5	a
	120	2.7	5.81×10^{10}	1.06	1.00	1.06	3.3	−104.7	a
	120	2.7	2.35×10^{10}	1.06	1.00	1.06	3.0	−109.7	a
	120	2.7	4.22×10^{10}	1.06	1.00	1.06	3.0	−113.0	a
	120	2.7	4.70×10^{10}	1.06	1.00	1.06	3.5	−122.5	a
	120	2.7	8.98×10^{10}	1.06	1.00	1.06	6.0	−133.8	a
	120	2.7	1.74×10^{11}	1.06	1.00	1.06	4.5	−139.0	a
	120	2.7	7.39×10^{10}	1.06	1.00	1.06	4.0	−144.1	a
	120	2.7	4.96×10^{10}	1.06	1.00	1.06	5.0	−148.3	a
	120	2.7	4.12×10^{10}	1.06	1.00	1.06	4.0	−152.5	a
	120	2.7	1.16×10^{11}	1.06	1.00	1.06	4.0	−157.0	a
	120	2.7	2.32×10^{10}	1.06	1.00	1.06	4.0	−161.5	a
	120	2.7	4.70×10^{10}	1.06	1.00	1.06	4.0	−165.8	a
	120	2.7	2.22×10^{11}	1.06	1.00	1.06	4.0	−170.2	a

Table 13. Parameters of our best-fit model of CCH toward Sgr B2(N).

Molecule[a]	Size[b] ('')	T_{rot}[c] (K)	N[d] (cm^{-2})	C_{int}[e]	C_{vib}[f]	C_N[g]	ΔV[h]	V_{off}[i] (km s^{-1})	F[j]
(1)	(2)	(3)	(4)	(5)	(6)	(7)	(8)	(9)	(10)
CCH	200	20	2.00×10^{15}	1.00	1.00	1.00	15.0	3.0	e
	20	2.7	2.43×10^{15}	1.43	1.00	1.43	8.0	0.0	a
	20	2.7	2.85×10^{14}	1.43	1.00	1.43	6.0	19.0	a
	120	2.7	2.57×10^{13}	1.43	1.00	1.43	5.0	−29.5	a
	120	2.7	4.99×10^{13}	1.43	1.00	1.43	5.0	−33.5	a
	120	2.7	4.99×10^{13}	1.43	1.00	1.43	5.0	−38.0	a
	120	2.7	5.71×10^{13}	1.43	1.00	1.43	5.0	−43.0	a
	120	2.7	9.99×10^{13}	1.43	1.00	1.43	5.0	−47.5	a
	120	2.7	4.71×10^{13}	1.43	1.00	1.43	4.5	−51.5	a
	120	2.7	1.21×10^{14}	1.43	1.00	1.43	5.0	−55.5	a
	120	2.7	9.28×10^{13}	1.43	1.00	1.43	4.5	−60.5	a
	120	2.7	6.42×10^{13}	1.43	1.00	1.43	4.5	−64.0	a
	120	2.7	7.13×10^{13}	1.43	1.00	1.43	5.0	−67.2	a
	120	2.7	1.43×10^{13}	1.43	1.00	1.43	4.0	−79.0	a
	120	2.7	2.28×10^{13}	1.43	1.00	1.43	3.0	−82.5	a
	120	2.7	4.42×10^{13}	1.43	1.00	1.43	4.0	−85.5	a
	120	2.7	5.71×10^{13}	1.43	1.00	1.43	4.0	−90.5	a
	120	2.7	2.85×10^{13}	1.43	1.00	1.43	3.5	−94.8	a
	120	2.7	1.86×10^{13}	1.43	1.00	1.43	4.0	−99.5	a
	120	2.7	9.99×10^{13}	1.43	1.00	1.43	4.7	−104.5	a

Notes. See notes of Table 6.

Table 13. continued.

Molecule[a]	Size[b] ('')	T_{rot}[c] (K)	N[d] (cm^{-2})	C_{int}[e]	C_{vib}[f]	C_N[g]	ΔV[h]	V_{off}[i]	F[j]
(1)	(2)	(3)	(4)	(5)	(6)	(7)	(8)	(9)	(10)
	120	2.7	2.57×10^{13}	1.43	1.00	1.43	3.0	−110.0	a
	120	2.7	3.57×10^{13}	1.43	1.00	1.43	4.5	−113.0	a
	120	2.7	8.56×10^{12}	1.43	1.00	1.43	4.5	−117.0	a
	120	2.7	2.14×10^{13}	1.43	1.00	1.43	3.0	−121.0	a
	120	2.7	7.13×10^{12}	1.43	1.00	1.43	4.0	−125.0	a
	120	2.7	1.43×10^{13}	1.43	1.00	1.43	5.0	−131.2	a
	120	2.7	1.28×10^{13}	1.43	1.00	1.43	4.0	−134.0	a
	120	2.7	6.42×10^{13}	1.43	1.00	1.43	4.5	−138.5	a
	120	2.7	4.00×10^{13}	1.43	1.00	1.43	5.0	−144.1	a
	120	2.7	9.99×10^{12}	1.43	1.00	1.43	6.0	−151.0	a
	120	2.7	5.71×10^{13}	1.43	1.00	1.43	5.0	−157.0	a
	120	2.7	9.99×10^{12}	1.43	1.00	1.43	3.0	−161.7	a
	120	2.7	3.28×10^{13}	1.43	1.00	1.43	5.0	−166.0	a
	120	2.7	8.28×10^{13}	1.43	1.00	1.43	4.0	−170.0	a
	120	2.7	5.71×10^{12}	1.43	1.00	1.43	8.0	−175.0	a
	120	2.7	2.85×10^{12}	1.43	1.00	1.43	4.0	−180.5	a
	120	2.7	8.56×10^{12}	1.43	1.00	1.43	4.0	−184.0	a
	120	2.7	4.28×10^{12}	1.43	1.00	1.43	4.0	−187.1	a
	120	2.7	4.28×10^{12}	1.43	1.00	1.43	8.0	−194.4	a
^{13}CCH	200	20	9.93×10^{13}	0.99	1.00	0.99	15.0	3.0	e
	20	2.7	1.01×10^{14}	1.19	1.00	1.19	8.0	0.0	a
	20	2.7	1.19×10^{13}	1.19	1.00	1.19	6.0	19.0	a
	120	2.7	5.34×10^{11}	1.19	1.00	1.19	5.0	−29.5	a
	120	2.7	1.04×10^{12}	1.19	1.00	1.19	5.0	−33.5	a
	120	2.7	1.04×10^{12}	1.19	1.00	1.19	5.0	−38.0	a
	120	2.7	7.91×10^{11}	1.19	1.00	1.19	5.0	−43.0	a
	120	2.7	1.39×10^{12}	1.19	1.00	1.19	5.0	−47.5	a
	120	2.7	6.52×10^{11}	1.19	1.00	1.19	4.5	−51.5	a
	120	2.7	5.04×10^{12}	1.19	1.00	1.19	5.0	−55.5	a
	120	2.7	3.85×10^{12}	1.19	1.00	1.19	4.5	−60.5	a
	120	2.7	2.67×10^{12}	1.19	1.00	1.19	4.5	−64.0	a
	120	2.7	2.96×10^{12}	1.19	1.00	1.19	5.0	−67.2	a
	120	2.7	2.96×10^{11}	1.19	1.00	1.19	4.0	−79.0	a
	120	2.7	4.74×10^{11}	1.19	1.00	1.19	3.0	−82.5	a
	120	2.7	9.19×10^{11}	1.19	1.00	1.19	4.0	−85.5	a
	120	2.7	1.19×10^{12}	1.19	1.00	1.19	4.0	−90.5	a
	120	2.7	5.93×10^{11}	1.19	1.00	1.19	3.5	−94.8	a
	120	2.7	3.85×10^{11}	1.19	1.00	1.19	4.0	−99.5	a
	120	2.7	2.08×10^{12}	1.19	1.00	1.19	4.7	−104.5	a
	120	2.7	5.34×10^{11}	1.19	1.00	1.19	3.0	−110.0	a
	120	2.7	7.41×10^{11}	1.19	1.00	1.19	4.5	−113.0	a
	120	2.7	3.56×10^{11}	1.19	1.00	1.19	4.5	−117.0	a
	120	2.7	8.89×10^{11}	1.19	1.00	1.19	3.0	−121.0	a
	120	2.7	2.96×10^{11}	1.19	1.00	1.19	4.0	−125.0	a
	120	2.7	5.93×10^{11}	1.19	1.00	1.19	5.0	−131.2	a
	120	2.7	5.34×10^{11}	1.19	1.00	1.19	4.0	−134.0	a
	120	2.7	2.67×10^{12}	1.19	1.00	1.19	4.5	−138.5	a
	120	2.7	1.66×10^{12}	1.19	1.00	1.19	5.0	−144.1	a
	120	2.7	4.15×10^{11}	1.19	1.00	1.19	6.0	−151.0	a
	120	2.7	2.37×10^{12}	1.19	1.00	1.19	5.0	−157.0	a
	120	2.7	4.15×10^{11}	1.19	1.00	1.19	3.0	−161.7	a
	120	2.7	1.36×10^{12}	1.19	1.00	1.19	5.0	−166.0	a
	120	2.7	3.44×10^{12}	1.19	1.00	1.19	4.0	−170.0	a
	120	2.7	2.37×10^{11}	1.19	1.00	1.19	8.0	−175.0	a
	120	2.7	1.19×10^{11}	1.19	1.00	1.19	4.0	−180.5	a
	120	2.7	3.56×10^{11}	1.19	1.00	1.19	4.0	−184.0	a
	120	2.7	1.78×10^{11}	1.19	1.00	1.19	4.0	−187.1	a
	120	2.7	1.78×10^{11}	1.19	1.00	1.19	8.0	−194.4	a

Table 13. continued.

Molecule[a]	Size[b] (″)	T_{rot}[c] (K)	N[d] (cm^{-2})	C_{int}[e]	C_{vib}[f]	C_N[g]	ΔV[h] (km s^{-1})	V_{off}[i]	F[j]
(1)	(2)	(3)	(4)	(5)	(6)	(7)	(8)	(9)	(10)
C^{13}CH	200	20	9.92×10^{13}	0.99	1.00	0.99	15.0	3.0	e
	20	2.7	1.02×10^{14}	1.20	1.00	1.20	8.0	0.0	a
	20	2.7	1.20×10^{13}	1.20	1.00	1.20	6.0	19.0	a
	120	2.7	5.39×10^{11}	1.20	1.00	1.20	5.0	−29.5	a
	120	2.7	1.05×10^{12}	1.20	1.00	1.20	5.0	−33.5	a
	120	2.7	1.05×10^{12}	1.20	1.00	1.20	5.0	−38.0	a
	120	2.7	7.98×10^{11}	1.20	1.00	1.20	5.0	−43.0	a
	120	2.7	1.40×10^{12}	1.20	1.00	1.20	5.0	−47.5	a
	120	2.7	6.58×10^{11}	1.20	1.00	1.20	4.5	−51.5	a
	120	2.7	5.09×10^{12}	1.20	1.00	1.20	5.0	−55.5	a
	120	2.7	3.89×10^{12}	1.20	1.00	1.20	4.5	−60.5	a
	120	2.7	2.69×10^{12}	1.20	1.00	1.20	4.5	−64.0	a
	120	2.7	2.99×10^{12}	1.20	1.00	1.20	5.0	−67.2	a
	120	2.7	2.99×10^{11}	1.20	1.00	1.20	4.0	−79.0	a
	120	2.7	4.79×10^{11}	1.20	1.00	1.20	3.0	−82.5	a
	120	2.7	9.28×10^{11}	1.20	1.00	1.20	4.0	−85.5	a
	120	2.7	1.20×10^{12}	1.20	1.00	1.20	4.0	−90.5	a
	120	2.7	5.99×10^{11}	1.20	1.00	1.20	3.5	−94.8	a
	120	2.7	3.89×10^{11}	1.20	1.00	1.20	4.0	−99.5	a
	120	2.7	2.09×10^{12}	1.20	1.00	1.20	4.7	−104.5	a
	120	2.7	5.39×10^{11}	1.20	1.00	1.20	3.0	−110.0	a
	120	2.7	7.48×10^{11}	1.20	1.00	1.20	4.5	−113.0	a
	120	2.7	3.59×10^{11}	1.20	1.00	1.20	4.5	−117.0	a
	120	2.7	8.98×10^{11}	1.20	1.00	1.20	3.0	−121.0	a
	120	2.7	2.99×10^{11}	1.20	1.00	1.20	4.0	−125.0	a
	120	2.7	5.99×10^{11}	1.20	1.00	1.20	5.0	−131.2	a
	120	2.7	5.39×10^{11}	1.20	1.00	1.20	4.0	−134.0	a
	120	2.7	2.69×10^{12}	1.20	1.00	1.20	4.5	−138.5	a
	120	2.7	1.68×10^{12}	1.20	1.00	1.20	5.0	−144.1	a
	120	2.7	4.19×10^{11}	1.20	1.00	1.20	6.0	−151.0	a
	120	2.7	2.39×10^{12}	1.20	1.00	1.20	5.0	−157.0	a
	120	2.7	4.19×10^{11}	1.20	1.00	1.20	3.0	−161.7	a
	120	2.7	1.38×10^{12}	1.20	1.00	1.20	5.0	−166.0	a
	120	2.7	3.47×10^{12}	1.20	1.00	1.20	4.0	−170.0	a
	120	2.7	2.39×10^{11}	1.20	1.00	1.20	8.0	−175.0	a
	120	2.7	1.20×10^{11}	1.20	1.00	1.20	4.0	−180.5	a
	120	2.7	3.59×10^{11}	1.20	1.00	1.20	4.0	−184.0	a
	120	2.7	1.80×10^{11}	1.20	1.00	1.20	4.0	−187.1	a
	120	2.7	1.80×10^{11}	1.20	1.00	1.20	8.0	−194.4	a

Table 14. Parameters of our best-fit model of CCS toward Sgr B2(N).

Molecule[a]	Size[b] (″)	T_{rot}[c] (K)	N[d] (cm^{-2})	C_{int}[e]	C_{vib}[f]	C_N[g]	ΔV[h] (km s^{-1})	V_{off}[i]	F[j]
(1)	(2)	(3)	(4)	(5)	(6)	(7)	(8)	(9)	(10)
CCS	60	20	8.29×10^{13}	1.04	1.00	1.04	13.0	1.0	e

Notes. See notes of Table 6.

Table 15. Parameters of our best-fit model of CH$_2$NH toward Sgr B2(N).

Molecule[a]	Size[b] (″)	T_{rot}[c] (K)	N[d] (cm^{-2})	C_{int}[e]	C_{vib}[f]	C_N[g]	ΔV[h] (km s^{-1})	V_{off}[i]	F[j]
(1)	(2)	(3)	(4)	(5)	(6)	(7)	(8)	(9)	(10)
CH$_2$NH	2.0	200	8.02×10^{17}	1.00	1.00	1.00	7.0	−1.0	e
	2.0	200	3.01×10^{17}	1.00	1.00	1.00	7.0	9.0	e

Notes. See notes of Table 6.

Table 16. Parameters of our best-fit model of aGg'-$(CH_2OH)_2$ toward Sgr B2(N).

Molecule[a]	Size[b] (″)	T_{rot}[c] (K)	N[d] (cm^{-2})	C_{int}[e]	C_{vib}[f]	C_N[g]	ΔV[h] (km s^{-1})	V_{off}[i]	F[j]
(1)	(2)	(3)	(4)	(5)	(6)	(7)	(8)	(9)	(10)
aGg'-$(CH_2OH)_2$	10	50	2.30×10^{15}	1.00	1.00	1.00	6.0	-1.0	e

Notes. See notes of Table 6.

Table 17. Parameters of our best-fit model of $CH_2(OH)CHO$ toward Sgr B2(N).

Molecule[a]	Size[b] (″)	T_{rot}[c] (K)	N[d] (cm^{-2})	C_{int}[e]	C_{vib}[f]	C_N[g]	ΔV[h] (km s^{-1})	V_{off}[i]	F[j]
(1)	(2)	(3)	(4)	(5)	(6)	(7)	(8)	(9)	(10)
$CH_2(OH)CHO$	10	80	1.80×10^{15}	1.00	1.00	1.00	6.0	-1.0	e

Notes. See notes of Table 6.

Table 18. Parameters of our best-fit model of CH_3C_3N toward Sgr B2(N).

Molecule[a]	Size[b] (″)	T_{rot}[c] (K)	N[d] (cm^{-2})	C_{int}[e]	C_{vib}[f]	C_N[g]	ΔV[h] (km s^{-1})	V_{off}[i]	F[j]
(1)	(2)	(3)	(4)	(5)	(6)	(7)	(8)	(9)	(10)
CH_3C_3N	3.0	100	1.09×10^{15}	0.99	1.00	0.99	7.0	0.0	e
	3.0	100	5.54×10^{14}	0.99	1.00	0.99	7.0	10.0	e

Notes. See notes of Table 6.

Table 19. Parameters of our best-fit model of CH_3CCH toward Sgr B2(N).

Molecule[a]	Size[b] (″)	T_{rot}[c] (K)	N[d] (cm^{-2})	C_{int}[e]	C_{vib}[f]	C_N[g]	ΔV[h] (km s^{-1})	V_{off}[i]	F[j]
(1)	(2)	(3)	(4)	(5)	(6)	(7)	(8)	(9)	(10)
CH_3CCH	10	75	3.84×10^{16}	0.85	1.00	0.85	7.0	0.0	e
	10	75	2.39×10^{16}	0.85	1.00	0.85	7.0	8.5	e
$CH_3C^{13}CH$	10	75	2.21×10^{15}	0.98	1.00	0.98	7.0	0.0	e
$CH_3^{13}CCH$	10	75	2.21×10^{15}	0.98	1.00	0.98	7.0	0.0	e
$^{13}CH_3CCH$	10	75	2.21×10^{15}	0.98	1.00	0.98	7.0	0.0	e

Notes. See notes of Table 6.

Table 20. Parameters of our best-fit model of $CH_3C(O)CH_3$ toward Sgr B2(N).

Molecule[a]	Size[b] (″)	T_{rot}[c] (K)	N[d] (cm^{-2})	C_{int}[e]	C_{vib}[f]	C_N[g]	ΔV[h] (km s^{-1})	V_{off}[i]	F[j]
(1)	(2)	(3)	(4)	(5)	(6)	(7)	(8)	(9)	(10)
$CH_3C(O)CH_3$	3.0	100	1.49×10^{17}	0.50	1.00	0.50	7.0	0.0	e
	3.0	100	3.73×10^{16}	0.50	1.00	0.50	7.0	10.0	e
$CH_3C(O)CH_3$, $v_{12}=1$	3.0	100	1.79×10^{17}	0.50	1.00	0.50	7.0	0.0	e
	3.0	100	4.47×10^{16}	0.50	1.00	0.50	7.0	10.0	e

Notes. See notes of Table 6.

Table 21. Parameters of our best-fit model of CH_3CHO toward Sgr B2(N).

Molecule[a]	Size[b] ('')	T_{rot}[c] (K)	N[d] (cm^{-2})	C_{int}[e]	C_{vib}[f]	C_N[g]	ΔV[h]	V_{off}[i]	F[j]
(1)	(2)	(3)	(4)	(5)	(6)	(7)	(8)	(9)	(10)
							(km s^{-1})		
CH_3CHO	3.0	100	1.43×10^{17}	0.89	1.00	0.89	8.0	−1.0	e
	3.0	100	8.04×10^{16}	0.89	1.00	0.89	8.0	9.0	e
$CH_3CHO, v_t = 1$	3.0	100	2.86×10^{17}	0.89	1.00	0.89	8.0	−1.0	e
	3.0	100	1.61×10^{17}	0.89	1.00	0.89	8.0	9.0	e

Notes. See notes of Table 6.

Table 22. Parameters of our best-fit model of CH_3CN toward Sgr B2(N).

Molecule[a]	Size[b] ('')	T_{rot}[c] (K)	N[d] (cm^{-2})	C_{int}[e]	C_{vib}[f]	C_N[g]	ΔV[h] (km s^{-1})	V_{off}[i]	F[j]
(1)	(2)	(3)	(4)	(5)	(6)	(7)	(8)	(9)	(10)
CH_3CN	2.7	200	1.97×10^{18}	0.98	1.00	0.98	6.5	−1.0	e
	2.7	200	7.87×10^{17}	0.98	1.00	0.98	6.5	9.0	e
	2.7	200	9.84×10^{16}	0.98	1.00	0.98	8.0	−11.0	e
$CH_3CN, v_8 = 1$	2.2	200	4.98×10^{18}	1.00	1.00	1.00	6.5	−1.0	e
	1.4	200	3.98×10^{18}	1.00	1.00	1.00	6.5	9.0	e
	1.8	200	3.49×10^{17}	1.00	1.00	1.00	8.0	−10.0	e
$CH_3CN, v_8 = 2$	2.2	200	1.10×10^{19}	1.00	1.00	1.00	6.5	−1.0	e
	1.4	200	8.96×10^{18}	1.00	1.00	1.00	6.5	9.0	e
$CH_3CN, v_4 = 1$	2.2	200	2.49×10^{19}	1.00	1.00	1.00	6.5	−1.0	e
	1.4	200	1.99×10^{19}	1.00	1.00	1.00	6.5	9.0	e
$^{13}CH_3CN$	2.7	200	1.16×10^{17}	1.01	1.15	1.16	6.5	−1.0	e
	2.7	200	4.65×10^{16}	1.01	1.15	1.16	6.5	9.0	e
	2.7	200	5.82×10^{15}	1.01	1.15	1.16	8.0	−11.0	e
$CH_3^{13}CN$	2.7	200	1.16×10^{17}	1.01	1.15	1.16	6.5	−1.0	e
	2.7	200	4.65×10^{16}	1.01	1.15	1.16	6.5	9.0	e
	2.7	200	5.82×10^{15}	1.01	1.15	1.16	8.0	−11.0	e
$^{13}CH_3CN, v_8 = 1$	2.2	200	3.61×10^{17}	1.01	1.15	1.16	6.5	−1.0	e
	1.4	200	2.91×10^{17}	1.01	1.15	1.16	6.5	9.0	e
$CH_3^{13}CN, v_8 = 1$	2.2	200	3.61×10^{17}	1.01	1.15	1.16	6.5	−1.0	e
	1.4	200	2.91×10^{17}	1.01	1.15	1.16	6.5	9.0	e
$^{13}CH_3^{13}CN$	2.7	200	5.82×10^{15}	1.01	1.15	1.16	6.5	−1.0	e
	2.7	200	2.33×10^{15}	1.01	1.15	1.16	6.5	9.0	e
	2.7	200	2.91×10^{14}	1.01	1.15	1.16	8.0	−11.0	e
$CH_3C^{15}N$	2.7	200	7.76×10^{15}	1.01	1.15	1.16	6.5	−1.0	e
	2.7	200	3.11×10^{15}	1.01	1.15	1.16	6.5	9.0	e
	2.7	200	3.87×10^{14}	1.01	1.15	1.16	8.0	−11.0	e

Notes. See notes of Table 6.

Table 23. Parameters of our best-fit model of $CH_3C(O)NH_2$-A toward Sgr B2(N).

Molecule[a]	Size[b] ('')	T_{rot}[c] (K)	N[d] (cm^{-2})	C_{int}[e]	C_{vib}[f]	C_N[g]	ΔV[h] (km s^{-1})	V_{off}[i]	F[j]
(1)	(2)	(3)	(4)	(5)	(6)	(7)	(8)	(9)	(10)
$CH_3C(O)NH_2$-A	2.4	170	8.10×10^{16}	1.01	1.00	1.01	7.0	0.0	e
$CH_3C(O)NH_2$-E	2.4	170	5.99×10^{16}	1.00	1.00	1.00	7.0	0.0	e
$CH_3C(O)NH_2$-A, v=1	2.4	170	8.10×10^{16}	1.01	1.00	1.01	7.0	0.0	e
$CH_3C(O)NH_2$-E, v=1	2.4	170	5.99×10^{16}	1.00	1.00	1.00	7.0	0.0	e
$CH_3C(O)NH_2$-A, v=2	2.4	170	8.10×10^{16}	1.01	1.00	1.01	7.0	0.0	e
$CH_3C(O)NH_2$-E, v=2	2.4	170	5.99×10^{16}	1.00	1.00	1.00	7.0	0.0	e

Notes. See notes of Table 6.

Table 24. Parameters of our best-fit model of CH_3COOH toward Sgr B2(N).

Molecule[a]	Size[b] (″)	T_{rot}[c] (K)	N[d] (cm^{-2})	C_{int}[e]	C_{vib}[f]	C_N[g]	ΔV[h] (km s^{-1})	V_{off}[i]	F[j]
(1)	(2)	(3)	(4)	(5)	(6)	(7)	(8)	(9)	(10)
CH_3COOH	4.0	100	1.05×10^{16}	0.88	1.00	0.88	7.0	−1.0	e
	4.0	100	3.59×10^{15}	0.88	1.00	0.88	7.0	8.0	e

Notes. See notes of Table 6.

Table 25. Parameters of our best-fit model of CH_3NH_2 toward Sgr B2(N).

Molecule[a]	Size[b] (″)	T_{rot}[c] (K)	N[d] (cm^{-2})	C_{int}[e]	C_{vib}[f]	C_N[g]	ΔV[h] (km s^{-1})	V_{off}[i]	F[j]
(1)	(2)	(3)	(4)	(5)	(6)	(7)	(8)	(9)	(10)
CH_3NH_2	3.0	100	6.00×10^{17}	1.00	1.00	1.00	9.0	0.0	e
	3.0	100	1.70×10^{17}	1.00	1.00	1.00	9.0	10.0	e
	120	2.7	1.01×10^{14}	1.01	1.00	1.01	9.0	17.0	a
	120	2.7	3.54×10^{14}	1.01	1.00	1.01	12.0	0.0	a

Notes. See notes of Table 6.

Table 26. Parameters of our best-fit model of CH_3OCH_3 toward Sgr B2(N).

Molecule[a]	Size[b] (″)	T_{rot}[c] (K)	N[d] (cm^{-2})	C_{int}[e]	C_{vib}[f]	C_N[g]	ΔV[h] (km s^{-1})	V_{off}[i]	F[j]
(1)	(2)	(3)	(4)	(5)	(6)	(7)	(8)	(9)	(10)
CH_3OCH_3	2.5	130	1.96×10^{18}	0.85	1.00	0.85	6.0	0.0	e
	2.5	130	9.37×10^{17}	0.85	1.00	0.85	6.0	10.0	e
$CH_3OCH_3, v_{11} = 1$	2.5	130	1.96×10^{18}	0.85	1.00	0.85	6.0	0.0	e
	2.5	130	9.37×10^{17}	0.85	1.00	0.85	6.0	10.0	e
$CH_3OCH_3, v_{15} = 1$	2.5	130	1.96×10^{18}	0.85	1.00	0.85	6.0	0.0	e
	2.5	130	9.37×10^{17}	0.85	1.00	0.85	6.0	10.0	e
$CH_3O^{13}CH_3$	2.5	130	9.83×10^{16}	0.85	1.00	0.85	6.0	0.0	e
	2.5	130	4.70×10^{16}	0.85	1.00	0.85	6.0	10.0	e

Notes. See notes of Table 6.

Table 27. Parameters of our best-fit model of CH_3OCHO toward Sgr B2(N).

Molecule[a]	Size[b] (″)	T_{rot}[c] (K)	N[d] (cm^{-2})	C_{int}[e]	C_{vib}[f]	C_N[g]	ΔV[h] (km s^{-1})	V_{off}[i]	F[j]
(1)	(2)	(3)	(4)	(5)	(6)	(7)	(8)	(9)	(10)
CH_3OCHO	4.0	80	4.37×10^{17}	0.91	1.00	0.91	7.0	−0.5	e
	4.0	80	1.46×10^{17}	0.91	1.00	0.91	7.0	9.5	e
$CH_3OCHO, v_t = 1$	4.0	80	1.00×10^{18}	0.91	1.00	0.91	7.0	−0.5	e
	4.0	80	3.37×10^{17}	0.91	1.00	0.91	7.0	9.5	e

Notes. See notes of Table 6.

Table 28. Parameters of our best-fit model of CH_3OH toward Sgr B2(N).

Molecule[a]	Size[b] (″)	T_{rot}[c] (K)	N[d] (cm^{-2})	C_{int}[e]	C_{vib}[f]	C_N[g]	ΔV[h] (km s^{-1})	V_{off}[i]	F[j]
(1)	(2)	(3)	(4)	(5)	(6)	(7)	(8)	(9)	(10)
CH_3OH	3.0	200	1.76×10^{19}	0.98	1.00	0.98	7.0	−0.5	e
	3.0	200	4.39×10^{18}	0.98	1.00	0.98	7.0	9.5	e
	60	15	1.94×10^{16}	1.02	1.00	1.02	16.0	4.0	e
	60	4.5	1.82×10^{15}	0.96	1.00	0.96	18.0	2.0	a
	120	2.7	4.57×10^{12}	0.93	1.00	0.93	3.5	−163.7	a
	120	2.7	6.06×10^{12}	0.93	1.00	0.93	3.0	−169.6	a
CH_3OH, $v_t = 1$	2.5	200	1.76×10^{19}	0.98	1.00	0.98	7.0	−0.5	e
	2.5	200	4.39×10^{18}	0.98	1.00	0.98	7.0	9.5	e
CH_3OH, $v_t = 2$	2.5	200	1.76×10^{19}	0.98	1.00	0.98	7.0	−0.5	e
	2.5	200	4.39×10^{18}	0.98	1.00	0.98	7.0	9.5	e
$^{13}CH_3OH$	3.0	200	7.00×10^{17}	1.00	1.00	1.00	7.0	−0.5	e
	3.0	200	1.80×10^{17}	1.00	1.00	1.00	7.0	9.5	e
	60	15	1.50×10^{15}	1.00	1.00	1.00	16.0	4.0	e
	60	4.5	2.00×10^{14}	1.00	1.00	1.00	18.0	2.0	a
$^{13}CH_3OH$, $v_t = 1$	2.5	200	7.00×10^{17}	1.00	1.00	1.00	7.0	−0.5	e
	2.5	200	1.80×10^{17}	1.00	1.00	1.00	7.0	9.5	e
$CH_3^{18}OH$	3.0	200	5.60×10^{16}	1.00	1.00	1.00	7.0	−0.5	e
	3.0	200	1.44×10^{16}	1.00	1.00	1.00	7.0	9.5	e
	60	15	1.20×10^{14}	1.00	1.00	1.00	16.0	4.0	e

Notes. See notes of Table 6.

Table 29. Parameters of our best-fit model of CH_3SH toward Sgr B2(N).

Molecule[a]	Size[b] (″)	T_{rot}[c] (K)	N[d] (cm^{-2})	C_{int}[e]	C_{vib}[f]	C_N[g]	ΔV[h] (km s^{-1})	V_{off}[i]	F[j]
(1)	(2)	(3)	(4)	(5)	(6)	(7)	(8)	(9)	(10)
CH_3SH	5.0	60	2.94×10^{16}	0.91	1.00	0.91	8.0	−1.2	e
	5.0	60	2.04×10^{16}	0.91	1.00	0.91	8.0	9.0	e

Notes. See notes of Table 6.

Table 30. Parameters of our best-fit model of CN toward Sgr B2(N).

Molecule[a]	Size[b] (″)	T_{rot}[c] (K)	N[d] (cm^{-2})	C_{int}[e]	C_{vib}[f]	C_N[g]	ΔV[h] (km s^{-1})	V_{off}[i]	F[j]
(1)	(2)	(3)	(4)	(5)	(6)	(7)	(8)	(9)	(10)
CN	200	20	6.93×10^{14}	0.99	1.00	0.99	32.0	5.0	e
	120	3.5	1.40×10^{15}	1.21	1.00	1.21	9.0	17.0	a
	120	3.5	4.34×10^{14}	1.21	1.00	1.21	5.0	8.8	a
	120	3.5	5.30×10^{15}	1.21	1.00	1.21	9.0	0.0	a
	120	2.7	3.20×10^{13}	1.28	1.00	1.28	3.0	−27.0	a
	120	2.7	4.48×10^{13}	1.28	1.00	1.28	3.0	−31.0	a
	120	2.7	7.67×10^{13}	1.28	1.00	1.28	4.5	−36.0	a
	120	2.7	2.81×10^{13}	1.28	1.00	1.28	3.5	−40.0	a
	120	2.7	1.09×10^{14}	1.28	1.00	1.28	3.0	−46.7	a
	120	2.7	1.53×10^{14}	1.28	1.00	1.28	2.8	−50.3	a
	120	2.7	2.30×10^{14}	1.28	1.00	1.28	3.8	−54.0	a
	120	2.7	1.79×10^{14}	1.28	1.00	1.28	4.0	−58.0	a
	120	2.7	2.94×10^{14}	1.28	1.00	1.28	6.0	−63.0	a
	120	2.7	7.67×10^{12}	1.28	1.00	1.28	2.5	−73.2	a
	120	2.7	3.07×10^{13}	1.28	1.00	1.28	3.5	−79.1	a
	120	2.7	7.03×10^{13}	1.28	1.00	1.28	2.5	−83.7	a
	120	2.7	3.84×10^{13}	1.28	1.00	1.28	4.0	−86.5	a
	120	2.7	7.03×10^{13}	1.28	1.00	1.28	2.7	−89.5	a
	120	2.7	5.76×10^{13}	1.28	1.00	1.28	2.5	−92.7	a
	120	2.7	1.28×10^{13}	1.28	1.00	1.28	4.0	−97.5	a

Notes. See notes of Table 6.

Table 30. continued.

Molecule[a]	Size[b] ('')	T_{rot}[c] (K)	N[d] (cm^{-2})	C_{int}[e]	C_{vib}[f]	C_N[g]	ΔV[h]	V_{off}[i] (km s^{-1})	F[j]
(1)	(2)	(3)	(4)	(5)	(6)	(7)	(8)	(9)	(10)
	120	2.7	1.92×10^{14}	1.28	1.00	1.28	3.0	−104.1	a
	120	2.7	3.84×10^{13}	1.28	1.00	1.28	3.0	−107.2	a
	120	2.7	6.39×10^{13}	1.28	1.00	1.28	3.0	−110.3	a
	120	2.7	3.07×10^{13}	1.28	1.00	1.28	3.0	−115.5	a
	120	2.7	1.02×10^{13}	1.28	1.00	1.28	1.6	−122.2	a
	120	2.7	1.28×10^{12}	1.28	1.00	1.28	3.0	−127.0	a
	120	2.7	1.92×10^{13}	1.28	1.00	1.28	3.5	−134.0	a
	120	2.7	1.09×10^{14}	1.28	1.00	1.28	3.0	−137.5	a
	120	2.7	6.39×10^{13}	1.28	1.00	1.28	4.5	−140.5	a
	120	2.7	9.85×10^{13}	1.28	1.00	1.28	3.4	−144.6	a
	120	2.7	1.53×10^{13}	1.28	1.00	1.28	4.0	−148.3	a
	120	2.7	2.81×10^{13}	1.28	1.00	1.28	6.0	−152.5	a
	120	2.7	7.03×10^{13}	1.28	1.00	1.28	3.0	−157.0	a
	120	2.7	2.05×10^{13}	1.28	1.00	1.28	3.0	−160.5	a
	120	2.7	3.84×10^{13}	1.28	1.00	1.28	4.0	−166.0	a
	120	2.7	3.45×10^{14}	1.28	1.00	1.28	4.0	−169.5	a
	120	2.7	1.92×10^{13}	1.28	1.00	1.28	3.4	−174.7	a
	120	2.7	8.95×10^{12}	1.28	1.00	1.28	4.0	−179.5	a
^{13}CN	200	20	3.46×10^{13}	0.99	1.00	0.99	32.0	5.0	e
	120	2.7	7.30×10^{13}	1.26	1.00	1.26	9.0	17.0	a
	120	2.7	2.27×10^{13}	1.26	1.00	1.26	5.0	8.8	a
	120	2.7	2.77×10^{14}	1.26	1.00	1.26	9.0	0.0	a
	120	2.7	7.87×10^{11}	1.26	1.00	1.26	3.0	−27.0	a
	120	2.7	1.10×10^{12}	1.26	1.00	1.26	3.0	−31.0	a
	120	2.7	1.89×10^{12}	1.26	1.00	1.26	4.5	−36.0	a
	120	2.7	6.92×10^{11}	1.26	1.00	1.26	3.5	−40.0	a
	120	2.7	1.79×10^{12}	1.26	1.00	1.26	3.0	−46.7	a
	120	2.7	2.52×10^{12}	1.26	1.00	1.26	2.8	−50.3	a
	120	2.7	1.13×10^{13}	1.26	1.00	1.26	3.8	−54.0	a
	120	2.7	8.81×10^{12}	1.26	1.00	1.26	4.0	−58.0	a
	120	2.7	1.45×10^{13}	1.26	1.00	1.26	6.0	−63.0	a
	120	2.7	3.78×10^{11}	1.26	1.00	1.26	2.5	−73.2	a
	120	2.7	7.55×10^{11}	1.26	1.00	1.26	3.5	−79.1	a
	120	2.7	1.74×10^{12}	1.26	1.00	1.26	2.5	−83.7	a
	120	2.7	9.44×10^{11}	1.26	1.00	1.26	4.0	−86.5	a
	120	2.7	1.74×10^{12}	1.26	1.00	1.26	2.7	−89.5	a
	120	2.7	1.42×10^{12}	1.26	1.00	1.26	2.5	−92.7	a
	120	2.7	3.15×10^{11}	1.26	1.00	1.26	4.0	−97.5	a
	120	2.7	4.72×10^{12}	1.26	1.00	1.26	3.0	−104.1	a
	120	2.7	9.44×10^{11}	1.26	1.00	1.26	3.0	−107.2	a
	120	2.7	1.57×10^{12}	1.26	1.00	1.26	3.0	−110.3	a
	120	2.7	7.55×10^{11}	1.26	1.00	1.26	3.0	−115.5	a
	120	2.7	5.04×10^{11}	1.26	1.00	1.26	1.6	−122.2	a
	120	2.7	6.29×10^{10}	1.26	1.00	1.26	3.0	−127.0	a
	120	2.7	9.44×10^{11}	1.26	1.00	1.26	3.5	−134.0	a
	120	2.7	5.35×10^{12}	1.26	1.00	1.26	3.0	−137.5	a
	120	2.7	3.15×10^{12}	1.26	1.00	1.26	4.5	−140.5	a
	120	2.7	4.85×10^{12}	1.26	1.00	1.26	3.4	−144.6	a
	120	2.7	7.55×10^{11}	1.26	1.00	1.26	4.0	−148.3	a
	120	2.7	1.38×10^{12}	1.26	1.00	1.26	6.0	−152.5	a
	120	2.7	3.46×10^{12}	1.26	1.00	1.26	3.0	−157.0	a
	120	2.7	1.01×10^{12}	1.26	1.00	1.26	3.0	−160.5	a
	120	2.7	1.89×10^{12}	1.26	1.00	1.26	4.0	−166.0	a
	120	2.7	1.70×10^{13}	1.26	1.00	1.26	4.0	−169.5	a
	120	2.7	9.44×10^{11}	1.26	1.00	1.26	3.4	−174.7	a
	120	2.7	4.41×10^{11}	1.26	1.00	1.26	4.0	−179.5	a
C^{15}N	200	20	2.31×10^{12}	0.99	1.00	0.99	32.0	5.0	e
	120	2.7	4.91×10^{12}	1.27	1.00	1.27	9.0	17.0	a
	120	2.7	1.52×10^{12}	1.27	1.00	1.27	5.0	8.8	a
	120	2.7	1.87×10^{13}	1.27	1.00	1.27	9.0	0.0	a

Table 31. Parameters of our best-fit model of CO toward Sgr B2(N).

Molecule[a]	Size[b] ($''$)	T_{rot}[c] (K)	N[d] (cm^{-2})	C_{int}[e]	C_{vib}[f]	C_N[g]	ΔV[h] (km s^{-1})	V_{off}[i] (km s^{-1})	F[j]
(1)	(2)	(3)	(4)	(5)	(6)	(7)	(8)	(9)	(10)
CO	200	48	6.15×10^{19}	0.98	1.00	0.98	18.0	6.5	e
	20	20	7.92×10^{18}	0.99	1.00	0.99	20.0	23.0	e
	20	18	1.98×10^{18}	0.99	1.00	0.99	20.0	−23.0	e
	200	10	1.12×10^{17}	1.02	1.00	1.02	18.0	1.5	a
	200	2.7	4.63×10^{16}	1.29	1.00	1.29	2.0	−72.7	a
	200	2.7	2.57×10^{16}	1.29	1.00	1.29	2.0	−82.0	a
	200	2.7	4.37×10^{16}	1.29	1.00	1.29	2.0	−84.2	a
	200	2.7	2.31×10^{17}	1.29	1.00	1.29	2.0	−89.9	a
	200	2.7	2.06×10^{16}	1.29	1.00	1.29	2.0	−92.8	a
	200	2.7	2.11×10^{17}	1.29	1.00	1.29	2.4	−102.6	a
	200	2.7	2.02×10^{17}	1.29	1.00	1.29	2.4	−105.3	a
	200	2.7	2.57×10^{16}	1.29	1.00	1.29	2.5	−107.5	a
	200	2.7	3.09×10^{16}	1.29	1.00	1.29	2.0	−112.8	a
	200	2.7	4.63×10^{15}	1.29	1.00	1.29	2.1	−137.0	a
	200	2.7	1.41×10^{16}	1.29	1.00	1.29	2.4	−138.8	a
	200	2.7	6.69×10^{15}	1.29	1.00	1.29	2.0	−144.0	a
	200	2.7	6.17×10^{15}	1.29	1.00	1.29	2.0	−157.0	a
	200	2.7	9.00×10^{15}	1.29	1.00	1.29	2.5	−169.0	a
^{13}CO	200	48	3.08×10^{18}	0.98	1.00	0.98	18.0	5.0	e
	20	20	3.96×10^{17}	0.99	1.00	0.99	20.0	23.0	e
	20	18	9.93×10^{16}	0.99	1.00	0.99	20.0	−23.0	e
	200	7.0	8.45×10^{16}	1.06	1.00	1.06	16.0	1.5	a
	200	2.7	2.29×10^{15}	1.27	1.00	1.27	2.0	−72.7	a
	200	2.7	6.35×10^{14}	1.27	1.00	1.27	2.0	−82.0	a
	200	2.7	1.08×10^{15}	1.27	1.00	1.27	2.0	−84.2	a
	200	2.7	5.71×10^{15}	1.27	1.00	1.27	2.0	−89.9	a
	200	2.7	5.08×10^{14}	1.27	1.00	1.27	2.0	−92.8	a
	200	2.7	5.21×10^{15}	1.27	1.00	1.27	2.4	−102.6	a
	200	2.7	4.98×10^{15}	1.27	1.00	1.27	2.4	−105.3	a
	200	2.7	6.35×10^{14}	1.27	1.00	1.27	2.5	−107.5	a
	200	2.7	7.62×10^{14}	1.27	1.00	1.27	2.0	−112.8	a
	200	2.7	2.29×10^{14}	1.27	1.00	1.27	2.1	−137.0	a
	200	2.7	6.99×10^{14}	1.27	1.00	1.27	2.4	−138.8	a
	200	2.7	3.30×10^{14}	1.27	1.00	1.27	2.0	−144.0	a
	200	2.7	3.05×10^{14}	1.27	1.00	1.27	2.0	−157.0	a
	200	2.7	4.45×10^{14}	1.27	1.00	1.27	2.5	−169.0	a
C^{18}O	200	48	2.46×10^{17}	0.98	1.00	0.98	18.0	5.0	e
	20	20	3.17×10^{16}	0.99	1.00	0.99	20.0	23.0	e
	20	18	7.94×10^{15}	0.99	1.00	0.99	20.0	−23.0	e
	200	7.0	6.76×10^{15}	1.06	1.00	1.06	16.0	1.5	a
	200	2.7	1.83×10^{14}	1.27	1.00	1.27	2.0	−72.7	a
	200	2.7	7.77×10^{13}	1.27	1.00	1.27	2.0	−82.0	a
	200	2.7	1.32×10^{14}	1.27	1.00	1.27	2.0	−84.2	a
	200	2.7	6.98×10^{14}	1.27	1.00	1.27	2.0	−89.9	a
	200	2.7	6.21×10^{13}	1.27	1.00	1.27	2.0	−92.8	a
	200	2.7	6.37×10^{14}	1.27	1.00	1.27	2.4	−102.6	a
	200	2.7	6.09×10^{14}	1.27	1.00	1.27	2.4	−105.3	a
	200	2.7	7.77×10^{13}	1.27	1.00	1.27	2.5	−107.5	a
	200	2.7	9.30×10^{13}	1.27	1.00	1.27	2.0	−112.8	a
	200	2.7	1.83×10^{13}	1.27	1.00	1.27	2.1	−137.0	a
	200	2.7	5.58×10^{13}	1.27	1.00	1.27	2.4	−138.8	a
	200	2.7	2.64×10^{13}	1.27	1.00	1.27	2.0	−144.0	a
	200	2.7	2.44×10^{13}	1.27	1.00	1.27	2.0	−157.0	a
	200	2.7	3.55×10^{13}	1.27	1.00	1.27	2.5	−169.0	a

Notes. See notes of Table 6.

Table 31. continued.

Molecule[a]	Size[b]	$T_{\rm rot}$[c]	N[d]	$C_{\rm int}$[e]	$C_{\rm vib}$[f]	C_N[g]	ΔV[h]	$V_{\rm off}$[i]	F[j]
	('')	(K)	(cm^{-2})				(km s^{-1})		
(1)	(2)	(3)	(4)	(5)	(6)	(7)	(8)	(9)	(10)
C^{17}O	200	48	8.55×10^{16}	0.98	1.00	0.98	18.0	5.0	e
	20	20	1.10×10^{16}	0.99	1.00	0.99	20.0	23.0	e
	20	18	2.76×10^{15}	0.99	1.00	0.99	20.0	−23.0	e
	200	7.0	2.35×10^{15}	1.06	1.00	1.06	16.0	1.5	a
	200	2.7	6.43×10^{13}	1.29	1.00	1.29	2.0	−72.7	a
	200	2.7	1.89×10^{13}	1.29	1.00	1.29	2.0	−82.0	a
	200	2.7	3.21×10^{13}	1.29	1.00	1.29	2.0	−84.2	a
	200	2.7	1.70×10^{14}	1.29	1.00	1.29	2.0	−89.9	a
	200	2.7	1.52×10^{13}	1.29	1.00	1.29	2.0	−92.8	a
	200	2.7	1.56×10^{14}	1.29	1.00	1.29	2.4	−102.6	a
	200	2.7	1.48×10^{14}	1.29	1.00	1.29	2.4	−105.3	a
	200	2.7	1.89×10^{13}	1.29	1.00	1.29	2.5	−107.5	a
	200	2.7	2.26×10^{13}	1.29	1.00	1.29	2.0	−112.8	a
	200	2.7	6.43×10^{12}	1.29	1.00	1.29	2.1	−137.0	a
	200	2.7	1.97×10^{13}	1.29	1.00	1.29	2.4	−138.8	a
	200	2.7	9.28×10^{12}	1.29	1.00	1.29	2.0	−144.0	a
	200	2.7	8.58×10^{12}	1.29	1.00	1.29	2.0	−157.0	a
	200	2.7	1.25×10^{13}	1.29	1.00	1.29	2.5	−169.0	a
^{13}C^{18}O	200	48	1.23×10^{16}	0.99	1.00	0.99	18.0	5.0	e
	20	20	1.59×10^{15}	0.99	1.00	0.99	20.0	23.0	e
	20	18	3.97×10^{14}	0.99	1.00	0.99	20.0	−23.0	e
	200	7.0	3.38×10^{14}	1.06	1.00	1.06	16.0	1.5	a
^{13}C^{17}O	200	48	4.27×10^{15}	0.98	1.00	0.98	18.0	5.0	e
	20	20	5.49×10^{14}	0.99	1.00	0.99	20.0	23.0	e
	20	18	1.38×10^{14}	0.99	1.00	0.99	20.0	−23.0	e
	200	7.0	1.17×10^{14}	1.06	1.00	1.06	16.0	1.5	a

Table 32. Parameters of our best-fit model of CS toward Sgr B2(N).

Molecule[a]	Size[b]	$T_{\rm rot}$[c]	N[d]	$C_{\rm int}$[e]	$C_{\rm vib}$[f]	C_N[g]	ΔV[h]	$V_{\rm off}$[i]	F[j]
	('')	(K)	(cm^{-2})				(km s^{-1})		
(1)	(2)	(3)	(4)	(5)	(6)	(7)	(8)	(9)	(10)
CS	4.0	150	2.59×10^{17}	1.00	1.00	1.00	12.0	1.5	e
	200	13	3.01×10^{15}	1.00	1.00	1.00	24.0	6.0	e
	120	6.3	3.91×10^{14}	1.03	1.00	1.03	10.0	17.0	a
	120	4.6	2.73×10^{13}	1.05	1.00	1.05	2.0	11.0	a
	120	4.6	1.31×10^{15}	1.05	1.00	1.05	10.0	2.0	a
	120	2.7	8.87×10^{11}	1.11	1.00	1.11	3.5	−32.7	a
	120	2.7	6.65×10^{12}	1.11	1.00	1.11	5.0	−47.3	a
	120	2.7	9.32×10^{13}	1.11	1.00	1.11	5.0	−55.6	a
	120	2.7	1.44×10^{13}	1.11	1.00	1.11	3.0	−60.2	a
	120	2.7	8.54×10^{13}	1.11	1.00	1.11	4.0	−63.0	a
	120	2.7	8.87×10^{12}	1.11	1.00	1.11	3.8	−84.7	a
	120	2.7	1.66×10^{13}	1.11	1.00	1.11	3.0	−90.0	a
	120	2.7	2.22×10^{13}	1.11	1.00	1.11	3.0	−93.0	a
	120	2.7	1.11×10^{12}	1.11	1.00	1.11	2.5	−97.0	a
	120	2.7	9.32×10^{13}	1.11	1.00	1.11	3.8	−104.0	a
	120	2.7	4.66×10^{12}	1.11	1.00	1.11	2.5	−110.0	a
	120	2.7	1.44×10^{12}	1.11	1.00	1.11	4.0	−113.0	a
	120	2.7	1.89×10^{12}	1.11	1.00	1.11	3.5	−122.0	a
	120	2.7	2.66×10^{12}	1.11	1.00	1.11	5.0	−127.0	a
	120	2.7	4.44×10^{12}	1.11	1.00	1.11	3.5	−133.3	a
	120	2.7	7.32×10^{13}	1.11	1.00	1.11	5.0	−137.0	a
	120	2.7	1.55×10^{13}	1.11	1.00	1.11	4.5	−143.9	a

Notes. See notes of Table 6.

Table 32. continued.

Molecule[a]	Size[b] ('')	T_{rot}[c] (K)	N[d] (cm^{-2})	C_{int}[e]	C_{vib}[f]	C_N[g]	ΔV[h] (km s^{-1})	V_{off}[i] (km s^{-1})	F[j]
(1)	(2)	(3)	(4)	(5)	(6)	(7)	(8)	(9)	(10)
	120	2.7	8.32×10^{12}	1.11	1.00	1.11	5.0	−151.0	a
	120	2.7	1.22×10^{13}	1.11	1.00	1.11	3.5	−156.3	a
	120	2.7	2.22×10^{12}	1.11	1.00	1.11	3.0	−159.3	a
	120	2.7	5.54×10^{12}	1.11	1.00	1.11	3.8	−161.9	a
	120	2.7	4.44×10^{12}	1.11	1.00	1.11	3.2	−166.0	a
	120	2.7	6.10×10^{13}	1.11	1.00	1.11	2.7	−169.5	a
	120	2.7	4.44×10^{12}	1.11	1.00	1.11	3.5	−175.0	a
	120	2.7	1.11×10^{12}	1.11	1.00	1.11	4.0	−179.7	a
^{13}CS	4.0	150	1.30×10^{16}	1.00	1.00	1.00	12.0	1.5	e
	200	13	1.50×10^{14}	1.00	1.00	1.00	24.0	6.0	e
	120	2.7	2.11×10^{13}	1.11	1.00	1.11	10.0	17.0	a
	120	2.7	1.44×10^{12}	1.11	1.00	1.11	2.0	11.0	a
	120	2.7	6.93×10^{13}	1.11	1.00	1.11	10.0	2.0	a
	120	2.7	2.22×10^{10}	1.11	1.00	1.11	3.5	−32.7	a
	120	2.7	1.11×10^{11}	1.11	1.00	1.11	5.0	−47.3	a
	120	2.7	4.66×10^{12}	1.11	1.00	1.11	5.0	−55.6	a
	120	2.7	7.21×10^{11}	1.11	1.00	1.11	3.0	−60.2	a
	120	2.7	4.27×10^{12}	1.11	1.00	1.11	4.0	−63.0	a
	120	2.7	2.22×10^{11}	1.11	1.00	1.11	3.8	−84.7	a
	120	2.7	4.16×10^{11}	1.11	1.00	1.11	3.0	−90.0	a
	120	2.7	5.54×10^{11}	1.11	1.00	1.11	3.0	−93.0	a
	120	2.7	2.77×10^{10}	1.11	1.00	1.11	2.5	−97.0	a
	120	2.7	2.33×10^{12}	1.11	1.00	1.11	3.8	−104.0	a
	120	2.7	1.16×10^{11}	1.11	1.00	1.11	2.5	−110.0	a
	120	2.7	3.60×10^{10}	1.11	1.00	1.11	4.0	−113.0	a
	120	2.7	9.43×10^{10}	1.11	1.00	1.11	3.5	−122.0	a
	120	2.7	1.33×10^{11}	1.11	1.00	1.11	5.0	−127.0	a
	120	2.7	2.22×10^{11}	1.11	1.00	1.11	3.5	−133.3	a
	120	2.7	3.66×10^{12}	1.11	1.00	1.11	5.0	−137.0	a
	120	2.7	7.76×10^{11}	1.11	1.00	1.11	4.5	−143.9	a
	120	2.7	4.16×10^{11}	1.11	1.00	1.11	5.0	−151.0	a
	120	2.7	6.10×10^{11}	1.11	1.00	1.11	3.5	−156.3	a
	120	2.7	1.11×10^{11}	1.11	1.00	1.11	3.0	−159.3	a
	120	2.7	2.77×10^{11}	1.11	1.00	1.11	3.8	−161.9	a
	120	2.7	2.22×10^{11}	1.11	1.00	1.11	3.2	−166.0	a
	120	2.7	3.05×10^{12}	1.11	1.00	1.11	2.7	−169.5	a
	120	2.7	2.22×10^{11}	1.11	1.00	1.11	3.5	−175.0	a
	120	2.7	5.54×10^{10}	1.11	1.00	1.11	4.0	−179.7	a
C^{34}S	4.0	150	1.18×10^{16}	1.00	1.00	1.00	12.0	1.5	e
	200	13	1.37×10^{14}	1.00	1.00	1.00	24.0	6.0	e
	120	2.7	1.92×10^{13}	1.11	1.00	1.11	10.0	17.0	a
	120	2.7	1.31×10^{12}	1.11	1.00	1.11	2.0	11.0	a
	120	2.7	6.30×10^{13}	1.11	1.00	1.11	10.0	2.0	a
	120	2.7	4.04×10^{10}	1.11	1.00	1.11	3.5	−32.7	a
	120	2.7	3.03×10^{11}	1.11	1.00	1.11	5.0	−47.3	a
	120	2.7	4.24×10^{12}	1.11	1.00	1.11	5.0	−55.6	a
	120	2.7	6.55×10^{11}	1.11	1.00	1.11	3.0	−60.2	a
	120	2.7	3.88×10^{12}	1.11	1.00	1.11	4.0	−63.0	a
	120	2.7	4.04×10^{11}	1.11	1.00	1.11	3.8	−84.7	a
	120	2.7	7.56×10^{11}	1.11	1.00	1.11	3.0	−90.0	a
	120	2.7	1.01×10^{12}	1.11	1.00	1.11	3.0	−93.0	a
	120	2.7	5.05×10^{10}	1.11	1.00	1.11	2.5	−97.0	a
	120	2.7	4.24×10^{12}	1.11	1.00	1.11	3.8	−104.0	a
	120	2.7	2.12×10^{11}	1.11	1.00	1.11	2.5	−110.0	a
	120	2.7	6.55×10^{10}	1.11	1.00	1.11	4.0	−113.0	a
	120	2.7	8.57×10^{10}	1.11	1.00	1.11	3.5	−122.0	a
	120	2.7	1.21×10^{11}	1.11	1.00	1.11	5.0	−127.0	a
	120	2.7	2.02×10^{11}	1.11	1.00	1.11	3.5	−133.3	a
	120	2.7	3.33×10^{12}	1.11	1.00	1.11	5.0	−137.0	a
	120	2.7	7.05×10^{11}	1.11	1.00	1.11	4.5	−143.9	a
	120	2.7	3.78×10^{11}	1.11	1.00	1.11	5.0	−151.0	a

Table 32. continued.

Molecule[a]	Size[b] (″)	T_{rot}[c] (K)	N[d] (cm^{-2})	C_{int}[e]	C_{vib}[f]	C_N[g]	ΔV[h] (km s^{-1})	V_{off}[i] (km s^{-1})	F[j]
(1)	(2)	(3)	(4)	(5)	(6)	(7)	(8)	(9)	(10)
	120	2.7	5.54×10^{11}	1.11	1.00	1.11	3.5	−156.3	a
	120	2.7	1.01×10^{11}	1.11	1.00	1.11	3.0	−159.3	a
	120	2.7	2.52×10^{11}	1.11	1.00	1.11	3.8	−161.9	a
	120	2.7	2.02×10^{11}	1.11	1.00	1.11	3.2	−166.0	a
	120	2.7	2.77×10^{12}	1.11	1.00	1.11	2.7	−169.5	a
	120	2.7	2.02×10^{11}	1.11	1.00	1.11	3.5	−175.0	a
	120	2.7	5.05×10^{10}	1.11	1.00	1.11	4.0	−179.7	a
C^{33}S	4.0	150	2.36×10^{15}	1.00	1.00	1.00	12.0	1.5	e
	200	13	2.73×10^{13}	1.00	1.00	1.00	24.0	6.0	e
	120	2.7	3.83×10^{12}	1.11	1.00	1.11	10.0	17.0	a
	120	2.7	2.62×10^{11}	1.11	1.00	1.11	2.0	11.0	a
	120	2.7	1.26×10^{13}	1.11	1.00	1.11	10.0	2.0	a
	120	2.7	8.06×10^{9}	1.11	1.00	1.11	3.5	−32.7	a
	120	2.7	6.04×10^{10}	1.11	1.00	1.11	5.0	−47.3	a
	120	2.7	8.47×10^{11}	1.11	1.00	1.11	5.0	−55.6	a
	120	2.7	1.31×10^{11}	1.11	1.00	1.11	3.0	−60.2	a
	120	2.7	7.76×10^{11}	1.11	1.00	1.11	4.0	−63.0	a
	120	2.7	8.06×10^{10}	1.11	1.00	1.11	3.8	−84.7	a
	120	2.7	1.51×10^{11}	1.11	1.00	1.11	3.0	−90.0	a
	120	2.7	2.02×10^{11}	1.11	1.00	1.11	3.0	−93.0	a
	120	2.7	1.01×10^{10}	1.11	1.00	1.11	2.5	−97.0	a
	120	2.7	8.47×10^{11}	1.11	1.00	1.11	3.8	−104.0	a
	120	2.7	4.24×10^{10}	1.11	1.00	1.11	2.5	−110.0	a
	120	2.7	1.31×10^{10}	1.11	1.00	1.11	4.0	−113.0	a
	120	2.7	1.72×10^{10}	1.11	1.00	1.11	3.5	−122.0	a
	120	2.7	2.42×10^{10}	1.11	1.00	1.11	5.0	−127.0	a
	120	2.7	4.04×10^{10}	1.11	1.00	1.11	3.5	−133.3	a
	120	2.7	6.65×10^{11}	1.11	1.00	1.11	5.0	−137.0	a
	120	2.7	1.41×10^{11}	1.11	1.00	1.11	4.5	−143.9	a
	120	2.7	7.56×10^{10}	1.11	1.00	1.11	5.0	−151.0	a
	120	2.7	1.11×10^{11}	1.11	1.00	1.11	3.5	−156.3	a
	120	2.7	2.02×10^{10}	1.11	1.00	1.11	3.0	−159.3	a
	120	2.7	5.05×10^{10}	1.11	1.00	1.11	3.8	−161.9	a
	120	2.7	4.04×10^{10}	1.11	1.00	1.11	3.2	−166.0	a
	120	2.7	5.54×10^{11}	1.11	1.00	1.11	2.7	−169.5	a
	120	2.7	4.04×10^{10}	1.11	1.00	1.11	3.5	−175.0	a
	120	2.7	1.01×10^{10}	1.11	1.00	1.11	4.0	−179.7	a
^{13}C^{34}S	4.0	150	5.90×10^{14}	1.00	1.00	1.00	12.0	1.5	e
	200	13	6.84×10^{12}	1.00	1.00	1.00	24.0	6.0	e
	120	2.7	9.58×10^{11}	1.11	1.00	1.11	10.0	17.0	a
	120	2.7	6.55×10^{10}	1.11	1.00	1.11	2.0	11.0	a
	120	2.7	3.15×10^{12}	1.11	1.00	1.11	10.0	2.0	a

Table 33. Parameters of our best-fit model of CH$_2$CO toward Sgr B2(N).

Molecule[a]	Size[b] (″)	T_{rot}[c] (K)	N[d] (cm^{-2})	C_{int}[e]	C_{vib}[f]	C_N[g]	ΔV[h] (km s^{-1})	V_{off}[i] (km s^{-1})	F[j]
(1)	(2)	(3)	(4)	(5)	(6)	(7)	(8)	(9)	(10)
CH$_2$CO	2.2	150	5.99×10^{17}	1.00	1.00	1.00	7.0	0.0	e
	1.9	150	2.99×10^{17}	1.00	1.00	1.00	7.0	10.0	e
^{13}CH$_2$CO	2.2	150	2.99×10^{16}	1.00	1.00	1.00	7.0	0.0	e
	1.9	150	1.50×10^{16}	1.00	1.00	1.00	7.0	10.0	e
CH$_2^{13}$CO	2.2	150	2.99×10^{16}	1.00	1.00	1.00	7.0	0.0	e
	1.9	150	1.50×10^{16}	1.00	1.00	1.00	7.0	10.0	e

Notes. See notes of Table 6.

Table 34. Parameters of our best-fit model of H_2CO toward Sgr B2(N).

Molecule[a]	Size[b] (″)	T_{rot}[c] (K)	N[d] (cm^{-2})	C_{int}[e]	C_{vib}[f]	C_N[g]	ΔV[h] (km s^{-1})	V_{off}[i]	F[j]
(1)	(2)	(3)	(4)	(5)	(6)	(7)	(8)	(9)	(10)
H_2CO	4.5	100	5.05×10^{17}	1.01	1.00	1.01	9.0	–0.8	e
	4.5	100	1.82×10^{17}	1.01	1.00	1.01	10.0	9.2	e
	40	11	3.07×10^{16}	0.96	1.00	0.96	25.0	0.0	e
	120	2.7	2.16×10^{16}	0.90	1.00	0.90	11.0	17.0	a
	120	2.7	6.76×10^{16}	0.90	1.00	0.90	17.0	1.9	a
$H_2^{13}CO$	4.5	100	2.52×10^{16}	1.01	1.00	1.01	9.0	–0.8	e
	4.5	100	9.09×10^{15}	1.01	1.00	1.01	10.0	9.2	e
	40	11	1.53×10^{15}	0.96	1.00	0.96	25.0	0.0	e
	120	2.7	1.08×10^{15}	0.90	1.00	0.90	11.0	17.0	a
	120	2.7	3.37×10^{15}	0.90	1.00	0.90	17.0	1.9	a

Notes. See notes of Table 6.

Table 35. Parameters of our best-fit model of H_2CS toward Sgr B2(N).

Molecule[a]	Size[b] (″)	T_{rot}[c] (K)	N[d] (cm^{-2})	C_{int}[e]	C_{vib}[f]	C_N[g]	ΔV[h] (km s^{-1})	V_{off}[i]	F[j]
(1)	(2)	(3)	(4)	(5)	(6)	(7)	(8)	(9)	(10)
H_2CS	3.0	150	2.50×10^{17}	1.00	1.00	1.00	8.0	–1.0	e
	2.0	150	3.99×10^{17}	1.00	1.00	1.00	8.0	9.0	e
	120	15	1.51×10^{14}	1.01	1.00	1.01	12.0	–7.0	e
$H_2^{13}CS$	3.0	150	1.25×10^{16}	1.00	1.00	1.00	8.0	–1.0	e
	2.0	150	2.00×10^{16}	1.00	1.00	1.00	8.0	9.0	e
	120	15	7.56×10^{12}	1.01	1.00	1.01	12.0	–7.0	e
$H_2C^{34}S$	3.0	150	1.14×10^{16}	1.00	1.00	1.00	8.0	–1.0	e
	2.0	150	1.82×10^{16}	1.00	1.00	1.00	8.0	9.0	e
	120	15	6.87×10^{12}	1.01	1.00	1.01	12.0	–7.0	e

Notes. See notes of Table 6.

Table 36. Parameters of our best-fit model of NH_2CH_2CN toward Sgr B2(N).

Molecule[a]	Size[b] (″)	T_{rot}[c] (K)	N[d] (cm^{-2})	C_{int}[e]	C_{vib}[f]	C_N[g]	ΔV[h] (km s^{-1})	V_{off}[i]	F[j]
(1)	(2)	(3)	(4)	(5)	(6)	(7)	(8)	(9)	(10)
NH_2CH_2CN	2.0	100	2.99×10^{16}	1.00	1.07	1.07	7.0	0.0	e

Notes. See notes of Table 6.

Table 37. Parameters of our best-fit model of H_2S toward Sgr B2(N).

Molecule[a]	Size[b] (″)	T_{rot}[c] (K)	N[d] (cm^{-2})	C_{int}[e]	C_{vib}[f]	C_N[g]	ΔV[h] (km s^{-1})	V_{off}[i]	F[j]
(1)	(2)	(3)	(4)	(5)	(6)	(7)	(8)	(9)	(10)
H_2S	5.0	200	6.27×10^{17}	0.99	1.00	0.99	13.0	3.0	e
	5.0	200	6.47×10^{16}	0.99	1.00	0.99	18.0	20.0	e
	5.0	200	6.17×10^{16}	0.99	1.00	0.99	15.0	–14.0	e

Notes. See notes of Table 6.

Table 38. Parameters of our best-fit model of HC_3N toward Sgr B2(N).

Molecule[a]	Size[b] ($''$)	T_{rot}[c] (K)	N[d] (cm^{-2})	C_{int}[e]	C_{vib}[f]	C_N[g]	ΔV[h] (km s^{-1})	V_{off}[i] (km s^{-1})	F[j]
(1)	(2)	(3)	(4)	(5)	(6)	(7)	(8)	(9)	(10)
HC_3N	9.0	60	1.20×10^{16}	1.00	1.00	1.00	9.0	−1.0	e
	9.0	60	7.59×10^{15}	1.00	1.00	1.00	9.0	8.5	e
	2.5	80	5.99×10^{16}	1.00	1.00	1.00	10.0	14.0	e
	2.5	80	6.99×10^{16}	1.00	1.00	1.00	10.0	−13.0	e
$HC_3N, v_7 = 1$	2.2	230	8.03×10^{17}	1.00	2.01	2.01	7.0	−1.5	e
	2.5	200	1.69×10^{17}	1.00	1.69	1.69	7.0	8.0	e
	1.8	200	1.52×10^{17}	1.00	1.69	1.69	10.0	14.0	e
	1.8	200	2.03×10^{17}	1.00	1.69	1.69	10.0	−13.0	e
$HC_3N, v_7 = 2$	1.8	200	2.37×10^{18}	1.00	1.69	1.69	7.0	−1.0	e
	2.5	200	1.69×10^{17}	1.00	1.69	1.69	7.0	8.0	e
	1.8	200	1.52×10^{17}	1.00	1.69	1.69	10.0	14.0	e
	1.8	200	2.03×10^{17}	1.00	1.69	1.69	10.0	−13.0	e
$HC_3N, v_6 = 1$	1.8	200	2.70×10^{18}	1.00	1.69	1.69	7.0	−1.0	e
	2.5	200	2.37×10^{17}	1.00	1.69	1.69	7.0	8.0	e
	1.8	200	1.52×10^{17}	1.00	1.69	1.69	10.0	14.0	e
	1.8	200	2.03×10^{17}	1.00	1.69	1.69	10.0	−13.0	e
$HC_3N, v_5 = 1/v_7 = 3$	1.4	200	7.61×10^{18}	1.00	1.69	1.69	7.0	−1.0	e
	2.5	200	5.07×10^{17}	1.00	1.69	1.69	7.0	8.0	e
$HC_3N, v_6 = v_7 = 1$	1.4	200	7.61×10^{18}	1.00	1.69	1.69	7.0	−2.0	e
	2.5	200	5.07×10^{17}	1.00	1.69	1.69	7.0	8.0	e
$HC_3N, v_4 = 1$	1.4	200	7.61×10^{18}	1.00	1.69	1.69	7.0	−2.0	e
	2.5	200	1.01×10^{18}	1.00	1.69	1.69	7.0	7.0	e
$HC_3N, v_7 = 4/v_5 = v_7 = 1$	1.4	200	6.76×10^{18}	1.00	1.69	1.69	7.0	−1.0	e
	2.5	200	6.76×10^{17}	1.00	1.69	1.69	7.0	8.0	e
$HC_3N, v_6 = 2$	1.4	200	1.01×10^{19}	1.00	1.69	1.69	7.0	−1.0	e
	2.5	200	1.01×10^{18}	1.00	1.69	1.69	7.0	8.0	e
$H^{13}CCCN$	9.0	60	5.99×10^{14}	1.00	1.00	1.00	9.0	−1.0	e
	9.0	60	3.80×10^{14}	1.00	1.00	1.00	9.0	8.5	e
	2.5	80	3.80×10^{15}	1.00	1.00	1.00	10.0	14.0	e
	2.5	80	4.50×10^{15}	1.00	1.00	1.00	10.0	−13.0	e
$HC^{13}CCN$	9.0	60	5.99×10^{14}	1.00	1.00	1.00	9.0	−1.0	e
	9.0	60	3.80×10^{14}	1.00	1.00	1.00	9.0	8.5	e
	2.5	80	3.80×10^{15}	1.00	1.00	1.00	10.0	14.0	e
	2.5	80	4.50×10^{15}	1.00	1.00	1.00	10.0	−13.0	e
$HCC^{13}CN$	9.0	60	5.99×10^{14}	1.00	1.00	1.00	9.0	−1.0	e
	9.0	60	3.80×10^{14}	1.00	1.00	1.00	9.0	8.5	e
	2.5	80	3.80×10^{15}	1.00	1.00	1.00	10.0	14.0	e
	2.5	80	4.50×10^{15}	1.00	1.00	1.00	10.0	−13.0	e
$H^{13}CCCN, v_7 = 1$	2.2	230	4.02×10^{16}	1.00	2.01	2.01	7.0	−1.5	e
	2.5	200	8.45×10^{15}	1.00	1.69	1.69	7.0	8.0	e
	1.8	200	7.61×10^{15}	1.00	1.69	1.69	10.0	14.0	e
	1.8	200	1.01×10^{16}	1.00	1.69	1.69	10.0	−13.0	e
$HC^{13}CCN, v_7 = 1$	2.2	230	4.02×10^{16}	1.00	2.01	2.01	7.0	−1.5	e
	2.5	200	8.45×10^{15}	1.00	1.69	1.69	7.0	8.0	e
	1.8	200	7.61×10^{15}	1.00	1.69	1.69	10.0	14.0	e
	1.8	200	1.01×10^{16}	1.00	1.69	1.69	10.0	−13.0	e
$HCC^{13}CN, v_7 = 1$	2.2	230	4.02×10^{16}	1.00	2.01	2.01	7.0	−1.5	e
	2.5	200	8.45×10^{15}	1.00	1.69	1.69	7.0	8.0	e
	1.8	200	7.61×10^{15}	1.00	1.69	1.69	10.0	14.0	e
	1.8	200	1.01×10^{16}	1.00	1.69	1.69	10.0	−13.0	e
$H^{13}CCCN, v_7 = 2$	1.8	200	1.18×10^{17}	1.00	1.69	1.69	7.0	−1.0	e
	2.5	200	8.45×10^{15}	1.00	1.69	1.69	7.0	8.0	e
	1.8	200	7.61×10^{15}	1.00	1.69	1.69	10.0	14.0	e
	1.8	200	1.01×10^{16}	1.00	1.69	1.69	10.0	−13.0	e

Notes. See notes of Table 6.

Table 38. continued.

Molecule[a]	Size[b] ('')	$T_{\rm rot}$[c] (K)	N[d] (cm^{-2})	$C_{\rm int}$[e]	$C_{\rm vib}$[f]	C_N[g]	ΔV[h] (km s^{-1})	$V_{\rm off}$[i]	F[j]
(1)	(2)	(3)	(4)	(5)	(6)	(7)	(8)	(9)	(10)
HC^{13}CCN, $v_7 = 2$	1.8	200	1.18×10^{17}	1.00	1.69	1.69	7.0	−1.0	e
	2.5	200	8.45×10^{15}	1.00	1.69	1.69	7.0	8.0	e
	1.8	200	7.61×10^{15}	1.00	1.69	1.69	10.0	14.0	e
	1.8	200	1.01×10^{16}	1.00	1.69	1.69	10.0	−13.0	e
HCC^{13}CN, $v_7 = 2$	1.8	200	1.18×10^{17}	1.00	1.69	1.69	7.0	−1.0	e
	2.5	200	8.45×10^{15}	1.00	1.69	1.69	7.0	8.0	e
	1.8	200	7.61×10^{15}	1.00	1.69	1.69	10.0	14.0	e
	1.8	200	1.01×10^{16}	1.00	1.69	1.69	10.0	−13.0	e
H^{13}CCCN, $v_6 = 1$	1.8	200	1.35×10^{17}	1.00	1.69	1.69	7.0	−1.0	e
	2.5	200	1.18×10^{16}	1.00	1.69	1.69	7.0	8.0	e
	1.8	200	7.61×10^{15}	1.00	1.69	1.69	10.0	14.0	e
	1.8	200	1.01×10^{16}	1.00	1.69	1.69	10.0	−13.0	e
HC^{13}CCN, $v_6 = 1$	1.8	200	1.35×10^{17}	1.00	1.69	1.69	7.0	−1.0	e
	2.5	200	1.18×10^{16}	1.00	1.69	1.69	7.0	8.0	e
	1.8	200	7.61×10^{15}	1.00	1.69	1.69	10.0	14.0	e
	1.8	200	1.01×10^{16}	1.00	1.69	1.69	10.0	−13.0	e
HCC^{13}CN, $v_6 = 1$	1.8	200	1.35×10^{17}	1.00	1.69	1.69	7.0	−1.0	e
	2.5	200	1.18×10^{16}	1.00	1.69	1.69	7.0	8.0	e
	1.8	200	7.61×10^{15}	1.00	1.69	1.69	10.0	14.0	e
	1.8	200	1.01×10^{16}	1.00	1.69	1.69	10.0	−13.0	e
H^{13}CCCN, $v_5 = 1/v_7 = 3$	1.4	200	3.80×10^{17}	1.00	1.69	1.69	7.0	−1.0	e
	2.5	200	2.54×10^{16}	1.00	1.69	1.69	7.0	8.0	e
HC^{13}CCN, $v_5 = 1/v_7 = 3$	1.4	200	3.80×10^{17}	1.00	1.69	1.69	7.0	−1.0	e
	2.5	200	2.54×10^{16}	1.00	1.69	1.69	7.0	8.0	e
HCC^{13}CN, $v_5 = 1/v_7 = 3$	1.4	200	3.80×10^{17}	1.00	1.69	1.69	7.0	−1.0	e
	2.5	200	2.54×10^{16}	1.00	1.69	1.69	7.0	8.0	e
H^{13}CCCN, $v_6 = v_7 = 1$	1.4	200	3.80×10^{17}	1.00	1.69	1.69	7.0	−2.0	e
	2.5	200	2.54×10^{16}	1.00	1.69	1.69	7.0	8.0	e
HC^{13}CCN, $v_6 = v_7 = 1$	1.4	200	3.80×10^{17}	1.00	1.69	1.69	7.0	−2.0	e
	2.5	200	2.54×10^{16}	1.00	1.69	1.69	7.0	8.0	e
HCC^{13}CN, $v_6 = v_7 = 1$	1.4	200	3.80×10^{17}	1.00	1.69	1.69	7.0	−2.0	e
	2.5	200	2.54×10^{16}	1.00	1.69	1.69	7.0	8.0	e
HCCC^{15}N	9.0	60	4.00×10^{13}	1.00	1.00	1.00	9.0	−1.0	e
	9.0	60	2.50×10^{13}	1.00	1.00	1.00	9.0	8.5	e
	2.5	80	2.50×10^{14}	1.00	1.00	1.00	10.0	14.0	e
	2.5	80	3.00×10^{14}	1.00	1.00	1.00	10.0	−13.0	e
HC^{13}C^{13}CN	9.0	60	3.00×10^{13}	1.00	1.00	1.00	9.0	−1.0	e
	9.0	60	1.90×10^{13}	1.00	1.00	1.00	9.0	8.5	e
	2.5	80	1.90×10^{14}	1.00	1.00	1.00	10.0	14.0	e
	2.5	80	2.25×10^{14}	1.00	1.00	1.00	10.0	−13.0	e
H^{13}CC^{13}CN	9.0	60	3.00×10^{13}	1.00	1.00	1.00	9.0	−1.0	e
	9.0	60	1.90×10^{13}	1.00	1.00	1.00	9.0	8.5	e
	2.5	80	1.90×10^{14}	1.00	1.00	1.00	10.0	14.0	e
	2.5	80	2.25×10^{14}	1.00	1.00	1.00	10.0	−13.0	e
H^{13}C^{13}CCN	9.0	60	3.00×10^{13}	1.00	1.00	1.00	9.0	−1.0	e
	9.0	60	1.90×10^{13}	1.00	1.00	1.00	9.0	8.5	e
	2.5	80	1.90×10^{14}	1.00	1.00	1.00	10.0	14.0	e
	2.5	80	2.25×10^{14}	1.00	1.00	1.00	10.0	−13.0	e

Table 39. Parameters of our best-fit model of HCCNC toward Sgr B2(N).

Molecule[a]	Size[b] (″)	$T_{\rm rot}$[c] (K)	N[d] (cm^{-2})	$C_{\rm int}$[e]	$C_{\rm vib}$[f]	C_N[g]	ΔV[h] (km s^{-1})	$V_{\rm off}$[i]	F[j]
(1)	(2)	(3)	(4)	(5)	(6)	(7)	(8)	(9)	(10)
HCCNC	9.0	60	4.00×10^{13}	1.00	1.00	1.00	8.0	0.0	e

Notes. See notes of Table 6.

Table 40. Parameters of our best-fit model of HCN toward Sgr B2(N).

Molecule[a]	Size[b] (″)	$T_{\rm rot}$[c] (K)	N[d] (cm^{-2})	$C_{\rm int}$[e]	$C_{\rm vib}$[f]	C_N[g]	ΔV[h] (km s^{-1})	$V_{\rm off}$[i]	F[j]
(1)	(2)	(3)	(4)	(5)	(6)	(7)	(8)	(9)	(10)
HCN	200	20	1.07×10^{17}	0.99	1.00	0.99	22.0	3.0	e
	20	20	2.78×10^{14}	0.99	1.00	0.99	22.0	43.0	e
	120	4.3	5.66×10^{13}	1.13	1.00	1.13	13.0	21.0	a
	120	5.0	7.69×10^{14}	1.10	1.00	1.10	26.0	−1.0	a
	120	2.7	1.99×10^{13}	1.24	1.00	1.24	7.0	−29.0	a
	120	2.7	4.97×10^{12}	1.24	1.00	1.24	4.0	−34.5	a
	120	2.7	4.97×10^{12}	1.24	1.00	1.24	3.0	−38.5	a
	120	2.7	2.01×10^{14}	1.24	1.00	1.24	9.0	−45.0	a
	120	2.7	1.94×10^{14}	1.24	1.00	1.24	6.0	−52.0	a
	120	2.7	4.97×10^{13}	1.24	1.00	1.24	4.2	−56.6	a
	120	2.7	1.02×10^{14}	1.24	1.00	1.24	7.0	−61.9	a
	120	2.7	4.47×10^{13}	1.24	1.00	1.24	8.0	−69.5	a
	120	2.7	1.24×10^{13}	1.24	1.00	1.24	4.5	−79.5	a
	120	2.7	1.24×10^{13}	1.24	1.00	1.24	5.0	−85.2	a
	120	2.7	9.31×10^{12}	1.24	1.00	1.24	5.0	−90.6	a
	120	2.7	4.97×10^{12}	1.24	1.00	1.24	5.0	−94.5	a
	120	2.7	1.39×10^{13}	1.24	1.00	1.24	3.8	−100.0	a
	120	2.7	2.73×10^{13}	1.24	1.00	1.24	3.3	−104.5	a
	120	2.7	1.03×10^{13}	1.24	1.00	1.24	4.4	−110.3	a
	120	2.7	4.35×10^{12}	1.24	1.00	1.24	3.0	−113.5	a
	120	2.7	3.48×10^{12}	1.24	1.00	1.24	3.5	−118.0	a
	120	2.7	3.35×10^{12}	1.24	1.00	1.24	3.5	−122.6	a
	120	2.7	2.24×10^{12}	1.24	1.00	1.24	3.0	−126.5	a
	120	2.7	1.29×10^{13}	1.24	1.00	1.24	4.7	−132.0	a
	120	2.7	9.94×10^{12}	1.24	1.00	1.24	3.5	−137.2	a
	120	2.7	8.07×10^{12}	1.24	1.00	1.24	4.0	−141.2	a
	120	2.7	5.71×10^{12}	1.24	1.00	1.24	3.8	−145.0	a
	120	2.7	4.35×10^{12}	1.24	1.00	1.24	5.0	−148.3	a
	120	2.7	4.10×10^{12}	1.24	1.00	1.24	4.0	−152.5	a
	120	2.7	4.35×10^{12}	1.24	1.00	1.24	4.0	−157.0	a
	120	2.7	3.23×10^{12}	1.24	1.00	1.24	4.0	−161.2	a
	120	2.7	2.24×10^{13}	1.24	1.00	1.24	5.0	−166.7	a
	120	2.7	2.48×10^{13}	1.24	1.00	1.24	3.2	−171.0	a
	120	2.7	8.57×10^{12}	1.24	1.00	1.24	4.7	−176.8	a
	120	2.7	2.48×10^{12}	1.24	1.00	1.24	4.0	−180.0	a
	120	2.7	1.99×10^{12}	1.24	1.00	1.24	4.0	−184.0	a
	120	2.7	6.21×10^{11}	1.24	1.00	1.24	4.0	−188.0	a
	120	2.7	4.35×10^{11}	1.24	1.00	1.24	3.5	−191.7	a
	120	2.7	2.73×10^{11}	1.24	1.00	1.24	4.0	−195.0	a
HCN, $v_2 = 1$	0.9	500	6.81×10^{19}	1.14	1.00	1.14	12.0	0.0	e
HCN, $v_2 = 2$	0.9	500	6.81×10^{19}	1.14	1.00	1.14	12.0	0.0	e
H^{13}CN	200	20	5.37×10^{15}	0.99	1.00	0.99	22.0	3.0	e
	20	20	1.39×10^{13}	0.99	1.00	0.99	22.0	43.0	e
	120	2.7	3.97×10^{13}	1.24	1.00	1.24	13.0	19.0	a
	120	3.7	4.08×10^{14}	1.17	1.00	1.17	24.0	0.0	a
	120	2.7	4.97×10^{11}	1.24	1.00	1.24	7.0	−29.0	a
	120	2.7	1.24×10^{11}	1.24	1.00	1.24	4.0	−34.5	a
	120	2.7	1.24×10^{11}	1.24	1.00	1.24	3.0	−38.5	a
	120	2.7	3.35×10^{12}	1.24	1.00	1.24	9.0	−45.0	a

Notes. See notes of Table 6.

Table 40. continued.

Molecule[a]	Size[b] (″)	T_{rot}[c] (K)	N[d] (cm^{-2})	C_{int}[e]	C_{vib}[f]	C_N[g]	ΔV[h]	V_{off}[i] (km s^{-1})	F[j]
(1)	(2)	(3)	(4)	(5)	(6)	(7)	(8)	(9)	(10)
	120	2.7	3.23×10^{12}	1.24	1.00	1.24	6.0	−52.0	a
	120	2.7	2.48×10^{12}	1.24	1.00	1.24	4.2	−56.6	a
	120	2.7	5.09×10^{12}	1.24	1.00	1.24	7.0	−61.9	a
	120	2.7	2.24×10^{12}	1.24	1.00	1.24	8.0	−69.5	a
	120	2.7	3.10×10^{11}	1.24	1.00	1.24	4.5	−79.5	a
	120	2.7	3.10×10^{11}	1.24	1.00	1.24	5.0	−85.2	a
	120	2.7	2.33×10^{11}	1.24	1.00	1.24	5.0	−90.6	a
	120	2.7	1.24×10^{11}	1.24	1.00	1.24	5.0	−94.5	a
	120	2.7	3.48×10^{11}	1.24	1.00	1.24	3.8	−100.0	a
	120	2.7	6.83×10^{11}	1.24	1.00	1.24	3.3	−104.5	a
	120	2.7	2.58×10^{11}	1.24	1.00	1.24	4.4	−110.3	a
	120	2.7	1.09×10^{11}	1.24	1.00	1.24	3.0	−113.5	a
	120	2.7	1.74×10^{11}	1.24	1.00	1.24	3.5	−118.0	a
	120	2.7	1.68×10^{11}	1.24	1.00	1.24	3.5	−122.6	a
	120	2.7	1.12×10^{11}	1.24	1.00	1.24	3.0	−126.5	a
	120	2.7	6.46×10^{11}	1.24	1.00	1.24	4.7	−132.0	a
	120	2.7	4.97×10^{11}	1.24	1.00	1.24	3.5	−137.2	a
	120	2.7	4.04×10^{11}	1.24	1.00	1.24	4.0	−141.2	a
	120	2.7	2.86×10^{11}	1.24	1.00	1.24	3.8	−145.0	a
	120	2.7	2.17×10^{11}	1.24	1.00	1.24	5.0	−148.3	a
	120	2.7	2.05×10^{11}	1.24	1.00	1.24	4.0	−152.5	a
	120	2.7	2.17×10^{11}	1.24	1.00	1.24	4.0	−157.0	a
	120	2.7	1.61×10^{11}	1.24	1.00	1.24	4.0	−161.2	a
	120	2.7	1.12×10^{12}	1.24	1.00	1.24	5.0	−166.7	a
	120	2.7	1.24×10^{12}	1.24	1.00	1.24	3.2	−171.0	a
	120	2.7	4.28×10^{11}	1.24	1.00	1.24	4.7	−176.8	a
	120	2.7	1.24×10^{11}	1.24	1.00	1.24	4.0	−180.0	a
	120	2.7	9.94×10^{10}	1.24	1.00	1.24	4.0	−184.0	a
	120	2.7	3.10×10^{10}	1.24	1.00	1.24	4.0	−188.0	a
	120	2.7	2.17×10^{10}	1.24	1.00	1.24	3.5	−191.7	a
	120	2.7	1.37×10^{10}	1.24	1.00	1.24	4.0	−195.0	a
H^{13}CN, $v_2 = 1$	0.9	500	3.39×10^{18}	1.13	1.00	1.13	12.0	0.0	e
HC^{15}N	200	20	3.58×10^{14}	0.99	1.00	0.99	22.0	3.0	e
	20	20	9.27×10^{11}	0.99	1.00	0.99	22.0	43.0	e
	120	2.7	2.11×10^{13}	1.24	1.00	1.24	12.5	16.0	a
	120	2.7	4.22×10^{13}	1.24	1.00	1.24	14.5	1.0	a
	120	2.7	5.67×10^{10}	1.24	1.00	1.24	7.0	−29.0	a
	120	2.7	1.41×10^{10}	1.24	1.00	1.24	4.0	−34.5	a
	120	2.7	1.41×10^{10}	1.24	1.00	1.24	3.0	−38.5	a
	120	2.7	4.47×10^{11}	1.24	1.00	1.24	9.0	−45.0	a
	120	2.7	4.31×10^{11}	1.24	1.00	1.24	6.0	−52.0	a
	120	2.7	1.65×10^{11}	1.24	1.00	1.24	4.2	−56.6	a
	120	2.7	3.39×10^{11}	1.24	1.00	1.24	7.0	−61.9	a
	120	2.7	1.49×10^{11}	1.24	1.00	1.24	8.0	−69.5	a
	120	2.7	3.55×10^{10}	1.24	1.00	1.24	4.5	−79.5	a
	120	2.7	3.55×10^{10}	1.24	1.00	1.24	5.0	−85.2	a
	120	2.7	2.66×10^{10}	1.24	1.00	1.24	5.0	−90.6	a
	120	2.7	1.41×10^{10}	1.24	1.00	1.24	5.0	−94.5	a
	120	2.7	3.97×10^{10}	1.24	1.00	1.24	3.8	−100.0	a
	120	2.7	7.81×10^{10}	1.24	1.00	1.24	3.3	−104.5	a
	120	2.7	2.94×10^{10}	1.24	1.00	1.24	4.4	−110.3	a
	120	2.7	1.24×10^{10}	1.24	1.00	1.24	3.0	−113.5	a
	120	2.7	1.16×10^{10}	1.24	1.00	1.24	3.5	−118.0	a
	120	2.7	1.12×10^{10}	1.24	1.00	1.24	3.5	−122.6	a
	120	2.7	7.45×10^{9}	1.24	1.00	1.24	3.0	−126.5	a
	120	2.7	4.31×10^{10}	1.24	1.00	1.24	4.7	−132.0	a
	120	2.7	3.31×10^{10}	1.24	1.00	1.24	3.5	−137.2	a
	120	2.7	2.69×10^{10}	1.24	1.00	1.24	4.0	−141.2	a
	120	2.7	1.90×10^{10}	1.24	1.00	1.24	3.8	−145.0	a
	120	2.7	1.45×10^{10}	1.24	1.00	1.24	5.0	−148.3	a
	120	2.7	1.37×10^{10}	1.24	1.00	1.24	4.0	−152.5	a

Table 40. continued.

Molecule[a]	Size[b] (″)	T_{rot}[c] (K)	N[d] (cm^{-2})	C_{int}[e]	C_{vib}[f]	C_N[g]	ΔV[h] (km s^{-1})	V_{off}[i]	F[j]
(1)	(2)	(3)	(4)	(5)	(6)	(7)	(8)	(9)	(10)
	120	2.7	1.45×10^{10}	1.24	1.00	1.24	4.0	−157.0	a
	120	2.7	1.08×10^{10}	1.24	1.00	1.24	4.0	−161.2	a
	120	2.7	7.45×10^{10}	1.24	1.00	1.24	5.0	−166.7	a
	120	2.7	8.28×10^{10}	1.24	1.00	1.24	3.2	−171.0	a
	120	2.7	2.85×10^{10}	1.24	1.00	1.24	4.7	−176.8	a
	120	2.7	8.28×10^{9}	1.24	1.00	1.24	4.0	−180.0	a
	120	2.7	6.61×10^{9}	1.24	1.00	1.24	4.0	−184.0	a
	120	2.7	2.07×10^{9}	1.24	1.00	1.24	4.0	−188.0	a
	120	2.7	1.45×10^{9}	1.24	1.00	1.24	3.5	−191.7	a
	120	2.7	9.10×10^{8}	1.24	1.00	1.24	4.0	−195.0	a
H^{13}C^{15}N	200	20	1.79×10^{13}	0.99	1.00	0.99	22.0	3.0	e
	20	20	4.65×10^{10}	0.99	1.00	0.99	22.0	43.0	e
	120	2.7	6.21×10^{11}	1.24	1.00	1.24	7.0	17.0	a
	120	2.7	4.97×10^{11}	1.24	1.00	1.24	4.0	3.8	a

Table 41. Parameters of our best-fit model of NH$_2$CHO toward Sgr B2(N).

Molecule[a]	Size[b] (″)	T_{rot}[c] (K)	N[d] (cm^{-2})	C_{int}[e]	C_{vib}[f]	C_N[g]	ΔV[h] (km s^{-1})	V_{off}[i]	F[j]
(1)	(2)	(3)	(4)	(5)	(6)	(7)	(8)	(9)	(10)
NH$_2$CHO	2.4	180	1.35×10^{18}	1.00	1.12	1.12	7.0	−1.0	e
	1.4	180	8.97×10^{17}	1.00	1.12	1.12	7.0	9.0	e
	60	2.7	3.13×10^{13}	1.04	1.00	1.04	8.0	19.0	a
NH$_2$CHO, $v_{12} = 1$	2.4	180	1.35×10^{18}	1.00	1.12	1.12	7.0	−1.0	e
	1.4	180	8.97×10^{17}	1.00	1.12	1.12	7.0	9.0	e
NH$_2^{13}$CHO	2.4	180	6.73×10^{16}	1.00	1.12	1.12	7.0	−1.0	e
	1.4	180	4.48×10^{16}	1.00	1.12	1.12	7.0	9.0	e
	60	2.7	1.57×10^{12}	1.04	1.00	1.04	8.0	19.0	a
NH$_2^{13}$CHO, $v_{12} = 1$	2.4	180	7.57×10^{16}	1.00	1.12	1.12	7.0	−1.0	e
	1.4	180	5.04×10^{16}	1.00	1.12	1.12	7.0	9.0	e

Notes. See notes of Table 6.

Table 42. Parameters of our best-fit model of HCO$^+$ toward Sgr B2(N).

Molecule[a]	Size[b] (″)	T_{rot}[c] (K)	N[d] (cm^{-2})	C_{int}[e]	C_{vib}[f]	C_N[g]	ΔV[h] (km s^{-1})	V_{off}[i]	F[j]
(1)	(2)	(3)	(4)	(5)	(6)	(7)	(8)	(9)	(10)
HCO$^+$	200	12	5.07×10^{15}	1.01	1.00	1.01	24.0	3.0	e
	20	20	1.19×10^{14}	0.99	1.00	0.99	26.0	43.0	e
	120	4.3	2.80×10^{13}	1.12	1.00	1.12	12.0	19.0	a
	120	4.3	2.80×10^{14}	1.12	1.00	1.12	25.0	−1.0	a
	120	2.7	1.72×10^{13}	1.23	1.00	1.23	6.0	−28.3	a
	120	2.7	2.01×10^{13}	1.23	1.00	1.23	5.0	−34.6	a
	120	2.7	8.84×10^{12}	1.23	1.00	1.23	3.0	−38.5	a
	120	2.7	5.16×10^{13}	1.23	1.00	1.23	5.0	−42.0	a
	120	2.7	7.74×10^{13}	1.23	1.00	1.23	5.0	−46.7	a
	120	2.7	1.25×10^{14}	1.23	1.00	1.23	6.0	−52.0	a
	120	2.7	2.46×10^{13}	1.23	1.00	1.23	3.5	−55.7	a
	120	2.7	2.58×10^{13}	1.23	1.00	1.23	3.5	−58.8	a
	120	2.7	4.67×10^{13}	1.23	1.00	1.23	6.0	−62.7	a
	120	2.7	2.09×10^{13}	1.23	1.00	1.23	7.0	−70.4	a
	120	2.7	1.52×10^{13}	1.23	1.00	1.23	6.0	−77.5	a
	120	2.7	1.77×10^{13}	1.23	1.00	1.23	4.5	−84.0	a
	120	2.7	1.38×10^{13}	1.23	1.00	1.23	5.0	−89.7	a
	120	2.7	4.91×10^{12}	1.23	1.00	1.23	5.0	−95.0	a
	120	2.7	8.84×10^{12}	1.23	1.00	1.23	4.0	−100.0	a

Notes. See notes of Table 6.

Table 42. continued.

Molecule[a]	Size[b] ('')	T_{rot}[c] (K)	N[d] (cm^{-2})	C_{int}[e]	C_{vib}[f]	C_N[g]	ΔV[h]	V_{off}[i] (km s^{-1})	F[j]
(1)	(2)	(3)	(4)	(5)	(6)	(7)	(8)	(9)	(10)
	120	2.7	4.67×10^{13}	1.23	1.00	1.23	3.7	−104.2	a
	120	2.7	1.72×10^{13}	1.23	1.00	1.23	4.5	−110.9	a
	120	2.7	2.95×10^{12}	1.23	1.00	1.23	3.0	−114.0	a
	120	2.7	2.46×10^{12}	1.23	1.00	1.23	4.0	−118.0	a
	120	2.7	6.14×10^{12}	1.23	1.00	1.23	5.0	−122.0	a
	120	2.7	2.21×10^{12}	1.23	1.00	1.23	4.0	−126.0	a
	120	2.7	5.65×10^{12}	1.23	1.00	1.23	5.0	−130.0	a
	120	2.7	2.70×10^{13}	1.23	1.00	1.23	6.8	−137.2	a
	120	2.7	1.23×10^{13}	1.23	1.00	1.23	4.5	−143.9	a
	120	2.7	4.67×10^{12}	1.23	1.00	1.23	5.0	−148.3	a
	120	2.7	4.30×10^{12}	1.23	1.00	1.23	5.0	−152.5	a
	120	2.7	4.54×10^{12}	1.23	1.00	1.23	4.5	−156.6	a
	120	2.7	4.18×10^{12}	1.23	1.00	1.23	4.5	−161.2	a
	120	2.7	8.60×10^{12}	1.23	1.00	1.23	5.0	−166.2	a
	120	2.7	2.95×10^{13}	1.23	1.00	1.23	3.5	−170.5	a
	120	2.7	6.14×10^{12}	1.23	1.00	1.23	5.5	−176.0	a
	120	2.7	3.07×10^{12}	1.23	1.00	1.23	4.0	−180.5	a
	120	2.7	4.42×10^{12}	1.23	1.00	1.23	5.0	−184.0	a
	120	2.7	1.84×10^{12}	1.23	1.00	1.23	4.0	−187.7	a
	120	2.7	6.14×10^{11}	1.23	1.00	1.23	8.0	−193.5	a
H^{13}CO$^+$	200	12	2.52×10^{14}	1.01	1.00	1.01	24.0	3.0	e
	20	20	5.95×10^{12}	0.99	1.00	0.99	26.0	43.0	e
	120	2.7	9.62×10^{12}	1.20	1.00	1.20	12.0	18.0	a
	120	2.7	5.17×10^{13}	1.20	1.00	1.20	21.0	0.5	a
	120	2.7	4.21×10^{11}	1.20	1.00	1.20	6.0	−28.3	a
	120	2.7	4.93×10^{11}	1.20	1.00	1.20	5.0	−34.6	a
	120	2.7	2.17×10^{11}	1.20	1.00	1.20	3.0	−38.5	a
	120	2.7	8.42×10^{11}	1.20	1.00	1.20	5.0	−42.0	a
	120	2.7	1.26×10^{12}	1.20	1.00	1.20	5.0	−46.7	a
	120	2.7	2.05×10^{12}	1.20	1.00	1.20	6.0	−52.0	a
	120	2.7	1.20×10^{12}	1.20	1.00	1.20	3.5	−55.7	a
	120	2.7	1.26×10^{12}	1.20	1.00	1.20	3.5	−58.8	a
	120	2.7	2.29×10^{12}	1.20	1.00	1.20	6.0	−62.7	a
	120	2.7	1.02×10^{12}	1.20	1.00	1.20	7.0	−70.4	a
	120	2.7	3.73×10^{11}	1.20	1.00	1.20	6.0	−77.5	a
	120	2.7	4.33×10^{11}	1.20	1.00	1.20	4.5	−84.0	a
	120	2.7	3.37×10^{11}	1.20	1.00	1.20	5.0	−89.7	a
	120	2.7	1.20×10^{11}	1.20	1.00	1.20	5.0	−95.0	a
	120	2.7	2.17×10^{11}	1.20	1.00	1.20	4.0	−100.0	a
	120	2.7	1.14×10^{12}	1.20	1.00	1.20	3.7	−104.2	a
	120	2.7	4.21×10^{11}	1.20	1.00	1.20	4.5	−110.9	a
	120	2.7	7.22×10^{10}	1.20	1.00	1.20	3.0	−114.0	a
	120	2.7	1.20×10^{11}	1.20	1.00	1.20	4.0	−118.0	a
	120	2.7	3.01×10^{11}	1.20	1.00	1.20	5.0	−122.0	a
	120	2.7	1.08×10^{11}	1.20	1.00	1.20	4.0	−126.0	a
	120	2.7	2.77×10^{11}	1.20	1.00	1.20	5.0	−130.0	a
	120	2.7	1.32×10^{12}	1.20	1.00	1.20	6.8	−137.2	a
	120	2.7	6.01×10^{11}	1.20	1.00	1.20	4.5	−143.9	a
	120	2.7	2.29×10^{11}	1.20	1.00	1.20	5.0	−148.3	a
	120	2.7	2.11×10^{11}	1.20	1.00	1.20	5.0	−152.5	a
	120	2.7	2.23×10^{11}	1.20	1.00	1.20	4.5	−156.6	a
	120	2.7	2.05×10^{11}	1.20	1.00	1.20	4.5	−161.2	a
	120	2.7	4.21×10^{11}	1.20	1.00	1.20	5.0	−166.2	a
	120	2.7	1.44×10^{12}	1.20	1.00	1.20	3.5	−170.5	a
	120	2.7	3.01×10^{11}	1.20	1.00	1.20	5.5	−176.0	a
	120	2.7	1.50×10^{11}	1.20	1.00	1.20	4.0	−180.5	a
	120	2.7	2.17×10^{11}	1.20	1.00	1.20	5.0	−184.0	a
	120	2.7	9.02×10^{10}	1.20	1.00	1.20	4.0	−187.7	a
	120	2.7	3.01×10^{10}	1.20	1.00	1.20	8.0	−193.5	a

Table 42. continued.

Molecule[a]	Size[b] ('')	T_{rot}[c] (K)	N[d] (cm^{-2})	C_{int}[e]	C_{vib}[f]	C_N[g]	ΔV[h] (km s^{-1})	V_{off}[i] (km s^{-1})	F[j]
(1)	(2)	(3)	(4)	(5)	(6)	(7)	(8)	(9)	(10)
HC^{18}O$^+$	200	12	2.02×10^{13}	1.01	1.00	1.01	24.0	0.0	e
	20	20	4.76×10^{11}	0.99	1.00	0.99	26.0	43.0	e
	120	2.7	2.76×10^{12}	1.20	1.00	1.20	10.0	16.0	a
	120	2.7	8.27×10^{12}	1.20	1.00	1.20	11.0	−0.5	a
	120	2.7	5.13×10^{10}	1.20	1.00	1.20	6.0	−28.3	a
	120	2.7	6.02×10^{10}	1.20	1.00	1.20	5.0	−34.6	a
	120	2.7	2.64×10^{10}	1.20	1.00	1.20	3.0	−38.5	a
	120	2.7	8.99×10^{10}	1.20	1.00	1.20	5.0	−42.0	a
	120	2.7	1.35×10^{11}	1.20	1.00	1.20	5.0	−46.7	a
	120	2.7	2.18×10^{11}	1.20	1.00	1.20	6.0	−52.0	a
	120	2.7	9.59×10^{10}	1.20	1.00	1.20	3.5	−55.7	a
	120	2.7	1.01×10^{11}	1.20	1.00	1.20	3.5	−58.8	a
	120	2.7	1.82×10^{11}	1.20	1.00	1.20	6.0	−62.7	a
	120	2.7	8.15×10^{10}	1.20	1.00	1.20	7.0	−70.4	a
	120	2.7	4.54×10^{10}	1.20	1.00	1.20	6.0	−77.5	a
	120	2.7	5.28×10^{10}	1.20	1.00	1.20	4.5	−84.0	a
	120	2.7	4.11×10^{10}	1.20	1.00	1.20	5.0	−89.7	a
	120	2.7	1.46×10^{10}	1.20	1.00	1.20	5.0	−95.0	a
	120	2.7	2.64×10^{10}	1.20	1.00	1.20	4.0	−100.0	a
	120	2.7	1.39×10^{11}	1.20	1.00	1.20	3.7	−104.2	a
	120	2.7	5.13×10^{10}	1.20	1.00	1.20	4.5	−110.9	a
	120	2.7	8.80×10^{9}	1.20	1.00	1.20	3.0	−114.0	a
	120	2.7	9.59×10^{9}	1.20	1.00	1.20	4.0	−118.0	a
	120	2.7	2.40×10^{10}	1.20	1.00	1.20	5.0	−122.0	a
	120	2.7	8.63×10^{9}	1.20	1.00	1.20	4.0	−126.0	a
	120	2.7	2.21×10^{10}	1.20	1.00	1.20	5.0	−130.0	a
	120	2.7	1.06×10^{11}	1.20	1.00	1.20	6.8	−137.2	a
	120	2.7	4.80×10^{10}	1.20	1.00	1.20	4.5	−143.9	a
	120	2.7	1.82×10^{10}	1.20	1.00	1.20	5.0	−148.3	a
	120	2.7	1.68×10^{10}	1.20	1.00	1.20	5.0	−152.5	a
	120	2.7	1.77×10^{10}	1.20	1.00	1.20	4.5	−156.6	a
	120	2.7	1.63×10^{10}	1.20	1.00	1.20	4.5	−161.2	a
	120	2.7	3.36×10^{10}	1.20	1.00	1.20	5.0	−166.2	a
	120	2.7	1.15×10^{11}	1.20	1.00	1.20	3.5	−170.5	a
	120	2.7	2.40×10^{10}	1.20	1.00	1.20	5.5	−176.0	a
	120	2.7	1.20×10^{10}	1.20	1.00	1.20	4.0	−180.5	a
	120	2.7	1.73×10^{10}	1.20	1.00	1.20	5.0	−184.0	a
	120	2.7	7.19×10^{9}	1.20	1.00	1.20	4.0	−187.7	a
	120	2.7	2.40×10^{9}	1.20	1.00	1.20	8.0	−193.5	a
HC^{17}O$^+$	200	12	7.00×10^{12}	1.01	1.00	1.01	24.0	0.0	e
	20	20	1.66×10^{11}	0.99	1.00	0.99	26.0	43.0	e
	120	2.7	9.62×10^{11}	1.20	1.00	1.20	10.0	16.0	a
	120	2.7	2.89×10^{12}	1.20	1.00	1.20	11.0	−0.5	a
	120	2.7	1.24×10^{10}	1.20	1.00	1.20	6.0	−28.3	a
	120	2.7	1.46×10^{10}	1.20	1.00	1.20	5.0	−34.6	a
	120	2.7	6.37×10^{9}	1.20	1.00	1.20	3.0	−38.5	a
	120	2.7	2.17×10^{10}	1.20	1.00	1.20	5.0	−42.0	a
	120	2.7	3.25×10^{10}	1.20	1.00	1.20	5.0	−46.7	a
	120	2.7	5.27×10^{10}	1.20	1.00	1.20	6.0	−52.0	a
	120	2.7	3.35×10^{10}	1.20	1.00	1.20	3.5	−55.7	a
	120	2.7	3.52×10^{10}	1.20	1.00	1.20	3.5	−58.8	a
	120	2.7	6.36×10^{10}	1.20	1.00	1.20	6.0	−62.7	a
	120	2.7	2.84×10^{10}	1.20	1.00	1.20	7.0	−70.4	a
	120	2.7	1.10×10^{10}	1.20	1.00	1.20	6.0	−77.5	a
	120	2.7	1.28×10^{10}	1.20	1.00	1.20	4.5	−84.0	a
	120	2.7	9.91×10^{9}	1.20	1.00	1.20	5.0	−89.7	a
	120	2.7	3.54×10^{9}	1.20	1.00	1.20	5.0	−95.0	a
	120	2.7	6.37×10^{9}	1.20	1.00	1.20	4.0	−100.0	a
	120	2.7	3.36×10^{10}	1.20	1.00	1.20	3.7	−104.2	a
	120	2.7	1.24×10^{10}	1.20	1.00	1.20	4.5	−110.9	a
	120	2.7	2.12×10^{9}	1.20	1.00	1.20	3.0	−114.0	a
	120	2.7	3.35×10^{9}	1.20	1.00	1.20	4.0	−118.0	a

Table 42. continued.

Molecule[a]	Size[b] (″)	T_{rot}[c] (K)	N[d] (cm^{-2})	C_{int}[e]	C_{vib}[f]	C_N[g]	ΔV[h] (km s^{-1})	V_{off}[i]	F[j]
(1)	(2)	(3)	(4)	(5)	(6)	(7)	(8)	(9)	(10)
	120	2.7	8.36×10^9	1.20	1.00	1.20	5.0	−122.0	a
	120	2.7	3.01×10^9	1.20	1.00	1.20	4.0	−126.0	a
	120	2.7	7.69×10^9	1.20	1.00	1.20	5.0	−130.0	a
	120	2.7	3.68×10^{10}	1.20	1.00	1.20	6.8	−137.2	a
	120	2.7	1.67×10^{10}	1.20	1.00	1.20	4.5	−143.9	a
	120	2.7	6.36×10^9	1.20	1.00	1.20	5.0	−148.3	a
	120	2.7	5.85×10^9	1.20	1.00	1.20	5.0	−152.5	a
	120	2.7	6.19×10^9	1.20	1.00	1.20	4.5	−156.6	a
	120	2.7	5.68×10^9	1.20	1.00	1.20	4.5	−161.2	a
	120	2.7	1.17×10^{10}	1.20	1.00	1.20	5.0	−166.2	a
	120	2.7	4.01×10^{10}	1.20	1.00	1.20	3.5	−170.5	a
	120	2.7	8.36×10^9	1.20	1.00	1.20	5.5	−176.0	a
	120	2.7	4.18×10^9	1.20	1.00	1.20	4.0	−180.5	a
	120	2.7	6.02×10^9	1.20	1.00	1.20	5.0	−184.0	a
	120	2.7	2.50×10^9	1.20	1.00	1.20	4.0	−187.7	a
	120	2.7	8.36×10^8	1.20	1.00	1.20	8.0	−193.5	a

Table 43. Parameters of our best-fit model of HCS$^+$ toward Sgr B2(N).

Molecule[a]	Size[b] (″)	T_{rot}[c] (K)	N[d] (cm^{-2})	C_{int}[e]	C_{vib}[f]	C_N[g]	ΔV[h] (km s^{-1})	V_{off}[i]	F[j]
(1)	(2)	(3)	(4)	(5)	(6)	(7)	(8)	(9)	(10)
HCS$^+$	8.0	50	2.48×10^{14}	0.99	1.00	0.99	12.0	2.0	e

Notes. See notes of Table 6.

Table 44. Parameters of our best-fit model of HDO toward Sgr B2(N).

Molecule[a]	Size[b] (″)	T_{rot}[c] (K)	N[d] (cm^{-2})	C_{int}[e]	C_{vib}[f]	C_N[g]	ΔV[h] (km s^{-1})	V_{off}[i]	F[j]
(1)	(2)	(3)	(4)	(5)	(6)	(7)	(8)	(9)	(10)
HDO	3.0	200	1.59×10^{17}	1.03	1.00	1.03	6.5	−1.0	e
	3.0	200	4.82×10^{16}	1.03	1.00	1.03	7.0	8.5	e

Notes. See notes of Table 6.

Table 45. Parameters of our best-fit model of HNC toward Sgr B2(N).

Molecule[a]	Size[b] (″)	T_{rot}[c] (K)	N[d] (cm^{-2})	C_{int}[e]	C_{vib}[f]	C_N[g]	ΔV[h] (km s^{-1})	V_{off}[i]	F[j]
(1)	(2)	(3)	(4)	(5)	(6)	(7)	(8)	(9)	(10)
HNC	200	20	4.79×10^{15}	1.00	1.00	1.00	24.0	4.0	e
	20	20	2.29×10^{13}	1.00	1.00	1.00	22.0	40.0	e
	120	2.7	2.46×10^{13}	1.33	1.00	1.33	14.0	20.0	a
	120	2.7	1.18×10^{14}	1.33	1.00	1.33	25.0	0.0	a
	120	2.7	2.13×10^{12}	1.33	1.00	1.33	7.0	−29.0	a
	120	2.7	1.33×10^{12}	1.33	1.00	1.33	4.0	−33.3	a
	120	2.7	2.93×10^{12}	1.33	1.00	1.33	5.0	−38.0	a
	120	2.7	3.99×10^{12}	1.33	1.00	1.33	6.0	−45.0	a
	120	2.7	5.19×10^{12}	1.33	1.00	1.33	5.0	−49.8	a
	120	2.7	1.33×10^{13}	1.33	1.00	1.33	6.0	−55.3	a
	120	2.7	1.86×10^{13}	1.33	1.00	1.33	5.0	−60.9	a
	120	2.7	5.32×10^{12}	1.33	1.00	1.33	5.0	−65.3	a
	120	2.7	6.65×10^{11}	1.33	1.00	1.33	7.0	−69.5	a
	120	2.7	7.98×10^{11}	1.33	1.00	1.33	5.0	−79.5	a
	120	2.7	2.53×10^{12}	1.33	1.00	1.33	3.5	−84.5	a
	120	2.7	3.19×10^{12}	1.33	1.00	1.33	4.5	−90.6	a

Notes. See notes of Table 6.

Table 45. continued.

Molecule[a]	Size[b] (″)	$T_{\rm rot}$[c] (K)	N[d] (cm^{-2})	$C_{\rm int}$[e]	$C_{\rm vib}$[f]	C_N[g]	ΔV[h]	$V_{\rm off}$[i]	F[j]
							(km s^{-1})		
(1)	(2)	(3)	(4)	(5)	(6)	(7)	(8)	(9)	(10)
	120	2.7	6.65×10^{11}	1.33	1.00	1.33	5.0	−95.0	a
	120	2.7	5.32×10^{11}	1.33	1.00	1.33	4.0	−100.5	a
	120	2.7	7.32×10^{12}	1.33	1.00	1.33	3.5	−104.0	a
	120	2.7	2.26×10^{12}	1.33	1.00	1.33	4.0	−110.0	a
	120	2.7	6.65×10^{11}	1.33	1.00	1.33	3.0	−113.5	a
	120	2.7	2.00×10^{11}	1.33	1.00	1.33	3.0	−119.5	a
	120	2.7	9.31×10^{11}	1.33	1.00	1.33	3.0	−122.3	a
	120	2.7	6.65×10^{11}	1.33	1.00	1.33	5.0	−130.0	a
	120	2.7	7.32×10^{12}	1.33	1.00	1.33	5.5	−137.5	a
	120	2.7	4.66×10^{12}	1.33	1.00	1.33	5.0	−144.0	a
	120	2.7	5.32×10^{11}	1.33	1.00	1.33	5.0	−148.3	a
	120	2.7	5.32×10^{11}	1.33	1.00	1.33	4.0	−152.5	a
	120	2.7	2.66×10^{12}	1.33	1.00	1.33	4.0	−157.0	a
	120	2.7	5.32×10^{11}	1.33	1.00	1.33	4.0	−161.2	a
	120	2.7	2.66×10^{12}	1.33	1.00	1.33	5.0	−166.0	a
	120	2.7	8.64×10^{12}	1.33	1.00	1.33	4.0	−170.0	a
	120	2.7	1.06×10^{12}	1.33	1.00	1.33	4.0	−175.5	a
	120	2.7	2.39×10^{11}	1.33	1.00	1.33	4.0	−180.0	a
	120	2.7	6.38×10^{11}	1.33	1.00	1.33	4.5	−184.7	a
	120	2.7	1.60×10^{11}	1.33	1.00	1.33	4.0	−188.0	a
HN^{13}C	200	20	2.38×10^{14}	0.99	1.00	0.99	24.0	4.0	e
	20	20	1.14×10^{12}	0.99	1.00	0.99	22.0	40.0	e
	120	2.7	1.81×10^{13}	1.20	1.00	1.20	12.0	17.0	a
	120	2.7	5.18×10^{13}	1.20	1.00	1.20	15.5	0.3	a
	120	2.7	4.82×10^{10}	1.20	1.00	1.20	7.0	−29.0	a
	120	2.7	3.01×10^{10}	1.20	1.00	1.20	4.0	−33.3	a
	120	2.7	6.62×10^{10}	1.20	1.00	1.20	5.0	−38.0	a
	120	2.7	6.02×10^{10}	1.20	1.00	1.20	6.0	−45.0	a
	120	2.7	7.83×10^{10}	1.20	1.00	1.20	5.0	−49.8	a
	120	2.7	6.02×10^{11}	1.20	1.00	1.20	6.0	−55.3	a
	120	2.7	8.43×10^{11}	1.20	1.00	1.20	5.0	−60.9	a
	120	2.7	2.41×10^{11}	1.20	1.00	1.20	5.0	−65.3	a
	120	2.7	3.01×10^{10}	1.20	1.00	1.20	7.0	−69.5	a
	120	2.7	1.81×10^{10}	1.20	1.00	1.20	5.0	−79.5	a
	120	2.7	5.72×10^{10}	1.20	1.00	1.20	3.5	−84.5	a
	120	2.7	7.22×10^{10}	1.20	1.00	1.20	4.5	−90.6	a
	120	2.7	1.50×10^{10}	1.20	1.00	1.20	5.0	−95.0	a
	120	2.7	1.20×10^{10}	1.20	1.00	1.20	4.0	−100.5	a
	120	2.7	1.66×10^{11}	1.20	1.00	1.20	3.5	−104.0	a
	120	2.7	5.12×10^{10}	1.20	1.00	1.20	4.0	−110.0	a
	120	2.7	1.50×10^{10}	1.20	1.00	1.20	3.0	−113.5	a
	120	2.7	9.03×10^{9}	1.20	1.00	1.20	3.0	−119.5	a
	120	2.7	4.21×10^{10}	1.20	1.00	1.20	3.0	−122.3	a
	120	2.7	3.01×10^{10}	1.20	1.00	1.20	5.0	−130.0	a
	120	2.7	3.31×10^{11}	1.20	1.00	1.20	5.5	−137.5	a
	120	2.7	2.11×10^{11}	1.20	1.00	1.20	5.0	−144.0	a
	120	2.7	2.41×10^{10}	1.20	1.00	1.20	5.0	−148.3	a
	120	2.7	2.41×10^{10}	1.20	1.00	1.20	4.0	−152.5	a
	120	2.7	1.20×10^{11}	1.20	1.00	1.20	4.0	−157.0	a
	120	2.7	2.41×10^{10}	1.20	1.00	1.20	4.0	−161.2	a
	120	2.7	1.20×10^{11}	1.20	1.00	1.20	5.0	−166.0	a
	120	2.7	3.91×10^{11}	1.20	1.00	1.20	4.0	−170.0	a
	120	2.7	4.82×10^{10}	1.20	1.00	1.20	4.0	−175.5	a
	120	2.7	1.08×10^{10}	1.20	1.00	1.20	4.0	−180.0	a
	120	2.7	2.89×10^{10}	1.20	1.00	1.20	4.5	−184.7	a
	120	2.7	7.22×10^{9}	1.20	1.00	1.20	4.0	−188.0	a
H^{15}NC	200	20	1.59×10^{13}	0.99	1.00	0.99	24.0	4.0	e
	20	20	7.61×10^{10}	0.99	1.00	0.99	22.0	40.0	e
	120	2.7	1.94×10^{12}	1.21	1.00	1.21	8.0	17.0	a
	120	2.7	6.07×10^{12}	1.21	1.00	1.21	9.0	0.0	a

Table 46. Parameters of our best-fit model of HNCO toward Sgr B2(N).

Molecule[a]	Size[b] (″)	T_{rot}[c] (K)	N[d] (cm^{-2})	C_{int}[e]	C_{vib}[f]	C_N[g]	ΔV[h] (km s^{-1})	V_{off}[i]	F[j]
(1)	(2)	(3)	(4)	(5)	(6)	(7)	(8)	(9)	(10)
HNCO	60	14	1.71×10^{15}	1.01	1.00	1.01	9.0	−1.0	e
	60	14	1.21×10^{15}	1.01	1.00	1.01	12.0	14.0	e
	2.4	200	1.32×10^{18}	1.02	1.00	1.02	7.0	−1.0	e
	1.9	200	8.13×10^{17}	1.02	1.00	1.02	7.0	9.0	e
HNCO, $v_5 = 1$	2.4	200	5.99×10^{18}	1.00	1.00	1.00	7.0	−1.0	e
	1.9	200	2.99×10^{18}	1.00	1.00	1.00	7.0	9.0	e
HNCO, $v_6 = 1$	2.4	200	5.99×10^{18}	1.00	1.00	1.00	7.0	−1.0	e
HNCO, $v_4 = 1$	2.4	200	2.00×10^{19}	1.00	1.00	1.00	7.0	−1.0	e
HN^{13}CO	60	14	8.49×10^{13}	1.00	1.00	1.00	9.0	−1.0	e
	60	14	5.99×10^{13}	1.00	1.00	1.00	12.0	14.0	e
	2.4	200	6.67×10^{16}	1.03	1.00	1.03	7.0	−1.0	e
	1.9	200	4.10×10^{16}	1.03	1.00	1.03	7.0	9.0	e
HNC^{18}O	60	14	6.82×10^{12}	1.00	1.00	1.00	9.0	−1.0	e
	60	14	4.81×10^{12}	1.00	1.00	1.00	12.0	14.0	e
	2.4	200	5.31×10^{15}	1.02	1.00	1.02	7.0	−1.0	e
	1.9	200	3.27×10^{15}	1.02	1.00	1.02	7.0	9.0	e

Notes. See notes of Table 6.

Table 47. Parameters of our best-fit model of HNCS toward Sgr B2(N).

Molecule[a]	Size[b] (″)	T_{rot}[c] (K)	N[d] (cm^{-2})	C_{int}[e]	C_{vib}[f]	C_N[g]	ΔV[h] (km s^{-1})	V_{off}[i]	F[j]
(1)	(2)	(3)	(4)	(5)	(6)	(7)	(8)	(9)	(10)
HNCS	200	20	9.22×10^{13}	0.92	1.00	0.92	20.0	5.0	e

Notes. See notes of Table 6.

Table 48. Parameters of our best-fit model of HOCN toward Sgr B2(N).

Molecule[a]	Size[b] (″)	T_{rot}[c] (K)	N[d] (cm^{-2})	C_{int}[e]	C_{vib}[f]	C_N[g]	ΔV[h] (km s^{-1})	V_{off}[i]	F[j]
(1)	(2)	(3)	(4)	(5)	(6)	(7)	(8)	(9)	(10)
HOCN	60	14	8.01×10^{12}	1.00	1.00	1.00	10.0	0.0	e
	60	14	9.01×10^{12}	1.00	1.00	1.00	12.0	11.0	e

Notes. See notes of Table 6.

Table 49. Parameters of our best-fit model of HOCO$^+$ toward Sgr B2(N).

Molecule[a]	Size[b] (″)	T_{rot}[c] (K)	N[d] (cm^{-2})	C_{int}[e]	C_{vib}[f]	C_N[g]	ΔV[h] (km s^{-1})	V_{off}[i]	F[j]
(1)	(2)	(3)	(4)	(5)	(6)	(7)	(8)	(9)	(10)
HOCO$^+$	200	10	1.23×10^{14}	1.03	1.00	1.03	12.0	0.0	e

Notes. See notes of Table 6.

Table 50. Parameters of our best-fit model of HOC$^+$ toward Sgr B2(N).

Molecule[a]	Size[b] (″)	T_{rot}[c] (K)	N[d] (cm^{-2})	C_{int}[e]	C_{vib}[f]	C_N[g]	ΔV[h] (km s^{-1})	V_{off}[i]	F[j]
(1)	(2)	(3)	(4)	(5)	(6)	(7)	(8)	(9)	(10)
HOC$^+$	200	20	1.10×10^{13}	1.00	1.00	1.00	18.0	3.0	e
	120	2.7	1.89×10^{12}	1.58	1.00	1.58	8.5	−0.2	a

Notes. See notes of Table 6.

Table 51. Parameters of our best-fit model of HSCN toward Sgr B2(N).

Molecule^a	Size^b (")	T_{rot}^{c} (K)	N^d (cm^{-2})	C_{int}^{e}	C_{vib}^{f}	C_N^{g}	ΔV^h (km s^{-1})	V_{off}^{i}	F^j
(1)	(2)	(3)	(4)	(5)	(6)	(7)	(8)	(9)	(10)
HSCN	200	20	4.49×10^{13}	1.00	1.00	1.00	20.0	5.0	e

Notes. See notes of Table 6.

Table 52. Parameters of our best-fit model of N$_2$H$^+$ toward Sgr B2(N).

Molecule^a	Size^b (")	T_{rot}^{c} (K)	N^d (cm^{-2})	C_{int}^{e}	C_{vib}^{f}	C_N^{g}	ΔV^h (km s^{-1})	V_{off}^{i}	F^j
(1)	(2)	(3)	(4)	(5)	(6)	(7)	(8)	(9)	(10)
N$_2$H$^+$	200	20	4.97×10^{14}	0.99	1.00	0.99	23.0	3.5	e
	200	4.0	1.62×10^{14}	1.08	1.00	1.08	17.0	0.0	a
	120	2.7	9.91×10^{11}	1.10	1.00	1.10	3.0	−55.3	a
	120	2.7	1.10×10^{12}	1.10	1.00	1.10	3.3	−58.5	a
	120	2.7	9.91×10^{11}	1.10	1.00	1.10	5.0	−61.9	a
	120	2.7	1.65×10^{11}	1.10	1.00	1.10	5.0	−85.0	a
	120	2.7	1.54×10^{11}	1.10	1.00	1.10	3.0	−90.6	a
	120	2.7	2.75×10^{11}	1.10	1.00	1.10	3.0	−99.3	a
	120	2.7	4.95×10^{11}	1.10	1.00	1.10	3.5	−104.0	a
	120	2.7	3.85×10^{11}	1.10	1.00	1.10	5.0	−108.3	a
	120	2.7	2.20×10^{11}	1.10	1.00	1.10	3.0	−124.0	a
	120	2.7	1.65×10^{11}	1.10	1.00	1.10	3.5	−133.8	a
	120	2.7	2.75×10^{11}	1.10	1.00	1.10	3.5	−137.0	a
	120	2.7	3.30×10^{11}	1.10	1.00	1.10	5.0	−142.5	a
	120	2.7	2.20×10^{11}	1.10	1.00	1.10	3.0	−167.0	a
	120	2.7	1.65×10^{12}	1.10	1.00	1.10	2.8	−169.9	a
	120	2.7	1.65×10^{11}	1.10	1.00	1.10	3.0	−181.0	a

Notes. See notes of Table 6.

Table 53. Parameters of our best-fit model of NH$_2$CN toward Sgr B2(N).

Molecule^a	Size^b (")	T_{rot}^{c} (K)	N^d (cm^{-2})	C_{int}^{e}	C_{vib}^{f}	C_N^{g}	ΔV^h (km s^{-1})	V_{off}^{i}	F^j
(1)	(2)	(3)	(4)	(5)	(6)	(7)	(8)	(9)	(10)
NH$_2$CN	2.0	150	5.13×10^{16}	1.03	1.00	1.03	8.0	−1.0	e
	2.0	150	2.05×10^{16}	1.03	1.00	1.03	8.0	9.0	e
	60	20	2.53×10^{13}	1.01	1.00	1.01	14.0	0.0	e
NH$_2^{13}$CN	2.0	150	2.56×10^{15}	1.03	1.00	1.03	8.0	−1.0	e
	2.0	150	1.03×10^{15}	1.03	1.00	1.03	8.0	9.0	e
	60	20	1.26×10^{12}	1.01	1.00	1.01	14.0	0.0	e

Notes. See notes of Table 6.

Table 54. Parameters of our best-fit model of NH$_2$D toward Sgr B2(N).

Molecule^a	Size^b (")	T_{rot}^{c} (K)	N^d (cm^{-2})	C_{int}^{e}	C_{vib}^{f}	C_N^{g}	ΔV^h (km s^{-1})	V_{off}^{i}	F^j
(1)	(2)	(3)	(4)	(5)	(6)	(7)	(8)	(9)	(10)
NH$_2$D	3.0	200	3.83×10^{16}	1.01	1.00	1.01	7.0	−1.0	e
	3.0	200	2.52×10^{16}	1.01	1.00	1.01	7.0	9.0	e

Notes. See notes of Table 6.

Table 55. Parameters of our best-fit model of NS toward Sgr B2(N).

Molecule[a]	Size[b] (″)	T_{rot}[c] (K)	N[d] (cm^{-2})	C_{int}[e]	C_{vib}[f]	C_N[g]	ΔV[h] (km s^{-1})	V_{off}[i]	F[j]
(1)	(2)	(3)	(4)	(5)	(6)	(7)	(8)	(9)	(10)
NS	200	30	1.05×10^{15}	0.96	1.00	0.96	13.0	1.0	e
	120	2.7	3.84×10^{14}	1.48	1.00	1.48	8.0	1.0	a

Notes. See notes of Table 6.

Table 56. Parameters of our best-fit model of OCS toward Sgr B2(N).

Molecule[a]	Size[b] (″)	T_{rot}[c] (K)	N[d] (cm^{-2})	C_{int}[e]	C_{vib}[f]	C_N[g]	ΔV[h] (km s^{-1})	V_{off}[i]	F[j]
(1)	(2)	(3)	(4)	(5)	(6)	(7)	(8)	(9)	(10)
OCS	8.0	60	1.80×10^{17}	1.00	1.00	1.00	6.5	–0.5	e
	8.0	60	7.98×10^{16}	1.00	1.00	1.00	6.5	8.8	e
	8.0	15	3.00×10^{16}	1.00	1.00	1.00	13.0	15.0	e
	8.0	15	3.00×10^{16}	1.00	1.00	1.00	10.0	–10.0	e
OCS, $v_2 = 1$	8.0	150	6.50×10^{17}	1.00	1.00	1.00	6.5	–0.5	e
	8.0	150	2.20×10^{17}	1.00	1.00	1.00	6.5	8.8	e
O^{13}CS	8.0	60	8.98×10^{15}	1.00	1.00	1.00	6.5	–0.5	e
	8.0	60	3.99×10^{15}	1.00	1.00	1.00	6.5	8.8	e
	8.0	15	1.50×10^{15}	1.00	1.00	1.00	13.0	15.0	e
	8.0	15	1.50×10^{15}	1.00	1.00	1.00	10.0	–10.0	e
OC^{34}S	8.0	60	8.16×10^{15}	1.00	1.00	1.00	6.5	–0.5	e
	8.0	60	3.63×10^{15}	1.00	1.00	1.00	6.5	8.8	e
	8.0	15	1.36×10^{15}	1.00	1.00	1.00	13.0	15.0	e
	8.0	15	1.36×10^{15}	1.00	1.00	1.00	10.0	–10.0	e
OC^{33}S	8.0	60	1.64×10^{15}	1.00	1.00	1.00	6.5	–0.5	e
	8.0	60	7.26×10^{14}	1.00	1.00	1.00	6.5	8.8	e
	8.0	15	2.73×10^{14}	1.00	1.00	1.00	13.0	15.0	e
	8.0	15	2.73×10^{14}	1.00	1.00	1.00	10.0	–10.0	e
^{18}OCS	8.0	60	7.19×10^{14}	1.00	1.00	1.00	6.5	–0.5	e
	8.0	60	3.20×10^{14}	1.00	1.00	1.00	6.5	8.8	e
	8.0	15	1.20×10^{14}	1.00	1.00	1.00	13.0	15.0	e
	8.0	15	1.20×10^{14}	1.00	1.00	1.00	10.0	–10.0	e

Notes. See notes of Table 6.

Table 57. Parameters of our best-fit model of PN toward Sgr B2(N).

Molecule[a]	Size[b] (″)	T_{rot}[c] (K)	N[d] (cm^{-2})	C_{int}[e]	C_{vib}[f]	C_N[g]	ΔV[h] (km s^{-1})	V_{off}[i]	F[j]
(1)	(2)	(3)	(4)	(5)	(6)	(7)	(8)	(9)	(10)
PN	120	2.7	8.82×10^{11}	1.10	1.00	1.10	7.0	0.0	a
	120	2.7	1.65×10^{12}	1.10	1.00	1.10	8.0	18.0	a

Notes. See notes of Table 6.

Table 58. Parameters of our best-fit model of SiO toward Sgr B2(N).

Molecule[a]	Size[b] ('')	T_{rot}[c] (K)	N[d] (cm^{-2})	C_{int}[e]	C_{vib}[f]	C_N[g]	ΔV[h] (km s^{-1})	V_{off}[i] (km s^{-1})	F[j]
(1)	(2)	(3)	(4)	(5)	(6)	(7)	(8)	(9)	(10)
SiO	200	16	3.00×10^{14}	1.00	1.00	1.00	14.0	0.5	e
	20	10	8.06×10^{13}	1.01	1.00	1.01	15.0	26.0	e
	20	10	6.05×10^{13}	1.01	1.00	1.01	15.0	−18.0	e
	120	4.6	1.44×10^{14}	1.04	1.00	1.04	9.0	19.5	a
	120	4.6	6.27×10^{13}	1.04	1.00	1.04	7.0	10.2	a
	120	3.9	3.50×10^{14}	1.06	1.00	1.06	9.0	0.0	a
	120	3.9	5.41×10^{13}	1.06	1.00	1.06	7.0	−8.0	a
	120	2.7	5.92×10^{12}	1.10	1.00	1.10	9.0	−48.9	a
	120	2.7	5.70×10^{12}	1.10	1.00	1.10	9.0	−59.5	a
	120	2.7	7.67×10^{11}	1.10	1.00	1.10	6.0	−130.8	a
	120	2.7	1.53×10^{12}	1.10	1.00	1.10	4.5	−136.9	a
	120	2.7	8.77×10^{11}	1.10	1.00	1.10	4.0	−142.0	a
	120	2.7	5.59×10^{11}	1.10	1.00	1.10	3.5	−146.5	a
	120	2.7	6.58×10^{11}	1.10	1.00	1.10	4.0	−156.5	a
	120	2.7	5.48×10^{11}	1.10	1.00	1.10	4.0	−160.5	a
	120	2.7	2.19×10^{12}	1.10	1.00	1.10	6.0	−170.0	a
^{29}SiO	200	16	1.50×10^{13}	1.00	1.00	1.00	14.0	0.5	e
	20	10	4.03×10^{12}	1.01	1.00	1.01	15.0	26.0	e
	20	10	3.02×10^{12}	1.01	1.00	1.01	15.0	−18.0	e
	120	2.7	7.56×10^{12}	1.09	1.00	1.09	9.0	19.5	a
	120	2.7	3.29×10^{12}	1.09	1.00	1.09	7.0	10.2	a
	120	2.7	1.81×10^{13}	1.09	1.00	1.09	9.0	0.0	a
	120	2.7	2.79×10^{12}	1.09	1.00	1.09	7.0	−8.0	a
	120	2.7	2.96×10^{11}	1.09	1.00	1.09	9.0	−48.9	a
	120	2.7	2.85×10^{11}	1.09	1.00	1.09	9.0	−59.5	a
	120	2.7	3.83×10^{10}	1.09	1.00	1.09	6.0	−130.8	a
	120	2.7	7.67×10^{10}	1.09	1.00	1.09	4.5	−136.9	a
	120	2.7	4.38×10^{10}	1.09	1.00	1.09	4.0	−142.0	a
	120	2.7	2.79×10^{10}	1.09	1.00	1.09	3.5	−146.5	a
	120	2.7	3.29×10^{10}	1.09	1.00	1.09	4.0	−156.5	a
	120	2.7	2.74×10^{10}	1.09	1.00	1.09	4.0	−160.5	a
	120	2.7	1.09×10^{11}	1.09	1.00	1.09	6.0	−170.0	a
^{30}SiO	200	16	9.99×10^{12}	1.00	1.00	1.00	14.0	0.5	e
	20	10	2.69×10^{12}	1.01	1.00	1.01	15.0	26.0	e
	20	10	2.02×10^{12}	1.01	1.00	1.01	15.0	−18.0	e
	120	2.7	5.03×10^{12}	1.09	1.00	1.09	9.0	19.5	a
	120	2.7	2.19×10^{12}	1.09	1.00	1.09	7.0	10.2	a
	120	2.7	1.20×10^{13}	1.09	1.00	1.09	9.0	0.0	a
	120	2.7	1.86×10^{12}	1.09	1.00	1.09	7.0	−8.0	a
	120	2.7	1.97×10^{11}	1.09	1.00	1.09	9.0	−48.9	a
	120	2.7	1.89×10^{11}	1.09	1.00	1.09	9.0	−59.5	a
	120	2.7	2.55×10^{10}	1.09	1.00	1.09	6.0	−130.8	a
	120	2.7	5.10×10^{10}	1.09	1.00	1.09	4.5	−136.9	a
	120	2.7	2.92×10^{10}	1.09	1.00	1.09	4.0	−142.0	a
	120	2.7	1.86×10^{10}	1.09	1.00	1.09	3.5	−146.5	a
	120	2.7	2.19×10^{10}	1.09	1.00	1.09	4.0	−156.5	a
	120	2.7	1.83×10^{10}	1.09	1.00	1.09	4.0	−160.5	a
	120	2.7	7.29×10^{10}	1.09	1.00	1.09	6.0	−170.0	a

Notes. See notes of Table 6.

Table 59. Parameters of our best-fit model of SO_2 toward Sgr B2(N).

Molecule[a]	Size[b] (″)	T_{rot}[c] (K)	N[d] (cm^{-2})	C_{int}[e]	C_{vib}[f]	C_N[g]	ΔV[h] (km s^{-1})	V_{off}[i]	F[j]
(1)	(2)	(3)	(4)	(5)	(6)	(7)	(8)	(9)	(10)
SO_2	3.0	150	7.80×10^{17}	0.97	1.00	0.97	7.0	−1.0	e
	30	20	1.60×10^{15}	1.00	1.00	1.00	14.0	2.0	e
	2.0	150	8.78×10^{17}	0.97	1.00	0.97	10.0	12.0	e
	2.0	150	5.85×10^{17}	0.97	1.00	0.97	10.0	−12.0	e
	20	20	1.10×10^{15}	1.00	1.00	1.00	24.0	28.0	e
	120	2.7	1.83×10^{14}	1.08	1.00	1.08	9.5	0.2	a
	120	2.7	9.69×10^{13}	1.08	1.00	1.08	12.0	17.0	a
$^{34}SO_2$	3.0	150	3.64×10^{16}	1.00	1.00	1.00	7.0	−1.0	e
	30	20	7.26×10^{13}	1.00	1.00	1.00	14.0	2.0	e
	2.0	150	4.09×10^{16}	1.00	1.00	1.00	10.0	12.0	e
	2.0	150	2.73×10^{16}	1.00	1.00	1.00	10.0	−12.0	e
	20	20	4.99×10^{13}	1.00	1.00	1.00	24.0	28.0	e

Notes. See notes of Table 6.

Table 60. Parameters of our best-fit model of SO toward Sgr B2(N).

Molecule[a]	Size[b] (″)	T_{rot}[c] (K)	N[d] (cm^{-2})	C_{int}[e]	C_{vib}[f]	C_N[g]	ΔV[h] (km s^{-1})	V_{off}[i]	F[j]
(1)	(2)	(3)	(4)	(5)	(6)	(7)	(8)	(9)	(10)
SO	3.0	150	8.11×10^{17}	1.01	1.00	1.01	8.0	0.0	e
	3.0	150	3.55×10^{17}	1.01	1.00	1.01	8.0	9.0	e
	3.0	150	2.03×10^{17}	1.01	1.00	1.01	14.0	−12.0	e
	30	20	3.07×10^{15}	1.02	1.00	1.02	12.0	0.0	e
	20	20	1.54×10^{15}	1.02	1.00	1.02	14.0	20.0	e
	120	2.7	7.26×10^{14}	0.95	1.00	0.95	14.0	1.0	a
	120	2.7	1.53×10^{14}	0.95	1.00	0.95	12.0	19.0	a
^{34}SO	3.0	150	3.69×10^{16}	1.01	1.00	1.01	8.0	0.0	e
	3.0	150	1.61×10^{16}	1.01	1.00	1.01	8.0	9.0	e
	3.0	150	9.22×10^{15}	1.01	1.00	1.01	14.0	−12.0	e
	30	20	1.39×10^{14}	1.02	1.00	1.02	12.0	0.0	e
	20	20	6.99×10^{13}	1.02	1.00	1.02	14.0	20.0	e
	120	2.7	3.28×10^{13}	0.95	1.00	0.95	14.0	1.0	a
	120	2.7	6.92×10^{12}	0.95	1.00	0.95	12.0	19.0	a
^{33}SO	3.0	150	7.37×10^{15}	1.01	1.00	1.01	8.0	0.0	e
	3.0	150	3.22×10^{15}	1.01	1.00	1.01	8.0	9.0	e
	3.0	150	1.84×10^{15}	1.01	1.00	1.01	14.0	−12.0	e
	30	20	2.80×10^{13}	1.02	1.00	1.02	12.0	0.0	e
	20	20	1.39×10^{13}	1.02	1.00	1.02	14.0	20.0	e
	120	2.7	6.59×10^{12}	0.95	1.00	0.95	14.0	1.0	a
	120	2.7	1.38×10^{12}	0.95	1.00	0.95	12.0	19.0	a

Notes. See notes of Table 6.

Table 61. Parameters of our best-fit model of t-HCOOH toward Sgr B2(N).

Molecule[a]	Size[b] (″)	T_{rot}[c] (K)	N[d] (cm^{-2})	C_{int}[e]	C_{vib}[f]	C_N[g]	ΔV[h] (km s^{-1})	V_{off}[i]	F[j]
(1)	(2)	(3)	(4)	(5)	(6)	(7)	(8)	(9)	(10)
t-HCOOH	5.0	70	1.50×10^{16}	1.00	1.00	1.00	8.0	−1.0	e
	5.0	70	7.48×10^{15}	1.00	1.00	1.00	8.0	9.0	e

Notes. See notes of Table 6.

Table 62. Parameters of our best-fit model of C_2H_3CN toward Sgr B2(M).

Molecule[a]	Size[b] ('')	T_{rot}[c] (K)	N[d] (cm^{-2})	C_{int}[e]	C_{vib}[f]	C_N[g]	ΔV[h] (km s^{-1})	V_{off}[i] (km s^{-1})	F[j]
(1)	(2)	(3)	(4)	(5)	(6)	(7)	(8)	(9)	(10)
C_2H_3CN	5.0	50	3.54×10^{15}	0.89	1.00	0.89	10.0	2.0	e
C_2H_3CN, $v_{11} = 1$	2.0	150	1.14×10^{17}	0.88	1.00	0.88	10.0	2.0	e

Notes. [a] Torsionally or vibrationally excited states are indicated after the name of the molecule and are modeled as separate entries. Entries with only the name of the molecule correspond to the ground state. [b] Source diameter (FWHM). [c] Rotational temperature. [d] Column density. [e] Correction factor that was applied to the column density to account for the correction to the approximate interpolation performed by XCLASS to compute the partition function. [f] Correction factor that was applied to the column density to account for the contribution of vibrationally or torsionally excited states or other conformers to the partition function. [g] Global correction factor that was applied to the column density ($C_{int} \times C_{vib}$). [h] Linewidth (FWHM). [i] Velocity offset with respect to the systemic velocity of Sgr B2(M) $V_{lsr} = 62$ km s^{-1}. [j] Flag indicating if the component belongs to the "emission" (e) or "absorption" (a) group.

Table 63. Parameters of our best-fit model of C_2H_5CN toward Sgr B2(M).

Molecule[a]	Size[b] ('')	T_{rot}[c] (K)	N[d] (cm^{-2})	C_{int}[e]	C_{vib}[f]	C_N[g]	ΔV[h] (km s^{-1})	V_{off}[i] (km s^{-1})	F[j]
(1)	(2)	(3)	(4)	(5)	(6)	(7)	(8)	(9)	(10)
C_2H_5CN	4.0	70	9.98×10^{15}	1.00	1.00	1.00	12.0	2.0	e
C_2H_5CN, $v_{13} + v_{21} = 1$	4.0	200	5.43×10^{16}	1.00	1.81	1.81	10.0	2.0	e

Notes. See notes of Table 62.

Table 64. Parameters of our best-fit model of C_2H_5OH toward Sgr B2(M).

Molecule[a]	Size[b] ('')	T_{rot}[c] (K)	N[d] (cm^{-2})	C_{int}[e]	C_{vib}[f]	C_N[g]	ΔV[h] (km s^{-1})	V_{off}[i] (km s^{-1})	F[j]
(1)	(2)	(3)	(4)	(5)	(6)	(7)	(8)	(9)	(10)
C_2H_5OH	60	20	5.54×10^{14}	0.92	1.00	0.92	13.0	−1.0	e
	5.0	100	2.11×10^{16}	1.05	1.00	1.05	8.0	0.0	e

Notes. See notes of Table 62.

Table 65. Parameters of our best-fit model of c-C_3H_2 toward Sgr B2(M).

Molecule[a]	Size[b] ('')	T_{rot}[c] (K)	N[d] (cm^{-2})	C_{int}[e]	C_{vib}[f]	C_N[g]	ΔV[h] (km s^{-1})	V_{off}[i] (km s^{-1})	F[j]
(1)	(2)	(3)	(4)	(5)	(6)	(7)	(8)	(9)	(10)
c-C_3H_2	200	15	2.60×10^{14}	1.00	1.00	1.00	15.0	−1.0	e
	120	3.0	2.11×10^{14}	1.05	1.00	1.05	11.0	3.0	a
	120	2.7	4.55×10^{12}	1.06	1.00	1.06	5.0	−23.5	a
	120	2.7	5.18×10^{12}	1.06	1.00	1.06	5.0	−30.0	a
	120	2.7	4.44×10^{12}	1.06	1.00	1.06	5.0	−40.0	a
	120	2.7	6.45×10^{12}	1.06	1.00	1.06	5.0	−45.0	a
	120	2.7	2.96×10^{12}	1.06	1.00	1.06	6.0	−50.0	a
	120	2.7	8.78×10^{12}	1.06	1.00	1.06	5.0	−53.8	a
	120	2.7	1.06×10^{13}	1.06	1.00	1.06	5.0	−59.5	a
	120	2.7	5.82×10^{12}	1.06	1.00	1.06	4.5	−64.5	a
	120	2.7	1.48×10^{12}	1.06	1.00	1.06	5.0	−70.7	a
	120	2.7	3.49×10^{12}	1.06	1.00	1.06	6.0	−77.5	a
	120	2.7	2.96×10^{12}	1.06	1.00	1.06	5.0	−82.0	a
	120	2.7	6.14×10^{12}	1.06	1.00	1.06	6.0	−87.0	a
	120	2.7	2.33×10^{12}	1.06	1.00	1.06	4.0	−91.5	a
	120	2.7	2.96×10^{11}	1.06	1.00	1.06	4.0	−97.5	a
	120	2.7	4.97×10^{12}	1.06	1.00	1.06	3.3	−103.3	a
	120	2.7	2.86×10^{12}	1.06	1.00	1.06	3.0	−107.7	a
	120	2.7	3.28×10^{12}	1.06	1.00	1.06	3.0	−111.0	a
	120	2.7	1.27×10^{12}	1.06	1.00	1.06	4.0	−115.5	a
	120	2.7	3.49×10^{12}	1.06	1.00	1.06	4.0	−120.7	a

Notes. See notes of Table 62.

Table 65. continued.

Molecule[a]	Size[b] ('')	T_{rot}[c] (K)	N[d] (cm^{-2})	C_{int}[e]	C_{vib}[f]	C_N[g]	ΔV[h]	V_{off}[i]	F[j]
(1)	(2)	(3)	(4)	(5)	(6)	(7)	(8)	(9)	(10)
	120	2.7	1.80×10^{12}	1.06	1.00	1.06	6.0	−131.8	a
	120	2.7	3.60×10^{12}	1.06	1.00	1.06	4.5	−138.0	a
	120	2.7	5.29×10^{11}	1.06	1.00	1.06	4.0	−142.1	a
	120	2.7	9.95×10^{11}	1.06	1.00	1.06	5.0	−146.3	a
	120	2.7	1.69×10^{12}	1.06	1.00	1.06	4.0	−150.5	a
	120	2.7	2.75×10^{12}	1.06	1.00	1.06	4.0	−155.0	a
	120	2.7	2.22×10^{12}	1.06	1.00	1.06	4.0	−159.5	a
	120	2.7	4.66×10^{12}	1.06	1.00	1.06	4.0	−163.8	a
	120	2.7	4.44×10^{12}	1.06	1.00	1.06	4.0	−168.2	a
	120	2.7	9.42×10^{11}	1.06	1.00	1.06	4.0	−173.6	a
	120	2.7	4.66×10^{11}	1.06	1.00	1.06	4.0	−178.0	a
c-CC^{13}CH$_2$	200	15	1.30×10^{13}	1.00	1.00	1.00	15.0	−1.0	e
	120	3.0	1.06×10^{13}	1.06	1.00	1.06	11.0	3.0	a
	120	2.7	1.16×10^{11}	1.07	1.00	1.07	5.0	−23.5	a
	120	2.7	1.31×10^{11}	1.07	1.00	1.07	5.0	−30.0	a
	120	2.7	7.51×10^{10}	1.07	1.00	1.07	5.0	−40.0	a
	120	2.7	1.09×10^{11}	1.07	1.00	1.07	5.0	−45.0	a
	120	2.7	5.01×10^{10}	1.07	1.00	1.07	6.0	−50.0	a
	120	2.7	4.45×10^{11}	1.07	1.00	1.07	5.0	−53.8	a
	120	2.7	5.37×10^{11}	1.07	1.00	1.07	5.0	−59.5	a
	120	2.7	2.95×10^{11}	1.07	1.00	1.07	4.5	−64.5	a
	120	2.7	3.76×10^{10}	1.07	1.00	1.07	5.0	−70.7	a
	120	2.7	8.85×10^{10}	1.07	1.00	1.07	6.0	−77.5	a
	120	2.7	7.51×10^{10}	1.07	1.00	1.07	5.0	−82.0	a
	120	2.7	1.56×10^{11}	1.07	1.00	1.07	6.0	−87.0	a
	120	2.7	5.90×10^{10}	1.07	1.00	1.07	4.0	−91.5	a
	120	2.7	7.51×10^{9}	1.07	1.00	1.07	4.0	−97.5	a
	120	2.7	1.27×10^{11}	1.07	1.00	1.07	3.3	−103.3	a
	120	2.7	7.24×10^{10}	1.07	1.00	1.07	3.0	−107.7	a
	120	2.7	8.32×10^{10}	1.07	1.00	1.07	3.0	−111.0	a
	120	2.7	6.44×10^{10}	1.07	1.00	1.07	4.0	−115.5	a
	120	2.7	1.77×10^{11}	1.07	1.00	1.07	4.0	−120.7	a
	120	2.7	9.12×10^{10}	1.07	1.00	1.07	6.0	−131.8	a
	120	2.7	1.82×10^{11}	1.07	1.00	1.07	4.5	−138.0	a
	120	2.7	2.68×10^{10}	1.07	1.00	1.07	4.0	−142.1	a
	120	2.7	5.04×10^{10}	1.07	1.00	1.07	5.0	−146.3	a
	120	2.7	8.58×10^{10}	1.07	1.00	1.07	4.0	−150.5	a
	120	2.7	1.39×10^{11}	1.07	1.00	1.07	4.0	−155.0	a
	120	2.7	1.13×10^{11}	1.07	1.00	1.07	4.0	−159.5	a
	120	2.7	2.36×10^{11}	1.07	1.00	1.07	4.0	−163.8	a
	120	2.7	2.25×10^{11}	1.07	1.00	1.07	4.0	−168.2	a
	120	2.7	4.77×10^{10}	1.07	1.00	1.07	4.0	−173.6	a
	120	2.7	2.36×10^{10}	1.07	1.00	1.07	4.0	−178.0	a
c-^{13}CC$_2$H$_2$	200	15	1.30×10^{13}	1.00	1.00	1.00	15.0	−1.0	e
	120	3.0	1.05×10^{13}	1.05	1.00	1.05	11.0	3.0	a
	120	2.7	1.14×10^{11}	1.06	1.00	1.06	5.0	−23.5	a
	120	2.7	1.29×10^{11}	1.06	1.00	1.06	5.0	−30.0	a
	120	2.7	7.39×10^{10}	1.06	1.00	1.06	5.0	−40.0	a
	120	2.7	1.08×10^{11}	1.06	1.00	1.06	5.0	−45.0	a
	120	2.7	4.93×10^{10}	1.06	1.00	1.06	6.0	−50.0	a
	120	2.7	4.38×10^{11}	1.06	1.00	1.06	5.0	−53.8	a
	120	2.7	5.28×10^{11}	1.06	1.00	1.06	5.0	−59.5	a
	120	2.7	2.90×10^{11}	1.06	1.00	1.06	4.5	−64.5	a
	120	2.7	3.70×10^{10}	1.06	1.00	1.06	5.0	−70.7	a
	120	2.7	8.71×10^{10}	1.06	1.00	1.06	6.0	−77.5	a
	120	2.7	7.39×10^{10}	1.06	1.00	1.06	5.0	−82.0	a
	120	2.7	1.53×10^{11}	1.06	1.00	1.06	6.0	−87.0	a
	120	2.7	5.81×10^{10}	1.06	1.00	1.06	4.0	−91.5	a
	120	2.7	7.39×10^{9}	1.06	1.00	1.06	4.0	−97.5	a
	120	2.7	1.25×10^{11}	1.06	1.00	1.06	3.3	−103.3	a

Table 65. continued.

Molecule[a]	Size[b] ('')	T_{rot}[c] (K)	N[d] (cm^{-2})	C_{int}[e]	C_{vib}[f]	C_N[g]	ΔV[h]	V_{off}[i] (km s^{-1})	F[j]
(1)	(2)	(3)	(4)	(5)	(6)	(7)	(8)	(9)	(10)
	120	2.7	7.13×10^{10}	1.06	1.00	1.06	3.0	−107.7	a
	120	2.7	8.18×10^{10}	1.06	1.00	1.06	3.0	−111.0	a
	120	2.7	6.34×10^{10}	1.06	1.00	1.06	4.0	−115.5	a
	120	2.7	1.74×10^{11}	1.06	1.00	1.06	4.0	−120.7	a
	120	2.7	8.98×10^{10}	1.06	1.00	1.06	6.0	−131.8	a
	120	2.7	1.80×10^{11}	1.06	1.00	1.06	4.5	−138.0	a
	120	2.7	2.64×10^{10}	1.06	1.00	1.06	4.0	−142.1	a
	120	2.7	4.96×10^{10}	1.06	1.00	1.06	5.0	−146.3	a
	120	2.7	8.45×10^{10}	1.06	1.00	1.06	4.0	−150.5	a
	120	2.7	1.37×10^{11}	1.06	1.00	1.06	4.0	−155.0	a
	120	2.7	1.11×10^{11}	1.06	1.00	1.06	4.0	−159.5	a
	120	2.7	2.32×10^{11}	1.06	1.00	1.06	4.0	−163.8	a
	120	2.7	2.22×10^{11}	1.06	1.00	1.06	4.0	−168.2	a
	120	2.7	4.70×10^{10}	1.06	1.00	1.06	4.0	−173.6	a
	120	2.7	2.32×10^{10}	1.06	1.00	1.06	4.0	−178.0	a

Table 66. Parameters of our best-fit model of CCH toward Sgr B2(M).

Molecule[a]	Size[b] ('')	T_{rot}[c] (K)	N[d] (cm^{-2})	C_{int}[e]	C_{vib}[f]	C_N[g]	ΔV[h]	V_{off}[i] (km s^{-1})	F[j]
(1)	(2)	(3)	(4)	(5)	(6)	(7)	(8)	(9)	(10)
CCH	200	20	5.00×10^{15}	1.00	1.00	1.00	15.0	1.0	e
	20	16	5.13×10^{15}	1.03	1.00	1.03	20.0	23.0	e
	120	3.9	5.18×10^{15}	1.29	1.00	1.29	11.0	4.0	a
	120	2.7	4.99×10^{13}	1.43	1.00	1.43	7.0	−27.0	a
	120	2.7	7.85×10^{13}	1.43	1.00	1.43	5.0	−32.0	a
	120	2.7	1.28×10^{14}	1.43	1.00	1.43	5.0	−41.0	a
	120	2.7	1.43×10^{14}	1.43	1.00	1.43	5.0	−45.5	a
	120	2.7	4.28×10^{13}	1.43	1.00	1.43	6.0	−50.0	a
	120	2.7	1.78×10^{14}	1.43	1.00	1.43	5.7	−54.0	a
	120	2.7	2.14×10^{14}	1.43	1.00	1.43	6.0	−60.0	a
	120	2.7	8.56×10^{13}	1.43	1.00	1.43	5.0	−65.2	a
	120	2.7	5.71×10^{13}	1.43	1.00	1.43	4.0	−77.0	a
	120	2.7	2.28×10^{13}	1.43	1.00	1.43	3.0	−80.5	a
	120	2.7	1.14×10^{14}	1.43	1.00	1.43	6.0	−84.5	a
	120	2.7	1.14×10^{14}	1.43	1.00	1.43	6.0	−90.0	a
	120	2.7	1.71×10^{14}	1.43	1.00	1.43	4.7	−102.5	a
	120	2.7	3.57×10^{13}	1.43	1.00	1.43	3.0	−107.7	a
	120	2.7	8.56×10^{13}	1.43	1.00	1.43	4.5	−111.0	a
	120	2.7	7.13×10^{12}	1.43	1.00	1.43	4.0	−116.0	a
	120	2.7	4.99×10^{13}	1.43	1.00	1.43	3.0	−120.5	a
	120	2.7	8.56×10^{12}	1.43	1.00	1.43	5.0	−128.0	a
	120	2.7	1.86×10^{13}	1.43	1.00	1.43	5.0	−134.0	a
	120	2.7	4.28×10^{13}	1.43	1.00	1.43	3.0	−138.0	a
	120	2.7	1.43×10^{13}	1.43	1.00	1.43	4.0	−142.1	a
	120	2.7	4.99×10^{13}	1.43	1.00	1.43	6.0	−148.0	a
	120	2.7	9.99×10^{13}	1.43	1.00	1.43	6.0	−155.0	a
	120	2.7	3.57×10^{13}	1.43	1.00	1.43	4.0	−159.2	a
	120	2.7	1.21×10^{14}	1.43	1.00	1.43	5.0	−164.0	a
	120	2.7	4.28×10^{13}	1.43	1.00	1.43	4.0	−168.0	a
	120	2.7	5.71×10^{13}	1.43	1.00	1.43	8.0	−173.0	a
	120	2.7	9.99×10^{12}	1.43	1.00	1.43	4.0	−178.0	a
	120	2.7	7.13×10^{12}	1.43	1.00	1.43	4.0	−182.0	a
	120	2.7	8.56×10^{12}	1.43	1.00	1.43	4.0	−185.7	a
	120	2.7	1.28×10^{13}	1.43	1.00	1.43	8.0	−192.4	a

Notes. See notes of Table 62.

Table 66. continued.

Molecule[a]	Size[b] (″)	T_{rot}[c] (K)	N[d] (cm^{-2})	C_{int}[e]	C_{vib}[f]	C_N[g]	ΔV[h]	V_{off}[i]	F[j]
(1)	(2)	(3)	(4)	(5)	(6)	(7)	(8)	(9)	(10)
^{13}CCH	200	20	2.48×10^{14}	0.99	1.00	0.99	15.0	1.0	e
	20	16	2.50×10^{14}	1.00	1.00	1.00	20.0	23.0	e
	120	3.9	2.23×10^{14}	1.11	1.00	1.11	11.0	4.0	a
	120	2.7	1.04×10^{12}	1.19	1.00	1.19	7.0	−27.0	a
	120	2.7	1.64×10^{12}	1.19	1.00	1.19	5.0	−32.0	a
	120	2.7	1.78×10^{12}	1.19	1.00	1.19	5.0	−41.0	a
	120	2.7	1.98×10^{12}	1.19	1.00	1.19	5.0	−45.5	a
	120	2.7	5.93×10^{11}	1.19	1.00	1.19	6.0	−50.0	a
	120	2.7	7.41×10^{12}	1.19	1.00	1.19	5.7	−54.0	a
	120	2.7	8.89×10^{12}	1.19	1.00	1.19	6.0	−60.0	a
	120	2.7	3.56×10^{12}	1.19	1.00	1.19	5.0	−65.2	a
	120	2.7	1.19×10^{12}	1.19	1.00	1.19	4.0	−77.0	a
	120	2.7	4.74×10^{11}	1.19	1.00	1.19	3.0	−80.5	a
	120	2.7	2.37×10^{12}	1.19	1.00	1.19	6.0	−84.5	a
	120	2.7	2.37×10^{12}	1.19	1.00	1.19	6.0	−90.0	a
	120	2.7	3.56×10^{12}	1.19	1.00	1.19	4.7	−102.5	a
	120	2.7	7.41×10^{11}	1.19	1.00	1.19	3.0	−107.7	a
	120	2.7	1.78×10^{12}	1.19	1.00	1.19	4.5	−111.0	a
	120	2.7	2.96×10^{11}	1.19	1.00	1.19	4.0	−116.0	a
	120	2.7	2.08×10^{12}	1.19	1.00	1.19	3.0	−120.5	a
	120	2.7	3.56×10^{11}	1.19	1.00	1.19	5.0	−128.0	a
	120	2.7	7.71×10^{11}	1.19	1.00	1.19	5.0	−134.0	a
	120	2.7	1.78×10^{12}	1.19	1.00	1.19	3.0	−138.0	a
	120	2.7	5.93×10^{11}	1.19	1.00	1.19	4.0	−142.1	a
	120	2.7	2.08×10^{12}	1.19	1.00	1.19	6.0	−148.0	a
	120	2.7	4.15×10^{12}	1.19	1.00	1.19	6.0	−155.0	a
	120	2.7	1.48×10^{12}	1.19	1.00	1.19	4.0	−159.2	a
	120	2.7	5.04×10^{12}	1.19	1.00	1.19	5.0	−164.0	a
	120	2.7	1.78×10^{12}	1.19	1.00	1.19	4.0	−168.0	a
	120	2.7	2.37×10^{12}	1.19	1.00	1.19	8.0	−173.0	a
	120	2.7	4.15×10^{11}	1.19	1.00	1.19	4.0	−178.0	a
	120	2.7	2.96×10^{11}	1.19	1.00	1.19	4.0	−182.0	a
	120	2.7	3.56×10^{11}	1.19	1.00	1.19	4.0	−185.7	a
	120	2.7	5.34×10^{11}	1.19	1.00	1.19	8.0	−192.4	a
C^{13}CH	200	20	2.48×10^{14}	0.99	1.00	0.99	15.0	1.0	e
	20	16	2.50×10^{14}	1.00	1.00	1.00	20.0	23.0	e
	120	3.9	2.24×10^{14}	1.12	1.00	1.12	11.0	4.0	a
	120	2.7	1.05×10^{12}	1.20	1.00	1.20	7.0	−27.0	a
	120	2.7	1.65×10^{12}	1.20	1.00	1.20	5.0	−32.0	a
	120	2.7	1.80×10^{12}	1.20	1.00	1.20	5.0	−41.0	a
	120	2.7	2.00×10^{12}	1.20	1.00	1.20	5.0	−45.5	a
	120	2.7	5.99×10^{11}	1.20	1.00	1.20	6.0	−50.0	a
	120	2.7	7.48×10^{12}	1.20	1.00	1.20	5.7	−54.0	a
	120	2.7	8.98×10^{12}	1.20	1.00	1.20	6.0	−60.0	a
	120	2.7	3.59×10^{12}	1.20	1.00	1.20	5.0	−65.2	a
	120	2.7	1.20×10^{12}	1.20	1.00	1.20	4.0	−77.0	a
	120	2.7	4.79×10^{11}	1.20	1.00	1.20	3.0	−80.5	a
	120	2.7	2.39×10^{12}	1.20	1.00	1.20	6.0	−84.5	a
	120	2.7	2.39×10^{12}	1.20	1.00	1.20	6.0	−90.0	a
	120	2.7	3.59×10^{12}	1.20	1.00	1.20	4.7	−102.5	a
	120	2.7	7.48×10^{11}	1.20	1.00	1.20	3.0	−107.7	a
	120	2.7	1.80×10^{12}	1.20	1.00	1.20	4.5	−111.0	a
	120	2.7	2.99×10^{11}	1.20	1.00	1.20	4.0	−116.0	a
	120	2.7	2.09×10^{12}	1.20	1.00	1.20	3.0	−120.5	a
	120	2.7	3.59×10^{11}	1.20	1.00	1.20	5.0	−128.0	a
	120	2.7	7.78×10^{11}	1.20	1.00	1.20	5.0	−134.0	a
	120	2.7	1.80×10^{12}	1.20	1.00	1.20	3.0	−138.0	a
	120	2.7	5.99×10^{11}	1.20	1.00	1.20	4.0	−142.1	a
	120	2.7	2.09×10^{12}	1.20	1.00	1.20	6.0	−148.0	a
	120	2.7	4.19×10^{12}	1.20	1.00	1.20	6.0	−155.0	a
	120	2.7	1.50×10^{12}	1.20	1.00	1.20	4.0	−159.2	a

Table 66. continued.

Molecule[a]	Size[b] (″)	$T_{rot}{}^c$ (K)	N^d (cm^{-2})	$C_{int}{}^e$	$C_{vib}{}^f$	$C_N{}^g$	ΔV^h (km s^{-1})	$V_{off}{}^i$	F^j
(1)	(2)	(3)	(4)	(5)	(6)	(7)	(8)	(9)	(10)
	120	2.7	5.09×10^{12}	1.20	1.00	1.20	5.0	−164.0	a
	120	2.7	1.80×10^{12}	1.20	1.00	1.20	4.0	−168.0	a
	120	2.7	2.39×10^{12}	1.20	1.00	1.20	8.0	−173.0	a
	120	2.7	4.19×10^{11}	1.20	1.00	1.20	4.0	−178.0	a
	120	2.7	2.99×10^{11}	1.20	1.00	1.20	4.0	−182.0	a
	120	2.7	3.59×10^{11}	1.20	1.00	1.20	4.0	−185.7	a
	120	2.7	5.39×10^{11}	1.20	1.00	1.20	8.0	−192.4	a

Table 67. Parameters of our best-fit model of CCS toward Sgr B2(M).

Molecule[a]	Size[b] (″)	$T_{rot}{}^c$ (K)	N^d (cm^{-2})	$C_{int}{}^e$	$C_{vib}{}^f$	$C_N{}^g$	ΔV^h (km s^{-1})	$V_{off}{}^i$	F^j
(1)	(2)	(3)	(4)	(5)	(6)	(7)	(8)	(9)	(10)
CCS	60	20	1.24×10^{14}	1.04	1.00	1.04	15.0	−1.0	e

Notes. See notes of Table 62.

Table 68. Parameters of our best-fit model of CH$_2$NH toward Sgr B2(M).

Molecule[a]	Size[b] (″)	$T_{rot}{}^c$ (K)	N^d (cm^{-2})	$C_{int}{}^e$	$C_{vib}{}^f$	$C_N{}^g$	ΔV^h (km s^{-1})	$V_{off}{}^i$	F^j
(1)	(2)	(3)	(4)	(5)	(6)	(7)	(8)	(9)	(10)
CH$_2$NH	120	14	1.45×10^{15}	1.00	1.00	1.00	10.0	0.0	e

Notes. See notes of Table 62.

Table 69. Parameters of our best-fit model of CH$_3$C$_3$N toward Sgr B2(M).

Molecule[a]	Size[b] (″)	$T_{rot}{}^c$ (K)	N^d (cm^{-2})	$C_{int}{}^e$	$C_{vib}{}^f$	$C_N{}^g$	ΔV^h (km s^{-1})	$V_{off}{}^i$	F^j
(1)	(2)	(3)	(4)	(5)	(6)	(7)	(8)	(9)	(10)
CH$_3$C$_3$N	5.0	100	2.97×10^{14}	0.99	1.00	0.99	8.0	0.0	e

Notes. See notes of Table 62.

Table 70. Parameters of our best-fit model of CH$_3$CCH toward Sgr B2(M).

Molecule[a]	Size[b] (″)	$T_{rot}{}^c$ (K)	N^d (cm^{-2})	$C_{int}{}^e$	$C_{vib}{}^f$	$C_N{}^g$	ΔV^h (km s^{-1})	$V_{off}{}^i$	F^j
(1)	(2)	(3)	(4)	(5)	(6)	(7)	(8)	(9)	(10)
CH$_3$CCH	30	70	7.72×10^{15}	0.86	1.00	0.86	10.0	0.0	e
CH$_3$C^{13}CH	30	70	4.42×10^{14}	0.98	1.00	0.98	10.0	0.0	e
CH$_3^{13}$CCH	30	70	4.42×10^{14}	0.98	1.00	0.98	10.0	0.0	e
^{13}CH$_3$CCH	30	70	4.42×10^{14}	0.98	1.00	0.98	10.0	0.0	e

Notes. See notes of Table 62.

Table 71. Parameters of our best-fit model of CH$_3$C(O)CH$_3$ toward Sgr B2(M).

Molecule[a]	Size[b] (″)	$T_{rot}{}^c$ (K)	N^d (cm^{-2})	$C_{int}{}^e$	$C_{vib}{}^f$	$C_N{}^g$	ΔV^h (km s^{-1})	$V_{off}{}^i$	F^j
(1)	(2)	(3)	(4)	(5)	(6)	(7)	(8)	(9)	(10)
CH$_3$C(O)CH$_3$	5.0	30	3.16×10^{15}	0.79	1.00	0.79	10.0	2.0	e

Notes. See notes of Table 62.

Table 72. Parameters of our best-fit model of CH_3CHO toward Sgr B2(M).

Molecule[a]	Size[b] (″)	T_{rot}[c] (K)	N[d] (cm^{-2})	C_{int}[e]	C_{vib}[f]	C_N[g]	ΔV[h] (km s^{-1})	V_{off}[i]	F[j]
(1)	(2)	(3)	(4)	(5)	(6)	(7)	(8)	(9)	(10)
CH_3CHO	30	40	5.82×10^{14}	0.90	1.00	0.90	12.0	0.0	e

Notes. See notes of Table 62.

Table 73. Parameters of our best-fit model of CH_3CN toward Sgr B2(M).

Molecule[a]	Size[b] (″)	T_{rot}[c] (K)	N[d] (cm^{-2})	C_{int}[e]	C_{vib}[f]	C_N[g]	ΔV[h] (km s^{-1})	V_{off}[i]	F[j]
(1)	(2)	(3)	(4)	(5)	(6)	(7)	(8)	(9)	(10)
CH_3CN	1.5	200	1.77×10^{17}	0.98	1.00	0.98	14.0	4.0	e
	60	60	2.69×10^{14}	0.90	1.00	0.90	13.0	1.0	e
$CH_3CN, v_8 = 1$	1.0	300	8.02×10^{17}	1.15	1.00	1.15	9.0	4.0	e
$CH_3CN, v_8 = 2$	1.0	300	8.02×10^{17}	1.15	1.00	1.15	9.0	4.0	e
$^{13}CH_3CN$	1.5	200	1.51×10^{16}	1.01	1.15	1.16	14.0	4.0	e
	60	60	1.95×10^{13}	0.97	1.00	0.97	13.0	1.0	e
$CH_3^{13}CN$	1.5	200	1.51×10^{16}	1.01	1.15	1.16	14.0	4.0	e
	60	60	1.95×10^{13}	0.97	1.00	0.97	13.0	1.0	e

Notes. See notes of Table 62.

Table 74. Parameters of our best-fit model of CH_3NH_2 toward Sgr B2(M).

Molecule[a]	Size[b] (″)	T_{rot}[c] (K)	N[d] (cm^{-2})	C_{int}[e]	C_{vib}[f]	C_N[g]	ΔV[h] (km s^{-1})	V_{off}[i]	F[j]
(1)	(2)	(3)	(4)	(5)	(6)	(7)	(8)	(9)	(10)
CH_3NH_2	5.0	50	4.50×10^{16}	1.00	1.00	1.00	15.0	0.0	e
	120	2.7	2.02×10^{14}	1.01	1.00	1.01	12.0	4.0	a

Notes. See notes of Table 62.

Table 75. Parameters of our best-fit model of CH_3OCH_3 toward Sgr B2(M).

Molecule[a]	Size[b] (″)	T_{rot}[c] (K)	N[d] (cm^{-2})	C_{int}[e]	C_{vib}[f]	C_N[g]	ΔV[h] (km s^{-1})	V_{off}[i]	F[j]
(1)	(2)	(3)	(4)	(5)	(6)	(7)	(8)	(9)	(10)
CH_3OCH_3	10	60	7.35×10^{15}	0.82	1.00	0.82	6.0	0.0	e

Notes. See notes of Table 62.

Table 76. Parameters of our best-fit model of CH_3OCHO toward Sgr B2(M).

Molecule[a]	Size[b] (″)	T_{rot}[c] (K)	N[d] (cm^{-2})	C_{int}[e]	C_{vib}[f]	C_N[g]	ΔV[h] (km s^{-1})	V_{off}[i]	F[j]
(1)	(2)	(3)	(4)	(5)	(6)	(7)	(8)	(9)	(10)
CH_3OCHO	5.0	40	2.29×10^{16}	0.92	1.00	0.92	9.0	0.0	e

Notes. See notes of Table 62.

Table 77. Parameters of our best-fit model of CH_3OH toward Sgr B2(M).

Molecule[a]	Size[b] (″)	T_{rot}[c] (K)	N[d] (cm^{-2})	C_{int}[e]	C_{vib}[f]	C_N[g]	ΔV[h] (km s^{-1})	V_{off}[i] (km s^{-1})	F[j]
(1)	(2)	(3)	(4)	(5)	(6)	(7)	(8)	(9)	(10)
CH_3OH	60	15	1.63×10^{16}	1.02	1.00	1.02	13.0	1.0	e
	60	4.5	3.83×10^{15}	0.96	1.00	0.96	11.0	3.0	a
	60	15	3.26×10^{15}	1.02	1.00	1.02	18.0	17.0	e
	1.3	200	5.66×10^{18}	0.98	1.00	0.98	11.0	3.0	e
	120	2.7	6.06×10^{12}	0.93	1.00	0.93	3.5	−57.0	a
	120	2.7	1.30×10^{12}	0.93	1.00	0.93	3.5	−62.0	a
	120	2.7	1.49×10^{12}	0.93	1.00	0.93	3.0	−97.0	a
	120	2.7	3.45×10^{12}	0.93	1.00	0.93	3.0	−102.7	a
	120	2.7	1.12×10^{12}	0.93	1.00	0.93	3.0	−149.0	a
	120	2.7	2.33×10^{12}	0.93	1.00	0.93	3.0	−153.2	a
	120	2.7	8.02×10^{12}	0.93	1.00	0.93	4.0	−158.2	a
	120	2.7	1.21×10^{13}	0.93	1.00	0.93	5.0	−163.7	a
	120	2.7	5.31×10^{12}	0.93	1.00	0.93	3.0	−168.0	a
$CH_3OH, v_t = 1$	1.3	200	5.66×10^{18}	0.98	1.00	0.98	11.0	3.0	e
$^{13}CH_3OH$	60	15	1.20×10^{15}	1.00	1.00	1.00	13.0	1.0	e
	60	4.5	5.00×10^{14}	1.00	1.00	1.00	11.0	3.0	a
	60	15	2.50×10^{14}	1.00	1.00	1.00	18.0	17.0	e
	1.3	200	2.20×10^{17}	1.00	1.00	1.00	11.0	3.0	e

Notes. See notes of Table 62.

Table 78. Parameters of our best-fit model of CH_3SH toward Sgr B2(M).

Molecule[a]	Size[b] (″)	T_{rot}[c] (K)	N[d] (cm^{-2})	C_{int}[e]	C_{vib}[f]	C_N[g]	ΔV[h] (km s^{-1})	V_{off}[i] (km s^{-1})	F[j]
(1)	(2)	(3)	(4)	(5)	(6)	(7)	(8)	(9)	(10)
CH_3SH	5.0	30	1.04×10^{16}	0.99	1.00	0.99	12.0	−2.0	e

Notes. See notes of Table 62.

Table 79. Parameters of our best-fit model of CN toward Sgr B2(M).

Molecule[a]	Size[b] (″)	T_{rot}[c] (K)	N[d] (cm^{-2})	C_{int}[e]	C_{vib}[f]	C_N[g]	ΔV[h] (km s^{-1})	V_{off}[i] (km s^{-1})	F[j]
(1)	(2)	(3)	(4)	(5)	(6)	(7)	(8)	(9)	(10)
CN	200	20	9.90×10^{15}	0.99	1.00	0.99	30.0	5.0	e
	120	3.0	7.48×10^{15}	1.25	1.00	1.25	12.0	4.0	a
	120	2.7	3.84×10^{13}	1.28	1.00	1.28	4.5	−26.0	a
	120	2.7	2.43×10^{14}	1.28	1.00	1.28	4.5	−31.0	a
	120	2.7	7.67×10^{13}	1.28	1.00	1.28	3.5	−39.0	a
	120	2.7	1.92×10^{14}	1.28	1.00	1.28	4.0	−43.8	a
	120	2.7	2.30×10^{14}	1.28	1.00	1.28	4.0	−48.5	a
	120	2.7	3.58×10^{14}	1.28	1.00	1.28	4.5	−53.8	a
	120	2.7	6.39×10^{14}	1.28	1.00	1.28	6.0	−60.5	a
	120	2.7	2.94×10^{13}	1.28	1.00	1.28	3.7	−70.5	a
	120	2.7	3.07×10^{13}	1.28	1.00	1.28	2.7	−77.1	a
	120	2.7	8.31×10^{13}	1.28	1.00	1.28	2.5	−80.5	a
	120	2.7	1.28×10^{14}	1.28	1.00	1.28	4.0	−84.5	a
	120	2.7	1.02×10^{14}	1.28	1.00	1.28	2.5	−88.0	a
	120	2.7	6.65×10^{13}	1.28	1.00	1.28	2.5	−91.2	a
	120	2.7	2.56×10^{13}	1.28	1.00	1.28	4.0	−95.5	a
	120	2.7	3.84×10^{14}	1.28	1.00	1.28	2.5	−102.5	a
	120	2.7	2.05×10^{14}	1.28	1.00	1.28	3.5	−108.0	a
	120	2.7	3.45×10^{13}	1.28	1.00	1.28	3.0	−113.5	a
	120	2.7	6.27×10^{13}	1.28	1.00	1.28	3.0	−120.5	a
	120	2.7	1.28×10^{13}	1.28	1.00	1.28	3.0	−125.0	a
	120	2.7	3.33×10^{13}	1.28	1.00	1.28	3.5	−130.7	a

Notes. See notes of Table 62.

Table 79. continued.

Molecule[a]	Size[b] ('')	$T_{\rm rot}$[c] (K)	N[d] (cm^{-2})	$C_{\rm int}$[e]	$C_{\rm vib}$[f]	C_N[g]	ΔV[h]	$V_{\rm off}$[i] (km s^{-1})	F[j]
(1)	(2)	(3)	(4)	(5)	(6)	(7)	(8)	(9)	(10)
	120	2.7	2.05×10^{13}	1.28	1.00	1.28	3.0	−134.0	a
	120	2.7	8.31×10^{13}	1.28	1.00	1.28	4.5	−138.5	a
	120	2.7	8.95×10^{13}	1.28	1.00	1.28	6.0	−150.5	a
	120	2.7	8.57×10^{13}	1.28	1.00	1.28	3.8	−155.3	a
	120	2.7	1.02×10^{14}	1.28	1.00	1.28	3.5	−159.3	a
	120	2.7	2.81×10^{14}	1.28	1.00	1.28	4.0	−164.0	a
	120	2.7	1.09×10^{14}	1.28	1.00	1.28	3.5	−168.0	a
	120	2.7	4.86×10^{13}	1.28	1.00	1.28	3.4	−173.0	a
	120	2.7	2.69×10^{13}	1.28	1.00	1.28	4.0	−177.5	a
^{13}CN	200	20	4.95×10^{14}	0.99	1.00	0.99	30.0	5.0	e
	120	3.0	3.69×10^{14}	1.23	1.00	1.23	12.0	4.0	a
	120	2.7	9.44×10^{11}	1.26	1.00	1.26	4.5	−26.0	a
	120	2.7	5.98×10^{12}	1.26	1.00	1.26	4.5	−31.0	a
	120	2.7	1.26×10^{12}	1.26	1.00	1.26	3.5	−39.0	a
	120	2.7	3.15×10^{12}	1.26	1.00	1.26	4.0	−43.8	a
	120	2.7	3.78×10^{12}	1.26	1.00	1.26	4.0	−48.5	a
	120	2.7	1.76×10^{13}	1.26	1.00	1.26	4.5	−53.8	a
	120	2.7	3.15×10^{13}	1.26	1.00	1.26	6.0	−60.5	a
	120	2.7	1.45×10^{12}	1.26	1.00	1.26	3.7	−70.5	a
	120	2.7	7.55×10^{11}	1.26	1.00	1.26	2.7	−77.1	a
	120	2.7	2.04×10^{12}	1.26	1.00	1.26	2.5	−80.5	a
	120	2.7	3.15×10^{12}	1.26	1.00	1.26	4.0	−84.5	a
	120	2.7	2.52×10^{12}	1.26	1.00	1.26	2.5	−88.0	a
	120	2.7	1.64×10^{12}	1.26	1.00	1.26	2.5	−91.2	a
	120	2.7	6.29×10^{11}	1.26	1.00	1.26	4.0	−95.5	a
	120	2.7	9.44×10^{12}	1.26	1.00	1.26	2.5	−102.5	a
	120	2.7	5.04×10^{12}	1.26	1.00	1.26	3.5	−108.0	a
	120	2.7	1.70×10^{12}	1.26	1.00	1.26	3.0	−113.5	a
	120	2.7	3.08×10^{12}	1.26	1.00	1.26	3.0	−120.5	a
	120	2.7	6.29×10^{11}	1.26	1.00	1.26	3.0	−125.0	a
	120	2.7	1.64×10^{12}	1.26	1.00	1.26	3.5	−130.7	a
	120	2.7	1.01×10^{12}	1.26	1.00	1.26	3.0	−134.0	a
	120	2.7	4.09×10^{12}	1.26	1.00	1.26	4.5	−138.5	a
	120	2.7	4.41×10^{12}	1.26	1.00	1.26	6.0	−150.5	a
	120	2.7	4.22×10^{12}	1.26	1.00	1.26	3.8	−155.3	a
	120	2.7	5.04×10^{12}	1.26	1.00	1.26	3.5	−159.3	a
	120	2.7	1.38×10^{13}	1.26	1.00	1.26	4.0	−164.0	a
	120	2.7	5.35×10^{12}	1.26	1.00	1.26	3.5	−168.0	a
	120	2.7	2.39×10^{12}	1.26	1.00	1.26	3.4	−173.0	a
	120	2.7	1.32×10^{12}	1.26	1.00	1.26	4.0	−177.5	a
C^{15}N	200	20	2.48×10^{13}	0.99	1.00	0.99	30.0	5.0	e
	120	2.7	1.90×10^{13}	1.27	1.00	1.27	12.0	4.0	a
	120	2.7	1.09×10^{11}	1.27	1.00	1.27	4.5	−26.0	a
	120	2.7	6.89×10^{11}	1.27	1.00	1.27	4.5	−31.0	a
	120	2.7	1.69×10^{11}	1.27	1.00	1.27	3.5	−39.0	a
	120	2.7	4.23×10^{11}	1.27	1.00	1.27	4.0	−43.8	a
	120	2.7	5.08×10^{11}	1.27	1.00	1.27	4.0	−48.5	a
	120	2.7	1.18×10^{12}	1.27	1.00	1.27	4.5	−53.8	a
	120	2.7	2.12×10^{12}	1.27	1.00	1.27	6.0	−60.5	a
	120	2.7	9.73×10^{10}	1.27	1.00	1.27	3.7	−70.5	a
	120	2.7	8.71×10^{10}	1.27	1.00	1.27	2.7	−77.1	a
	120	2.7	2.36×10^{11}	1.27	1.00	1.27	2.5	−80.5	a
	120	2.7	3.63×10^{11}	1.27	1.00	1.27	4.0	−84.5	a
	120	2.7	2.91×10^{11}	1.27	1.00	1.27	2.5	−88.0	a
	120	2.7	1.89×10^{11}	1.27	1.00	1.27	2.5	−91.2	a
	120	2.7	7.25×10^{10}	1.27	1.00	1.27	4.0	−95.5	a
	120	2.7	1.09×10^{12}	1.27	1.00	1.27	2.5	−102.5	a
	120	2.7	5.80×10^{11}	1.27	1.00	1.27	3.5	−108.0	a
	120	2.7	1.14×10^{11}	1.27	1.00	1.27	3.0	−113.5	a
	120	2.7	2.07×10^{11}	1.27	1.00	1.27	3.0	−120.5	a
	120	2.7	4.23×10^{10}	1.27	1.00	1.27	3.0	−125.0	a
	120	2.7	1.10×10^{11}	1.27	1.00	1.27	3.5	−130.7	a

Table 79. continued.

Molecule[a]	Size[b] (″)	T_{rot}[c] (K)	N[d] (cm^{-2})	C_{int}[e]	C_{vib}[f]	C_N[g]	ΔV[h] (km s^{-1})	V_{off}[i] (km s^{-1})	F[j]
(1)	(2)	(3)	(4)	(5)	(6)	(7)	(8)	(9)	(10)
	120	2.7	6.76×10^{10}	1.27	1.00	1.27	3.0	−134.0	a
	120	2.7	2.75×10^{11}	1.27	1.00	1.27	4.5	−138.5	a
	120	2.7	2.96×10^{11}	1.27	1.00	1.27	6.0	−150.5	a
	120	2.7	2.83×10^{11}	1.27	1.00	1.27	3.8	−155.3	a
	120	2.7	3.39×10^{11}	1.27	1.00	1.27	3.5	−159.3	a
	120	2.7	9.30×10^{11}	1.27	1.00	1.27	4.0	−164.0	a
	120	2.7	3.59×10^{11}	1.27	1.00	1.27	3.5	−168.0	a
	120	2.7	1.61×10^{11}	1.27	1.00	1.27	3.4	−173.0	a
	120	2.7	8.88×10^{10}	1.27	1.00	1.27	4.0	−177.5	a

Table 80. Parameters of our best-fit model of CO toward Sgr B2(M).

Molecule[a]	Size[b] (″)	T_{rot}[c] (K)	N[d] (cm^{-2})	C_{int}[e]	C_{vib}[f]	C_N[g]	ΔV[h] (km s^{-1})	V_{off}[i] (km s^{-1})	F[j]
(1)	(2)	(3)	(4)	(5)	(6)	(7)	(8)	(9)	(10)
CO	200	58	6.90×10^{19}	0.99	1.00	0.99	16.0	−1.0	e
	20	16	1.80×10^{19}	1.00	1.00	1.00	20.0	23.0	e
	20	16	2.00×10^{18}	1.00	1.00	1.00	20.0	−23.0	e
	200	10	1.53×10^{17}	1.02	1.00	1.02	15.0	3.0	a
	200	2.7	5.04×10^{16}	1.29	1.00	1.29	2.0	−31.0	a
	200	2.7	4.63×10^{16}	1.29	1.00	1.29	2.0	−70.7	a
	200	2.7	6.69×10^{16}	1.29	1.00	1.29	2.0	−80.7	a
	200	2.7	4.21×10^{16}	1.29	1.00	1.29	2.0	−83.0	a
	200	2.7	3.34×10^{17}	1.29	1.00	1.29	2.2	−87.9	a
	200	2.7	5.14×10^{16}	1.29	1.00	1.29	2.0	−91.1	a
	200	2.7	4.21×10^{17}	1.29	1.00	1.29	2.2	−103.0	a
	200	2.7	2.61×10^{17}	1.29	1.00	1.29	2.1	−108.0	a
	200	2.7	1.03×10^{17}	1.29	1.00	1.29	2.2	−111.4	a
	200	2.7	2.57×10^{16}	1.29	1.00	1.29	2.3	−120.8	a
	200	2.7	4.63×10^{15}	1.29	1.00	1.29	2.1	−135.2	a
	200	2.7	1.93×10^{16}	1.29	1.00	1.29	2.4	−138.0	a
	200	2.7	6.43×10^{15}	1.29	1.00	1.29	3.0	−149.0	a
	200	2.7	3.86×10^{15}	1.29	1.00	1.29	2.5	−152.5	a
	200	2.7	7.20×10^{15}	1.29	1.00	1.29	3.0	−155.8	a
	200	2.7	1.67×10^{16}	1.29	1.00	1.29	3.5	−160.0	a
	200	2.7	2.25×10^{16}	1.29	1.00	1.29	2.2	−164.0	a
	200	2.7	1.67×10^{16}	1.29	1.00	1.29	4.5	−168.3	a
	200	2.7	5.66×10^{15}	1.29	1.00	1.29	1.8	−172.8	a
	200	2.7	2.57×10^{15}	1.29	1.00	1.29	2.0	−177.5	a
^{13}CO	200	58	3.45×10^{18}	0.99	1.00	0.99	16.0	−1.0	e
	20	16	8.98×10^{17}	1.00	1.00	1.00	20.0	23.0	e
	20	16	9.98×10^{16}	1.00	1.00	1.00	20.0	−23.0	e
	200	8.0	1.04×10^{17}	1.04	1.00	1.04	14.0	2.5	a
	200	2.7	1.25×10^{15}	1.27	1.00	1.27	2.0	−31.0	a
	200	2.7	2.29×10^{15}	1.27	1.00	1.27	2.0	−70.7	a
	200	2.7	1.65×10^{15}	1.27	1.00	1.27	2.0	−80.7	a
	200	2.7	1.04×10^{15}	1.27	1.00	1.27	2.0	−83.0	a
	200	2.7	8.26×10^{15}	1.27	1.00	1.27	2.2	−87.9	a
	200	2.7	1.27×10^{15}	1.27	1.00	1.27	2.0	−91.1	a
	200	2.7	1.04×10^{16}	1.27	1.00	1.27	2.2	−103.0	a
	200	2.7	6.44×10^{15}	1.27	1.00	1.27	2.1	−108.0	a
	200	2.7	2.54×10^{15}	1.27	1.00	1.27	2.2	−111.4	a
	200	2.7	1.27×10^{15}	1.27	1.00	1.27	2.3	−120.8	a
	200	2.7	2.29×10^{14}	1.27	1.00	1.27	2.1	−135.2	a
	200	2.7	9.53×10^{14}	1.27	1.00	1.27	2.4	−138.0	a
	200	2.7	3.17×10^{14}	1.27	1.00	1.27	3.0	−149.0	a
	200	2.7	1.91×10^{14}	1.27	1.00	1.27	2.5	−152.5	a
	200	2.7	3.56×10^{14}	1.27	1.00	1.27	3.0	−155.8	a
	200	2.7	8.26×10^{14}	1.27	1.00	1.27	3.5	−160.0	a

Notes. See notes of Table 62.

Table 80. continued.

Molecule[a]	Size[b] ('')	$T_{\rm rot}$[c] (K)	N[d] (cm^{-2})	$C_{\rm int}$[e]	$C_{\rm vib}$[f]	C_N[g]	ΔV[h]	$V_{\rm off}$[i]	F[j]
							(km s^{-1})		
(1)	(2)	(3)	(4)	(5)	(6)	(7)	(8)	(9)	(10)
	200	2.7	1.11×10^{15}	1.27	1.00	1.27	2.2	−164.0	a
	200	2.7	8.26×10^{14}	1.27	1.00	1.27	4.5	−168.3	a
	200	2.7	2.79×10^{14}	1.27	1.00	1.27	1.8	−172.8	a
	200	2.7	1.27×10^{14}	1.27	1.00	1.27	2.0	−177.5	a
C^{18}O	200	58	3.50×10^{17}	0.99	1.00	0.99	16.0	−1.0	e
	20	16	7.88×10^{16}	1.00	1.00	1.00	20.0	23.0	e
	20	16	9.98×10^{15}	1.00	1.00	1.00	20.0	−23.0	e
	200	8.0	1.04×10^{15}	1.04	1.00	1.04	12.0	3.0	a
	200	2.7	1.52×10^{14}	1.27	1.00	1.27	2.0	−31.0	a
	200	2.7	1.83×10^{14}	1.27	1.00	1.27	2.0	−70.7	a
	200	2.7	2.02×10^{14}	1.27	1.00	1.27	2.0	−80.7	a
	200	2.7	1.27×10^{14}	1.27	1.00	1.27	2.0	−83.0	a
	200	2.7	1.01×10^{15}	1.27	1.00	1.27	2.2	−87.9	a
	200	2.7	1.55×10^{14}	1.27	1.00	1.27	2.0	−91.1	a
	200	2.7	1.27×10^{15}	1.27	1.00	1.27	2.2	−103.0	a
	200	2.7	7.87×10^{14}	1.27	1.00	1.27	2.1	−108.0	a
	200	2.7	3.11×10^{14}	1.27	1.00	1.27	2.2	−111.4	a
	200	2.7	1.02×10^{14}	1.27	1.00	1.27	2.3	−120.8	a
	200	2.7	1.83×10^{13}	1.27	1.00	1.27	2.1	−135.2	a
	200	2.7	7.61×10^{13}	1.27	1.00	1.27	2.4	−138.0	a
	200	2.7	2.54×10^{13}	1.27	1.00	1.27	3.0	−149.0	a
	200	2.7	1.52×10^{13}	1.27	1.00	1.27	2.5	−152.5	a
	200	2.7	2.84×10^{13}	1.27	1.00	1.27	3.0	−155.8	a
	200	2.7	6.60×10^{13}	1.27	1.00	1.27	3.5	−160.0	a
	200	2.7	8.88×10^{13}	1.27	1.00	1.27	2.2	−164.0	a
	200	2.7	6.60×10^{13}	1.27	1.00	1.27	4.5	−168.3	a
	200	2.7	2.23×10^{13}	1.27	1.00	1.27	1.8	−172.8	a
	200	2.7	1.02×10^{13}	1.27	1.00	1.27	2.0	−177.5	a
C^{17}O	200	58	1.15×10^{17}	0.99	1.00	0.99	16.0	−1.0	e
	20	16	2.40×10^{16}	1.00	1.00	1.00	20.0	23.0	e
	20	16	3.46×10^{15}	1.00	1.00	1.00	20.0	−23.0	e
	200	8.0	3.62×10^{14}	1.04	1.00	1.04	12.0	3.0	a
	200	2.7	3.70×10^{13}	1.29	1.00	1.29	2.0	−31.0	a
	200	2.7	6.43×10^{13}	1.29	1.00	1.29	2.0	−70.7	a
	200	2.7	4.91×10^{13}	1.29	1.00	1.29	2.0	−80.7	a
	200	2.7	3.09×10^{13}	1.29	1.00	1.29	2.0	−83.0	a
	200	2.7	2.46×10^{14}	1.29	1.00	1.29	2.2	−87.9	a
	200	2.7	3.77×10^{13}	1.29	1.00	1.29	2.0	−91.1	a
	200	2.7	3.09×10^{14}	1.29	1.00	1.29	2.2	−103.0	a
	200	2.7	1.92×10^{14}	1.29	1.00	1.29	2.1	−108.0	a
	200	2.7	7.57×10^{13}	1.29	1.00	1.29	2.2	−111.4	a
	200	2.7	3.58×10^{13}	1.29	1.00	1.29	2.3	−120.8	a
	200	2.7	6.43×10^{12}	1.29	1.00	1.29	2.1	−135.2	a
	200	2.7	2.67×10^{13}	1.29	1.00	1.29	2.4	−138.0	a
	200	2.7	8.92×10^{12}	1.29	1.00	1.29	3.0	−149.0	a
	200	2.7	5.36×10^{12}	1.29	1.00	1.29	2.5	−152.5	a
	200	2.7	1.00×10^{13}	1.29	1.00	1.29	3.0	−155.8	a
	200	2.7	2.33×10^{13}	1.29	1.00	1.29	3.5	−160.0	a
	200	2.7	3.12×10^{13}	1.29	1.00	1.29	2.2	−164.0	a
	200	2.7	2.33×10^{13}	1.29	1.00	1.29	4.5	−168.3	a
	200	2.7	7.86×10^{12}	1.29	1.00	1.29	1.8	−172.8	a
	200	2.7	3.58×10^{12}	1.29	1.00	1.29	2.0	−177.5	a
^{13}C^{18}O	200	58	1.38×10^{16}	0.99	1.00	0.99	16.0	−1.0	e
	20	16	3.94×10^{15}	1.00	1.00	1.00	20.0	23.0	e
	20	16	4.99×10^{14}	1.00	1.00	1.00	20.0	−23.0	e
	200	8.0	5.21×10^{13}	1.04	1.00	1.04	12.0	3.0	a
	200	2.7	3.86×10^{12}	1.29	1.00	1.29	2.0	−31.0	a
	200	2.7	9.26×10^{12}	1.29	1.00	1.29	2.0	−70.7	a
	200	2.7	5.12×10^{12}	1.29	1.00	1.29	2.0	−80.7	a
	200	2.7	3.21×10^{12}	1.29	1.00	1.29	2.0	−83.0	a

Table 80. continued.

Molecule[a]	Size[b] ($''$)	T_{rot}[c] (K)	N[d] (cm^{-2})	C_{int}[e]	C_{vib}[f]	C_N[g]	ΔV[h] (km s^{-1})	V_{off}[i] (km s^{-1})	F[j]
(1)	(2)	(3)	(4)	(5)	(6)	(7)	(8)	(9)	(10)
	200	2.7	2.56×10^{13}	1.29	1.00	1.29	2.2	−87.9	a
	200	2.7	3.92×10^{12}	1.29	1.00	1.29	2.0	−91.1	a
	200	2.7	3.21×10^{13}	1.29	1.00	1.29	2.2	−103.0	a
	200	2.7	1.99×10^{13}	1.29	1.00	1.29	2.1	−108.0	a
	200	2.7	7.88×10^{12}	1.29	1.00	1.29	2.2	−111.4	a
	200	2.7	5.14×10^{12}	1.29	1.00	1.29	2.3	−120.8	a
	200	2.7	9.26×10^{11}	1.29	1.00	1.29	2.1	−135.2	a
	200	2.7	3.86×10^{12}	1.29	1.00	1.29	2.4	−138.0	a
	200	2.7	1.29×10^{12}	1.29	1.00	1.29	3.0	−149.0	a
	200	2.7	7.72×10^{11}	1.29	1.00	1.29	2.5	−152.5	a
	200	2.7	1.44×10^{12}	1.29	1.00	1.29	3.0	−155.8	a
	200	2.7	3.34×10^{12}	1.29	1.00	1.29	3.5	−160.0	a
	200	2.7	4.50×10^{12}	1.29	1.00	1.29	2.2	−164.0	a
	200	2.7	3.34×10^{12}	1.29	1.00	1.29	4.5	−168.3	a
	200	2.7	1.13×10^{12}	1.29	1.00	1.29	1.8	−172.8	a
	200	2.7	5.14×10^{11}	1.29	1.00	1.29	2.0	−177.5	a
$^{13}C^{17}O$	200	58	3.95×10^{15}	0.99	1.00	0.99	16.0	−1.0	e
	20	16	1.20×10^{15}	1.00	1.00	1.00	20.0	23.0	e
	20	16	1.74×10^{14}	1.00	1.00	1.00	20.0	−23.0	e
	200	8.0	1.81×10^{13}	1.04	1.00	1.04	12.0	3.0	a
	200	2.7	9.26×10^{11}	1.29	1.00	1.29	2.0	−31.0	a
	200	2.7	3.21×10^{12}	1.29	1.00	1.29	2.0	−70.7	a
	200	2.7	1.23×10^{12}	1.29	1.00	1.29	2.0	−80.7	a
	200	2.7	7.72×10^{11}	1.29	1.00	1.29	2.0	−83.0	a
	200	2.7	6.15×10^{12}	1.29	1.00	1.29	2.2	−87.9	a
	200	2.7	9.43×10^{11}	1.29	1.00	1.29	2.0	−91.1	a
	200	2.7	7.72×10^{12}	1.29	1.00	1.29	2.2	−103.0	a
	200	2.7	4.80×10^{12}	1.29	1.00	1.29	2.1	−108.0	a
	200	2.7	1.89×10^{12}	1.29	1.00	1.29	2.2	−111.4	a
	200	2.7	1.79×10^{12}	1.29	1.00	1.29	2.3	−120.8	a
	200	2.7	3.21×10^{11}	1.29	1.00	1.29	2.1	−135.2	a
	200	2.7	1.34×10^{12}	1.29	1.00	1.29	2.4	−138.0	a
	200	2.7	4.46×10^{11}	1.29	1.00	1.29	3.0	−149.0	a
	200	2.7	2.69×10^{11}	1.29	1.00	1.29	2.5	−152.5	a
	200	2.7	5.00×10^{11}	1.29	1.00	1.29	3.0	−155.8	a
	200	2.7	1.16×10^{12}	1.29	1.00	1.29	3.5	−160.0	a
	200	2.7	1.57×10^{12}	1.29	1.00	1.29	2.2	−164.0	a
	200	2.7	1.16×10^{12}	1.29	1.00	1.29	4.5	−168.3	a
	200	2.7	3.94×10^{11}	1.29	1.00	1.29	1.8	−172.8	a
	200	2.7	1.79×10^{11}	1.29	1.00	1.29	2.0	−177.5	a

Table 81. Parameters of our best-fit model of CS toward Sgr B2(M).

Molecule[a]	Size[b] ($''$)	T_{rot}[c] (K)	N[d] (cm^{-2})	C_{int}[e]	C_{vib}[f]	C_N[g]	ΔV[h] (km s^{-1})	V_{off}[i] (km s^{-1})	F[j]
(1)	(2)	(3)	(4)	(5)	(6)	(7)	(8)	(9)	(10)
CS	200	20	1.49×10^{16}	1.00	1.00	1.00	18.0	0.0	e
	20	16	5.00×10^{15}	1.00	1.00	1.00	20.0	20.0	e
	120	4.2	1.06×10^{15}	1.06	1.00	1.06	14.5	4.0	a
	120	2.7	1.05×10^{13}	1.11	1.00	1.11	3.5	−30.7	a
	120	2.7	1.06×10^{14}	1.11	1.00	1.11	6.5	−44.2	a
	120	2.7	5.86×10^{13}	1.11	1.00	1.11	6.5	−53.8	a
	120	2.7	2.48×10^{14}	1.11	1.00	1.11	5.7	−59.8	a
	120	2.7	3.88×10^{12}	1.11	1.00	1.11	6.0	−78.0	a
	120	2.7	4.88×10^{13}	1.11	1.00	1.11	4.3	−82.7	a
	120	2.7	9.98×10^{12}	1.11	1.00	1.11	3.0	−88.0	a
	120	2.7	5.54×10^{12}	1.11	1.00	1.11	4.0	−91.5	a
	120	2.7	1.39×10^{14}	1.11	1.00	1.11	2.5	−103.2	a
	120	2.7	4.15×10^{13}	1.11	1.00	1.11	2.5	−108.0	a

Notes. See notes of Table 62.

Table 81. continued.

Molecule[a]	Size[b] ('')	T_{rot}[c] (K)	N[d] (cm^{-2})	C_{int}[e]	C_{vib}[f]	C_N[g]	ΔV[h]	V_{off}[i] (km s^{-1})	F[j]
(1)	(2)	(3)	(4)	(5)	(6)	(7)	(8)	(9)	(10)
	120	2.7	5.54×10^{12}	1.11	1.00	1.11	4.0	−111.0	a
	120	2.7	2.00×10^{12}	1.11	1.00	1.11	3.5	−120.0	a
	120	2.7	2.99×10^{12}	1.11	1.00	1.11	5.0	−125.0	a
	120	2.7	5.54×10^{12}	1.11	1.00	1.11	3.5	−131.3	a
	120	2.7	1.22×10^{13}	1.11	1.00	1.11	3.5	−139.0	a
	120	2.7	9.98×10^{12}	1.11	1.00	1.11	5.0	−149.0	a
	120	2.7	3.17×10^{13}	1.11	1.00	1.11	4.0	−153.7	a
	120	2.7	2.07×10^{13}	1.11	1.00	1.11	3.0	−157.3	a
	120	2.7	1.33×10^{13}	1.11	1.00	1.11	3.8	−159.9	a
	120	2.7	5.12×10^{13}	1.11	1.00	1.11	3.2	−164.0	a
	120	2.7	4.15×10^{13}	1.11	1.00	1.11	3.5	−168.2	a
	120	2.7	3.33×10^{12}	1.11	1.00	1.11	3.0	−173.3	a
	120	2.7	2.22×10^{12}	1.11	1.00	1.11	4.0	−177.7	a
^{13}CS	200	20	7.47×10^{14}	1.00	1.00	1.00	18.0	0.0	e
	20	16	2.50×10^{14}	1.00	1.00	1.00	20.0	20.0	e
	120	2.7	1.55×10^{14}	1.11	1.00	1.11	14.5	4.0	a
	120	2.7	2.64×10^{11}	1.11	1.00	1.11	3.5	−30.7	a
	120	2.7	1.77×10^{12}	1.11	1.00	1.11	6.5	−44.2	a
	120	2.7	2.93×10^{12}	1.11	1.00	1.11	6.5	−53.8	a
	120	2.7	1.24×10^{13}	1.11	1.00	1.11	5.7	−59.8	a
	120	2.7	9.70×10^{10}	1.11	1.00	1.11	6.0	−78.0	a
	120	2.7	1.22×10^{12}	1.11	1.00	1.11	3.3	−82.7	a
	120	2.7	2.50×10^{11}	1.11	1.00	1.11	3.0	−88.0	a
	120	2.7	1.39×10^{11}	1.11	1.00	1.11	4.0	−91.5	a
	120	2.7	3.48×10^{12}	1.11	1.00	1.11	2.5	−103.2	a
	120	2.7	1.04×10^{12}	1.11	1.00	1.11	2.5	−108.0	a
	120	2.7	1.39×10^{11}	1.11	1.00	1.11	4.0	−111.0	a
	120	2.7	9.98×10^{10}	1.11	1.00	1.11	3.5	−120.0	a
	120	2.7	1.50×10^{11}	1.11	1.00	1.11	5.0	−125.0	a
	120	2.7	2.77×10^{11}	1.11	1.00	1.11	3.5	−131.3	a
	120	2.7	6.10×10^{11}	1.11	1.00	1.11	3.5	−139.0	a
	120	2.7	4.99×10^{11}	1.11	1.00	1.11	5.0	−149.0	a
	120	2.7	1.59×10^{12}	1.11	1.00	1.11	4.0	−153.7	a
	120	2.7	1.04×10^{12}	1.11	1.00	1.11	3.0	−157.3	a
	120	2.7	6.65×10^{11}	1.11	1.00	1.11	3.8	−159.9	a
	120	2.7	2.56×10^{12}	1.11	1.00	1.11	3.2	−164.0	a
	120	2.7	2.07×10^{12}	1.11	1.00	1.11	3.5	−168.2	a
	120	2.7	1.66×10^{11}	1.11	1.00	1.11	3.0	−173.3	a
	120	2.7	1.11×10^{11}	1.11	1.00	1.11	4.0	−177.7	a
C^{34}S	200	20	6.78×10^{14}	1.00	1.00	1.00	18.0	0.0	e
	20	16	2.27×10^{14}	1.00	1.00	1.00	20.0	20.0	e
	120	2.7	1.77×10^{14}	1.11	1.00	1.11	14.5	4.0	a
	120	2.7	4.79×10^{11}	1.11	1.00	1.11	3.5	−30.7	a
	120	2.7	4.84×10^{12}	1.11	1.00	1.11	6.5	−44.2	a
	120	2.7	2.66×10^{12}	1.11	1.00	1.11	6.5	−53.8	a
	120	2.7	1.13×10^{13}	1.11	1.00	1.11	5.7	−59.8	a
	120	2.7	1.76×10^{11}	1.11	1.00	1.11	6.0	−78.0	a
	120	2.7	2.22×10^{12}	1.11	1.00	1.11	3.3	−82.7	a
	120	2.7	4.54×10^{11}	1.11	1.00	1.11	3.0	−88.0	a
	120	2.7	2.52×10^{11}	1.11	1.00	1.11	4.0	−91.5	a
	120	2.7	6.32×10^{12}	1.11	1.00	1.11	2.5	−103.2	a
	120	2.7	1.89×10^{12}	1.11	1.00	1.11	2.5	−108.0	a
	120	2.7	2.52×10^{11}	1.11	1.00	1.11	4.0	−111.0	a
	120	2.7	9.07×10^{10}	1.11	1.00	1.11	3.5	−120.0	a
	120	2.7	1.36×10^{11}	1.11	1.00	1.11	5.0	−125.0	a
	120	2.7	2.52×10^{11}	1.11	1.00	1.11	3.5	−131.3	a
	120	2.7	5.54×10^{11}	1.11	1.00	1.11	3.5	−139.0	a
	120	2.7	4.54×10^{11}	1.11	1.00	1.11	5.0	−149.0	a
	120	2.7	1.44×10^{12}	1.11	1.00	1.11	4.0	−153.7	a
	120	2.7	9.43×10^{11}	1.11	1.00	1.11	3.0	−157.3	a

Table 81. continued.

Molecule[a]	Size[b] (")	$T_{\rm rot}$[c] (K)	N[d] (cm^{-2})	$C_{\rm int}$[e]	$C_{\rm vib}$[f]	C_N[g]	ΔV[h]	$V_{\rm off}$[i] (km s^{-1})	F[j]
(1)	(2)	(3)	(4)	(5)	(6)	(7)	(8)	(9)	(10)
	120	2.7	6.04×10^{11}	1.11	1.00	1.11	3.8	−159.9	a
	120	2.7	2.33×10^{12}	1.11	1.00	1.11	3.2	−164.0	a
	120	2.7	1.89×10^{12}	1.11	1.00	1.11	3.5	−168.2	a
	120	2.7	1.51×10^{11}	1.11	1.00	1.11	3.0	−173.3	a
	120	2.7	1.01×10^{11}	1.11	1.00	1.11	4.0	−177.7	a
C^{33}S	200	20	1.35×10^{14}	1.00	1.00	1.00	18.0	0.0	e
	20	16	4.54×10^{13}	1.00	1.00	1.00	20.0	20.0	e
	120	2.7	3.88×10^{13}	1.11	1.00	1.11	14.5	4.0	a
	120	2.7	9.58×10^{10}	1.11	1.00	1.11	3.5	−30.7	a
	120	2.7	9.67×10^{11}	1.11	1.00	1.11	6.5	−44.2	a
	120	2.7	5.32×10^{11}	1.11	1.00	1.11	6.5	−53.8	a
	120	2.7	2.26×10^{12}	1.11	1.00	1.11	5.7	−59.8	a
	120	2.7	3.53×10^{10}	1.11	1.00	1.11	6.0	−78.0	a
	120	2.7	4.44×10^{11}	1.11	1.00	1.11	3.3	−82.7	a
	120	2.7	9.07×10^{10}	1.11	1.00	1.11	3.0	−88.0	a
	120	2.7	5.03×10^{10}	1.11	1.00	1.11	4.0	−91.5	a
	120	2.7	1.26×10^{12}	1.11	1.00	1.11	2.5	−103.2	a
	120	2.7	3.77×10^{11}	1.11	1.00	1.11	2.5	−108.0	a
	120	2.7	5.03×10^{10}	1.11	1.00	1.11	4.0	−111.0	a
	120	2.7	1.82×10^{10}	1.11	1.00	1.11	3.5	−120.0	a
	120	2.7	2.73×10^{10}	1.11	1.00	1.11	5.0	−125.0	a
	120	2.7	5.03×10^{10}	1.11	1.00	1.11	3.5	−131.3	a
	120	2.7	1.11×10^{11}	1.11	1.00	1.11	3.5	−139.0	a
	120	2.7	9.07×10^{10}	1.11	1.00	1.11	5.0	−149.0	a
	120	2.7	2.88×10^{11}	1.11	1.00	1.11	4.0	−153.7	a
	120	2.7	1.89×10^{11}	1.11	1.00	1.11	3.0	−157.3	a
	120	2.7	1.21×10^{11}	1.11	1.00	1.11	3.8	−159.9	a
	120	2.7	4.66×10^{11}	1.11	1.00	1.11	3.2	−164.0	a
	120	2.7	3.77×10^{11}	1.11	1.00	1.11	3.5	−168.2	a
	120	2.7	3.02×10^{10}	1.11	1.00	1.11	3.0	−173.3	a
	120	2.7	2.02×10^{10}	1.11	1.00	1.11	4.0	−177.7	a
^{13}C^{34}S	200	20	3.40×10^{13}	1.00	1.00	1.00	18.0	0.0	e
	20	16	1.14×10^{13}	1.00	1.00	1.00	20.0	20.0	e
	120	2.7	8.87×10^{12}	1.11	1.00	1.11	14.5	4.0	a
	120	2.7	1.20×10^{10}	1.11	1.00	1.11	3.5	−30.7	a
	120	2.7	8.06×10^{10}	1.11	1.00	1.11	6.5	−44.2	a
	120	2.7	1.33×10^{11}	1.11	1.00	1.11	6.5	−53.8	a
	120	2.7	5.64×10^{11}	1.11	1.00	1.11	5.7	−59.8	a
	120	2.7	4.41×10^{9}	1.11	1.00	1.11	6.0	−78.0	a
	120	2.7	5.54×10^{10}	1.11	1.00	1.11	3.3	−82.7	a
	120	2.7	1.13×10^{10}	1.11	1.00	1.11	3.0	−88.0	a
	120	2.7	6.30×10^{9}	1.11	1.00	1.11	4.0	−91.5	a
	120	2.7	1.59×10^{11}	1.11	1.00	1.11	2.5	−103.2	a
	120	2.7	4.71×10^{10}	1.11	1.00	1.11	2.5	−108.0	a
	120	2.7	6.30×10^{9}	1.11	1.00	1.11	4.0	−111.0	a
	120	2.7	4.54×10^{9}	1.11	1.00	1.11	3.5	−120.0	a
	120	2.7	6.81×10^{9}	1.11	1.00	1.11	5.0	−125.0	a
	120	2.7	1.26×10^{10}	1.11	1.00	1.11	3.5	−131.3	a
	120	2.7	2.77×10^{10}	1.11	1.00	1.11	3.5	−139.0	a
	120	2.7	2.27×10^{10}	1.11	1.00	1.11	5.0	−149.0	a
	120	2.7	7.21×10^{10}	1.11	1.00	1.11	4.0	−153.7	a
	120	2.7	4.71×10^{10}	1.11	1.00	1.11	3.0	−157.3	a
	120	2.7	3.03×10^{10}	1.11	1.00	1.11	3.8	−159.9	a
	120	2.7	1.16×10^{11}	1.11	1.00	1.11	3.2	−164.0	a
	120	2.7	9.43×10^{10}	1.11	1.00	1.11	3.5	−168.2	a
	120	2.7	7.56×10^{9}	1.11	1.00	1.11	3.0	−173.3	a
	120	2.7	5.05×10^{9}	1.11	1.00	1.11	4.0	−177.7	a

Table 82. Parameters of our best-fit model of CH_2CO toward Sgr B2(M).

Molecule[a]	Size[b] (")	T_{rot}[c] (K)	N[d] (cm^{-2})	C_{int}[e]	C_{vib}[f]	C_N[g]	ΔV[h] (km s^{-1})	V_{off}[i] (km s^{-1})	F[j]
(1)	(2)	(3)	(4)	(5)	(6)	(7)	(8)	(9)	(10)
CH_2CO	60	20	2.10×10^{14}	1.05	1.00	1.05	14.0	0.0	e
	1.1	200	3.95×10^{17}	0.99	1.00	0.99	12.0	3.0	e
$CH_2^{13}CO$	60	20	1.05×10^{13}	1.05	1.00	1.05	14.0	0.0	e
	1.1	200	1.97×10^{16}	0.99	1.00	0.99	12.0	3.0	e
$^{13}CH_2CO$	60	20	1.05×10^{13}	1.05	1.00	1.05	14.0	0.0	e
	1.1	200	1.97×10^{16}	0.99	1.00	0.99	12.0	3.0	e

Notes. See notes of Table 62.

Table 83. Parameters of our best-fit model of H_2CO toward Sgr B2(M).

Molecule[a]	Size[b] (")	T_{rot}[c] (K)	N[d] (cm^{-2})	C_{int}[e]	C_{vib}[f]	C_N[g]	ΔV[h] (km s^{-1})	V_{off}[i] (km s^{-1})	F[j]
(1)	(2)	(3)	(4)	(5)	(6)	(7)	(8)	(9)	(10)
H_2CO	4.0	100	2.32×10^{17}	1.01	1.00	1.01	13.0	3.0	e
	200	5.0	3.17×10^{15}	0.79	1.00	0.79	16.0	4.0	a
$H_2^{13}CO$	4.0	100	1.16×10^{16}	1.01	1.00	1.01	13.0	3.0	e
	200	2.7	1.80×10^{14}	0.90	1.00	0.90	16.0	4.0	a
$H_2C^{18}O$	4.0	100	9.29×10^{14}	1.01	1.00	1.01	13.0	3.0	e
	200	2.7	1.43×10^{13}	0.90	1.00	0.90	16.0	4.0	a

Notes. See notes of Table 62.

Table 84. Parameters of our best-fit model of H_2CS toward Sgr B2(M).

Molecule[a]	Size[b] (")	T_{rot}[c] (K)	N[d] (cm^{-2})	C_{int}[e]	C_{vib}[f]	C_N[g]	ΔV[h] (km s^{-1})	V_{off}[i] (km s^{-1})	F[j]
(1)	(2)	(3)	(4)	(5)	(6)	(7)	(8)	(9)	(10)
H_2CS	2.0	150	1.60×10^{17}	1.00	1.00	1.00	13.0	2.0	e
	120	15	2.72×10^{14}	1.01	1.00	1.01	12.0	−5.0	e
	20	15	3.33×10^{14}	1.01	1.00	1.01	17.0	20.0	e
$H_2^{13}CS$	2.0	150	7.98×10^{15}	1.00	1.00	1.00	13.0	2.0	e
	120	15	1.36×10^{13}	1.01	1.00	1.01	12.0	−5.0	e
	20	15	1.66×10^{13}	1.01	1.00	1.01	17.0	20.0	e
$H_2C^{34}S$	2.0	150	7.98×10^{15}	1.00	1.00	1.00	13.0	2.0	e
	120	15	1.36×10^{13}	1.01	1.00	1.01	12.0	−5.0	e
	20	15	1.66×10^{13}	1.01	1.00	1.01	17.0	20.0	e

Notes. See notes of Table 62.

Table 85. Parameters of our best-fit model of H_2S toward Sgr B2(M).

Molecule[a]	Size[b] (")	T_{rot}[c] (K)	N[d] (cm^{-2})	C_{int}[e]	C_{vib}[f]	C_N[g]	ΔV[h] (km s^{-1})	V_{off}[i] (km s^{-1})	F[j]
(1)	(2)	(3)	(4)	(5)	(6)	(7)	(8)	(9)	(10)
H_2S	5.0	145	6.77×10^{17}	0.99	1.00	0.99	12.0	−1.5	e
	5.0	145	1.29×10^{16}	0.99	1.00	0.99	13.0	18.0	e
	5.0	145	1.79×10^{16}	0.99	1.00	0.99	13.0	−18.0	e
$H_2^{34}S$	5.0	145	3.08×10^{16}	0.99	1.00	0.99	12.0	−1.5	e
	5.0	145	5.87×10^{14}	0.99	1.00	0.99	13.0	18.0	e
	5.0	145	8.12×10^{14}	0.99	1.00	0.99	13.0	−18.0	e
$H_2^{33}S$	5.0	145	6.16×10^{15}	0.99	1.00	0.99	12.0	−1.5	e
	5.0	145	1.17×10^{14}	0.99	1.00	0.99	13.0	18.0	e
	5.0	145	1.63×10^{14}	0.99	1.00	0.99	13.0	−18.0	e

Notes. See notes of Table 62.

Table 86. Parameters of our best-fit model of HC_3N toward Sgr B2(M).

Molecule[a]	Size[b] ('')	T_{rot}[c] (K)	N[d] (cm^{-2})	C_{int}[e]	C_{vib}[f]	C_N[g]	ΔV[h] (km s^{-1})	V_{off}[i]	F[j]
(1)	(2)	(3)	(4)	(5)	(6)	(7)	(8)	(9)	(10)
HC_3N	60	60	4.50×10^{14}	1.00	1.00	1.00	14.0	0.0	e
	20	20	2.40×10^{14}	1.00	1.00	1.00	30.0	11.0	e
	20	20	2.40×10^{14}	1.00	1.00	1.00	30.0	−8.0	e
$HC_3N, v_7 = 1$	1.3	200	5.07×10^{17}	1.00	1.69	1.69	10.0	3.0	e
$HC_3N, v_7 = 2$	1.3	200	5.07×10^{17}	1.00	1.69	1.69	10.0	3.0	e
$HC_3N, v_6 = 1$	1.3	200	6.76×10^{17}	1.00	1.69	1.69	10.0	3.0	e
$HC_3N, v_5 = 1/v_7 = 3$	1.3	200	1.35×10^{18}	1.00	1.69	1.69	10.0	3.0	e
$HC_3N, v_6 = v_7 = 1$	1.3	200	1.35×10^{18}	1.00	1.69	1.69	10.0	3.0	e
$HC_3N, v_4 = 1$	1.3	200	2.54×10^{18}	1.00	1.69	1.69	10.0	3.0	e
$H^{13}CCCN$	60	60	3.40×10^{13}	1.00	1.00	1.00	14.0	0.0	e
	20	20	1.20×10^{13}	1.00	1.00	1.00	30.0	11.0	e
	20	20	1.20×10^{13}	1.00	1.00	1.00	30.0	−8.0	e
$HC^{13}CCN$	60	60	3.40×10^{13}	1.00	1.00	1.00	14.0	0.0	e
	20	20	1.20×10^{13}	1.00	1.00	1.00	30.0	11.0	e
	20	20	1.20×10^{13}	1.00	1.00	1.00	30.0	−8.0	e
$HCC^{13}CN$	60	60	3.40×10^{13}	1.00	1.00	1.00	14.0	0.0	e
	20	20	1.20×10^{13}	1.00	1.00	1.00	30.0	11.0	e
	20	20	1.20×10^{13}	1.00	1.00	1.00	30.0	−8.0	e
$H^{13}CCCN, v_7 = 1$	1.3	200	2.54×10^{16}	1.00	1.69	1.69	10.0	3.0	e
$HC^{13}CCN, v_7 = 1$	1.3	200	2.54×10^{16}	1.00	1.69	1.69	10.0	3.0	e
$HCC^{13}CN, v_7 = 1$	1.3	200	2.54×10^{16}	1.00	1.69	1.69	10.0	3.0	e
$H^{13}CCCN, v_7 = 2$	1.3	200	2.54×10^{16}	1.00	1.69	1.69	10.0	3.0	e
$HC^{13}CCN, v_7 = 2$	1.3	200	2.54×10^{16}	1.00	1.69	1.69	10.0	3.0	e
$HCC^{13}CN, v_7 = 2$	1.3	200	2.54×10^{16}	1.00	1.69	1.69	10.0	3.0	e
$H^{13}CCCN, v_6 = 1$	1.3	200	4.22×10^{16}	1.00	1.69	1.69	10.0	3.0	e
$HC^{13}CCN, v_6 = 1$	1.3	200	4.22×10^{16}	1.00	1.69	1.69	10.0	3.0	e
$HCC^{13}CN, v_6 = 1$	1.3	200	4.22×10^{16}	1.00	1.69	1.69	10.0	3.0	e

Notes. See notes of Table 62.

Table 87. Parameters of our best-fit model of HC_5N toward Sgr B2(M).

Molecule[a]	Size[b] ('')	T_{rot}[c] (K)	N[d] (cm^{-2})	C_{int}[e]	C_{vib}[f]	C_N[g]	ΔV[h] (km s^{-1})	V_{off}[i]	F[j]
(1)	(2)	(3)	(4)	(5)	(6)	(7)	(8)	(9)	(10)
HC_5N	2.0	200	1.16×10^{16}	1.00	5.79	5.79	8.0	−1.0	e
	60	20	1.30×10^{14}	1.00	1.00	1.00	10.0	−1.0	e
$HC_5N, v_{11} = 1$	2.0	200	1.16×10^{16}	1.00	5.79	5.79	8.0	−1.0	e

Notes. See notes of Table 62.

Table 88. Parameters of our best-fit model of HCN toward Sgr B2(M).

Molecule[a]	Size[b] (″)	$T_{\rm rot}$[c] (K)	N[d] (cm^{-2})	$C_{\rm int}$[e]	$C_{\rm vib}$[f]	C_N[g]	ΔV[h] (km s^{-1})	$V_{\rm off}$[i] (km s^{-1})	F[j]
(1)	(2)	(3)	(4)	(5)	(6)	(7)	(8)	(9)	(10)
HCN	200	20	1.79×10^{16}	0.99	1.00	0.99	25.0	3.0	e
	20	16	2.61×10^{15}	1.00	1.00	1.00	20.0	28.0	e
	120	4.4	1.13×10^{15}	1.13	1.00	1.13	18.0	2.0	a
	120	2.7	8.94×10^{13}	1.24	1.00	1.24	7.0	−27.0	a
	120	2.7	3.97×10^{13}	1.24	1.00	1.24	4.0	−32.5	a
	120	2.7	1.04×10^{13}	1.24	1.00	1.24	3.0	−36.5	a
	120	2.7	2.01×10^{14}	1.24	1.00	1.24	9.0	−43.0	a
	120	2.7	1.79×10^{14}	1.24	1.00	1.24	6.0	−50.0	a
	120	2.7	7.70×10^{13}	1.24	1.00	1.24	4.2	−54.6	a
	120	2.7	2.11×10^{14}	1.24	1.00	1.24	7.0	−59.9	a
	120	2.7	4.22×10^{13}	1.24	1.00	1.24	8.0	−67.5	a
	120	2.7	1.24×10^{13}	1.24	1.00	1.24	4.5	−77.5	a
	120	2.7	2.61×10^{13}	1.24	1.00	1.24	5.0	−83.2	a
	120	2.7	2.36×10^{13}	1.24	1.00	1.24	5.0	−88.3	a
	120	2.7	1.14×10^{13}	1.24	1.00	1.24	5.0	−93.0	a
	120	2.7	2.63×10^{13}	1.24	1.00	1.24	3.8	−98.5	a
	120	2.7	3.63×10^{13}	1.24	1.00	1.24	2.6	−103.9	a
	120	2.7	1.61×10^{13}	1.24	1.00	1.24	3.0	−108.0	a
	120	2.7	1.74×10^{13}	1.24	1.00	1.24	3.0	−111.5	a
	120	2.7	8.45×10^{12}	1.24	1.00	1.24	3.5	−116.5	a
	120	2.7	8.32×10^{12}	1.24	1.00	1.24	3.5	−121.3	a
	120	2.7	5.59×10^{12}	1.24	1.00	1.24	5.0	−128.0	a
	120	2.7	9.56×10^{12}	1.24	1.00	1.24	5.5	−134.2	a
	120	2.7	7.33×10^{12}	1.24	1.00	1.24	4.0	−139.2	a
	120	2.7	7.45×10^{12}	1.24	1.00	1.24	5.0	−146.3	a
	120	2.7	8.69×10^{12}	1.24	1.00	1.24	4.0	−150.5	a
	120	2.7	1.24×10^{13}	1.24	1.00	1.24	4.0	−154.6	a
	120	2.7	2.24×10^{13}	1.24	1.00	1.24	4.0	−159.2	a
	120	2.7	4.97×10^{13}	1.24	1.00	1.24	5.0	−164.7	a
	120	2.7	1.49×10^{13}	1.24	1.00	1.24	4.0	−170.0	a
	120	2.7	9.44×10^{12}	1.24	1.00	1.24	4.0	−174.0	a
	120	2.7	2.48×10^{12}	1.24	1.00	1.24	4.0	−178.0	a
	120	2.7	1.24×10^{12}	1.24	1.00	1.24	4.0	−182.0	a
	120	2.7	9.94×10^{11}	1.24	1.00	1.24	4.0	−186.0	a
	120	2.7	4.35×10^{11}	1.24	1.00	1.24	5.0	−193.0	a
HCN, $v_2 = 1$	0.6	500	7.95×10^{19}	1.14	1.00	1.14	12.0	0.0	e
HCN, $v_2 = 2$	0.6	500	7.95×10^{19}	1.14	1.00	1.14	12.0	0.0	e
H^{13}CN	200	20	8.95×10^{14}	0.99	1.00	0.99	25.0	3.0	e
	20	16	1.30×10^{14}	1.00	1.00	1.00	20.0	28.0	e
	120	3.0	2.43×10^{14}	1.22	1.00	1.22	18.0	3.0	a
	120	2.7	2.24×10^{12}	1.24	1.00	1.24	7.0	−27.0	a
	120	2.7	9.94×10^{11}	1.24	1.00	1.24	4.0	−32.5	a
	120	2.7	2.61×10^{11}	1.24	1.00	1.24	3.0	−36.5	a
	120	2.7	3.35×10^{12}	1.24	1.00	1.24	9.0	−43.0	a
	120	2.7	2.98×10^{12}	1.24	1.00	1.24	6.0	−50.0	a
	120	2.7	3.85×10^{12}	1.24	1.00	1.24	4.2	−54.6	a
	120	2.7	1.06×10^{13}	1.24	1.00	1.24	7.0	−59.9	a
	120	2.7	2.11×10^{12}	1.24	1.00	1.24	8.0	−67.5	a
	120	2.7	3.10×10^{11}	1.24	1.00	1.24	4.5	−77.5	a
	120	2.7	6.52×10^{11}	1.24	1.00	1.24	5.0	−83.2	a
	120	2.7	5.90×10^{11}	1.24	1.00	1.24	5.0	−88.3	a
	120	2.7	2.86×10^{11}	1.24	1.00	1.24	5.0	−93.0	a
	120	2.7	6.58×10^{11}	1.24	1.00	1.24	3.8	−98.5	a
	120	2.7	9.07×10^{11}	1.24	1.00	1.24	2.6	−103.9	a
	120	2.7	4.04×10^{11}	1.24	1.00	1.24	3.0	−108.0	a
	120	2.7	4.35×10^{11}	1.24	1.00	1.24	3.0	−111.5	a
	120	2.7	4.22×10^{11}	1.24	1.00	1.24	3.5	−116.5	a
	120	2.7	4.16×10^{11}	1.24	1.00	1.24	3.5	−121.3	a
	120	2.7	2.79×10^{11}	1.24	1.00	1.24	5.0	−128.0	a

Notes. See notes of Table 62.

Table 88. continued.

Molecule[a]	Size[b] (″)	T_{rot}[c] (K)	N[d] (cm^{-2})	C_{int}[e]	C_{vib}[f]	C_N[g]	ΔV[h] (km s^{-1})	V_{off}[i]	F[j]
(1)	(2)	(3)	(4)	(5)	(6)	(7)	(8)	(9)	(10)
	120	2.7	4.78×10^{11}	1.24	1.00	1.24	5.5	−134.2	a
	120	2.7	3.66×10^{11}	1.24	1.00	1.24	4.0	−139.2	a
	120	2.7	3.73×10^{11}	1.24	1.00	1.24	5.0	−146.3	a
	120	2.7	4.35×10^{11}	1.24	1.00	1.24	4.0	−150.5	a
	120	2.7	6.21×10^{11}	1.24	1.00	1.24	4.0	−154.6	a
	120	2.7	1.12×10^{12}	1.24	1.00	1.24	4.0	−159.2	a
	120	2.7	2.48×10^{12}	1.24	1.00	1.24	5.0	−164.7	a
	120	2.7	7.45×10^{11}	1.24	1.00	1.24	4.0	−170.0	a
	120	2.7	4.72×10^{11}	1.24	1.00	1.24	4.0	−174.0	a
	120	2.7	1.24×10^{11}	1.24	1.00	1.24	4.0	−178.0	a
	120	2.7	6.21×10^{10}	1.24	1.00	1.24	4.0	−182.0	a
	120	2.7	4.97×10^{10}	1.24	1.00	1.24	4.0	−186.0	a
	120	2.7	2.17×10^{10}	1.24	1.00	1.24	5.0	−193.0	a
HC^{15}N	200	20	5.96×10^{13}	0.99	1.00	0.99	25.0	3.0	e
	20	16	8.70×10^{12}	1.00	1.00	1.00	20.0	28.0	e
	120	3.0	3.04×10^{13}	1.22	1.00	1.22	14.0	4.0	a
	120	2.7	2.56×10^{11}	1.24	1.00	1.24	7.0	−27.0	a
	120	2.7	1.13×10^{11}	1.24	1.00	1.24	4.0	−32.5	a
	120	2.7	2.98×10^{10}	1.24	1.00	1.24	3.0	−36.5	a
	120	2.7	4.47×10^{11}	1.24	1.00	1.24	9.0	−43.0	a
	120	2.7	3.97×10^{11}	1.24	1.00	1.24	6.0	−50.0	a
	120	2.7	2.57×10^{11}	1.24	1.00	1.24	4.2	−54.6	a
	120	2.7	7.04×10^{11}	1.24	1.00	1.24	7.0	−59.9	a
	120	2.7	1.40×10^{11}	1.24	1.00	1.24	8.0	−67.5	a
	120	2.7	3.55×10^{10}	1.24	1.00	1.24	4.5	−77.5	a
	120	2.7	7.45×10^{10}	1.24	1.00	1.24	5.0	−83.2	a
	120	2.7	6.74×10^{10}	1.24	1.00	1.24	5.0	−88.3	a
	120	2.7	3.26×10^{10}	1.24	1.00	1.24	5.0	−93.0	a
	120	2.7	7.52×10^{10}	1.24	1.00	1.24	3.8	−98.5	a
	120	2.7	1.03×10^{11}	1.24	1.00	1.24	2.6	−103.9	a
	120	2.7	4.60×10^{10}	1.24	1.00	1.24	3.0	−108.0	a
	120	2.7	4.96×10^{10}	1.24	1.00	1.24	3.0	−111.5	a
	120	2.7	2.82×10^{10}	1.24	1.00	1.24	3.5	−116.5	a
	120	2.7	2.77×10^{10}	1.24	1.00	1.24	3.5	−121.3	a
	120	2.7	1.86×10^{10}	1.24	1.00	1.24	5.0	−128.0	a
	120	2.7	3.19×10^{10}	1.24	1.00	1.24	5.5	−134.2	a
	120	2.7	2.44×10^{10}	1.24	1.00	1.24	4.0	−139.2	a
	120	2.7	2.48×10^{10}	1.24	1.00	1.24	5.0	−146.3	a
	120	2.7	2.89×10^{10}	1.24	1.00	1.24	4.0	−150.5	a
	120	2.7	4.13×10^{10}	1.24	1.00	1.24	4.0	−154.6	a
	120	2.7	7.45×10^{10}	1.24	1.00	1.24	4.0	−159.2	a
	120	2.7	1.65×10^{11}	1.24	1.00	1.24	5.0	−164.7	a
	120	2.7	4.96×10^{10}	1.24	1.00	1.24	4.0	−170.0	a
	120	2.7	3.14×10^{10}	1.24	1.00	1.24	4.0	−174.0	a
	120	2.7	8.28×10^{9}	1.24	1.00	1.24	4.0	−178.0	a
	120	2.7	4.13×10^{9}	1.24	1.00	1.24	4.0	−182.0	a
	120	2.7	3.31×10^{9}	1.24	1.00	1.24	4.0	−186.0	a
	120	2.7	1.45×10^{9}	1.24	1.00	1.24	5.0	−193.0	a
H^{13}C^{15}N	200	20	2.98×10^{12}	0.99	1.00	0.99	25.0	3.0	e
	20	16	4.34×10^{11}	1.00	1.00	1.00	20.0	28.0	e
	120	3.0	2.43×10^{12}	1.22	1.00	1.22	18.0	3.0	a
DCN	200	20	3.99×10^{12}	1.00	1.00	1.00	9.0	1.5	e

Table 89. Parameters of our best-fit model of NH_2CHO toward Sgr B2(M).

Molecule[a]	Size[b] ($''$)	T_{rot}[c] (K)	N[d] (cm^{-2})	C_{int}[e]	C_{vib}[f]	C_N[g]	ΔV[h] (km s^{-1})	V_{off}[i]	F[j]
(1)	(2)	(3)	(4)	(5)	(6)	(7)	(8)	(9)	(10)
NH_2CHO	3.0	200	1.40×10^{16}	1.00	1.17	1.17	12.0	2.0	e
	60	20	2.40×10^{14}	1.00	1.00	1.00	12.0	0.0	e
	60	5.0	2.12×10^{14}	1.02	1.00	1.02	8.0	−0.2	a
	60	5.0	8.14×10^{13}	1.02	1.00	1.02	5.0	6.0	a

Notes. See notes of Table 62.

Table 90. Parameters of our best-fit model of HCO^+ toward Sgr B2(M).

Molecule[a]	Size[b] ($''$)	T_{rot}[c] (K)	N[d] (cm^{-2})	C_{int}[e]	C_{vib}[f]	C_N[g]	ΔV[h] (km s^{-1})	V_{off}[i]	F[j]
(1)	(2)	(3)	(4)	(5)	(6)	(7)	(8)	(9)	(10)
HCO^+	200	20	7.45×10^{15}	0.99	1.00	0.99	12.0	0.0	e
	50	20	9.93×10^{14}	0.99	1.00	0.99	20.0	18.0	e
	50	20	7.94×10^{13}	0.99	1.00	0.99	20.0	42.0	e
	50	20	7.94×10^{14}	0.99	1.00	0.99	12.0	−11.0	e
	120	3.8	2.59×10^{15}	1.15	1.00	1.15	12.0	2.5	a
	120	2.7	1.96×10^{13}	1.23	1.00	1.23	7.0	−27.0	a
	120	2.7	3.19×10^{13}	1.23	1.00	1.23	5.0	−32.0	a
	120	2.7	1.23×10^{13}	1.23	1.00	1.23	3.0	−36.5	a
	120	2.7	1.55×10^{14}	1.23	1.00	1.23	5.0	−40.0	a
	120	2.7	1.25×10^{14}	1.23	1.00	1.23	5.0	−45.0	a
	120	2.7	1.11×10^{14}	1.23	1.00	1.23	6.0	−50.0	a
	120	2.7	2.46×10^{13}	1.23	1.00	1.23	4.5	−54.4	a
	120	2.7	8.47×10^{13}	1.23	1.00	1.23	6.2	−60.9	a
	120	2.7	1.23×10^{13}	1.23	1.00	1.23	7.0	−67.5	a
	120	2.7	1.23×10^{13}	1.23	1.00	1.23	5.0	−75.5	a
	120	2.7	2.70×10^{13}	1.23	1.00	1.23	5.0	−81.5	a
	120	2.7	2.95×10^{13}	1.23	1.00	1.23	5.0	−88.3	a
	120	2.7	8.84×10^{12}	1.23	1.00	1.23	5.0	−93.0	a
	120	2.7	4.91×10^{12}	1.23	1.00	1.23	4.0	−98.5	a
	120	2.7	6.39×10^{13}	1.23	1.00	1.23	3.3	−103.0	a
	120	2.7	2.46×10^{13}	1.23	1.00	1.23	3.0	−107.7	a
	120	2.7	1.23×10^{13}	1.23	1.00	1.23	3.0	−111.5	a
	120	2.7	4.05×10^{12}	1.23	1.00	1.23	4.0	−116.0	a
	120	2.7	1.17×10^{13}	1.23	1.00	1.23	4.0	−121.3	a
	120	2.7	8.60×10^{12}	1.23	1.00	1.23	5.0	−128.0	a
	120	2.7	8.60×10^{12}	1.23	1.00	1.23	5.0	−134.0	a
	120	2.7	8.60×10^{12}	1.23	1.00	1.23	4.0	−138.3	a
	120	2.7	5.53×10^{12}	1.23	1.00	1.23	4.0	−142.1	a
	120	2.7	1.04×10^{13}	1.23	1.00	1.23	5.0	−146.3	a
	120	2.7	8.60×10^{12}	1.23	1.00	1.23	3.5	−150.5	a
	120	2.7	1.11×10^{13}	1.23	1.00	1.23	3.5	−154.6	a
	120	2.7	1.35×10^{13}	1.23	1.00	1.23	4.0	−159.2	a
	120	2.7	3.19×10^{13}	1.23	1.00	1.23	5.0	−164.2	a
	120	2.7	7.37×10^{12}	1.23	1.00	1.23	4.0	−170.0	a
	120	2.7	9.82×10^{12}	1.23	1.00	1.23	4.0	−174.0	a
	120	2.7	7.37×10^{12}	1.23	1.00	1.23	4.0	−178.0	a
	120	2.7	2.46×10^{12}	1.23	1.00	1.23	4.0	−182.0	a
	120	2.7	2.46×10^{12}	1.23	1.00	1.23	4.0	−185.7	a
	120	2.7	4.05×10^{12}	1.23	1.00	1.23	8.0	−192.4	a
$H^{13}CO^+$	200	20	3.72×10^{14}	0.99	1.00	0.99	12.0	0.0	e
	50	20	4.96×10^{13}	0.99	1.00	0.99	20.0	18.0	e
	50	20	3.97×10^{12}	0.99	1.00	0.99	20.0	42.0	e
	50	20	3.97×10^{13}	0.99	1.00	0.99	12.0	−11.0	e
	120	3.1	1.33×10^{14}	1.17	1.00	1.17	12.0	2.5	a
	120	2.7	4.81×10^{11}	1.20	1.00	1.20	7.0	−27.0	a
	120	2.7	7.82×10^{11}	1.20	1.00	1.20	5.0	−32.0	a
	120	2.7	3.01×10^{11}	1.20	1.00	1.20	3.0	−36.5	a

Notes. See notes of Table 62.

Table 90. continued.

Molecule[a]	Size[b] ('')	$T_{\rm rot}$[c] (K)	N[d] (cm^{-2})	$C_{\rm int}$[e]	$C_{\rm vib}$[f]	C_N[g]	ΔV[h] (km s^{-1})	$V_{\rm off}$[i] (km s^{-1})	F[j]
(1)	(2)	(3)	(4)	(5)	(6)	(7)	(8)	(9)	(10)
	120	2.7	2.53×10^{12}	1.20	1.00	1.20	5.0	−40.0	a
	120	2.7	2.05×10^{12}	1.20	1.00	1.20	5.0	−45.0	a
	120	2.7	1.80×10^{12}	1.20	1.00	1.20	6.0	−50.0	a
	120	2.7	1.20×10^{12}	1.20	1.00	1.20	4.5	−54.4	a
	120	2.7	4.15×10^{12}	1.20	1.00	1.20	6.2	−60.9	a
	120	2.7	6.01×10^{11}	1.20	1.00	1.20	7.0	−67.5	a
	120	2.7	3.01×10^{11}	1.20	1.00	1.20	5.0	−75.5	a
	120	2.7	6.62×10^{11}	1.20	1.00	1.20	5.0	−81.5	a
	120	2.7	7.22×10^{11}	1.20	1.00	1.20	5.0	−88.3	a
	120	2.7	2.17×10^{11}	1.20	1.00	1.20	5.0	−93.0	a
	120	2.7	1.20×10^{11}	1.20	1.00	1.20	4.0	−98.5	a
	120	2.7	1.56×10^{12}	1.20	1.00	1.20	3.3	−103.0	a
	120	2.7	6.01×10^{11}	1.20	1.00	1.20	3.0	−107.7	a
	120	2.7	3.01×10^{11}	1.20	1.00	1.20	3.0	−111.5	a
	120	2.7	1.98×10^{11}	1.20	1.00	1.20	4.0	−116.0	a
	120	2.7	5.71×10^{11}	1.20	1.00	1.20	4.0	−121.3	a
	120	2.7	4.21×10^{11}	1.20	1.00	1.20	5.0	−128.0	a
	120	2.7	4.21×10^{11}	1.20	1.00	1.20	5.0	−134.0	a
	120	2.7	4.21×10^{11}	1.20	1.00	1.20	4.0	−138.3	a
	120	2.7	2.71×10^{11}	1.20	1.00	1.20	4.0	−142.1	a
	120	2.7	5.11×10^{11}	1.20	1.00	1.20	5.0	−146.3	a
	120	2.7	4.21×10^{11}	1.20	1.00	1.20	3.5	−150.5	a
	120	2.7	5.41×10^{11}	1.20	1.00	1.20	3.5	−154.6	a
	120	2.7	6.62×10^{11}	1.20	1.00	1.20	4.0	−159.2	a
	120	2.7	1.56×10^{12}	1.20	1.00	1.20	5.0	−164.2	a
	120	2.7	3.61×10^{11}	1.20	1.00	1.20	4.0	−170.0	a
	120	2.7	4.81×10^{11}	1.20	1.00	1.20	4.0	−174.0	a
	120	2.7	3.61×10^{11}	1.20	1.00	1.20	4.0	−178.0	a
	120	2.7	1.20×10^{11}	1.20	1.00	1.20	4.0	−182.0	a
	120	2.7	1.20×10^{11}	1.20	1.00	1.20	4.0	−185.7	a
	120	2.7	1.98×10^{11}	1.20	1.00	1.20	8.0	−192.4	a
HC^{18}O$^+$	200	20	2.98×10^{13}	0.99	1.00	0.99	12.0	1.0	e
	50	20	3.97×10^{12}	0.99	1.00	0.99	20.0	18.0	e
	50	20	3.17×10^{11}	0.99	1.00	0.99	20.0	42.0	e
	50	20	3.17×10^{12}	0.99	1.00	0.99	12.0	−11.0	e
	120	2.7	1.08×10^{13}	1.20	1.00	1.20	12.0	3.5	a
	120	2.7	5.86×10^{10}	1.20	1.00	1.20	7.0	−27.0	a
	120	2.7	9.53×10^{10}	1.20	1.00	1.20	5.0	−32.0	a
	120	2.7	3.67×10^{10}	1.20	1.00	1.20	3.0	−36.5	a
	120	2.7	2.70×10^{11}	1.20	1.00	1.20	5.0	−40.0	a
	120	2.7	2.18×10^{11}	1.20	1.00	1.20	5.0	−45.0	a
	120	2.7	1.93×10^{11}	1.20	1.00	1.20	6.0	−50.0	a
	120	2.7	9.59×10^{10}	1.20	1.00	1.20	4.5	−54.4	a
	120	2.7	3.31×10^{11}	1.20	1.00	1.20	6.2	−60.9	a
	120	2.7	4.80×10^{10}	1.20	1.00	1.20	7.0	−67.5	a
	120	2.7	3.67×10^{10}	1.20	1.00	1.20	5.0	−75.5	a
	120	2.7	8.07×10^{10}	1.20	1.00	1.20	5.0	−81.5	a
	120	2.7	8.80×10^{10}	1.20	1.00	1.20	5.0	−88.3	a
	120	2.7	2.64×10^{10}	1.20	1.00	1.20	5.0	−93.0	a
	120	2.7	1.46×10^{10}	1.20	1.00	1.20	4.0	−98.5	a
	120	2.7	1.91×10^{11}	1.20	1.00	1.20	3.3	−103.0	a
	120	2.7	7.34×10^{10}	1.20	1.00	1.20	3.0	−107.7	a
	120	2.7	3.67×10^{10}	1.20	1.00	1.20	3.0	−111.5	a
	120	2.7	1.58×10^{10}	1.20	1.00	1.20	4.0	−116.0	a
	120	2.7	4.56×10^{10}	1.20	1.00	1.20	4.0	−121.3	a
	120	2.7	3.36×10^{10}	1.20	1.00	1.20	5.0	−128.0	a
	120	2.7	3.36×10^{10}	1.20	1.00	1.20	5.0	−134.0	a
	120	2.7	3.36×10^{10}	1.20	1.00	1.20	4.0	−138.3	a
	120	2.7	2.16×10^{10}	1.20	1.00	1.20	4.0	−142.1	a
	120	2.7	4.08×10^{10}	1.20	1.00	1.20	5.0	−146.3	a
	120	2.7	3.36×10^{10}	1.20	1.00	1.20	3.5	−150.5	a

Table 90. continued.

Molecule[a]	Size[b] (″)	T_{rot}[c] (K)	N[d] (cm^{-2})	C_{int}[e]	C_{vib}[f]	C_N[g]	ΔV[h]	V_{off}[i] (km s^{-1})	F[j]
(1)	(2)	(3)	(4)	(5)	(6)	(7)	(8)	(9)	(10)
	120	2.7	4.32×10^{10}	1.20	1.00	1.20	3.5	−154.6	a
	120	2.7	5.28×10^{10}	1.20	1.00	1.20	4.0	−159.2	a
	120	2.7	1.25×10^{11}	1.20	1.00	1.20	5.0	−164.2	a
	120	2.7	2.88×10^{10}	1.20	1.00	1.20	4.0	−170.0	a
	120	2.7	3.84×10^{10}	1.20	1.00	1.20	4.0	−174.0	a
	120	2.7	2.88×10^{10}	1.20	1.00	1.20	4.0	−178.0	a
	120	2.7	9.59×10^{9}	1.20	1.00	1.20	4.0	−182.0	a
	120	2.7	9.59×10^{9}	1.20	1.00	1.20	4.0	−185.7	a
	120	2.7	1.58×10^{10}	1.20	1.00	1.20	8.0	−192.4	a
HC^{17}O$^+$	200	20	1.03×10^{13}	0.99	1.00	0.99	12.0	1.0	e
	50	20	1.37×10^{12}	0.99	1.00	0.99	20.0	18.0	e
	50	20	1.10×10^{11}	0.99	1.00	0.99	20.0	42.0	e
	50	20	1.10×10^{12}	0.99	1.00	0.99	12.0	−11.0	e
	120	2.7	3.78×10^{12}	1.20	1.00	1.20	12.0	3.5	a
	120	2.7	1.41×10^{10}	1.20	1.00	1.20	7.0	−27.0	a
	120	2.7	2.30×10^{10}	1.20	1.00	1.20	5.0	−32.0	a
	120	2.7	8.86×10^{9}	1.20	1.00	1.20	3.0	−36.5	a
	120	2.7	6.51×10^{10}	1.20	1.00	1.20	5.0	−40.0	a
	120	2.7	5.27×10^{10}	1.20	1.00	1.20	5.0	−45.0	a
	120	2.7	4.66×10^{10}	1.20	1.00	1.20	6.0	−50.0	a
	120	2.7	3.35×10^{10}	1.20	1.00	1.20	4.5	−54.4	a
	120	2.7	1.15×10^{11}	1.20	1.00	1.20	6.2	−60.9	a
	120	2.7	1.67×10^{10}	1.20	1.00	1.20	7.0	−67.5	a
	120	2.7	8.86×10^{9}	1.20	1.00	1.20	5.0	−75.5	a
	120	2.7	1.95×10^{10}	1.20	1.00	1.20	5.0	−81.5	a
	120	2.7	2.12×10^{10}	1.20	1.00	1.20	5.0	−88.3	a
	120	2.7	6.37×10^{9}	1.20	1.00	1.20	5.0	−93.0	a
	120	2.7	3.53×10^{9}	1.20	1.00	1.20	4.0	−98.5	a
	120	2.7	4.60×10^{10}	1.20	1.00	1.20	3.3	−103.0	a
	120	2.7	1.77×10^{10}	1.20	1.00	1.20	3.0	−107.7	a
	120	2.7	8.86×10^{9}	1.20	1.00	1.20	3.0	−111.5	a
	120	2.7	5.51×10^{9}	1.20	1.00	1.20	4.0	−116.0	a
	120	2.7	1.59×10^{10}	1.20	1.00	1.20	4.0	−121.3	a
	120	2.7	1.17×10^{10}	1.20	1.00	1.20	5.0	−128.0	a
	120	2.7	1.17×10^{10}	1.20	1.00	1.20	5.0	−134.0	a
	120	2.7	1.17×10^{10}	1.20	1.00	1.20	4.0	−138.3	a
	120	2.7	7.53×10^{9}	1.20	1.00	1.20	4.0	−142.1	a
	120	2.7	1.42×10^{10}	1.20	1.00	1.20	5.0	−146.3	a
	120	2.7	1.17×10^{10}	1.20	1.00	1.20	3.5	−150.5	a
	120	2.7	1.50×10^{10}	1.20	1.00	1.20	3.5	−154.6	a
	120	2.7	1.84×10^{10}	1.20	1.00	1.20	4.0	−159.2	a
	120	2.7	4.35×10^{10}	1.20	1.00	1.20	5.0	−164.2	a
	120	2.7	1.00×10^{10}	1.20	1.00	1.20	4.0	−170.0	a
	120	2.7	1.34×10^{10}	1.20	1.00	1.20	4.0	−174.0	a
	120	2.7	1.00×10^{10}	1.20	1.00	1.20	4.0	−178.0	a
	120	2.7	3.35×10^{9}	1.20	1.00	1.20	4.0	−182.0	a
	120	2.7	3.35×10^{9}	1.20	1.00	1.20	4.0	−185.7	a
	120	2.7	5.51×10^{9}	1.20	1.00	1.20	8.0	−192.4	a

Table 91. Parameters of our best-fit model of HCS$^+$ toward Sgr B2(M).

Molecule[a]	Size[b] (″)	T_{rot}[c] (K)	N[d] (cm^{-2})	C_{int}[e]	C_{vib}[f]	C_N[g]	ΔV[h]	V_{off}[i] (km s^{-1})	F[j]
(1)	(2)	(3)	(4)	(5)	(6)	(7)	(8)	(9)	(10)
HCS$^+$	8.0	50	2.98×10^{14}	0.99	1.00	0.99	17.0	0.0	e

Notes. See notes of Table 62.

Table 92. Parameters of our best-fit model of HDO toward Sgr B2(M).

Molecule[a]	Size[b] (″)	T_{rot}[c] (K)	N[d] (cm^{-2})	C_{int}[e]	C_{vib}[f]	C_N[g]	ΔV[h]	V_{off}[i]	F[j]
(1)	(2)	(3)	(4)	(5)	(6)	(7)	(8)	(9)	(10)
HDO	3.0	200	5.13×10^{16}	1.03	1.00	1.03	12.0	2.5	e

Notes. See notes of Table 62.

Table 93. Parameters of our best-fit model of HNC toward Sgr B2(M).

Molecule[a]	Size[b] (″)	T_{rot}[c] (K)	N[d] (cm^{-2})	C_{int}[e]	C_{vib}[f]	C_N[g]	ΔV[h]	V_{off}[i]	F[j]
(1)	(2)	(3)	(4)	(5)	(6)	(7)	(8)	(9)	(10)
HNC	200	20	5.98×10^{15}	1.00	1.00	1.00	22.0	3.5	e
	20	16	3.04×10^{14}	1.01	1.00	1.01	20.0	27.0	e
	120	3.7	9.88×10^{14}	1.24	1.00	1.24	13.0	4.5	a
	120	2.7	5.32×10^{12}	1.33	1.00	1.33	7.0	−27.0	a
	120	2.7	1.33×10^{13}	1.33	1.00	1.33	4.0	−31.3	a
	120	2.7	5.32×10^{11}	1.33	1.00	1.33	3.0	−36.5	a
	120	2.7	2.00×10^{13}	1.33	1.00	1.33	9.0	−43.0	a
	120	2.7	1.60×10^{13}	1.33	1.00	1.33	5.0	−47.3	a
	120	2.7	1.73×10^{13}	1.33	1.00	1.33	6.6	−54.0	a
	120	2.7	8.78×10^{13}	1.33	1.00	1.33	6.0	−60.0	a
	120	2.7	6.65×10^{11}	1.33	1.00	1.33	7.0	−67.5	a
	120	2.7	1.06×10^{12}	1.33	1.00	1.33	5.0	−77.5	a
	120	2.7	6.38×10^{12}	1.33	1.00	1.33	5.5	−83.0	a
	120	2.7	6.65×10^{12}	1.33	1.00	1.33	4.5	−88.6	a
	120	2.7	1.06×10^{12}	1.33	1.00	1.33	5.0	−93.0	a
	120	2.7	7.98×10^{11}	1.33	1.00	1.33	4.0	−98.5	a
	120	2.7	9.97×10^{12}	1.33	1.00	1.33	3.0	−103.0	a
	120	2.7	4.39×10^{12}	1.33	1.00	1.33	3.0	−108.0	a
	120	2.7	1.86×10^{12}	1.33	1.00	1.33	3.0	−111.5	a
	120	2.7	2.00×10^{11}	1.33	1.00	1.33	3.0	−116.5	a
	120	2.7	2.39×10^{12}	1.33	1.00	1.33	4.0	−121.0	a
	120	2.7	6.65×10^{11}	1.33	1.00	1.33	5.0	−128.0	a
	120	2.7	2.00×10^{12}	1.33	1.00	1.33	5.0	−132.5	a
	120	2.7	3.46×10^{12}	1.33	1.00	1.33	5.0	−138.7	a
	120	2.7	6.65×10^{11}	1.33	1.00	1.33	5.0	−146.3	a
	120	2.7	2.26×10^{12}	1.33	1.00	1.33	4.0	−150.5	a
	120	2.7	3.99×10^{12}	1.33	1.00	1.33	4.0	−155.0	a
	120	2.7	3.99×10^{12}	1.33	1.00	1.33	4.0	−159.2	a
	120	2.7	1.86×10^{13}	1.33	1.00	1.33	5.0	−164.3	a
	120	2.7	4.66×10^{12}	1.33	1.00	1.33	4.0	−169.0	a
	120	2.7	2.26×10^{12}	1.33	1.00	1.33	4.0	−173.5	a
	120	2.7	1.20×10^{12}	1.33	1.00	1.33	4.0	−178.0	a
	120	2.7	1.06×10^{11}	1.33	1.00	1.33	4.0	−182.0	a
	120	2.7	2.26×10^{11}	1.33	1.00	1.33	4.0	−186.0	a
HN^{13}C	200	20	2.98×10^{14}	0.99	1.00	0.99	22.0	3.5	e
	20	16	1.50×10^{13}	1.00	1.00	1.00	20.0	27.0	e
	120	3.0	9.45×10^{13}	1.18	1.00	1.18	13.0	4.5	a
	120	2.7	1.20×10^{11}	1.20	1.00	1.20	7.0	−27.0	a
	120	2.7	3.01×10^{11}	1.20	1.00	1.20	4.0	−31.3	a
	120	2.7	1.20×10^{10}	1.20	1.00	1.20	3.0	−36.5	a
	120	2.7	3.01×10^{11}	1.20	1.00	1.20	9.0	−43.0	a
	120	2.7	2.41×10^{11}	1.20	1.00	1.20	5.0	−47.3	a
	120	2.7	7.83×10^{11}	1.20	1.00	1.20	6.6	−54.0	a
	120	2.7	3.97×10^{12}	1.20	1.00	1.20	6.0	−60.0	a
	120	2.7	3.01×10^{10}	1.20	1.00	1.20	7.0	−67.5	a
	120	2.7	2.41×10^{10}	1.20	1.00	1.20	5.0	−77.5	a
	120	2.7	1.44×10^{11}	1.20	1.00	1.20	5.5	−83.0	a
	120	2.7	1.50×10^{11}	1.20	1.00	1.20	4.5	−88.6	a
	120	2.7	2.41×10^{10}	1.20	1.00	1.20	5.0	−93.0	a

Notes. See notes of Table 62.

Table 93. continued.

Molecule[a]	Size[b] ('')	T_{rot}[c] (K)	N[d] (cm^{-2})	C_{int}[e]	C_{vib}[f]	C_N[g]	ΔV[h]	V_{off}[i] (km s^{-1})	F[j]
(1)	(2)	(3)	(4)	(5)	(6)	(7)	(8)	(9)	(10)
	120	2.7	1.81×10^{10}	1.20	1.00	1.20	4.0	−98.5	a
	120	2.7	2.26×10^{11}	1.20	1.00	1.20	3.0	−103.0	a
	120	2.7	9.93×10^{10}	1.20	1.00	1.20	3.0	−108.0	a
	120	2.7	4.21×10^{10}	1.20	1.00	1.20	3.0	−111.5	a
	120	2.7	9.03×10^{9}	1.20	1.00	1.20	3.0	−116.5	a
	120	2.7	1.08×10^{11}	1.20	1.00	1.20	4.0	−121.0	a
	120	2.7	3.01×10^{10}	1.20	1.00	1.20	5.0	−128.0	a
	120	2.7	9.03×10^{10}	1.20	1.00	1.20	5.0	−132.5	a
	120	2.7	1.57×10^{11}	1.20	1.00	1.20	5.0	−138.7	a
	120	2.7	3.01×10^{10}	1.20	1.00	1.20	5.0	−146.3	a
	120	2.7	1.02×10^{11}	1.20	1.00	1.20	4.0	−150.5	a
	120	2.7	1.81×10^{11}	1.20	1.00	1.20	4.0	−155.0	a
	120	2.7	1.81×10^{11}	1.20	1.00	1.20	4.0	−159.2	a
	120	2.7	8.43×10^{11}	1.20	1.00	1.20	5.0	−164.3	a
	120	2.7	2.11×10^{11}	1.20	1.00	1.20	4.0	−169.0	a
	120	2.7	1.02×10^{11}	1.20	1.00	1.20	4.0	−173.5	a
	120	2.7	5.42×10^{10}	1.20	1.00	1.20	4.0	−178.0	a
	120	2.7	4.82×10^{9}	1.20	1.00	1.20	4.0	−182.0	a
	120	2.7	1.02×10^{10}	1.20	1.00	1.20	4.0	−186.0	a
H^{15}NC	200	20	1.98×10^{13}	0.99	1.00	0.99	22.0	3.5	e
	20	16	9.98×10^{11}	1.00	1.00	1.00	20.0	27.0	e
	120	3.0	1.01×10^{13}	1.19	1.00	1.19	13.0	4.2	a
	120	2.7	1.38×10^{10}	1.21	1.00	1.21	7.0	−27.0	a
	120	2.7	3.47×10^{10}	1.21	1.00	1.21	4.0	−31.3	a
	120	2.7	1.38×10^{9}	1.21	1.00	1.21	3.0	−36.5	a
	120	2.7	4.04×10^{10}	1.21	1.00	1.21	9.0	−43.0	a
	120	2.7	3.24×10^{10}	1.21	1.00	1.21	5.0	−47.3	a
	120	2.7	5.26×10^{10}	1.21	1.00	1.21	6.6	−54.0	a
	120	2.7	2.67×10^{11}	1.21	1.00	1.21	6.0	−60.0	a
	120	2.7	2.03×10^{9}	1.21	1.00	1.21	7.0	−67.5	a
	120	2.7	2.78×10^{9}	1.21	1.00	1.21	5.0	−77.5	a
	120	2.7	1.66×10^{10}	1.21	1.00	1.21	5.5	−83.0	a
	120	2.7	1.74×10^{10}	1.21	1.00	1.21	4.5	−88.6	a
	120	2.7	2.78×10^{9}	1.21	1.00	1.21	5.0	−93.0	a
	120	2.7	2.08×10^{9}	1.21	1.00	1.21	4.0	−98.5	a
	120	2.7	2.60×10^{10}	1.21	1.00	1.21	3.0	−103.0	a
	120	2.7	1.14×10^{10}	1.21	1.00	1.21	3.0	−108.0	a
	120	2.7	4.86×10^{9}	1.21	1.00	1.21	3.0	−111.5	a
	120	2.7	6.07×10^{8}	1.21	1.00	1.21	3.0	−116.5	a
	120	2.7	7.28×10^{9}	1.21	1.00	1.21	4.0	−121.0	a
	120	2.7	2.03×10^{9}	1.21	1.00	1.21	5.0	−128.0	a
	120	2.7	6.07×10^{9}	1.21	1.00	1.21	5.0	−132.5	a
	120	2.7	1.05×10^{10}	1.21	1.00	1.21	5.0	−138.7	a
	120	2.7	2.03×10^{9}	1.21	1.00	1.21	5.0	−146.3	a
	120	2.7	6.88×10^{9}	1.21	1.00	1.21	4.0	−150.5	a
	120	2.7	1.21×10^{10}	1.21	1.00	1.21	4.0	−155.0	a
	120	2.7	1.21×10^{10}	1.21	1.00	1.21	4.0	−159.2	a
	120	2.7	5.67×10^{10}	1.21	1.00	1.21	5.0	−164.3	a
	120	2.7	1.42×10^{10}	1.21	1.00	1.21	4.0	−169.0	a
	120	2.7	6.88×10^{9}	1.21	1.00	1.21	4.0	−173.5	a
	120	2.7	3.64×10^{9}	1.21	1.00	1.21	4.0	−178.0	a
	120	2.7	3.24×10^{8}	1.21	1.00	1.21	4.0	−182.0	a
	120	2.7	6.88×10^{8}	1.21	1.00	1.21	4.0	−186.0	a

Table 94. Parameters of our best-fit model of HNCO toward Sgr B2(M).

Molecule[a]	Size[b] (″)	$T_{\rm rot}$[c] (K)	N[d] (cm^{-2})	$C_{\rm int}$[e]	$C_{\rm vib}$[f]	C_N[g]	ΔV[h] (km s^{-1})	$V_{\rm off}$[i]	F[j]
(1)	(2)	(3)	(4)	(5)	(6)	(7)	(8)	(9)	(10)
HNCO	3.0	100	5.87×10^{16}	0.98	1.00	0.98	12.0	1.0	e
	60	12	1.78×10^{15}	1.04	1.00	1.04	14.0	1.0	e
	20	10	1.97×10^{15}	1.09	1.00	1.09	30.0	15.0	e
HN^{13}CO	3.0	100	2.99×10^{15}	1.00	1.00	1.00	12.0	1.0	e
	60	12	8.81×10^{13}	1.04	1.00	1.04	14.0	1.0	e
	20	10	9.73×10^{13}	1.08	1.00	1.08	30.0	15.0	e

Notes. See notes of Table 62.

Table 95. Parameters of our best-fit model of HNCS toward Sgr B2(M).

Molecule[a]	Size[b] (″)	$T_{\rm rot}$[c] (K)	N[d] (cm^{-2})	$C_{\rm int}$[e]	$C_{\rm vib}$[f]	C_N[g]	ΔV[h] (km s^{-1})	$V_{\rm off}$[i]	F[j]
(1)	(2)	(3)	(4)	(5)	(6)	(7)	(8)	(9)	(10)
HNCS	200	17	6.23×10^{13}	0.96	1.00	0.96	22.0	0.0	e

Notes. See notes of Table 62.

Table 96. Parameters of our best-fit model of HOCN toward Sgr B2(M).

Molecule[a]	Size[b] (″)	$T_{\rm rot}$[c] (K)	N[d] (cm^{-2})	$C_{\rm int}$[e]	$C_{\rm vib}$[f]	C_N[g]	ΔV[h] (km s^{-1})	$V_{\rm off}$[i]	F[j]
(1)	(2)	(3)	(4)	(5)	(6)	(7)	(8)	(9)	(10)
HOCN	60	12	7.67×10^{12}	1.02	1.00	1.02	14.0	0.0	e
	3.0	100	6.93×10^{14}	0.99	1.00	0.99	12.0	0.0	e

Notes. See notes of Table 62.

Table 97. Parameters of our best-fit model of HOCO$^+$ toward Sgr B2(M).

Molecule[a]	Size[b] (″)	$T_{\rm rot}$[c] (K)	N[d] (cm^{-2})	$C_{\rm int}$[e]	$C_{\rm vib}$[f]	C_N[g]	ΔV[h] (km s^{-1})	$V_{\rm off}$[i]	F[j]
(1)	(2)	(3)	(4)	(5)	(6)	(7)	(8)	(9)	(10)
HOCO$^+$	200	20	6.14×10^{13}	0.94	1.00	0.94	15.0	0.0	e

Notes. See notes of Table 62.

Table 98. Parameters of our best-fit model of HOC$^+$ toward Sgr B2(M).

Molecule[a]	Size[b] (″)	$T_{\rm rot}$[c] (K)	N[d] (cm^{-2})	$C_{\rm int}$[e]	$C_{\rm vib}$[f]	C_N[g]	ΔV[h] (km s^{-1})	$V_{\rm off}$[i]	F[j]
(1)	(2)	(3)	(4)	(5)	(6)	(7)	(8)	(9)	(10)
HOC$^+$	200	20	6.99×10^{13}	1.00	1.00	1.00	18.0	3.0	e
	120	2.7	1.29×10^{13}	1.58	1.00	1.58	17.0	3.0	a

Notes. See notes of Table 62.

Table 99. Parameters of our best-fit model of HSCN toward Sgr B2(M).

Molecule[a]	Size[b] (″)	$T_{\rm rot}$[c] (K)	N[d] (cm^{-2})	$C_{\rm int}$[e]	$C_{\rm vib}$[f]	C_N[g]	ΔV[h] (km s^{-1})	$V_{\rm off}$[i]	F[j]
(1)	(2)	(3)	(4)	(5)	(6)	(7)	(8)	(9)	(10)
HSCN	200	17	2.40×10^{13}	1.00	1.00	1.00	22.0	0.0	e

Notes. See notes of Table 62.

Table 100. Parameters of our best-fit model of N_2H^+ toward Sgr B2(M).

Molecule[a]	Size[b] (″)	T_{rot}[c] (K)	N[d] (cm^{-2})	C_{int}[e]	C_{vib}[f]	C_N[g]	ΔV[h] (km s^{-1})	V_{off}[i]	F[j]
(1)	(2)	(3)	(4)	(5)	(6)	(7)	(8)	(9)	(10)
N_2H^+	200	50	9.77×10^{14}	0.98	1.00	0.98	24.0	4.5	e
	120	3.5	1.63×10^{14}	1.09	1.00	1.09	14.0	2.5	a
	120	2.7	2.64×10^{12}	1.10	1.00	1.10	6.0	−40.5	a
	120	2.7	9.91×10^{11}	1.10	1.00	1.10	6.0	−47.0	a
	120	2.7	1.10×10^{13}	1.10	1.00	1.10	5.0	−60.0	a
	120	2.7	1.98×10^{11}	1.10	1.00	1.10	2.0	−82.3	a
	120	2.7	1.32×10^{11}	1.10	1.00	1.10	3.0	−86.0	a
	120	2.7	1.32×10^{11}	1.10	1.00	1.10	4.0	−89.5	a
	120	2.7	1.16×10^{12}	1.10	1.00	1.10	3.0	−103.0	a
	120	2.7	1.54×10^{12}	1.10	1.00	1.10	3.0	−163.3	a
	120	2.7	6.61×10^{11}	1.10	1.00	1.10	5.0	−168.0	a
$^{15}NNH^+$	200	50	3.29×10^{12}	0.99	1.00	0.99	24.0	4.5	e
	120	3.5	1.16×10^{12}	1.16	1.00	1.16	14.0	2.5	a
	120	2.7	6.47×10^{9}	1.21	1.00	1.21	6.0	−40.5	a
	120	2.7	2.43×10^{9}	1.21	1.00	1.21	6.0	−47.0	a
	120	2.7	4.04×10^{10}	1.21	1.00	1.21	5.0	−60.0	a
	120	2.7	6.24×10^{8}	1.21	1.00	1.21	2.0	−82.3	a
	120	2.7	4.16×10^{8}	1.21	1.00	1.21	3.0	−86.0	a
	120	2.7	4.16×10^{8}	1.21	1.00	1.21	4.0	−89.5	a
	120	2.7	3.64×10^{9}	1.21	1.00	1.21	3.0	−103.0	a
	120	2.7	5.67×10^{9}	1.21	1.00	1.21	3.0	−163.3	a
	120	2.7	2.43×10^{9}	1.21	1.00	1.21	5.0	−168.0	a
$N^{15}NH^+$	200	50	3.29×10^{12}	0.99	1.00	0.99	24.0	4.5	e
	120	3.5	1.16×10^{12}	1.16	1.00	1.16	14.0	2.5	a
	120	2.7	6.47×10^{9}	1.21	1.00	1.21	6.0	−40.5	a
	120	2.7	2.43×10^{9}	1.21	1.00	1.21	6.0	−47.0	a
	120	2.7	4.04×10^{10}	1.21	1.00	1.21	5.0	−60.0	a
	120	2.7	6.24×10^{8}	1.21	1.00	1.21	2.0	−82.3	a
	120	2.7	4.16×10^{8}	1.21	1.00	1.21	3.0	−86.0	a
	120	2.7	4.16×10^{8}	1.21	1.00	1.21	4.0	−89.5	a
	120	2.7	3.64×10^{9}	1.21	1.00	1.21	3.0	−103.0	a
	120	2.7	5.67×10^{9}	1.21	1.00	1.21	3.0	−163.3	a
	120	2.7	2.43×10^{9}	1.21	1.00	1.21	5.0	−168.0	a

Notes. See notes of Table 62.

Table 101. Parameters of our best-fit model of NH_2CN toward Sgr B2(M).

Molecule[a]	Size[b] (″)	T_{rot}[c] (K)	N[d] (cm^{-2})	C_{int}[e]	C_{vib}[f]	C_N[g]	ΔV[h] (km s^{-1})	V_{off}[i]	F[j]
(1)	(2)	(3)	(4)	(5)	(6)	(7)	(8)	(9)	(10)
NH_2CN	60	20	3.54×10^{13}	1.01	1.00	1.01	14.0	0.0	e

Notes. See notes of Table 62.

Table 102. Parameters of our best-fit model of NS toward Sgr B2(M).

Molecule[a]	Size[b] (″)	T_{rot}[c] (K)	N[d] (cm^{-2})	C_{int}[e]	C_{vib}[f]	C_N[g]	ΔV[h] (km s^{-1})	V_{off}[i]	F[j]
(1)	(2)	(3)	(4)	(5)	(6)	(7)	(8)	(9)	(10)
NS	200	20	5.96×10^{14}	0.99	1.00	0.99	18.0	1.0	e
	120	2.7	3.84×10^{14}	1.48	1.00	1.48	12.0	3.0	a

Notes. See notes of Table 62.

Table 103. Parameters of our best-fit model of OCS toward Sgr B2(M).

Molecule[a]	Size[b] (″)	$T_{\rm rot}$[c] (K)	N[d] (cm^{-2})	$C_{\rm int}$[e]	$C_{\rm vib}$[f]	C_N[g]	ΔV[h] (km s^{-1})	$V_{\rm off}$[i]	F[j]
(1)	(2)	(3)	(4)	(5)	(6)	(7)	(8)	(9)	(10)
OCS	60	20	2.80×10^{15}	1.00	1.00	1.00	12.0	1.0	e
	3.0	150	2.00×10^{17}	1.00	1.00	1.00	14.0	2.0	e
	60	20	6.99×10^{14}	1.00	1.00	1.00	28.0	14.0	e
O^{13}CS	60	20	2.00×10^{14}	1.00	1.00	1.00	12.0	1.0	e
	3.0	150	1.30×10^{16}	1.00	1.00	1.00	14.0	2.0	e
	60	20	5.00×10^{13}	1.00	1.00	1.00	28.0	14.0	e
OC^{34}S	60	20	2.50×10^{14}	1.00	1.00	1.00	12.0	1.0	e
	3.0	150	1.80×10^{16}	1.00	1.00	1.00	14.0	2.0	e
	60	20	6.24×10^{13}	1.00	1.00	1.00	28.0	14.0	e

Notes. See notes of Table 62.

Table 104. Parameters of our best-fit model of PN toward Sgr B2(M).

Molecule[a]	Size[b] (″)	$T_{\rm rot}$[c] (K)	N[d] (cm^{-2})	$C_{\rm int}$[e]	$C_{\rm vib}$[f]	C_N[g]	ΔV[h] (km s^{-1})	$V_{\rm off}$[i]	F[j]
(1)	(2)	(3)	(4)	(5)	(6)	(7)	(8)	(9)	(10)
PN	120	2.7	3.97×10^{12}	1.10	1.00	1.10	7.0	–0.2	a
	120	2.7	9.93×10^{11}	1.10	1.00	1.10	4.0	7.5	a

Notes. See notes of Table 62.

Table 105. Parameters of our best-fit model of SiO toward Sgr B2(M).

Molecule[a]	Size[b] ($''$)	T_{rot}[c] (K)	N[d] (cm^{-2})	C_{int}[e]	C_{vib}[f]	C_N[g]	ΔV[h] (km s^{-1})	V_{off}[i] (km s^{-1})	F[j]
(1)	(2)	(3)	(4)	(5)	(6)	(7)	(8)	(9)	(10)
SiO	200	16	4.50×10^{14}	1.00	1.00	1.00	22.0	0.5	e
	20	10	1.81×10^{14}	1.01	1.00	1.01	15.0	26.0	e
	20	10	1.21×10^{14}	1.01	1.00	1.01	15.0	−23.0	e
	120	3.3	3.23×10^{14}	1.08	1.00	1.08	7.5	6.8	a
	120	3.3	4.52×10^{14}	1.08	1.00	1.08	7.0	−1.3	a
	120	2.7	1.75×10^{12}	1.10	1.00	1.10	5.0	−44.5	a
	120	2.7	2.19×10^{12}	1.10	1.00	1.10	6.0	−50.0	a
	120	2.7	2.96×10^{12}	1.10	1.00	1.10	4.5	−54.0	a
	120	2.7	3.62×10^{12}	1.10	1.00	1.10	5.0	−58.5	a
	120	2.7	3.73×10^{12}	1.10	1.00	1.10	5.0	−64.0	a
	120	2.7	8.77×10^{11}	1.10	1.00	1.10	5.0	−86.0	a
	120	2.7	8.22×10^{11}	1.10	1.00	1.10	3.5	−103.5	a
	120	2.7	5.26×10^{12}	1.10	1.00	1.10	9.5	−154.0	a
	120	2.7	4.27×10^{12}	1.10	1.00	1.10	8.5	−165.5	a
^{29}SiO	200	16	2.25×10^{13}	1.00	1.00	1.00	22.0	0.5	e
	20	10	9.07×10^{12}	1.01	1.00	1.01	15.0	26.0	e
	20	10	6.05×10^{12}	1.01	1.00	1.01	15.0	−23.0	e
	120	3.3	1.61×10^{13}	1.07	1.00	1.07	7.5	6.8	a
	120	3.3	2.26×10^{13}	1.07	1.00	1.07	7.0	−1.3	a
	120	2.7	8.76×10^{10}	1.09	1.00	1.09	5.0	−44.5	a
	120	2.7	1.09×10^{11}	1.09	1.00	1.09	6.0	−50.0	a
	120	2.7	1.48×10^{11}	1.09	1.00	1.09	4.5	−54.0	a
	120	2.7	1.81×10^{11}	1.09	1.00	1.09	5.0	−58.5	a
	120	2.7	1.86×10^{11}	1.09	1.00	1.09	5.0	−64.0	a
	120	2.7	4.38×10^{10}	1.09	1.00	1.09	5.0	−86.0	a
	120	2.7	4.11×10^{10}	1.09	1.00	1.09	3.5	−103.5	a
	120	2.7	2.63×10^{11}	1.09	1.00	1.09	9.5	−154.0	a
	120	2.7	2.14×10^{11}	1.09	1.00	1.09	8.5	−165.5	a
^{30}SiO	200	16	1.50×10^{13}	1.00	1.00	1.00	22.0	0.5	e
	20	10	6.05×10^{12}	1.01	1.00	1.01	15.0	26.0	e
	20	10	4.03×10^{12}	1.01	1.00	1.01	15.0	−23.0	e
	120	3.3	1.07×10^{13}	1.07	1.00	1.07	7.5	6.8	a
	120	3.3	1.50×10^{13}	1.07	1.00	1.07	7.0	−1.3	a
	120	2.7	5.83×10^{10}	1.09	1.00	1.09	5.0	−44.5	a
	120	2.7	7.29×10^{10}	1.09	1.00	1.09	6.0	−50.0	a
	120	2.7	9.84×10^{10}	1.09	1.00	1.09	4.5	−54.0	a
	120	2.7	1.20×10^{11}	1.09	1.00	1.09	5.0	−58.5	a
	120	2.7	1.24×10^{11}	1.09	1.00	1.09	5.0	−64.0	a
	120	2.7	2.92×10^{10}	1.09	1.00	1.09	5.0	−86.0	a
	120	2.7	2.73×10^{10}	1.09	1.00	1.09	3.5	−103.5	a
	120	2.7	1.75×10^{11}	1.09	1.00	1.09	9.5	−154.0	a
	120	2.7	1.42×10^{11}	1.09	1.00	1.09	8.5	−165.5	a
Si^{18}O	200	16	1.80×10^{12}	1.00	1.00	1.00	26.0	1.0	e
	20	10	7.26×10^{11}	1.01	1.00	1.01	15.0	26.0	e
	20	10	4.84×10^{11}	1.01	1.00	1.01	15.0	−23.0	e
	120	3.3	1.29×10^{12}	1.07	1.00	1.07	7.5	6.8	a
	120	3.3	1.80×10^{12}	1.07	1.00	1.07	7.0	−1.3	a

Notes. See notes of Table 62.

Table 106. Parameters of our best-fit model of SO_2 toward Sgr B2(M).

Molecule[a]	Size[b] (″)	T_{rot}[c] (K)	N[d] (cm^{-2})	C_{int}[e]	C_{vib}[f]	C_N[g]	ΔV[h] (km s^{-1})	V_{off}[i]	F[j]
(1)	(2)	(3)	(4)	(5)	(6)	(7)	(8)	(9)	(10)
SO_2	2.0	200	1.98×10^{19}	0.99	1.00	0.99	13.0	−1.0	e
	60	50	5.90×10^{15}	0.98	1.00	0.98	14.0	−4.0	e
$SO_2, v_2 = 1$	1.2	200	7.94×10^{19}	0.99	1.00	0.99	13.0	−1.0	e
$^{34}SO_2$	2.0	200	9.09×10^{17}	1.00	1.00	1.00	13.0	−1.0	e
	60	50	2.72×10^{14}	1.00	1.00	1.00	14.0	−4.0	e
$^{33}SO_2$	2.0	200	1.82×10^{17}	1.00	1.00	1.00	13.0	−1.0	e
	60	50	5.43×10^{13}	1.00	1.00	1.00	14.0	−4.0	e
$SO^{18}O$	2.0	200	8.01×10^{16}	1.00	1.00	1.00	13.0	−1.0	e
	60	50	2.39×10^{13}	1.00	1.00	1.00	14.0	−4.0	e
$SO^{17}O$	2.0	200	2.78×10^{16}	1.00	1.00	1.00	13.0	−1.0	e
	60	50	8.31×10^{12}	1.00	1.00	1.00	14.0	−4.0	e

Notes. See notes of Table 62.

Table 107. Parameters of our best-fit model of SO toward Sgr B2(M).

Molecule[a]	Size[b] (″)	T_{rot}[c] (K)	N[d] (cm^{-2})	C_{int}[e]	C_{vib}[f]	C_N[g]	ΔV[h] (km s^{-1})	V_{off}[i]	F[j]
(1)	(2)	(3)	(4)	(5)	(6)	(7)	(8)	(9)	(10)
SO	30	30	8.98×10^{15}	1.06	1.00	1.06	15.0	−1.0	e
	2.0	200	2.46×10^{18}	0.99	1.00	0.99	14.0	−1.0	e
	20	20	2.56×10^{15}	1.02	1.00	1.02	20.0	11.0	e
	20	20	2.56×10^{15}	1.02	1.00	1.02	15.0	−13.0	e
	120	3.0	7.54×10^{14}	0.94	1.00	0.94	13.0	3.0	a
	120	2.7	5.44×10^{12}	0.95	1.00	0.95	3.0	−53.0	a
	120	2.7	2.67×10^{13}	0.95	1.00	0.95	6.0	−59.0	a
	120	2.7	2.20×10^{13}	0.95	1.00	0.95	6.0	−104.0	a
	120	2.7	5.73×10^{12}	0.95	1.00	0.95	6.0	−156.0	a
	120	2.7	7.64×10^{12}	0.95	1.00	0.95	6.0	−166.5	a
^{34}SO	30	30	8.46×10^{14}	1.06	1.00	1.06	15.0	−1.0	e
	2.0	200	1.23×10^{17}	0.99	1.00	0.99	14.0	−1.0	e
	20	20	1.54×10^{14}	1.02	1.00	1.02	20.0	11.0	e
	20	20	1.54×10^{14}	1.02	1.00	1.02	15.0	−13.0	e
	120	3.0	3.76×10^{13}	0.94	1.00	0.94	13.0	3.0	a
^{33}SO	30	30	3.17×10^{14}	1.06	1.00	1.06	15.0	−1.0	e
	2.0	200	2.46×10^{16}	0.99	1.00	0.99	14.0	−1.0	e
	120	3.0	8.46×10^{12}	0.94	1.00	0.94	13.0	3.0	a
$S^{18}O$	30	30	9.53×10^{13}	1.06	1.00	1.06	15.0	−1.0	e
	2.0	200	7.88×10^{15}	0.98	1.00	0.98	14.0	−1.0	e

Notes. See notes of Table 62.